

UNIVERSITY OF CANTABRIA

DEPARTMENT OF  
COMMUNICATIONS ENGINEERING



PhD DISSERTATION

BASEBAND PROCESSING IN ANALOG COMBINING  
MIMO SYSTEMS: FROM THEORETICAL  
DESIGN TO FPGA IMPLEMENTATION

Author: Víctor Elvira Arregui  
Supervisors: Jesús Ibáñez Díaz  
Javier Vía Rodríguez

2011



# **Procesado Banda Base en Sistemas MIMO basados en Combinación Analógica de Antenas: Del Diseño Teórico a la Implementación FPGA**

Tesis que se presenta para optar al título de  
Doctor por la Universidad de Cantabria

**Author:** Víctor Elvira Arregui

**Supervisors:** Jesús Ibáñez Díaz  
Javier Vía Rodríguez

Programa Oficial de Posgrado en Tecnologías de la Información  
y Comunicaciones en Sistemas de Telecomunicación

Grupo de Tratamiento Avanzado de Señal

Departamento de Ingeniería de Comunicaciones

Escuela Técnica Superior de Ingenieros Industriales y de Telecomunicación

Universidad de Cantabria

2011



Il piacere più nobile è la gioia di comprendere.

—*Leonardo da Vinci*

## **Affiliations**

Advanced Signal Processing Group  
Department of Communications Engineering  
University of Cantabria, Spain

The research leading to this work has received funding from the European Community's Seventh Framework Programme (FP7/2007-2013) under grant agreement n° 213952 (MIMAX).

# Acknowledgements

I would like to start by thanking my thesis supervisors, Javier Vía and Jesús Ibáñez, for all the work they have endeavored upon with me, their immense patience, and the great support that I have received from the first day that I began to work with them until the day that I am writing these lines. They have always helped me while having good demeanor and better disposition at whatever hour of the day without any single exception. Thank you to Vía for making simple what was difficult with the humility that usually resides within only the most brilliant people. Thank you to Jesús for your infinite optimism and for giving me the opportunity to work with one of the best professors I have ever had in my life. I would also like to extend this thanks to Ignacio Santamaría, an excellent professor and, even beyond that, an extraordinary boss; although he has not been a supervisor of this work, he gave me the opportunity to become a part of this group, and I have had the deep satisfaction to work with him within the MIMAX project. This thesis is as much mine as it is theirs.

I want to thank to all of the Grupo de Tratamiento Avanzado de Señal (GTAS), as much as to the rest of professors, to Jesús Pérez, who diligently managed my end of bachelor project, to Luis Vielva, who I have come to understand two of each three of his ingenious remarks, and to all my colleagues, whom I have been fortunate to work with. It is difficult for me to imagine a better work environment than what I have experienced in the last few years in GTAS. Thank you to Alfredo because you helped with the final stretch of the project, when I needed it the most. Thank you to Christian because you have just arrived and have been very willing to help me. Thank you to Chus for putting up with me as an office colleague (and friend) since the first day I arrived until the very end and always having a good sense of humor, which has made each work day much more agreeable. Thank you to Fouad because each afternoon without an attempted invitation from you for a cappuccino would have never been the same. Thank you to Gonzy because you are positively brilliant and it appears that you are unaware of this (which is fun), and because a conversation with you is always a genuine pleasure. Thank you to Miguel because, although we met recently, when I talk to you, due to your friendliness, it seems that we met years ago. Thank you to Ramírez for being always in the mood to help with anything and in any moment with a smile (although also with a certain comment that I cannot reproduce here). Thank you to Steven because of your irony and excellent sense of humor (I am not being ironic). Thank you so much to all of you. It has been an immense pleasure, and I hope to have the opportunity to work again with any of you.

The necessary work to be able to finish a doctoral dissertation is only possible thanks to the support of a lot of people at the professional level as well as at personal level. This work in good part can be attributed to many people, who have helped me in multiple facets of life within the past few years and especially within the last several months. I would like to thank these people that have supported me in different ways during the writing of this document, who have lived with me and put up with me day-to-day, or who have aided in the tedious revision of this final document (or both tasks simultaneously). Especially, I would like to give

thanks to you, Julie, because of your infinite patience. You have dedicated hours and hours to reading and rereading each chapter of this dissertation until sleepiness caught up with you. You cannot imagine how much I appreciate what you have done. Thanks.

Also, I would like to thank my friends for the support and fun we have shared. Thank you especially to my lifelong friends (they know who they are). This also extendible to all the friends that, even though we have met each other later on, are capable of making me believe that we have known each other of all our lives. I cannot conceive a life without the friends I have.

Finally, and most importantly, I want to dedicate this thesis to my parents. The first memories of my life are full of their affection, support, and effort to make me a better person. They, due to their values, which they have established within me, have tried each day to make me a happier person and a hard worker with humility. This work is for you. I also want to thank the support and affection of the rest of my small family: my cousin, my aunts and uncles, and my grandparents. I would like to especially mention my two grandfathers. One of them left us nearly 18 years ago, but I will never forget him. The other one, who each year harvests more than 1,500 kilograms of potatoes with his strong and octogenarian hands, has always inspired my way of thinking. He, for his extraordinary intelligence and for his diligence in everything he does, on top of having to abandon his studies at age 12 to maintain his family, is the sole, authentic engineer and doctor of the family. As for the rest of us, we are only and will only be the apprentices.

Víctor Elvira Arregui

Santander, 23 May 2011

# Abstract

Within the last several years, wireless communication has been one of the fastest growing segments of the communications industry. One of the major novelties in this field has been the shift from the single-input single-output (SISO) paradigm, where the system has one antenna for transmission and one antenna for reception, to the multi-input multi-output (MIMO) scheme, where there are several antennas both at the transmitter and the receiver side. Although MIMO systems exceed significantly the performance of SISO systems, the former has an extra cost in terms of production cost, size, and power consumption, which is in part responsible for the delay in the commercial deployment of MIMO wireless transceivers.

A novel MIMO architecture, called analog antenna combining, exploits some important MIMO benefits but with a cost comparable to that of the SISO systems. The analog antenna combining schemes basically use at each antenna branch a phase shifter and two variable gain amplifiers (VGA), which essentially implement a multiplication by a complex weight directly in the radio-frequency (RF) domain. This multiplication also may be performed by a vector modulator (VM). The research and the subsequent fabrication of wireless devices with this technology has been pursued within the European Union funded project MIMAX.

In the first part of this work, we consider the problem of selecting the transmit and receive RF weights (also called beamformers) for orthogonal frequency-division multiplexing (OFDM) transmissions under different assumptions on the channel state information. In particular, for the case of channel state information (CSI) at the transmitter and the receiver side (CSIT+CSIR), a general beamforming criterion is proposed, which depending on a single parameter establishes a tradeoff between the energy of the equivalent SISO channel (after transmit-receive beamforming) and its spectral flatness. Regarding the general criterion, we have proposed an efficient gradient search algorithm, which, in practice, provides satisfactory solutions for the calculation of the RF weights. The case with perfect CSI at the receiver but only statistical information at the transmitter has been also explored, considering transmit correlation knowledge at the transmitter side. A new scheme, which spreads the information over the time under different pairs of beamformers, has been proposed. For this case, we have designed the time and frequency precoders as well as the optimal transmit and receive beamformers. The performance of the proposed scheme has been compared by means of simulations with that of the traditional MIMO and SISO systems.

In the second part of the thesis, in the context of the European Union funded project MIMAX, we have participated in the development of a MIMO wireless transceiver, which performs analog antenna combining, the so-called MIMAX transceiver. Starting from the baseband processor of the widely used IEEE standard 802.11a, we have designed the FPGA-synthesizable baseband processor of the transceiver. An existing legacy 802.11a baseband processor has been modified, and several new baseband modules have been designed and implemented in order to allow the new functionalities of the MIMAX transceiver. These modules include a MIMO channel estimator and a RF weights calculation block. The latter has been the most challenging, because it must perform within the FPGA one of the algorithms

proposed in the first part of the work. The new baseband modules have been successfully integrated within the legacy IEEE 802.11a baseband processor, and they have been tested in real-time within a baseband board, jointly designed within the MIMAX project and manufactured by one of the project partners. Moreover, some tests of the whole physical layer of the MIMAX transceiver have been carried out in order to show, in a real environment and in real-time, the improvement of the MIMAX transceiver with respect to the SISO one.

In summary, this dissertation has two distinct parts. The theoretical first part addresses the calculation of the optimal beamformers under different types of channel knowledge in a MIMO system, which performs analog antenna combining at the RF domain. In the second part, emphasizing application, and while participating in a successful joint development of a novel MIMO wireless transceiver (MIMAX transceiver), we focus on the FPGA-design, implementation, integration, and real-time testing of the MIMAX baseband processor, which is based on the IEEE 802.11a baseband processor. For this purpose, some new baseband blocks are designed with RF weights calculation being the most challenging block, which performs one adapted algorithm of those described in the first part.

# Resumen y Conclusiones

Las comunicaciones inalámbricas permiten servicios que no son posibles en las tradicionales comunicaciones con cables. Desde principios de la década de los 90, y especialmente en los últimos años, los sistemas de comunicaciones inalámbricas constituyen uno de los sectores de mayor crecimiento de la industria de las comunicaciones. Esto es debido principalmente al enorme crecimiento del uso de dispositivos electrónicos portables, como los teléfonos móviles y ordenadores portátiles, y más recientemente los teléfonos inteligentes, ordenadores de bolsillo y demás dispositivos que permiten el acceso a Internet.

Como consecuencia, y en paralelo a este crecimiento, se han ido desarrollando sistemas de comunicaciones inalámbricas cada vez más fiables y eficientes. Los sistemas tradicionales de comunicaciones inalámbricas poseen una única antena en el transmisor y otra en el receptor. Estos sistemas, también llamados de una sola entrada y salida (*single-input single-output* o SISO), ofrecen un rendimiento y una tasa de transferencia bastante limitados. Una de las novedades más importantes en este campo ha sido el cambio de los sistemas SISO por los sistemas de múltiples antenas tanto en el transmisor como en el receptor (*multiple-input multiple-output* o MIMO). Los sistemas MIMO superan significativamente el rendimiento de los sistemas SISO debido a que el uso de múltiples antenas ofrece una dimensión especial extra que puede ser aprovechada para mejorar la fiabilidad (diversidad), la tasa de transmisión (ganancia por multiplexado) y la cobertura de los sistemas (ganancia de *array*).

Sin embargo, las mejoras que los sistemas MIMO ofrecen respecto a los sistemas SISO llevan asociadas una serie de desventajas. Las estaciones MIMO tradicionales requieren una rama de radiofrecuencia (RF) por cada antena y además el procesado en banda base también debe ser realizado para cada una de esas ramas. En consecuencia, para obtener todos los beneficios ofrecidos por las múltiples antenas, las estaciones MIMO tienen un aumento de coste, tamaño y consumo de potencia respecto a las estaciones SISO. Esta ha sido una de las causas por las que la inclusión de los sistemas MIMO en dispositivos comerciales se ha visto notablemente retrasada.

Impulsada por recientes avances en tecnologías SiGe-BiCMOS, ha sido propuesta una nueva arquitectura de combinación analógica de antenas. Esta arquitectura puede extraer algunas de las ventajas de los sistemas MIMO a la vez que mantiene un coste, tamaño y consumo similar al de los sistemas SISO. En este nuevo esquema, cada rama de RF contiene un desfaseador y un amplificador variable de ganancia (o, alternativamente, un modulador vectorial), que, básicamente, implementan la multiplicación en RF de la señal por un peso complejo. Las señales ponderadas son combinadas en RF en el receptor, de manera que se mantiene una sola cadena tanto en RF como en banda base, tal y como se puede apreciar en la Figura 1. En el marco del proyecto europeo MIMAX, en el cual ha participado el Grupo de Tratamiento Avanzado de Señal (GTAS) de la Universidad de Cantabria, se ha llevado a cabo

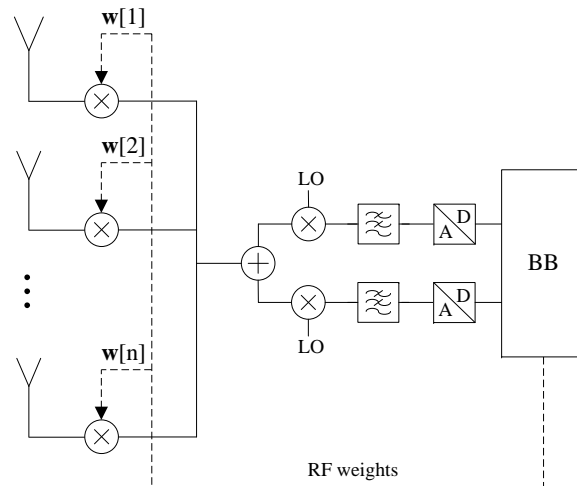


**Figura 1:** Combinación analógica de las antenas en radiofrecuencia en sistemas de comunicaciones MIMO. Ejemplo para receptor de la estación inalámbrica.

una profunda investigación sobre la arquitectura de combinación analógica de antenas, así como el desarrollo de un prototipo inalámbrico que implemente dicha arquitectura.

Esta tesis se divide en dos partes. En la primera parte se aborda el diseño teórico del algoritmo de cálculo de los pesos óptimos en un sistema MIMO que implementa la arquitectura de combinación analógica de antenas. El estudio sobre la selección de los pesos es abordado tanto en el caso en el que el transmisor conoce perfectamente el canal en transmisión como cuando sólo conoce la estadística del canal. En ambos casos se supone que el receptor conoce perfectamente el estado del canal, lo cual es común en la mayor parte de sistemas inalámbricos. La segunda parte, más aplicada, consiste en el diseño, implementación, integración y pruebas experimentales en tiempo real, de un procesador banda base que explota las nuevas funcionalidades de la arquitectura propuesta.

En el Capítulo 2, a modo de introducción, se analizan los sistemas MIMO tradicionales, y se presentan sus principales ventajas como el multiplexado espacial, la diversidad espacial o la ganancia de *array*. Sin embargo, la nueva arquitectura de combinación analógica de antenas permite conservar ciertas ventajas de los sistemas MIMO con un coste, tamaño y consumo similar al de los sistemas SISO. Para ello, nuevos desafíos se presentan en la banda base, la cual, entre otras cosas, debe decidir qué pesos son aplicados en RF.

## Parte I: Esquemas para la Selección Óptima de Pesos

En la primera parte de este trabajo se aborda el cálculo de los pesos que deben ser aplicados en RF en un sistema basado en combinación analógica de antenas. Hemos estudiado dicho problema en un sistema con multiplexación por división de frecuencias ortogonales (OFDM), y bajo diferentes suposiciones acerca del canal. Nótese que en un sistema multi-portadora como OFDM, debido a la naturaleza de la nueva arquitectura empleada, una única pareja de pesos se aplica a todas las subportadoras. Por esta razón, la selección de los pesos adecuados no es trivial.

## Conocimiento Perfecto del Canal en el Transmisor

En el Capítulo 3 se trata el diseño de los pesos cuando tanto el transmisor como el receptor tienen conocimiento perfecto del canal. Se propone un criterio general para la obtención de los pesos que, dependiendo de un parámetro  $\alpha$ , establece un compromiso entre la energía del canal SISO equivalente (después de la aplicación de los pesos) y la selectividad frecuencial de dicho canal. Ciertos valores del parámetro  $\alpha$  se analizan por ser casos especialmente interesantes. Por ejemplo, mediante el criterio general, es posible maximizar la relación señal a ruido (SNR) del canal SISO equivalente (criterio MaxSNR), maximizar la capacidad del canal SISO equivalente (criterio MaxCAP), o minimizar el error cuadrático medio (MSE) en el receptor (criterio MinMSE).

Se demuestra que el problema de optimización es no convexo y que se puede obtener una solución aproximada con técnicas de relajación semidefinida (SDR). Se propone un algoritmo de descenso por gradiente que es computacionalmente menos costoso que las técnicas SDR y que ofrece unos buenos resultados en la mayoría de los casos prácticos. Finalmente se exponen diversas simulaciones que muestran el rendimiento de los algoritmos propuestos.

## Conocimiento Estadístico del Canal en el Transmisor

El caso análogo al del Capítulo 3 cuando el transmisor sólo dispone de conocimiento estadístico del canal se estudia en el Capítulo 4. Para la selección de pesos se propone un método de multiplexación por división de pesos (BDM) que consiste en la transmisión de la información distribuida en distintos instantes temporales y transmitida bajo diferentes pesos. Mediante el diseño de los precodificadores adecuados (que dispersan esa información en el tiempo y en la frecuencia) y de un conjunto de pesos que apunte en distintas direcciones, la diversidad espacial de MIMO puede ser conservada convirtiéndose en una diversidad temporal.

Por tanto, el conjunto de pesos del transmisor puede ser visto como un conjunto de direcciones determinadas por los autovectores de la matriz de correlación en el transmisor. En función de los autovalores de cada una de las direcciones, y mediante el conocido algoritmo de *waterfilling*, se asignan distintas potencias a cada una de dichas direcciones. Finalmente, la matriz de pesos del transmisor se multiplica por una matriz con elementos de módulo constante, lo que permite mantener la potencia de transmisión también constante. El conjunto de pesos del receptor se obtiene aplicando a cada uno de los pesos del transmisor el algoritmo descrito en el Capítulo 3. También en este caso se muestra una serie de simulaciones que evalúan el rendimiento del diseño propuesto.

## Parte II: Nueva Banda Base MIMAX: Diseño, Implementación, Integración y Pruebas en Tiempo Real

En la segunda parte de la tesis se desarrollan tareas más cercanas a la implementación. Como se ha mencionado previamente, el objetivo final del proyecto europeo MIMAX consiste en el desarrollo de un prototipo inalámbrico MIMO basado en la arquitectura de combinación analógica de antenas. Dicho prototipo (llamado prototipo MIMAX) está basado en el conocido estándar IEEE 802.11a (que implementa OFDM), el cual se usa ampliamente en redes inalámbricas de área local. El trabajo relativo a esta tesis ha consistido en el diseño e implementación de una banda base que permita al prototipo MIMAX extraer los beneficios de la

nueva arquitectura MIMO (nótese que 802.11a como tal es un estándar que sólo puede ser implementado en un sistema SISO).

A continuación se resume el proceso de la creación de la nueva banda base, desde el inicio de su diseño hasta las pruebas en tiempo real de dicha banda base en conjunto con otras partes del prototipo.

### **Diseño de la Banda Base**

En el Capítulo 6 se aborda el diseño de la banda base de MIMAX partiendo de un preexistente procesador banda base del estándar IEEE 802.11a. Dicho procesador se modifica ligeramente y se propone la inclusión de un conjunto de nuevos bloques. Entre estos nuevos bloques MIMAX, destacan el bloque de estimación del canal MIMO y, especialmente, el bloque de cálculo de pesos. Este último, el más costoso de la nueva banda base tanto desde el punto de vista de esfuerzo como de recursos empleados, consiste en el diseño, en punto fijo y sintetizable en FPGA, de uno de los algoritmos estudiados en la primera parte de la tesis.

En MIMAX, mediante un proceso de entrenamiento, tanto el transmisor como el receptor conocen el canal. Por ello, se analizan los algoritmos propuestos en el Capítulo 3 para implementar uno de ellos en el diseño FPGA de la banda base. Finalmente se ha elegido una versión aproximada del criterio MaxSNR, debido a que proporciona unos buenos resultados con una complejidad notablemente reducida en comparación con los otros criterios.

Tanto el diseño como la implementación de todos los nuevos bloques de la banda base se realiza con el programa System Generator de Xilinx, integrado en el entorno Simulink de MATLAB. Este programa permite la creación de bloques complejos a través de otros más simples como sumadores y multiplicadores, todos ellos sintetizables. De esta manera, el proceso de diseño e implementación está totalmente interrelacionado desde el principio. Para el diseño de los bloques se ha partido de un modelo punto flotante de MATLAB de toda la banda base MIMAX. A partir de este modelo se crea un modelo en punto fijo asociado a cada bloque. Este modelo replica bit a bit el comportamiento de los diseños en System Generator. La utilidad de los modelos punto fijo es por un lado la validación del correcto funcionamiento de los bloques en System Generator y por otro, la inclusión de los mismos en el modelo punto flotante que permite evaluar el comportamiento de los bloques mediante simulaciones masivas y consecuentemente tomar decisiones de diseño.

### **Simulación, Generación e Integración del Procesador Banda Base**

Una vez que los nuevos bloques de la banda base MIMAX han sido diseñados e implementados, el Capítulo 7 describe la validación general por medio de una serie de campañas de simulación. Estas campañas validan tanto el comportamiento de los bloques individualmente como el funcionamiento conjunto de los mismos dentro de la banda base MIMAX. Las simulaciones se realizan tanto con System Generator como con ModelSim, siendo igualmente satisfactorias en ambos casos.

Finalmente, mediante System Generator, se genera un fichero netlist (NGC) con la descripción e interconexión de todos los nuevos bloques de la banda base MIMAX. Esa nueva entidad se incluye en un proyecto ISE de la banda base del estándar IEEE 802.11a que ha sido ligeramente modificado para integrar los nuevos bloques. El proyecto, cuyos componentes están programados principalmente en el lenguaje de descripción de hardware VHDL, se sintetiza e implementa dando como resultado un fichero `.bit` que permite programar la FPGA que contendrá el procesador banda base.

## Pruebas en Tiempo Real del Procesador Banda Base

Como se ha mencionado anteriormente, en el marco del proyecto MIMAX, se ha construido un prototipo de comunicaciones inalámbricas con la arquitectura previamente descrita. Cada uno de los miembros del proyecto ha sido responsable de una parcela delimitada. Así, en colaboración con el centro de investigación IHP (de Frankfurt Oder, Alemania), se ha diseñado la placa banda base que contiene la FPGA que debe albergar el procesador banda base. Esta placa ha sido fabricada y montada por IHP.

En el Capítulo 8 se desarrollan una serie de experimentos en tiempo real para probar el funcionamiento del procesador banda base en la placa desarrollada. Se hace especial hincapié en la validación de los nuevos bloques. Una vez validados los bloques en tiempo real, se integra la placa banda base con otros elementos de la capa física del prototipo, los cuales han sido previamente desarrollados por otros miembros del proyecto. Esta nueva configuración incluye tanto el frontal analógico MIMAX (encargado de aplicar los pesos mediante moduladores vectoriales), como el *array* de antenas. Con esta configuración se llevan a cabo distintos experimentos más generales que, además de probar el buen funcionamiento del procesador banda base, proporcionan una muestra cuantitativa de las ventajas del sistema MIMAX respecto al SISO. Concretamente se puede observar una mejora sustancial tanto en SNR como en cobertura y también una disminución muy significativa de la tasa de tramas erróneas.

## Conclusiones

En este trabajo se propone una nueva arquitectura de combinación analógica de antenas para un transceptor inalámbrico MIMO. Esta arquitectura ha constituido el hilo conductor de esta tesis puesto que en la primera parte de la misma se ha realizado un profundo estudio de la selección óptima de los pesos que se deben aplicar en RF, y en la segunda se ha diseñado e implementado un procesador banda base que implementa los nuevos requerimientos de la nueva arquitectura, incluido el cálculo de pesos.

En la primera parte de la tesis, se ha estudiado tanto el caso con conocimiento del canal en transmisión como el caso en el que el transmisor sólo conoce la estadística del canal. Se ha propuesto un criterio general para la selección de pesos para el primer caso y un nuevo método de transmisión basado en el envío de la información a través de diversas direcciones para el segundo caso. Para ambas situaciones se han propuesto algoritmos que calculan esos pesos. Se ha comprobado por medio de simulaciones que dichos algoritmos obtienen resultados que mejoran notablemente las prestaciones de los sistemas SISO, incluso aproximándose en ciertas ocasiones a los costosos sistemas tradicionales MIMO.

En la segunda parte de la tesis, se ha detallado nuestra participación en el proyecto europeo MIMAX, que ha desarrollado un prototipo con la nueva arquitectura propuesta. A partir del estándar IEEE 802.11a, se ha diseñado el procesador banda base que permite al prototipo MIMAX hacer uso de las nuevas funcionalidades. Especial mención merece el bloque de cálculo de pesos, que se ha diseñado a partir de uno de los algoritmos propuestos en la primera parte. El nuevo procesador banda base se ha implementado y testado tanto en solitario, como junto con otros componentes de la capa física de MIMAX. Se ha demostrado tanto el correcto funcionamiento del procesador banda base como la sustancial mejora de prestaciones del sistema MIMAX con respecto al SISO gracias a una mejora en la cobertura, fiabilidad y tasa de transmisión.



# Notation and Acronyms

## Used Notation

$a$	Scalar (lowercase)
$a^*$	Complex conjugate of $a$
$\mathbf{a}$	Column vector (lowercase boldface)
$a_i$	$i$ -th component of vector $\mathbf{a}$
$\ \mathbf{a}\ $	Euclidean norm of a vector, $\ \mathbf{a}\  = (\sum_i a_i^2)^{1/2}$
$\hat{\mathbf{a}}$	Estimate of $\mathbf{a}$
$E[\mathbf{x}]$	Mathematical expectation of a random vector $\mathbf{x}$
$\mathbf{A}$	Matrix (uppercase boldface)
$A_{i,j}$	Element $(i,j)$ of matrix $\mathbf{A}$
$\ \mathbf{A}\ $	Frobenius Norm of $\mathbf{A}$ , $\ \mathbf{A}\  = (\sum_i \sum_j A_{ij}^2)^{1/2}$
$\mathbf{A}^T$	Transpose
$\mathbf{A}^H$	Hermitian
$\mathbf{A}^+$	Moore-Penrose pseudo-inverse of $\mathbf{A}$ , i.e., $\mathbf{A}^+ = (\mathbf{A}^T \mathbf{A})^{-1} \mathbf{A}^T$
$\text{Tr}(\mathbf{A})$	Trace of matrix $\mathbf{A}$
$\text{rank}(\mathbf{A})$	Rank of matrix $\mathbf{A}$
$\text{vec}(\mathbf{A})$	Column-wise vectorized version of matrix $\mathbf{A}$
$\det(\mathbf{A})$	Determinant of matrix $\mathbf{A}$
$\text{diag}(\mathbf{a})$	Diagonal matrix defined by vector $\mathbf{a}$
$\mathbf{I}$	Identity matrix

## Acronyms

3GPP	3rd Generation Partnership Project
ADC	Analog-to-Digital Converter
AFE	Analog Front-End
AGC	Automatic Gain Control
ASC	Antenna Selection Combining
ASIC	Application-Specific Integrated Circuit
BB	Baseband
BDM	Beam-Division Multiplexing
BER	Bit Error Rate
BLAST	Bell Laboratories Layered Space-Time Architecture

BPF	Bandpass Filter
BPSK	Binary Phase Shift Keying
C2C	Car-to-Car Communication
CCA	Clear Channel Assessment
CDI	Channel Distribution Information
CDIR	Channel Distribution Information at the Receiver
CDIT	Channel Distribution Information at the Transmitter
CMOS	Complementary Metal-Oxide Semiconductor (transistor type)
COFDM	Coded Orthogonal Frequency-Division Multiplexing
CORDIC	Coordinate Rotation Digital Compute
CP	Cyclic Prefix
CQI	Channel Quality Indicator
CRC	Cyclic Redundancy Code
CSI	Channel State Information
CSIR	Channel State Information at the Receiver
CSIT	Channel State Information at the Transmitter
CTS	Clear To Send
DAC	Digital-to-Analog Converter
DCF	Distributed Coordination Function
DET	Dominant Eigenmode Transmission
DFT	Discrete Fourier Transform
DIP	Dual In-Line Packet (switch)
DSP	Digital Signal Processor
DSSS	Direct Sequence Spread Spectrum
DVB	Digital Video Broadcasting
EGC	Equal-Gain Combining
EPP	Enhanced Parallel Port
EU	European Union
EV	Eigenvalue
FDM	Frequency-Division Multiplex
FER	Frame Error Rate
FFT	Fast Fourier Transform
FHSS	Frequency Hopping Spread Spectrum
FIFO	First In, First Out
FPGA	Field-Programmable Gate Array
GUI	Graphical User Interface
HD	High Definition
HDL	High-level Design Language
IC	Integrated Circuit
IDFT	Inverse Discrete Fourier Transform
IEEE	Institute of Electrical and Electronics Engineers
IP	Intellectual Property
IPTV	Internet Protocol Television
ICI	Inter-Carrier Interference
ISI	Inter-Symbol Interference

---

ISM	Industrial, Scientific and Medical (radio spectrum)
JTAG	Joint Test Action Group (port)
LAN	Local Area Network
LED	Light Emitting Device
LMMSE	Linear Minimum Mean Squared Error
LNA	Low Noise Amplifier
LS	Least Squares
LSB	Less Significant Bit
LTE	Long Term Evolution (3GPP 4G technology)
LUT	Lookup Table
MAC	Media Access Control
MIMAX	Advanced MIMO Systems for MAXimum Reliability and Performance
MIMO	Multiple-Input Multiple-Output
MIPP	MIMAX Parallel Port
MISO	Multiple-Input Single-Output
ML	Maximum Likelihood
MMSE	Minimum Mean Square Error
MRC	Maximum-Ratio Combining
MRT	Maximum-Ratio Transmission
MSB	Most Significant Bit
MSE	Mean Square Error
NP	Nondeterministic Polynomial Time
OBDM	Orthogonal Beam-Division Multipleing
OFDM	Orthogonal Frequency-Division Multiplexing
PA	Power Amplifier
PC	Personal Computer
PCMCIA	Personal Computer Memory Card International Association
PDF	Probability Density Function
PDP	Power Delay Profile
PEP	Pairwise Error Probability
PER	Packet Error Rate
PHY	Physical Layer
PLL	Phase-Locked Loop
PM	Power Method
PROM	Programmable Read-Only Memory
PSD	Power Spectral Density
QAM	Quadrature Amplitude Modulation
QPSK	Quadrature Phase-Shift Keying
RAM	Random-Access Memory
RF	Radio-Frequency
RFCU	Radio-Frequency Control Unit
RFID	Radio-Frequency Identification
RMS	Root-Mean-Square
RSSI	Received Signal Strength Indicator
RTS	Request To Send
RX	Receiver

RXBF	Receive Beamforming
SDR	Semidefinite Relaxation
SER	Symbol Error Rate
SIMO	Single-Input Multiple-Output
SISO	Single-Input Single-Output
SLS	Scaled Least Squares
SMA	Sub-Miniature A Connector
SNR	Signal-to-Noise Ratio
SP	Serial Port
STBC	Space-Time Block Code
SVD	Singular Value Decomposition
SVGA	Super Video Graphics Array
TDD	Time-Division Duplex
TX	Transmitter
TXBF	Transmit Beamforming
USB	Universal Serial Bus
VGA	Variable Gain Amplifier
VHDL	Very High-level Design Language
VM	Vector Modulator
WLAN	Wireless Local Area Network
XST	Xilinx Synthesis Tool
ZMCSCG	Zero-Mean Circularly Symmetric Complex Gaussian

# Contents

<b>Acknowledgements</b>	<b>vii</b>
<b>Abstract</b>	<b>ix</b>
<b>Resumen y Conclusiones (Spanish Summary)</b>	<b>xi</b>
<b>Notation and Acronyms</b>	<b>xvii</b>
<b>Contents</b>	<b>xxiv</b>
<b>1 Introduction</b>	<b>1</b>
1.1 Goal of the Thesis . . . . .	1
1.2 Outline and Contributions . . . . .	2
<b>2 Review of MIMO Wireless Communications Systems</b>	<b>9</b>
2.1 Introduction . . . . .	9
2.2 Advantages of MIMO Systems . . . . .	10
2.2.1 Spatial Diversity Gain . . . . .	10
2.2.2 Multiplexing Gain . . . . .	10
2.2.3 Array Gain . . . . .	10
2.2.4 Coding Gain . . . . .	11
2.2.5 Fundamental Tradeoffs . . . . .	12
2.3 Design of MIMO Transceiver . . . . .	13
2.3.1 Channel Known at the Transmitter . . . . .	13
2.3.2 Channel Unknown at the Transmitter . . . . .	14
2.3.3 Multi-Carrier Transmissions: Orthogonal Frequency-Division Multiplexing Schemes . . . . .	14
2.4 Drawbacks of MIMO Systems . . . . .	16
2.4.1 Existing MIMO Combining Schemes and Algorithms . . . . .	17
2.5 A Novel Analog Antenna Combining System: MIMAX Project . . . . .	19
2.5.1 Transmission Schemes for MIMAX . . . . .	21
2.5.2 Channel Estimation . . . . .	23
2.5.3 MIMAX Capabilities . . . . .	23
2.5.4 MIMAX Consortium . . . . .	25
2.6 Conclusions . . . . .	27
<b>I Design of the Transmit and Receive Beamformers</b>	<b>29</b>
<b>3 Perfect Channel Knowledge at the Transmitter Side</b>	<b>31</b>
3.1 Introduction . . . . .	31
3.1.1 Previous Work . . . . .	32
3.2 Preliminaries . . . . .	33
3.2.1 Main Assumptions . . . . .	33
3.2.2 System Model . . . . .	33

3.2.3	LMMSE Receiver . . . . .	34
3.2.4	Problem Statement . . . . .	34
3.3	General Analog Beamforming Criterion . . . . .	34
3.3.1	Particular Cases . . . . .	35
3.3.2	Main Properties . . . . .	36
3.4	Optimization Problem and Proposed Algorithm . . . . .	39
3.4.1	Optimization Problem . . . . .	39
3.4.2	Analysis of the Cost Function Minima . . . . .	40
3.4.3	Approximated Solution based on Semidefinite Relaxation . . . . .	42
3.4.4	Proposed Beamforming Algorithm . . . . .	42
3.5	Simulation Results . . . . .	44
3.5.1	Equivalent Channel Properties . . . . .	44
3.5.2	Uncoded Transmissions . . . . .	46
3.5.3	Coded Transmissions . . . . .	49
3.5.4	Effects of RF Impairments and Channel Estimation Errors . . . . .	50
3.6	Conclusions . . . . .	51
<b>4</b>	<b>Statistical Channel Knowledge at the Transmitter Side</b>	<b>53</b>
4.1	Introduction . . . . .	53
4.2	Preliminaries . . . . .	54
4.2.1	Problem Statement . . . . .	54
4.2.2	General System Model . . . . .	54
4.3	General Analog Beamforming Criterion with Statistical CSIT and Perfect CSIR . . . . .	56
4.3.1	Design of the Frequency and Time Precoders . . . . .	56
4.3.2	Design of the Beamformers . . . . .	57
4.3.3	Further Discussion . . . . .	61
4.4	Simulation Results . . . . .	62
4.4.1	Studied Schemes . . . . .	62
4.4.2	Experiments . . . . .	63
4.5	Conclusions . . . . .	67
<b>II</b>	<b>New MIMAX Baseband: Design, Implementation, Integration, and Real-Time Testing</b>	<b>69</b>
<b>5</b>	<b>MIMAX Concept and Baseband Processor</b>	<b>71</b>
5.1	Introduction . . . . .	71
5.2	MIMAX Project . . . . .	72
5.2.1	MIMAX Concept . . . . .	72
5.2.2	MIMAX Demonstrator . . . . .	72
5.2.3	Focusing on WLAN: IEEE 802.11a Standard . . . . .	74
5.2.4	MIMAX Compatibility with Legacy 802.11a Devices . . . . .	75
5.3	Baseband Processor . . . . .	75
5.3.1	802.11a PHY Layer: A Technical Overview . . . . .	76
5.3.2	Types of Frames . . . . .	77
5.3.3	Required Baseband Processor Changes . . . . .	78
5.3.4	New MIMAX Baseband Blocks . . . . .	79
5.3.5	New MIMAX Blocks Interfaces . . . . .	81
5.4	Channel Estimation in MIMAX . . . . .	82
5.4.1	Channel Estimation Procedure and Frames . . . . .	83
5.4.2	Beamformers for Channel Estimation . . . . .	84
5.4.3	Channel Estimation Algorithms . . . . .	85
5.4.4	Simulation Results for 802.11a Transmissions . . . . .	90
5.5	Conclusions . . . . .	92

<b>6</b>	<b>FPGA Design of the New MIMAX Blocks</b>	<b>93</b>
6.1	Introduction . . . . .	93
6.2	Tools . . . . .	94
6.2.1	MATLAB and Simulink . . . . .	94
6.2.2	System Generator for DSP . . . . .	95
6.2.3	ModelSim . . . . .	95
6.2.4	Xilinx ISE Foundation . . . . .	95
6.2.5	Chipscope Pro . . . . .	96
6.2.6	AccelDSP . . . . .	96
6.3	Design Procedure . . . . .	96
6.3.1	MATLAB Floating-Point Model . . . . .	96
6.3.2	MATLAB Fixed-Point Model . . . . .	97
6.3.3	System Generator Model . . . . .	97
6.4	MIMAX Channel Estimation Block . . . . .	99
6.5	Frequency Offset Estimation Block . . . . .	100
6.6	Weights Correction Block . . . . .	101
6.7	MIMAX RF Weights Block (Transmit-Receive Beamforming Block) . . . . .	102
6.7.1	Criterion, Algorithm, and Pseudocode . . . . .	102
6.7.2	Design and Architecture . . . . .	105
6.7.3	Design Decisions . . . . .	110
6.8	Reconfigurability . . . . .	112
6.9	Conclusions . . . . .	113
<b>7</b>	<b>Simulation, Generation, and Integration</b>	<b>115</b>
7.1	Introduction . . . . .	115
7.2	Simulation of the New MIMAX Baseband Blocks . . . . .	115
7.2.1	System Generator Simulation . . . . .	115
7.2.2	ModelSim Simulation . . . . .	123
7.3	Generation Process . . . . .	125
7.3.1	Target FPGA . . . . .	128
7.3.2	First Generation Results . . . . .	128
7.3.3	New Baseband Blocks Frequency Clock . . . . .	128
7.4	FPGA Integration . . . . .	129
7.4.1	First Integration Tests . . . . .	129
7.4.2	Integration of the New MIMAX Blocks within the Legacy 802.11a Baseband Processor . . . . .	130
7.5	Conclusions . . . . .	132
<b>8</b>	<b>Real-Time Testing</b>	<b>133</b>
8.1	Introduction . . . . .	133
8.2	MIMAX Baseband Board . . . . .	133
8.3	MAC Emulator . . . . .	137
8.4	First Real-Time Testing of the MIMAX Blocks . . . . .	138
8.4.1	Setup . . . . .	138
8.4.2	Preliminary Basic Tests . . . . .	139
8.4.3	Basic Transmission and Reception Tests . . . . .	140
8.4.4	Reception of Training Frames . . . . .	140
8.5	Physical Layer Tests in MIMAX . . . . .	146
8.5.1	MIMAX Analog Front-End . . . . .	146
8.5.2	MIMAX Antenna Array . . . . .	147
8.5.3	Setup . . . . .	148
8.5.4	Figures of Merit and Testing Procedure . . . . .	149
8.5.5	Experiments . . . . .	150
8.5.6	Conclusion of the Physical Layer Tests . . . . .	151

8.6	User-Level Tests in MIMAX . . . . .	152
8.7	Conclusions . . . . .	152
<b>III</b>	<b>Conclusions and Future Directions</b>	<b>155</b>
<b>9</b>	<b>Conclusion and Future Directions</b>	<b>157</b>
9.1	Conclusions . . . . .	157
9.1.1	Part I: Design of the Transmit and Receive Beamformers . . . . .	157
9.1.2	Part II: New MIMAX Baseband . . . . .	158
9.2	Future Directions . . . . .	158
9.2.1	Theoretical Work . . . . .	158
9.2.2	Practical Work . . . . .	159
<b>A</b>	<b>Rewriting and Analyzing the Beamforming Function</b>	<b>161</b>
A.1	Rewriting the Cost Function . . . . .	161
A.2	Analysis of the Penalty Term . . . . .	161
A.2.1	Antisymmetry . . . . .	161
A.2.2	Monotonicity . . . . .	162
A.2.3	Schur-Convexity of $g_{\alpha,\beta}(\mathbf{p}_\beta)$ . . . . .	162
<b>B</b>	<b>Publications</b>	<b>163</b>
B.1	Book Chapter . . . . .	163
B.2	International Journals . . . . .	163
B.3	International Conferences . . . . .	163
	<b>List of Figures</b>	<b>168</b>
	<b>List of Tables</b>	<b>169</b>
	<b>List of Algorithms</b>	<b>171</b>
	<b>Bibliography</b>	<b>173</b>

# Chapter 1

## Introduction

### 1.1 Goal of the Thesis

Wireless communications allow services that are impossible or troublesome within traditional wired communications. The wireless communication systems field has undergone remarkable growth since the early 1990's, mostly due to the large increase of the use of mobile electronic devices that require communication and particularly internet access, such as handheld devices and laptops. Accordingly, the importance of the development of reliable and efficient wireless communications has also raised in parallel. Traditional wireless communication systems have a single antenna for transmission and a single antenna for reception. These systems, known as single-input single-output (SISO) systems, have a limited performance and data throughput. Since the pioneering work of Winters [Winters, 1987], Foschini [Foschini, 1996], Foschini and Gans [Foschini and Gans, 1998], and Telatar [Telatar, 1999], the spectral efficiencies for wireless systems with multiple transmit and receive antennas have remarkably improved. These systems that use several antennas at the transmitter and the receiver to achieve better performance, also called multiple-input multiple-output (MIMO) systems, significantly exceed the performance of SISO systems. The use of multiple antennas at wireless access points and mobile terminals offers an extra spatial dimension, which can be exploited to improve reliability (diversity), transmission rate (multiplexing), and coverage (array and coding gains) [Barbarossa, 2005]. Recent theoretical and technological progress has enabled the introduction of MIMO systems and concepts in current and future wireless communication systems, such as 802.11n [IEEE Standard 802.11n, 2007], WiMAX [Mobile WiMAX, 2006, Andrews et al., 2007], or 3GPP-LTE [E. Dahlman and Bemming, 2007].

Nevertheless, the performance enhancements obtained through MIMO techniques have certain associated drawbacks in comparison with SISO systems. Traditional MIMO transceivers require an RF branch as well as independent multidimensional signal processing in each baseband path [Goldsmith, 2005]. Therefore, the exploitation of all the MIMO benefits generate at each station an extra cost, size, and power consumption in comparison with SISO systems. The added cost of deploying multiple antennas, the space and circuit power requirements of these extra antennas (especially in small handheld units), and the added complexity required at the baseband processor are in part responsible for the delay in the commercial deployment of MIMO wireless transceivers, primarily in handsets or small cost terminals.

The combining schemes mitigate several of the drawbacks of the full MIMO systems while keeping certain advantages. Compared to antenna selection systems, where the antenna paths are selected and switched, or phased arrays, where only the phase can be adjusted,

in combining schemes, both the phases and amplitudes of the different branches are set. In the state-of-the-art combining approaches, this complex weighting is performed in the baseband. The combining schemes at the baseband have the advantage of a simple design using commercial off-the-shelf components. Although the baseband combining schemes have a single baseband path, they maintain multiple RF branches (i.e., multiple up/down converters), which still suppose an extra cost, size, and consumption. To decrease these parameters, the analog antenna combining schemes have been proposed. The combination is performed at the RF domain, thus, a single RF branch and baseband path is needed.

Considering the novel analog antenna combining scheme, the first goal of this thesis consists in the design of the transmit and receive RF weights under orthogonal frequency-division multiplexing (OFDM) transmissions for different channel knowledge cases. In particular, for the case of channel state information (CSI) at the transmitter and the receiver side (CSIT+CSIR), a general beamforming criterion is proposed, which depending on a single parameter, establishes a tradeoff between the energy of the equivalent SISO channel (after transmit-receive beamforming) and its spectral flatness. With the general criterion, by means of a gradient search algorithm, the calculation of the RF weights is proposed. The case with perfect CSI at the receiver but only statistical information at the transmitter is also studied. In particular, a new scheme, which spreads the information over the time using different pairs of beamformers, is proposed. For this case, the time and frequency precoders as well as the optimal transmit and receive beamformers are designed. The performance of these systems are compared by means of several simulations with the full MIMO and SISO performances.

As a second main goal, in the context of the European Union funded project MIMAX, an FPGA-synthesizable baseband processor for the analog antenna combining architecture is designed, implemented, and tested in real-time. This work is part of the practical development of a MIMO wireless transceiver that performs analog antenna combining (the so-called MIMAX transceiver). Starting from the baseband processor of the widely used IEEE 802.11a standard, we implement new baseband modules in order to allow the new functionalities of the MIMAX transceiver. These modules are for instance a MIMO channel estimator and a RF weights calculation block. The latter is the main challenge within the baseband processor development, and it performs one of the algorithms proposed in the first part of the thesis. Particularly, the RF weights calculation block provides the weights maximizing the received signal-to-noise ratio (SNR) under perfect channel knowledge at both sides. All the baseband modules are successfully integrated within the legacy IEEE 802.11a baseband processor, and they are tested in real-time within a baseband board manufactured by one of the project partners. Moreover, some tests of the MIMAX transceiver are carried out in order to show, in a real environment and in real-time, the advantages of the MIMAX transceiver with respect to the SISO one in terms of coverage, received SNR, and data throughput.

## 1.2 Outline and Contributions

This work starts with Chapter 2, where the MIMO wireless communications systems are introduced. We review the main benefits and drawbacks of traditional MIMO architectures. Alternatively, a novel MIMO architecture based on analog antenna combining is presented. This alternative, proposed in the EU funded MIMAX project within the 7<sup>th</sup> Framework Programme, maintains some of the MIMO benefits mitigating the most important drawbacks, such as cost and power consumption. This architecture represents the core of this thesis and

is used along the entire work, both in this first theoretical part and also in the second part addressing application.

The first part of this thesis presents a theoretical design of the transmit and receive beamformers in an analog antenna combining architecture. Several criteria and associated algorithms are proposed under different assumptions on the channel state information.

- In Chapter 3, we analyze the problem of selecting transmit and receive beamformers under OFDM transmissions with perfect channel state information at the receiver side and the transmitter side (CSIT+CSIR). Specifically, a general beamforming criterion is proposed, which, depending on a single parameter  $\alpha$ , can optimize different figures of merit of the equivalent SISO channel (after beamforming), such as the signal-to-noise ratio (SNR), the mean square error (MSE), or the capacity. Although the problem is non-convex and has no closed-form solution, we propose a suboptimal gradient search algorithm that provides very accurate results in practical cases.

The publications that have contributed to this chapter are the following:

- I. Santamaría, J. Vía, V. Elvira, J. Ibáñez, J. Pérez, R. Eickhoff, and U. Mayer. *Handbook of Smart Antennas for RFID Systems*, chapter Low cost and compact RF-MIMO transceivers. Wiley, 2009.
- J. Vía, I. Santamaría, V. Elvira, and R. Eickhoff. "A general criterion for analog Tx-Rx beamforming under OFDM transmissions". *IEEE Transactions on Signal Processing*, volume 58, no. 4, pages 2155-2167, 2010.
- J. Vía, V. Elvira, I. Santamaría, and R. Eickhoff. "Minimum BER beamforming in the RF domain for OFDM transmissions and linear receivers". In *IEEE International Conference on Acoustics, Speech, and Signal Processing (ICASSP 2009)*. Taipei, Taiwan, 2009.
- J. Vía, V. Elvira, I. Santamaría, and R. Eickhoff. "Analog antenna combining for maximum capacity under OFDM transmissions". In *IEEE International Conference on Communications (ICC 2009)*. Dresden, Germany, 2009.
- J. Vía, I. Santamaría, V. Elvira, J. Ibáñez, and R. Eickhoff. "OFDM system with pre-FFT processing for MIMO systems". In *FP7 Workshop on Advanced MIMO and Cooperative Communications*. Brussels, Belgium. 2009.
- J. Vía, I. Santamaría, V. Elvira, and R. Eickhoff. "A general pre-FFT criterion for MIMO-OFDM beamforming". In *IEEE International Conference on Communications (ICC 2010)*. Cape Town, South Africa. 2010.
- The counterpart of the problem presented in Chapter 3 is addressed in Chapter 4, which considers the case with perfect channel state information at the receiver side, but only statistical channel state information at the transmitter (CDIT+CSIR). In particular, we propose a new scheme, called beam-division multiplexing (BDM), where the information is spread among the OFDM subcarriers but also among different OFDM symbols transmitted under a different pair of transmit-receive beamformers. In this case, we design the frequency and time precoders as well as the optimal transmit and receive beamformers. Particularly, each of the optimal precoding matrices results in any unitary matrix with constant modulus elements, such as the DFT matrix. The selection of the transmit beamformers represents a new challenge; since transmit correlation is known at the transmitter, the design of the transmit beamformers is calculated with

power waterfilling, transmitting along the strongest modes of this transmit correlation matrix. The strongest modes are mixed with a DFT matrix in order to maintain constant energy at the transmitter and, as a result, a set of transmit beamformers is obtained. The design of the receive beamformers is performed as in the previous chapter.

The publications that have contributed to this chapter are the following:<sup>1</sup>

- I. Santamaría, J. Vía, V. Elvira, J. Ibáñez, J. Pérez, R. Eickhoff, and U. Mayer. *Handbook of Smart Antennas for RFID Systems*, chapter Low cost and compact RF-MIMO transceivers. Wiley, 2009.
- V. Elvira and J. Vía. "Analog antenna combining in transmit correlated channels: Transceiver design and performance evaluation". *Submitted to Signal Processing (Second Review)*. 2011.
- I. Santamaría, V. Elvira, J. Vía, D. Ramírez, J. Pérez, J. Ibáñez, R. Eickhoff, and F. Ellinger. "Optimal MIMO transmission schemes with adaptive antenna combining in the RF path". In *16th European Signal Processing Conference (EUSIPCO 2008)*. Lausanne, Switzerland, 2008.
- J. Vía, V. Elvira, J. Ibáñez, and I. Santamaría. "Optimal precoding for a novel RF-MIMO scheme in transmit correlated rayleigh channels". In *IEEE Workshop on Signal Processing Advances in Wireless Communications (SPAWC 2009)*. Perugia, Italy, 2009.
- V. Elvira and J. Vía, "Diversity techniques for analog combining schemes: design and performance evaluation". In *Proceedings of the 17th European Signal Processing Conference (EUSIPCO 2009)*. Glasgow, Scotland. 2009.
- J. Vía, I. Santamaría, V. Elvira, J. Ibáñez, and R. Eickhoff. "OFDM system with pre-FFT processing for MIMO systems". In *FP7 Workshop on Advanced MIMO and Cooperative Communications*. Brussels, Belgium. 2009.

The second part of the thesis takes place within the context of the prototype development of an analog antenna combining wireless transceiver. In particular, this part addresses the design and implementation of the required changes on a legacy baseband processor to allow the features provided by the new architecture.

- In Chapter 5, we present the European Union funded MIMAX project, which aims to investigate and develop a more powerful WLAN transceiver with an analog antenna combining architecture, which is also compatible with the IEEE 802.11a standard at 5 GHz (therefore, based on OFDM). We focus on the baseband processor, where our contribution will take place. After reviewing the legacy IEEE 802.11a PHY layer, we recommend some changes on it. Since this standard only considers SISO architecture, we also propose the addition of some new baseband modules (from now on, the new MIMAX baseband blocks), such as a block for the estimation of the MIMO channel, and a RF Weights Block, which, based on the algorithms studied in the first part, must compute the transmit and receive beamformers.

The publications that have contributed to this chapter are the following:

---

<sup>1</sup>Note that certain publications have made significant contributions to several chapters.

- R. Eickhoff, U. Mayer, M. Wickert, F. Ellinger, I. Santamaría, V. Elvira, J. Ibañez, and J. Vía. "Fully integrated MIMO transceiver with pre-FFT processing for 802.11a". In *FP7 Workshop on Advanced MIMO and Cooperative Communications*. Brussels, Belgium. 2009.
  - R. Kraemer, Z. Stamenkovic, K. Tittelbach-Helmrich, L. González, S. Ruiz, O. Gago, J. Ibañez, V. Elvira, M. Wickert, and R. Eickhoff. "RF-MIMO WLAN modem demonstrator". In *25th Wireless World Research Forum WWRF Meeting*. London, UK. 2010.
  - Z. Stamenkovic, K. Tittelbach-Helmrich, M. Krstic, J. Ibañez, V. Elvira, and I. Santamaría. "Mac and baseband hardware platforms for RF-MIMO WLAN". In *Proceedings of the 5th European Conference on Circuits and Systems for Communications*. Belgrade, Serbia. 2010.
  - V. Elvira, J. Ibañez, I. Santamaria, M. Krstic, K. Tittelbach-Helmrich, and Z. Stamenkovic. "Baseband processor for RF-MIMO WLAN". In *17th IEEE International Conference on Electronics, Circuits, and Systems (ICECS 2010)*. Athens, Greece. 2010.
  - R. Eickhoff, K. Tittelbach-Helmrich, M. Wickert, J. Wagner, U. Mayer, V. Elvira, and J. Ibañez. "Physical layer amendments for MIMO features in 802.11a". In *Proceedings of the Future Network and MobileSummit*. Warsaw, Poland. 2011.
- In Chapter 6, we describe the design procedure of the new MIMAX baseband blocks that must be included within the legacy IEEE 802.11a baseband processor. The second part of this thesis aims to obtain an FPGA version of the MIMAX baseband processor, and the main contribution of this chapter consists in the design of the new MIMAX block for this baseband processor. To achieve this goal, we generate a fixed-point model of each different MIMAX block that must be designed. We make use of the System Generator tool for the design/implementation process of all the new MIMAX baseband blocks. Because of the nature of this tool, the design and implementation decisions are interrelated, and the blocks designs can be directly synthesized to be downloaded onto an FPGA. The main achievement is an amenable fixed-point FPGA version of the beamforming calculation algorithms proposed in the first part.

The publications that have contributed to this chapter are:

- R. Kraemer, Z. Stamenkovic, K. Tittelbach-Helmrich, L. González, S. Ruiz, O. Gago, J. Ibañez, V. Elvira, M. Wickert, and R. Eickhoff. "RF-MIMO WLAN modem demonstrator". In *25th Wireless World Research Forum WWRF Meeting*. London, UK. 2010.
- Z. Stamenkovic, K. Tittelbach-Helmrich, M. Krstic, J. Ibañez, V. Elvira, and I. Santamaría. "Mac and baseband hardware platforms for RF-MIMO WLAN". In *Proceedings of the 5th European Conference on Circuits and Systems for Communications*. Belgrade, Serbia. 2010.
- V. Elvira, J. Ibañez, I. Santamaria, M. Krstic, K. Tittelbach-Helmrich, and Z. Stamenkovic. "Baseband processor for RF-MIMO WLAN". In *17th IEEE International Conference on Electronics, Circuits, and Systems (ICECS 2010)*. Athens, Greece. 2010.
- R. Eickhoff, K. Tittelbach-Helmrich, M. Wickert, J. Wagner, U. Mayer, V. Elvira, and J. Ibañez. "Physical layer amendments for MIMO features in 802.11a". In *Proceedings of the Future Network and MobileSummit*. Warsaw, Poland. 2011.

- In Chapter 7, some different campaigns of simulations are proposed and conducted with System Generator and also with ModelSim in order to test the correct behavior of the new MIMAX baseband blocks, both in a stand-alone way or within an entire baseband processor configuration. Once the blocks are validated in simulation, we generate the netlist files of the MIMAX entity, which comprises all the new MIMAX baseband blocks. This generation is required for integrating the MIMAX entity within the IEEE 802.11a baseband processor in a single MIMAX baseband processor project. This process is finished with the generation of a .bit file that configures the FPGA of the baseband board as seen in Chapter 8. Therefore, the main contribution of this chapter consists in the validation of the new MIMAX blocks by means of simulations, as well as the NGC generation and integration of these blocks within an existing project of the legacy 802.11a baseband processor in order to obtain the MIMAX baseband processor.

The publications that have contributed to this chapter are the following:

- R. Kraemer, Z. Stamenkovic, K. Tittelbach-Helmrich, L. González, S. Ruiz, O. Gago, J. Ibañez, V. Elvira, M. Wickert, and R. Eickhoff. "RF-MIMO WLAN modem demonstrator". In *25th Wireless World Research Forum WWRF Meeting*. London, UK. 2010.
  - Z. Stamenkovic, K. Tittelbach-Helmrich, M. Krstic, J. Ibañez, V. Elvira, and I. Santamaría. "Mac and baseband hardware platforms for RF-MIMO WLAN". In *Proceedings of the 5th European Conference on Circuits and Systems for Communications*. Belgrade, Serbia. 2010.
  - V. Elvira, J. Ibañez, I. Santamaria, M. Krstic, K. Tittelbach-Helmrich, and Z. Stamenkovic. "Baseband processor for RF-MIMO WLAN". In *17th IEEE International Conference on Electronics, Circuits, and Systems (ICECS 2010)*. Athens, Greece. 2010.
  - R. Eickhoff, K. Tittelbach-Helmrich, M. Wickert, J. Wagner, U. Mayer, V. Elvira, and J. Ibañez. "Physical layer amendments for MIMO features in 802.11a". In *Proceedings of the Future Network and MobileSummit*. Warsaw, Poland. 2011.
- The real-time testing of the new MIMAX baseband blocks within the baseband processor in FPGA is addressed in Chapter 8. We present the different parts of the MIMAX transceiver, developed by the partners of the MIMAX project, focusing on the baseband board where the baseband processor is placed. We describe different setups and scenarios where the new MIMAX blocks can be tested in real-time. The first campaign is devoted to test the blocks in a stand-alone setup within the MIMAX baseband processor. A more general setup is also described where the baseband processor, analog front-end, and antenna array are jointly tested. In this chapter, we finally present some experiments of the whole physical layer where the benefits of the MIMAX architecture with respect to the SISO system are shown in a prototype. In these experiments, a block of frames is sent with some random weights (equivalent to a SISO channel) and another block is sent under the optimal weights. This process is repeated a number of times sufficiently large for obtaining for both systems (SISO and MIMAX) some figures of merit, such as the frame error rate (FER) or the RSSI level after combination (SNR improvement). The role of the new MIMAX baseband blocks is one of the most critical challenges within the development of the MIMAX prototype, and this chapter validates the work carried out throughout the second part of the thesis.

The publications that have contributed to this chapter are the following:

- R. Kraemer, Z. Stamenkovic, K. Tittelbach-Helmrich, L. González, S. Ruiz, O. Gago, J. Ibañez, V. Elvira, M. Wickert, and R. Eickhoff. "RF-MIMO WLAN modem demonstrator". In *25th Wireless World Research Forum WWRF Meeting*. London, UK. 2010.
- Z. Stamenkovic, K. Tittelbach-Helmrich, M. Krstic, J. Ibañez, V. Elvira, and I. Santamaría. "Mac and baseband hardware platforms for RF-MIMO WLAN". In *Proceedings of the 5th European Conference on Circuits and Systems for Communications*. Belgrade, Serbia. 2010.
- V. Elvira, J. Ibañez, I. Santamaria, M. Krstic, K. Tittelbach-Helmrich, and Z. Stamenkovic. "Baseband processor for RF-MIMO WLAN". In *17th IEEE International Conference on Electronics, Circuits, and Systems (ICECS 2010)*. Athens, Greece. 2010.
- R. Eickhoff, K. Tittelbach-Helmrich, M. Wickert, J. Wagner, U. Mayer, V. Elvira, and J. Ibañez. "Physical layer amendments for MIMO features in 802.11a". In *Proceedings of the Future Network and Mobile Summit*. Warsaw, Poland. 2011.

In Chapter 9, the main conclusions of this work and the future directions are summarized. Two appendices and some bibliographic references are also included.

The contributions of this thesis are summarized at the end of each corresponding chapter. Additionally, a full listing of the resulting publications is included in Appendix B.



# Review of MIMO Wireless Communications Systems

## 2.1 Introduction

The past decade has witnessed important advances in the physical layer of the wireless communications. Traditional wireless communication systems have a single antenna for transmission and a single antenna for reception. These systems, well known as single-input single-output (SISO) systems, have a limited performance and data throughput. In recent years, significant developments have been made in systems that use several antennas at the transmitter (TX) and the receiver (RX) to achieve better performance. They are called multiple-input multiple-output (MIMO) systems and significantly exceed the performance of SISO systems. Since the pioneering work of Winters [Winters, 1987], Foschini [Foschini, 1996], Foschini and Gans [Foschini and Gans, 1998], and Telatar [Telatar, 1999], the spectral efficiencies for wireless systems with multiple transmit and receive antennas, have remarkably improved.

The use of multiple antennas at wireless access points and mobile terminals offers an extra spatial dimension, which can be exploited to improve reliability (diversity), transmission rate (multiplexing), and coverage (array and coding gains) [Barbarossa, 2005]. Recent theoretical and technological progress has enabled the introduction of MIMO systems and concepts in current and future wireless communication systems, such as 802.11n [IEEE Standard 802.11n, 2007], WiMAX [Mobile WiMAX, 2006, Andrews et al., 2007], or 3GPP-LTE [E. Dahlman and Bemming, 2007].

One of the main drawbacks of the performance enhancements obtained through MIMO techniques is the added cost of deploying multiple antennas, the space and circuit power requirements of these extra antennas (especially on small handheld units), and the added complexity required for multidimensional signal processing [Goldsmith, 2005].

Throughout this introductory chapter, the main benefits and drawbacks of traditional full MIMO architectures are explored. A novel analog combining architecture is proposed with the aim of maintaining some of the MIMO benefits and simultaneously reducing some of the MIMO disadvantages. This analog combining architecture is the core around which this thesis is built.

## 2.2 Advantages of MIMO Systems

In this section, we focus on the main benefits presented by the MIMO systems, which are essentially the spatial diversity gain, the multiplexing gain, and the array gain. The multiplexing-diversity tradeoff concept is also introduced.

### 2.2.1 Spatial Diversity Gain

One of the most obvious advantages obtained by placing multiple antennas at the transmitter and the receiver is that the additional spatial degree of freedom can be used to get supplementary diversity. If the antennas are placed sufficiently far apart, the channel gains between different antenna pairs fade independently, and, thus, independent signal paths are created. The required antenna separation needed to create independent paths depends on the local scattering environment as well as on the carrier frequency. Typically, the more scatterers and reflectors available, the less correlation there will be between the antennas.

The maximum spatial diversity gain of a flat-fading spatially white MIMO channel is equal to the product of the number of transmit and receive antennas. In general, to achieve this diversity, some form of space-time coding is needed as we will see in Subsection 2.2.4. The specific processing needed to extract the spatial diversity also depends on the channel state information (CSI) available at the transmitter or the receiver sides.

As shown in Figure 2.1, the diversity gain can be defined as the asymptotic negative slope of the bit error rate (BER), the symbol error rate (SER), or frame error rate (FER) versus the signal-to-noise ratio (SNR) in a log-log scale [A. Paulraj and Gore, 2003]. For instance, in Figure 2.1 for the case of  $n_T = 4$ , it can be shown that, in the high SNR regime, when the SNR is increased in 10 dB, the SER is decreased by a factor of  $10^{-4}$ , i.e.,

$$G_d = \lim_{\text{SNR} \rightarrow \infty} -\frac{\log_2(P_e)}{\log_2(\text{SNR})}.$$

### 2.2.2 Multiplexing Gain

In the baseband of full MIMO systems, where each antenna branch is demodulated and acquired independently, the capacity can be increased by a factor proportional to the channel rank (for independent and identically distributed (i.i.d.) channels this is the minimum of the number of transmit and receive antennas). This increase is characterized by the multiplexing gain, which is defined as

$$r = \lim_{\text{SNR} \rightarrow \infty} \frac{C_{out,p}}{\log_2(\text{SNR})},$$

where  $C_{out,p}$  is the outage capacity for a probability of outage  $p$ . For burst block-fading transmissions, this definition means that transmitting at a given fixed rate of  $C_{out,p}$  bps,  $p\%$  of the frames would be lost, while the remaining frames will be decoded without error, since, for these frames, we are transmitting at a rate lower than the capacity.

### 2.2.3 Array Gain

The array gain is defined as the increase in average output SNR (at the input of the detector) relative to the single-antenna average SNR. The array gain can be obtained at each side of

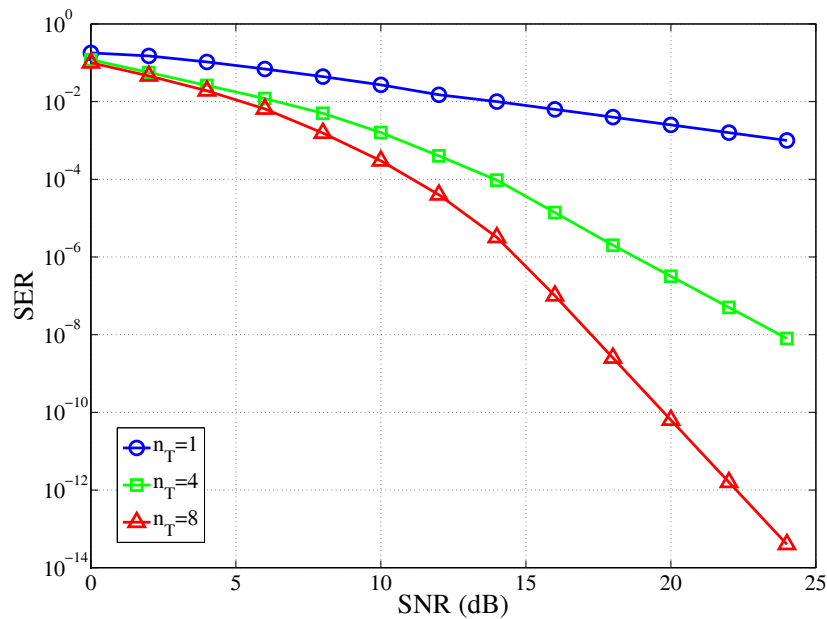


**Figure 2.1:** Effect of diversity on the SER performance in Rayleigh channel.

the link by coherent combination. This means that, under perfect channel state information at the transmitter and receiver (CSIT and CSIR, respectively), the transmit and receive array gains can be achieved, since the transmitted signals are constructively added in-phase at each receive antenna, and the signal at each receive antenna is further constructively combined with each other. However, with CDIT and CSIR, since the channel is unknown at the transmitter, only the receiver array gain can be achieved. It is important to notice that the array gain does not depend on the correlation between antennas, whereas the diversity gain is maximal for independent branches and decreases as the correlation between branches increases.

The effect of the array gain on the SER performance is a displacement of the SER curves, but it has no effect on their slopes [A. Paulraj and Gore, 2003]. Figure 2.2 shows the different effects of the array gain and the spatial diversity gain. It can be seen that the SNR advantage due to the spatial diversity gain increases with the SNR, but it remains constant with the array gain.

#### 2.2.4 Coding Gain

The coding gain is the improvement in terms of SNR between an uncoded system and the same system with a particular coding. This coding is usually performed with space-time block codes, which will be briefly reviewed in Subsection 2.3.1. The nature of the coding gain is similar to the one of the array gain, in the sense that coding gain also shifts the SNR vs SER performance curve to the left in a log-log scale, i.e., both gains obtain a SNR improvement. Figure 2.2 illustrates the effect that the different types of diversity have on the SER.

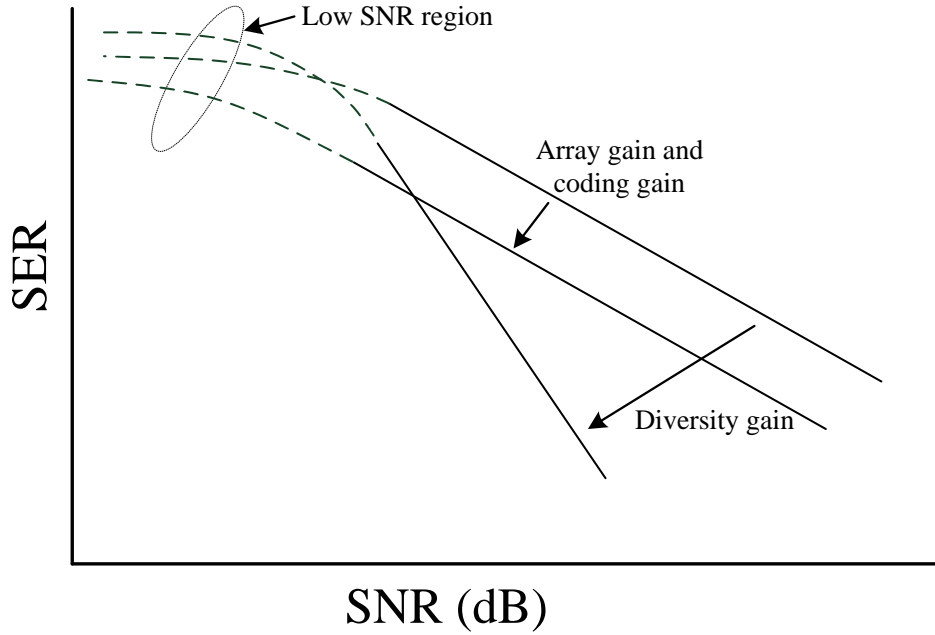


**Figure 2.2:** SER performance depending on the array gain, coding gain, and diversity gain.

### 2.2.5 Fundamental Tradeoffs

In this section, we have seen that, with a higher number of antennas, the throughput system can be enhanced (more transmitted data) and the BER can be reduced (more reliability). The question now is whether both improvements are possible simultaneously.

All MIMO systems have certain tradeoffs, such as the well-known multiplexing-diversity tradeoff [Zheng and Tse, 2003] that basically establishes a compromise between the two most important benefits of MIMO systems: increased rate (multiplexing gain) and increased reliability (spatial diversity gain). This tradeoff can be formally expressed as

$$G_d(r) = (n_T - r)(n_R - r), \quad 0 \leq r \leq \min(n_T, n_R). \quad (2.1)$$

In words, this tradeoff can be interpreted as follows: at each point,  $(r, G_d(r))$  of the piecewise linear curve given by 2.1, for each 3 dB of increase in SNR, it is theoretically possible to decrease the BER by  $2^{-G_d(r)}$ , while at the same time increasing the transmission rate by  $r$  bps/Hz. Accordingly, it is clear that any MIMO scheme that aims at improving the transmission reliability by exploiting all the diversity gain must transmit along a single spatial mode at a fixed rate. Conversely, a MIMO system that exploits all the multiplexing gain and sends information along all the spatial modes (probably with some kind of adaptive modulation scheme), then it will not achieve spatial diversity gain.<sup>1</sup>

Figure 2.3 shows the diversity-multiplexing tradeoff curves for a  $4 \times 4$  MIMO system. It can be seen that by using appropriate coding schemes in a full MIMO scheme, we can work at any point of the piecewise linear frontier depicted in dashed line. Nevertheless, a SISO system is obviously unable to exploit the spatial degrees of freedom of the MIMO channel.

<sup>1</sup>Note that the diversity gain can be also obtained in frequency and in time, and both can be extracted in a MIMO system which transmits along all the spatial modes or even in a SISO system.

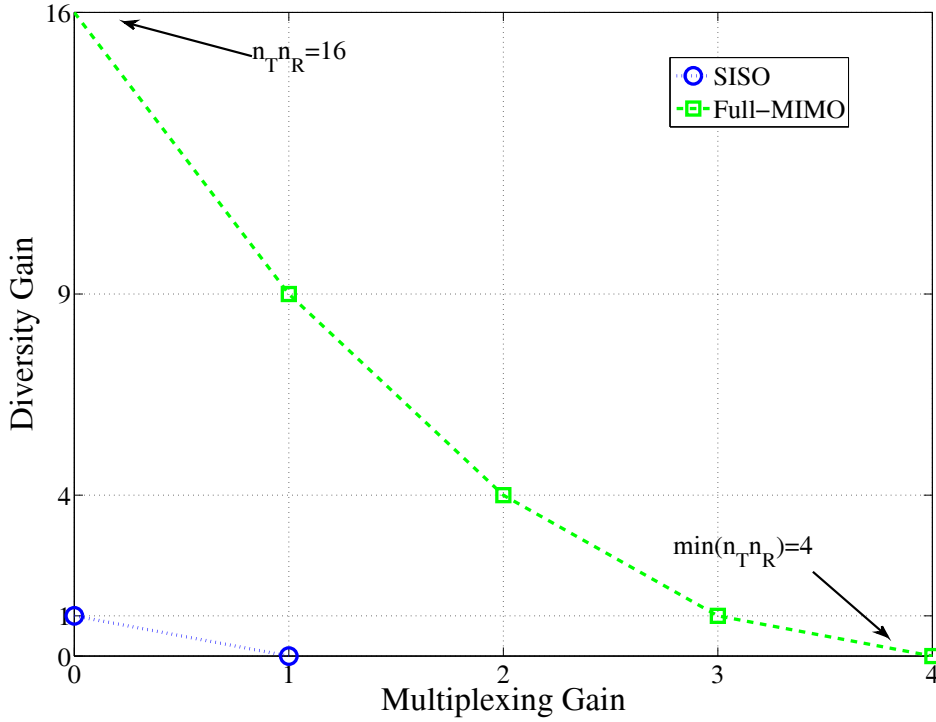


**Figure 2.3:** Achievable diversity-multiplexing curves for a  $4 \times 4$  system with full MIMO and SISO.

## 2.3 Design of MIMO Transceiver

In this section, we briefly review the design of the MIMO transceiver in single-carrier and multi-carrier systems. The channel state information is supposed to be perfect at the receiver, which is very common in practice. In the following two subsections, we start proposing the design for single-carrier schemes under different channel state information at the transmitter. Finally, we introduce the orthogonal frequency-division multiplexing (OFDM) schemes.

### 2.3.1 Channel Known at the Transmitter

Let us consider a system with  $n_T$  transmit antennas and  $n_R$  receive antennas. When the channel is known at the transmitter, the spatial diversity can be extracted through the dominant eigenmode transmission (DET). The same signal is transmitted from all antennas in the transmit array with weights vector  $\mathbf{w}$ . The receive signal vector is then given by

$$\mathbf{y} = \sqrt{\frac{E_s}{n_T}} \mathbf{H} \mathbf{w}_T s + \mathbf{n},$$

where  $\mathbf{y}$  is the  $n_R \times 1$  received signal vector,  $E_s$  is the average transmit symbol energy,  $\mathbf{H}$  is the  $n_R \times n_T$  channel matrix,  $\mathbf{w}_T$  is the  $n_T \times 1$  complex weights vector,  $s$  is the transmitted symbol, and  $\mathbf{n}$  is a  $n_R \times 1$  that represents the spatially white zero-mean circularly symmetric complex Gaussian (ZMCSCG) noise. Let the receiver form a weighted sum of antenna outputs according to  $z = \mathbf{w}_R^H \mathbf{y}$ , where  $\mathbf{w}_R$  is a  $n_R \times 1$  vector of complex weights. If the SVD of the  $\mathbf{H}$  matrix is given by  $\mathbf{H} = \mathbf{U} \mathbf{\Sigma} \mathbf{V}^H$ , it can be verified that the SNR at the receiver is maximized

when  $\mathbf{w}_T$  and  $\mathbf{w}_R$  are the singular vectors, corresponding to the maximum singular value  $\sigma_{\max}$  of  $\mathbf{H}$  [A. Paulraj and Gore, 2003].

### 2.3.2 Channel Unknown at the Transmitter

When the channel is not known at the transmitter, it is still possible to obtain spatial diversity by using specific transmission codes. Particularly, the space-time block coding (STBC) is a technique which allows the transmission of multiple copies of a data stream across a number of antennas in order to exploit the various received versions of the data to improve the reliability of data-transfer. As an example, we briefly describe the simplest STBCs: the Alamouti scheme [Alamouti, 1998].

Let us consider a  $2 \times 1$  multiple-input single-output (MISO) system,<sup>2</sup> where the channel vector is

$$\mathbf{h} = [h_1 \quad h_2].$$

The key point is that two different symbols  $s_1$  and  $s_2$  are transmitted simultaneously from antennas 1 and 2, respectively, during the first symbol period, followed by symbols  $-s_2^*$  and  $s_1^*$  from antennas 1 and 2, respectively, during the next symbol period. Therefore, the received signals over two consecutive symbol periods are

$$y_1 = \sqrt{\frac{E_s}{2}} [h_1 \quad h_2] \begin{bmatrix} s_1 \\ s_2 \end{bmatrix} + n_1$$

and

$$y_2 = \sqrt{\frac{E_s}{2}} [h_1 \quad h_2] \begin{bmatrix} -s_2^* \\ s_1^* \end{bmatrix} + n_2,$$

where  $n_1$  and  $n_2$  are uncorrelated ZMCSCG noise samples. It can be demonstrated that the optimal receiver is linear, and it provides a spatial diversity order of  $n_T n_R$  (second order in this case), even when channel knowledge is not available at the transmitter. The above Alamouti MISO scheme can be easily extended to the case when multiple antennas are used at the receiver [A. Paulraj and Gore, 2003, Tse, 2005].

### 2.3.3 Multi-Carrier Transmissions: Orthogonal Frequency-Division Multiplexing Schemes

Orthogonal frequency-division multiplexing (OFDM) is a widely used multi-carrier method in wideband digital communications. The idea consists in dividing the available bandwidth in several orthogonal parallel streams, each one ruled by a different subcarrier.

The data symbols modulate  $N_c$  subcarriers, which occupy the total bandwidth  $W$  and are uniformly separated by  $W/N_c$ . The data symbols on the subcarriers are then converted to time domain through the inverse discrete Fourier transform (IDFT). The transmitter includes a cyclic prefix in every OFDM symbol before the transmission of the frame.<sup>3</sup> At the receiver, the cyclic prefix is discarded, and the  $N_c$  symbols are converted to frequency domain through

<sup>2</sup>Note that throughout this work, we denote a MIMO system/channel as *the*  $n_T \times n_R$  *system/channel* but the MIMO channel matrix  $\mathbf{H}$  has  $n_R \times n_T$  dimension. In this example, the  $2 \times 1$  MISO system has two transmit and one receive antennas, and the dimension of the channel vector  $\mathbf{h}$  is  $1 \times 2$ .

<sup>3</sup>The cyclic prefix is a prefix of the OFDM symbols, discarded at the receiver, which avoids intersymbol interference (ISI). It is particularly useful in frequency-selective channels, because it allows the linear convolution of the multipath channel to be modeled as circular convolution.

a DFT. The data symbols on the subcarriers are maintained to be orthogonal as they propagate through narrowband parallel sub-channels [Tse, 2005].

Many wireless standards, like 802.11a, g, and n, DVB-T, DVB-H, WiMAX, or 3GPP, are based on OFDM due to its benefits with respect to single-carrier transmissions, such as ISI reduction/removal or frequency diversity gain (i.e., SNR improvement). In particular, as we will detail in Section 2.5, the developed MIMAX prototype is based on IEEE 802.11a standard. In OFDM, with the novel analog antenna combining architecture, the choice of transmit/receive beamformers is not as trivial as in single-carrier transmissions. Due to the nature of the novel RF-MIMO transceiver, the transceiver uses the same pair of beamformers for all the subcarriers, and, therefore, the problem is coupled. In Chapters 3 and 4, we will tackle the problem of selecting the beamformers under different channel state information conditions within this OFDM-based novel architecture.

**Table 2.1:** Transmission schemes under different scenarios.

	CSIR	CDIR
CSIT	TXBF + RXBF	TXBF + RX BDM
CDIT	TX BDM + RXBF	TX BDM + RX BDM

The signal model in MIMO systems is given by

$$\mathbf{y}_k = \mathbf{H}_k \mathbf{s}_k + \mathbf{n}_k, \quad k = 1, \dots, N_c,$$

where  $\mathbf{y}_k$  is the received signals vector,  $\mathbf{H}_k$  is the  $n_R \times n_T$  channel response matrix,  $s_k$  is the transmitted symbols vector,  $\mathbf{n}_k$  is the white ZMCSCG noise vector for the  $k$ -th subcarrier, and  $N_c$  is the number of subcarriers. It can be seen that the OFDM scheme can be split into  $N_c$  orthogonal single-carrier systems.

When the channel is known at the transmitter, we have seen that there are certain optimal transmit and receive weights that maximize the SNR at the receiver. Nevertheless, in the first approach, a constant power transmission has been considered. In multi-carrier schemes, the allocation of the available power at the transmitter among the different subcarriers represents an interesting problem. The waterfilling algorithm tackles this problem which, can be extended to any power allocation among independent subchannels.

### Waterfilling Algorithm

Focusing on the OFDM-MIMO system where the channel for all subcarriers is known at the transmitter, it has been seen that the transmit and receive weights are given by the input and output singular vectors, respectively, corresponding to the maximum singular value  $\sigma_{k,\max}$  of  $\mathbf{H}_k$  (see Subsection 2.3.1). The classical waterfilling algorithm solves iteratively the problem of maximizing the mutual information between the input and the output of a channel composed of several subchannels (such as frequency-selective channel, time-varying channel, etc) with a global power constraint at the transmitter [Cover and Thomas, 1991, Telatar, 1999, Palomar and Fonollosa, 2005]. The power allocated to the  $i$ -th subchannel is given by

$$\rho_k = \left( \mu - \frac{1}{\gamma \sigma_k^2} \right)_+, \quad k = 1, \dots, N_c, \quad (2.2)$$

where  $\gamma$  is the SNR at the receiver,  $\sigma_k^2$  is the maximum singular value of  $\mathbf{H}_k$ ,

$$(x)_+ = \begin{cases} 0 & x \leq 0, \\ x & x \geq 0, \end{cases}$$

and  $\mu$  is the water level, which is chosen to satisfy

$$\sum_{n=1}^n \rho_k = 1. \quad (2.3)$$

## 2.4 Drawbacks of MIMO Systems

As seen in the Section 2.2, MIMO systems present a significant improvement over SISO systems by either increasing the data throughput (rate) or reliability (for instance, the bit error rate). In particular, the best data throughput can be reached by the so-called full MIMO systems. These types of systems, with an appropriate transmission technique, can increase the data throughput by a factor proportional to the channel rank matrix. For instance, under a full-rank channel matrix, they can obtain full multiplexing gain, i.e., they can send  $\min(n_T, n_R)$  streams at the same time through the  $n_R \times n_T$  MIMO channel. Nevertheless, in order to reach full multiplexing gain, the system must also satisfy specific conditions. Each antenna branch must be demodulated, acquired, and processed independently at the receiver. Likewise, at the transmitter, each antenna branch must be processed, modulated, and upconverted independently [Barbarossa, 2005]. Therefore, the exploitation of all the MIMO benefits generate at each station an extra cost, size, and power consumption in comparison with the single-input single-output (SISO) systems, which is in part responsible for the delay in the commercial deployment of MIMO wireless transceivers, mainly in handsets or small cost terminals. Figure 2.4 shows the receiver part of the full MIMO architecture.

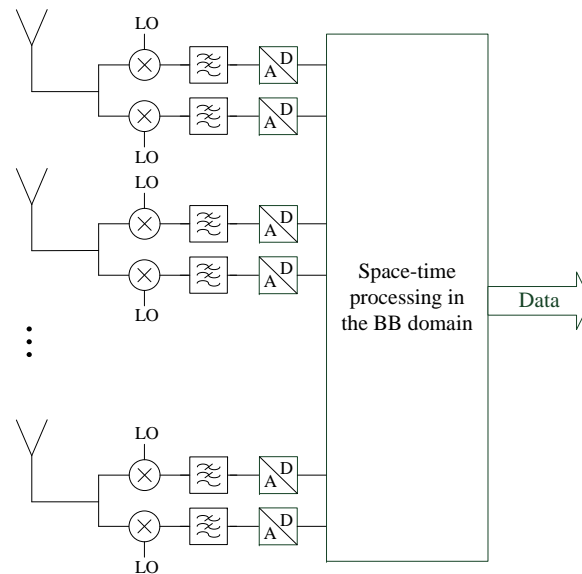


**Figure 2.4:** Full MIMO transceiver. Exemplarily shown for a direct-conversion receiver.

The combining schemes mitigate some of the drawbacks of the full MIMO systems. Compared to antenna selection systems, where the antenna paths are selected and switched, or phased arrays, where only the phase can be adjusted, in combining schemes, both the phases and amplitudes of the different branches are adjusted. In the state-of-the-art combining approaches, this complex weighting is performed in the baseband as illustrated in Figure 2.5. The combining schemes at the baseband have the advantage of a simple design using commercial off-the-shelf components. Although the baseband combining schemes have a single baseband path, they maintain multiple radio-frequency (RF) branches and analog-to-digital converters (ADCs), which still suppose an extra cost, size, and consumption. To decrease these parameters, the analog combining schemes were proposed.

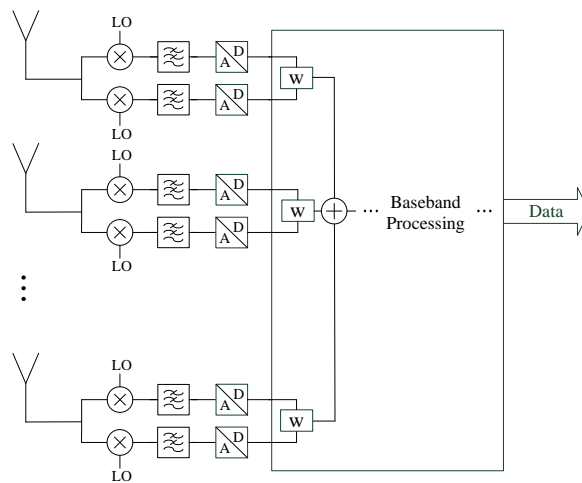


**Figure 2.5:** Conventional approach performing adaptive combining.

In order to reduce the costs of the multiple RF branches, several alternatives for the analog combining based on variable-gain amplifiers (VGA) and phase shifters applied on each branch have been proposed in the last decade [Sandhu and Ho, 2003, S. Jeon and Itoh, May 2002]. The analog combining architecture is similar to a pre-FFT scheme, which has been widely studied in the literature [Sandhu and Ho, 2003, Huang and Letaief, 2004b, Rahman et al., 2004, Li et al., 2007b]. The main motivation behind pre-FFT schemes consists in the reduction of the cost due to FFT calculations, and, to this end, beamforming is shifted before FFT processing.

### 2.4.1 Existing MIMO Combining Schemes and Algorithms

As described throughout Section 2.2, the performance benefits of MIMO schemes are numerous due to some gains with respect to the SISO schemes. Particularly, there is a tradeoff between the multiplexing and diversity gains. MIMO algorithms that exploit the multiplexing gain (e.g. spatial multiplexing) use multi-stream transmission and produce little or no diversity gain. On the other hand, the MIMO algorithms that are able to provide full diversity gain use single-stream transmission, and, therefore, they do not offer multiplexing gain. This is the case of the different combining schemes where no multiplexing gain is available.

In any case, after adaptive modulation and outer channel coding, diversity and multiplexing gains translate to BER, which is the performance metric of interest. Well-suited MIMO

combining algorithms are developed for different scenarios: point-to-point, multi-user, and cellular scenarios. In the following, we briefly characterize these schemes, pointing out their benefits and drawbacks. For each scheme, we explain the optimal selection of the beamformers when the system is single-carrier or when the channel is frequency flat in a multi-carrier system. The beamforming selection in a multi-carrier system is a more intricate problem when the channel is frequency-selective, because, as stated above, due to the combining architecture, a single beamformer is applied to all the subcarriers.

### Antenna Selection Combining

In the antenna selection combining algorithm (ASC), the combiner at the receiver selects and outputs the signal on the branch with the highest SNR  $S_i/N_i$ , where  $N_i$  and  $S_i$  are, respectively, the noise and the received signal power at the  $i$ -th branch. Assuming that the noise power  $N_i = N_0$  is the same on all branches, this is equivalent to select the highest  $S_i + N_i$ .<sup>4</sup> With ASC, the output of the combiner has a SNR equal to the maximum SNR of all the branches.

A receiver that implements ASC must monitor simultaneously the SNR on every branch. The complexity of an ASC receiver, with a single RF and baseband branch, is similar to a SISO receiver, but the performance of this algorithm is quite low in comparison with other MIMO combining schemes.

### Dominant Eigenmode Transmission

Among all MIMO algorithms that use a single channel mode for transmission, the so-called dominant eigenmode transmission (DET) provides the best performance. It maximizes the output signal-to-noise-ratio (SNR) at the receive at the expense of the highest complexity in point-to-point communications. DET is able to provide full array gain and full spatial diversity (diversity order is equal to the product of the number of transmit and receive antennas) without any penalty in the signalling rate. Moreover, in the low and medium SNR regime, the performance of DET is close to the MIMO multi-stream based algorithms [Tse, 2005, A. Paulraj and Gore, 2003]. Using DET, the optimum weights that maximize the resulting SNR at the receiver and transmitter arrays are obtained as a function of the MIMO channel matrix. Therefore, the application of DET requires full CSI at both the transmitter and receiver. Suboptimal MIMO diversity techniques also need some type of CSI at the receiver. Moreover, DET is intended for a flat-fading channel, hence, it cannot be used for a frequency selective channel as it is.

**Transmit and Receive Maximum-Ratio Combining:** In the particular cases of multiple-input single-output (MISO) and single-input multiple-output (SIMO) configurations, DET reduces to the maximum-ratio transmission (MRT) and maximum-ratio combining (MRC), respectively, and they are optimum in terms of capacity [Tse, 2005, A. Paulraj and Gore, 2003].

In MRC, the output is a weighted sum, where each branch is multiplied by the complex weight  $w[i] = a_i e^{j\theta_i}$ , where  $\theta_i$  is the phase of the incoming signal on the  $i$ -th branch. Assuming the same noise power spectral density (PSD), it can be demonstrated that  $a_i^2 = S_i/N_0$ , i.e.,  $a_i$

<sup>4</sup>In practice,  $S_i + N_i$  is easier to measure than SNR, since the former involves finding only the total power in the received signal.

is proportional to the SNR on the  $i$ -th branch [Goldsmith, 2005]. In a system with  $n_T$  receive antennas, the resulting combined SNR becomes

$$\gamma_{\Sigma} = \sum_{i=1}^{n_T} \frac{S_i}{N_0},$$

i.e., the SNR of the combiner output is the sum of SNRs on each branch. Thus, the SNR after the combiner, and, therefore, the array gain increase linearly with the number of receive antennas.

The reasoning for the MRT case in a MISO channel is analogous to the MRC one. In this case, the transmitter must have access to the channel state information (CSIT), and the square of the transmit weight on each branch must be proportional to the channel between each branch and the single antenna at the receiver.

### Equal-Gain Combining

DET technique requires knowledge of the time-varying SNR on each branch, which in practice can be difficult to be measured. A simpler technique is equal-gain combining (EGC), which co-phases the signals on each branch and then combines them with equal weighting, i.e., the weight at the  $i$ -th branch is  $\mathbf{w}[i] = e^{\theta_i}$ . Therefore, the SNR of the combiner output, assuming the same noise PSD of  $N_0/2$  in each branch, is then given by [Goldsmith, 2005]

$$\gamma_{\Sigma} = \frac{1}{N_0 M} \left( \sum_{i=1}^M \sqrt{S_i} \right)^2.$$

Along with ASC, MRC, and MRT, EGC is a suboptimal diversity scheme that, in certain cases, can provide performances close to DET but with lower complexity and lower requirements about the CSI. Figure 2.6 summarizes all these techniques providing an overview between the performance and the requirements of CSI.

## 2.5 A Novel Analog Antenna Combining System: MIMAX Project

Until very recently, the performance of the RF combining schemes introduced in Section 2.4 was quite limited, because phase shifters tend to exhibit significant amplitude variations. However, recent advances in SiGe-BiCMOS technology together with certain innovative concepts introduced for phase and amplitude control circuits [Ellinger, 2007] have made possible the development of a full  $360^\circ$  control range of the phase shifter together with an amplitude control of more than 20 dB. Propelled by these advances, a novel RF-MIMO transceiver architecture has been proposed, which is shown in Figure 2.7. The RF-MIMO transmitter operates analogously. With this architecture, the spatial processing is done at RF front-end, which significantly reduces the hardware cost and power consumption [Eickhoff et al., 2008].

The price to pay for the simplicity of the analog combining architecture is that a single branch is processed after the RF analog combining stage, and, consequently, the multiplexing gain is limited to one. Therefore, a single stream of data is transmitted and received through an equivalent SISO channel, which is optimized with respect to the transmit and receive analog beamformers (RF weights). Nevertheless, in low signal-to-noise ratio (SNR) scenarios or for highly correlated MIMO channels (which can even become rank-deficient), the spatial

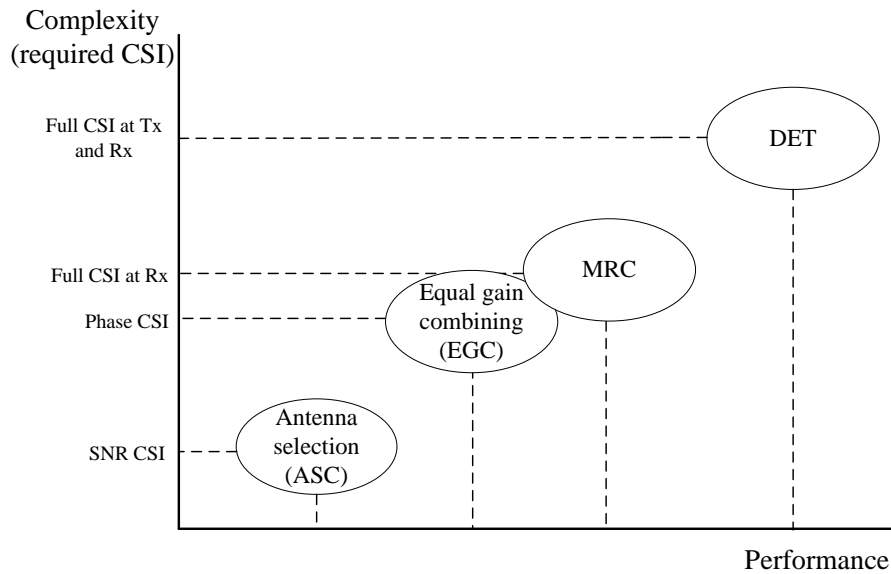


**Figure 2.6:** Comparison among the different MIMO combining algorithms.

degrees of freedom are limited, and the performance improvement of full MIMO due to spatial multiplexing is marginal compared to the analog combining architecture.

Finally, we must point out that the development of this type of analog weighting RF circuits in BiCMOS technology suitable for mass fabrication is currently being pursued within the European Union funded project MIMAX (*MIMO Systems for Maximum Reliability and Performance*, FP7/2007-2013 n° 213952) [MIMAX Web, 2008].

MIMAX is a research project within the 7<sup>th</sup> Framework Programme that aims to investigate and develop a more powerful wireless local area network (WLAN) device, which is compatible with the existing WLAN networks [Eickhoff et al., 2008, MIMAX Web, 2008]. The project's concepts are based on wireless MIMO communication, which are similar to the approaches used in new WLAN standard 802.11n, WiMAX, or LTE (advanced). Nevertheless, the main difference between MIMAX and the aforementioned standards is that, in MIMAX, the required signal processing is executed near the transmit and receive antennas, i.e., MIMAX architecture is based on analog antenna combining.

Although the analog antenna combining could be applied to any wireless technology,<sup>5</sup> market and technology analysis within the MIMAX project revealed the great potential offered by the WLANs. Especially, IEEE 802.11a provides promising market prospects for exploiting the benefits of spatial signal processing in the RF due to compact form factors, high revenues, and competitive system costs. For this reason, the MIMAX transceiver is based on 802.11a technology at 5 GHz with an analog antenna combining architecture as that shown in Figure 2.7. In Chapter 5, we will go into detail about this project, particularly describing the development of a prototype that implements this novel architecture.

<sup>5</sup>See [Santamaría et al., 2009b] for a thorough study of the feasibility and potential impact of MIMAX in several standards such as WiMAX or LTE.

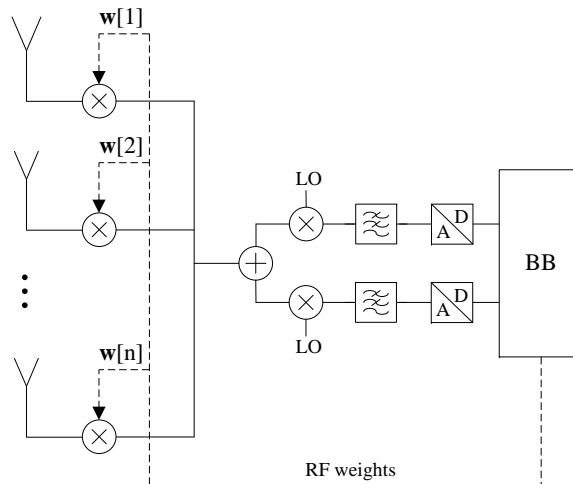


**Figure 2.7:** Analog antenna combining in the RF path for MIMO communications systems. Exemplarily shown for a direct-conversion receiver.

### 2.5.1 Transmission Schemes for MIMAX

The new challenge at the baseband part of the MIMAX transceiver consists in selecting the weights (also called beamformers) that must be applied in RF. Depending on the channel state knowledge at the transmitter and the receiver, the design of the beamformers to be applied in the RF part is distinct. Specifically, we can distinguish between two different scenarios regarding the channel knowledge at the transmitter or receiver. In the following, we review the different scenarios and the existent techniques for the calculation of the transmit/receive beamformers in a single-carrier scheme. Note that the MIMAX transceiver is based on OFDM, and, therefore, the selection of the beamformers is not that simple. In fact, in this analog combining RF architecture and under OFDM transmissions, the design of efficient transmission schemes constitutes one of the main challenges of this thesis.

- Perfect channel state information (CSI): If the channel is perfectly known, the RF weights (i.e., the RF beamformer) can be obtained following certain optimization criterion. We refer to this technique as transmit or receive beamforming: TXBF or RXBF, respectively.
- Statistical channel state information or channel distribution information (CDI): If the channel is not perfectly known, we must rely on its statistical information. Thus, in order to exploit the spatial diversity of the system, the information symbols have to be distributed among different transmission (or reception) directions (beamformers). Therefore, unlike the perfect CSI case, a data block has to be precoded and transmitted/received using different beamformers. We refer to this scheme as transmit or receive beam-division multiplexing (BDM): TX BDM or RX BDM, respectively. With this scheme, the spatial diversity is shifted to an equivalent time diversity. As we will see in the following chapter, if there is no channel correlation, the directions (beamformers) are orthogonal, and the scheme is called orthogonal beam-division multiplexing (OBDM).

Therefore, depending on the CSI available at each side, the optimal transmission schemes can be studied under four possible scenarios that are also summarized in Table 2.2. Neverthe-

less, the channel is usually known at the receiver, which makes two scenarios be particularly relevant:

- **CSIT+CSIR:** This is the principal scenario for MIMAX. If the channel has been estimated at both the transmitter and receiver sides, the beamformers can be selected to optimize certain figures of merit of the equivalent SISO channel. As an illustrative example, in the case of flat fading channels, all the different criteria reduce to the maximization of the SNR, which is achieved by the well-known dominant eigenmode transmission (DET) technique depicted in Subsection 2.4.1. This scheme will be deeply studied for a multi-carrier system (OFDM) in Chapter 3, and its implementation will be addressed in the second part of this thesis.
- **CDIT+CSIR:** If the channel is only available at the receiver side, the transmitter uses the BDM transmission technique. For instance, in a  $4 \times 4$  MIMO channel without channel correlation, in order to exploit the spatial diversity, the transmitter has to transmit in four orthogonal spatial directions (using four different transmit beamformers). In this case, we call the transmission technique orthogonal BDM (OBDM). On the other hand, for each transmit beamformer, the receiver has perfect knowledge of the equivalent SIMO channel, and, therefore, it can apply the RXBF technique. In the particular case of flat fading channels, the receiver architecture reduces to the well-known maximum ratio combining (MRC). This problem will be addressed in Chapter 4 for frequency-selective channels with transmit correlation knowledge.

**Table 2.2:** Transmission schemes under different scenarios.

	CSIR	CDIR
CSIT	TXBF + RXBF	TXBF + RX BDM
CDIT	TX BDM + RXBF	TX BDM + RX BDM

The other two possible scenarios are not as common in practice, and they are the following:

- **CSIT+CDIR:** This is the counterpart of the CDIT+CSIR scenario. Here, the transmitter can select an optimal beamformer, but, in order to exploit the spatial diversity at the receiver side, the information has to be distributed among  $n_T$  different OFDM symbols, which will be received using  $n_R$  different receive beamformers. For instance, this scenario occurs when the channel between two terminals is estimated in both directions. In this case, the terminal T1 sends a training frame to the terminal T2. Once T2 knows the channel, it sends a training frame to T1. This last frame is sent under CSIT+CDIR. In Chapter 5, we address the channel estimation problem in an analog antenna combining system, and we briefly review this scenario.
- **CDIT+CDIR:** If the channel is not known, typically the transmitter will initiate a channel estimation procedure. However, during this initial stage, it is also possible to transmit data with increased reliability even though the MIMO channel is unknown at both

sides. The general idea consists of applying BDM at both sides. To this end, the combination of  $n_T$  transmit and  $n_R$  receive beamformers guarantees the exploitation of the spatial diversity of the MIMO channel. In this case, the information bits have to be distributed (precoded) among  $n_T n_R$  consecutive OFDM symbols. If the MIMO matrix has i.i.d. entries, then OBDM is applied at both sides.

The MIMAX transceiver is designed in such a way that there is access to the channel state information at the transmission and the reception sides (CSIT+CSIR). In Chapter 3, we focus on this case and design the transmit and receive RF beamformers under OFDM transmissions. Although the CDIT+CSIR case is not the main scope of the MIMAX project, the problem of selecting the optimal beamformers under these circumstances is also addressed in Chapter 4.<sup>6</sup>

The MIMAX project aims to develop a demonstrator of the MIMAX transceiver. The whole second part of this thesis seeks to design, implement, and test in real-time an FPGA-synthesizable version of the new baseband blocks needed to estimate the MIMO channel and also to calculate the optimal weights to be applied in RF. The implemented algorithm is an approximated version of one proposed in Chapter 3, assuming perfect channel state information at the transmitter and at the receiver side (CSIT+CSIR). More details about the transmission schemes in MIMAX can be found in [Santamaría et al., 2009b].

### 2.5.2 Channel Estimation

The channel estimation procedure in the analog antenna combining architectures represents a challenging task since there is a single branch at the transmitter and the receiver. Note that, with this architecture, the MIMO channel is projected into a SISO channel by means of the transmit and receive beamformers. Therefore, an estimate of the  $n_R \times n_T$  frequency-selective MIMO channel must be obtained from the estimates of  $n_T n_R$  MIMO channel projections (equivalent SISO channels) under different transmit-receive beamformers. Consequently, these beamformers have to be carefully chosen.

In Section 5.4, the training process and the selection of the beamformers for this training process will be detailed for a system based on 802.11a. We will also study several channel estimation algorithms: different versions of the least squares (LS) estimator and the minimum mean-square error (MMSE) estimator. Finally, we will select the simple LS algorithm to be implemented in a real baseband processor.

### 2.5.3 MIMAX Capabilities

In Section 2.2, the main advantages of MIMO systems have been presented, i.e., the spatial diversity gain, the multiplexing gain, and the array gain. Moreover, it has been shown that there is a tradeoff between spatial diversity gain and multiplexing gain.

We have seen the benefits of the MIMAX architecture (analog combining); now, we analyze how these changes affect the different MIMO gains. Table 2.3 summarizes the maximum achievable gains for full MIMO, MIMAX, and SISO systems, taking into account the channel state information at each side.

<sup>6</sup>In the second part of this thesis, we will see that the MIMAX transceiver performs a channel estimation procedure in both directions in such a way that both transmitter and receiver know the channel state.

**Table 2.3:** Maximum achievable diversity, multiplexing, and array gains for full MIMO, MIMAX, and SISO systems.

	Diversity gain	Multiplexing gain	Array gain
Full MIMO	$n_T n_R$	$\min(n_T, n_R)$	$n_R$ (CSIR) $n_T n_R$ (CSIT+CSIR)
MIMAX	$n_T n_R$	1	$n_R$ (CSIR) $n_T n_R$ (CSIT+CSIR)
SISO	1	1	1

### Spatial Diversity Gain

The spatial diversity gain can be obtained in MIMAX as in the full-MIMO architecture. Note that the spatial diversity gain decreases with the antenna correlation, and, thus, for a MIMAX transceiver which operates on the 5 GHz band in indoor environments with many scatterers around, the channel should decorrelate over short distances, and typical antenna separation of  $\lambda/2$  would suffice (i.e., around 3 cm).

The particular processing needed to extract the spatial diversity also depends on the channel state information available at the transmitter or the receiver sides. For flat fading channels, all the spatial diversity can be extracted in MIMAX by using dominant eigenmode transmission (DET) if the channel is known at both sides or by using beam-division multiplexing (BDM) if the channel is unknown at the transmitter. The basic idea is that, when the channel is known, all the spatial diversity can be extracted by transmitting through the strongest mode of the MIMO channel. However, when the channel is unknown at the transmitter, it is necessary to distribute the symbols or codewords over a number of consecutive blocks (this number must be greater or equal to the number of transmit antennas), which are then transmitted through different spatial directions.

### Multiplexing Gain

In MIMAX, a single branch is processed after the RF analog combining stage, and, consequently, the multiplexing gain is limited to one. In comparison to a SISO link, the only increase in capacity comes from the increased SNR due to the array gain. Nevertheless, we must note that, in a full MIMO system, to obtain multiplexing gain, the channel matrix must have a rank higher than one, and the SNR regime must be medium or high. Thus, in many practical scenarios, this limitation of MIMAX has no effect. Therefore, for MIMAX, the multiplexing gain is one, and then the emphasis is placed on diversity gain or reliability as can be seen in Figure 2.8.

### Array Gain

As well as in the full MIMO scheme, in MIMAX architecture, the array gain can be obtained at each side of the link by coherent combining. To obtain the full array gain, the receiver needs to have perfect CSI in order to perform a coherent combination of the signals. The array gain, along with the spatial diversity gain, is one of the benefits that MIMAX can achieve without rising significantly the complexity and power consumption of the SISO architecture.

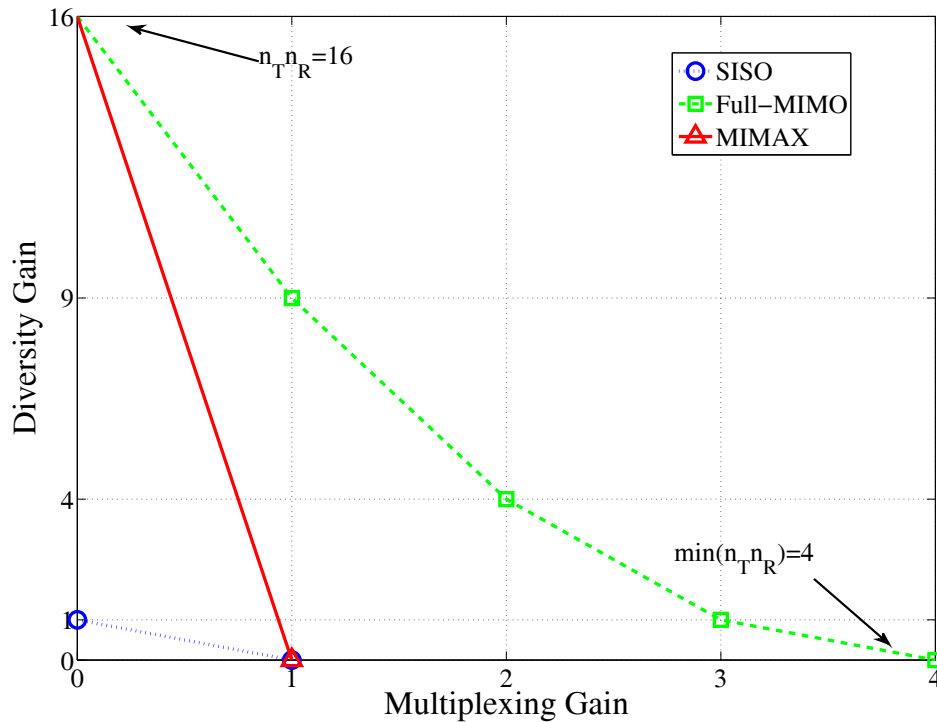


**Figure 2.8:** Achievable diversity-multiplexing curves for a  $4 \times 4$  system with full MIMO, MIMAX, and SISO.

#### 2.5.4 MIMAX Consortium

The MIMAX consortium combines multidisciplinary expertise and resources from academia, and industry including know-how in analog combining signal processing, software development, RF design, integrated circuit (IC) technology manufacturing, antenna arrays, and market-oriented service providers. MIMAX consists of three small/medium size enterprises, one large research institute, and two universities, which are from four EU countries (Cyprus, Germany, Italy, and Spain).

##### TU Dresden

The involved Chair for Circuit Design and Network Theory at the Dresden University of Technology (TUD) is devoted to the design of high-speed integrated circuits using advanced circuit techniques and technologies. Applications mainly involve wireless communications at up to 60 GHz and optical communications up to 40 Gbps.

TUD is responsible for project management and task coordination of MIMAX. Furthermore, TUD is designing the key components for the MIMAX transceiver, such as the vector modulators, the power amplifiers, the low noise amplifiers, and the mixers in the RF domain, i.e., the analog front-end (AFE).

##### University of Cantabria

The Advanced Signal Processing Group (GTAS) is one of the research groups of the University of Cantabria (UC). Since its creation, the group has carried out an important research

work in the field of signal processing algorithms for wireless communications, as well as in the cross-fertilization between machine-learning concepts and communications problems. During the past few years, the group's activity has been focused mainly on MIMO wireless communications systems.

In MIMAX, UC is responsible for designing the baseband processing tasks, including the MIMO algorithms as well as the baseband implementation of those algorithms within the final MIMAX baseband processor.

### **IHP Microelectronics**

The IHP (Institute for High-Performance Microelectronics) has a team of 204 R&D professionals with core competence in microelectronics: process technology, circuit design, and systems. As a member institute of the Gottfried Wilhelm Leibniz Society, the core funding comes from the German Federal Government and the State Government of Brandenburg.

Within the MIMAX project, IHP focuses on baseband and MAC processors. The availability of a big set of pre-developed modules will allow the consortium to concentrate on the innovative parts of MIMAX.

### **TTI Norte**

TTI is a small/medium size Spanish enterprise that comprises of an expanding team of more than 80 highly qualified engineers well supported by key lab and fabrication assets. Its main expertise areas are active antennas and microwave and RF technologies (active elements as frequency converters and synthesizers).

TTI is responsible for the architectural and detailed design, as well as the development and testing of the integrated antenna array, plus the various integration aspects of the transceiver front-end and the antenna array.

### **T-Connect**

T-Connect is set up in Trieste (Italy) in AREA science park, one of the leading multi-sectoral Science Parks in Europe. Its main expertise areas consist of supporting customer in the acquisition of localization data referred to their mobile's users, developing software solutions laying on a server, and developing software interfaces on client terminals for the correct usage of the services.

In MIMAX, T-Connect is responsible for the market analysis and for defining system requirements that arise from application scenarios. Moreover, the seamless user interface and the exploitation of the MIMAX achievements are the key tasks of T-Connect.

### **PrimeTel**

PrimeTel is an electronic communication and information technology company based in Cyprus that owns and operates a truly regional network, spanning Cyprus, Greece, UK, and Russia, providing voice, data, and Internet Protocol services to business and residential customers as well as wholesale services to carriers, mobile operators, content, application, and internet providers.

In MIMAX, PrimeTel is responsible for the marketing aspects in private networks and the exploitation of the MIMAX achievements in this area of networks. Moreover, PrimeTel

will develop the seamless application interface to the reconfigurable MAC processor and also perform demonstration activities for private communication networks.

## 2.6 Conclusions

Throughout this chapter, we have reviewed the main advantages and drawbacks of MIMO systems. We have presented some MIMO combining architectures, which, reducing part of the drawbacks of MIMO systems, extract most of the benefits of the traditional full MIMO systems. We have reviewed the available work in the literature about these combining schemes, and a novel analog antenna combining architecture has been proposed. We have seen that, from the signal processing point of view, the main challenge consist in the selection of the optimal transmit/receive weights to be applied in RF. This problem will be addressed in the next chapters for different channel knowledge at both sides of the channel. Finally, the MI-MAX project has been introduced, detailing its main objectives, the consortium, and the part of the work that must be done by the GTAS group.



Part **I**

**Design of the Transmit and Receive  
Beamformers**



# Perfect Channel Knowledge at the Transmitter Side

## 3.1 Introduction

In Chapter 2, the benefits (e.g., diversity or multiplexing gain) of multiple-input multiple-output (MIMO) wireless communication systems have been reviewed. Nevertheless, it has been seen that, in order to extract all these benefits, all antenna paths must be independently acquired and processed at baseband. Consequently, the hardware costs, size, and power consumption of conventional MIMO systems are increased accordingly. A RF-MIMO receiver architecture, shown in Figure 3.1, was proposed in Chapter 2 to mitigate some of these problems by shifting spatial signal processing from the baseband to the radio-frequency (RF) front-end. By applying the complex weights  $w[n]$  (gain factor and phase shift) to the received signals as shown in Figure 3.1, after combining the weighted RF signals, a single stream of data must be acquired and processed, and, thus, the hardware cost and the power consumption are significantly reduced [Eickhoff et al., 2008]. Although the multiplexing gain of the RF-MIMO transceiver is limited to one (since we transmit/receive a single data stream), in Chapter 2, we have shown that other benefits of the MIMO channel, such as full spatial diversity or full array gain can be retained by the proposed architecture if proper processing is carried out.

From a signal processing point of view, the adaptive antenna combining architecture in Figure 3.1 poses several challenging design problems. Specifically, in the case of OFDM transmissions, a conventional MIMO-OFDM receiver can compute the fast Fourier transform (FFT) of each baseband signal, and, hence, it can apply the optimal processing independently for each subcarrier. However, the new RF-MIMO transceiver uses the same pair of RF weights (or beamformers) for all the subcarriers and, therefore, the problem is inherently coupled.

In this chapter, we address the problem of selecting at the receiver side the transmit and receive beamformers under OFDM transmissions with perfect channel state information at the receiver side (CSIR). In Section 3.2, we propose a general beamforming criterion, which depends on a single parameter  $\alpha$ . This parameter establishes a tradeoff between the energy and the spectral flatness of the equivalent SISO channel (after transmit-transmit beamforming). Analogously to the MaxSNR approach for pre-FFT MIMO schemes [Huang and Letaief, 2004b], the proposed beamforming criterion results in a non-convex optimization problem and has no closed-form solution. In Section 3.4.1, we analyze the associated non-convex opti-

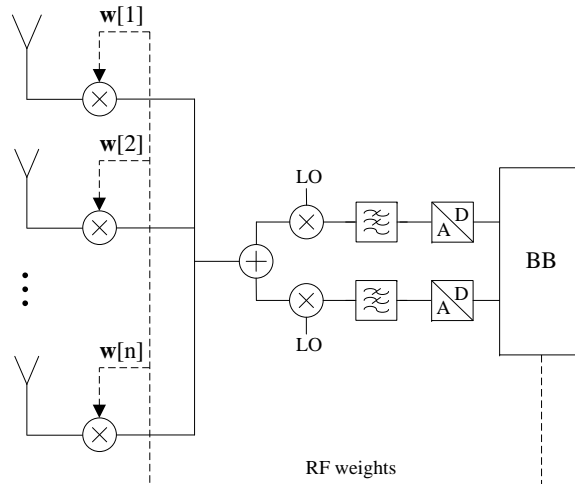


**Figure 3.1:** Analog antenna combining in the RF path for MIMO communications systems. Exemplarily shown for a direct-conversion receiver.

mization problem and show that, in certain cases, it can be approximately solved by means of semidefinite relaxation (SDR) techniques. Furthermore, in order to avoid the high complexity cost associated to SDR techniques, we propose a suboptimal gradient search algorithm that, in combination with a very effective initialization technique, provides very accurate results in most of the practical cases. Finally, in Section 3.5, several simulation examples show the advantage of the proposed technique over the MaxSNR approach for both coded and uncoded transmissions.

### 3.1.1 Previous Work

In the case of conventional MIMO-OFDM systems, which we also refer to as full MIMO systems or post-FFT processing [Rahman et al., 2004], the joint design of transmit-transmit beamformers has been widely explored in the literature. In particular, in [Palomar et al., 2003, Palomar and Jiang, 2006], a number of interesting design criteria have been solved in closed-form within the powerful frameworks of convex optimization and majorization [Boyd and Vandenberghe, 2004, Marshall and Olkin, 1979, Palomar and Jiang, 2006].

In Section 2.4, we have exhibited the drawbacks of MIMO systems, and we have exposed several alternatives existent in the literature to mitigate these handicaps. We have reviewed the so called pre-FFT paradigm, a widely studied scheme, which aims to reduce the cost of the MIMO transceivers by decreasing the FFT calculations. This is achieved by shifting the beamforming before FFT processing. However, from the point of view of beamforming design, most of these pre-FFT schemes only consider receive beamforming, and the design criterion reduces to the maximization of the received SNR (MaxSNR) [Sandhu and Ho, 2003, Huang and Letaief, 2004b, Rahman et al., 2004, Li et al., 2007b]. In this chapter, we show that other design criteria can provide significantly better performance. Thus, although the present work has been motivated by the novel RF-combining architecture, the obtained results can be directly applied to pre-FFT schemes.

Finally, the statistical eigen-beamforming transmission mode, defined in the WiMAX standard [Wang et al., 2007, Wang et al., 2008], is also based on the application of a common transmit beamformer to a set of subcarriers. This idea allows a feedback reduction when

compared with a maximum ratio transmission (MRT) approach [Wang et al., 2007, Wang et al., 2008, Proakis, 1988]. However, analogously to the pre-FFT schemes, the design of the beamformer only considers the MaxSNR criterion.

## 3.2 Preliminaries

### 3.2.1 Main Assumptions

The main assumptions in this chapter are the following:

- We must point out that recent advances in RF integrated circuits designed in SiGe-BiCMOS technology [Ellinger, 2007] have made feasible the combination of RF signals using precise phase shifters with  $360^\circ$  control range and an amplitude dynamic range of more than 20 dB. In the design of the beamformers, we do not consider RF impairments, such as I/Q imbalance, imperfections in the RF circuitry, or quantization errors in the RF weights. However, as it will be shown in the simulations section, we should not expect a high impact of RF impairments in the performance of the proposed architecture.
- The MIMO channel and noise variance are perfectly known at the receiver side. We do not consider channel estimation errors due to the noise, the limited number of pilots, or the channel estimation process. On the other hand, note that the channel estimation process can be reduced to the sequential estimation of several single-input single-output (SISO) frequency selective channels. Additionally, in the case of pre-FFT systems and for the MaxSNR criterion, the optimal beamformers can be extracted from the signal covariance matrix, i.e., the knowledge of the channel and noise variance is not required [Huang and Letaief, 2004b, Li et al., 2007b].
- Both the transmit and receive weights are computed at the receiver side. Comparable to the WiMAX statistical eigen-beamforming transmission mode [Wang et al., 2007, Wang et al., 2008], the only feedback from the receiver is the optimal transmit beamformer. Therefore, the feedback is significantly reduced in comparison to the transmission of all the coefficients of the frequency-selective MIMO channel. On the other hand, we must note that, under this assumption, the transmitter cannot apply adaptive power loading techniques.

### 3.2.2 System Model

Let us consider a RF-MIMO system with  $n_T$  transmit and  $n_R$  receive antennas and unit-energy transmit and receive beamformers defined by the RF weights in Figure 3.1. Assuming a transmission scheme based on OFDM with  $N_c$  data-carriers and using a cyclic prefix longer than the channel impulse response, the communication system after transmit-receive beamforming in RF may be decomposed into the following set of parallel and non-interfering single-input single-output (SISO) equivalent channels

$$y_k = h_k s_k + n_k, \quad k = 1, \dots, N_c,$$

where  $y_k \in \mathbb{C}$  is the observation associated to the  $k$ -th data carrier,  $n_k$  represents the complex circular i.i.d. Gaussian noise with zero mean and variance  $\sigma^2$ ,  $s_k$  is the transmitted signal, and  $h_k$  is the equivalent channel after transmit-receive beamforming, which is given by

$$h_k = \mathbf{w}_R^H \mathbf{H}_k \mathbf{w}_T, \quad k = 1, \dots, N_c,$$

where  $\mathbf{w}_T \in \mathbb{C}^{n_T \times 1}$  and  $\mathbf{w}_R \in \mathbb{C}^{n_R \times 1}$  are the transmit and receive beamformers, and  $\mathbf{H}_k \in \mathbb{C}^{n_R \times n_T}$  represents the MIMO channel for the  $k$ -th data-carrier.

### 3.2.3 LMMSE Receiver

Although the results in this chapter are not restricted to a particular receiver, it will be useful to review the linear minimum mean square error (LMMSE) receiver. In particular, under perfect knowledge of the equivalent channel, and assuming unit transmit power per data carrier ( $E[|s_k|^2] = 1$ ), the MMSE estimate of  $s_k$  is

$$\hat{s}_k = \frac{h_k^* y_k}{|h_k|^2 + \sigma^2},$$

which yields a per-carrier MSE

$$\text{MSE}_k = E[|\hat{s}_k - s_k|^2] = \frac{1}{1 + \gamma|h_k|^2}, \quad k = 1, \dots, N_c,$$

where  $\gamma = 1/\sigma^2$  is defined as the (expected) signal to noise ratio (SNR) at the transmitter side.

### 3.2.4 Problem Statement

Conventional MIMO-OFDM baseband schemes have access to the signals at each one of the transmit/receive antennas and, consequently, can obtain a different pair of beamformers for each subcarrier. However, with the novel analog RF combining architecture a per-carrier beamforming design is not possible since all the orthogonal MIMO channels  $\mathbf{H}_k$  are affected by the same pair of beamformers. Notice that, with the RF combining architecture, a single FFT must be computed after the analog beamforming (at the receiver side), which notably simplifies the hardware and the system computational complexity, but it also complicates the beamforming design problem due to the coupling among subcarriers. This coupling imposes some tradeoffs and represents the main challenge for the design of the beamformers. In the following section, we tackle the problem of joint transmit-receive analog beamforming design using a unifying cost function, which, by changing a single parameter, encompasses several interesting design criteria.

## 3.3 General Analog Beamforming Criterion

In this section, we introduce a general criterion for the design of the transmit-receive beamformers under perfect knowledge of the MIMO channel  $\mathbf{H}_k$ , as well as the noise variance, at the receiver side. Specifically, we propose to minimize the following cost function

$$f_\alpha(\mathbf{w}_T, \mathbf{w}_R) = \frac{1}{\alpha - 1} \log \left( \frac{1}{N_c} \sum_{k=1}^{N_c} \text{MSE}_k^{\alpha-1} \right), \quad (3.1)$$

where  $\alpha$  is a real parameter, which controls the overall system performance. Thus, our optimization problem can be written as

$$\begin{aligned} & \underset{\mathbf{w}_T, \mathbf{w}_R}{\text{minimize}} && f_\alpha(\mathbf{w}_T, \mathbf{w}_R) \\ & \text{subject to} && \|\mathbf{w}_T\| = 1, \\ & && \|\mathbf{w}_R\| = 1. \end{aligned} \quad (3.2)$$

It is interesting to mention that (3.1) structurally resembles the definition of Renyi's entropy of order  $\alpha$  for a discrete random variable [Renyi, 1976]. This is a parametric family of entropy measures that include conventional Shannon's entropy definition as a limiting case, when  $\alpha$  tends to 1 and which has recently been used by Principe and co-workers in a number of applications, such as blind source separation and blind deconvolution/equalization [Erdogmus et al., 2004, Santamaría et al., 2002].

Before addressing the optimization problem, let us analyze some interesting choices of  $\alpha$ , which will help us to shed some light on the properties of the cost function (3.1).

### 3.3.1 Particular Cases

#### MaxSNR ( $\alpha = 0$ )

If the parameter  $\alpha$  is set to zero, the optimization problem in (3.2) can be rewritten as

$$\underset{\mathbf{w}_T, \mathbf{w}_R}{\text{maximize}} \quad \frac{1}{N_c} \sum_{k=1}^{N_c} |h_k|^2 \quad \text{s. t.} \quad \|\mathbf{w}_T\| = \|\mathbf{w}_R\| = 1,$$

i.e., the proposed criterion reduces to the maximization of the energy of the equivalent channel or, in other words, to the maximization of the received SNR. This problem has been previously addressed by other authors in the contexts of analog combining [Okada and Komaki, 2001] and pre-FFT schemes [Sandhu and Ho, 2003, Huang and Letaief, 2004b, Rahman et al., 2004, Li et al., 2007b], and it is also closely related to the statistical eigen beamforming transmission mode defined in the WiMAX standard [Wang et al., 2007, Wang et al., 2008].

#### MaxCAP ( $\alpha = 1$ )

When  $\alpha$  approaches 1, it can be easily shown by direct application of the L'Hopital's rule, that the proposed criterion reduces to

$$\underset{\mathbf{w}_T, \mathbf{w}_R}{\text{maximize}} \quad \frac{1}{N_c} \sum_{k=1}^{N_c} \log(1 + \gamma |h_k|^2) \quad \text{s. t.} \quad \|\mathbf{w}_T\| = \|\mathbf{w}_R\| = 1,$$

which represents the capacity of the equivalent SISO channel after beamforming.

#### MinMSE ( $\alpha = 2$ )

In this case, (3.2) is equivalent to

$$\underset{\mathbf{w}_T, \mathbf{w}_R}{\text{minimize}} \quad \frac{1}{N_c} \sum_{k=1}^{N_c} \text{MSE}_k \quad \text{s. t.} \quad \|\mathbf{w}_T\| = \|\mathbf{w}_R\| = 1,$$

i.e., the proposed criterion amounts to minimizing the overall MSE of the optimal linear receiver. Moreover, in Chapter 4, we will see that, in the important case of quadrature amplitude modulation (QAM) constellations and, under optimal linear precoding of the information symbols, the minimization of the MSE is equivalent to the minimization of the bit error rate (BER) of the optimal linear receiver.

Although in this chapter we mainly focus on the three previous values of  $\alpha$ , it should be noted that any other choice would be in principle possible. In particular, two other interesting cases are the following:

### MaxMin ( $\alpha = \infty$ )

In this case, the summation in (3.1) is dominated by the worst data-carrier, i.e., by that with the smallest  $|h_k|^2$ . Therefore, for  $\alpha \rightarrow \infty$ , the proposed criterion reduces to the optimization of the worst data-carrier. Interestingly, in the particular single-input multiple-output (SIMO) and multiple-input single-output (MISO) cases, the proposed criterion is mathematically identical to that of the MaxMin fair multicast beamforming problem, which has been proven to be NP-hard [Sidiropoulos et al., 2006, Phan et al., 2009].

### MaxMax ( $\alpha = -\infty$ )

For  $\alpha < 1$ , the proposed criterion can be rewritten as

$$\underset{\mathbf{w}_T, \mathbf{w}_R}{\text{maximize}} \quad \sum_{k=1}^{N_c} \left(1 + \gamma |h_k|^2\right)^{1-\alpha} \quad \text{s. t.} \quad \|\mathbf{w}_T\| = \|\mathbf{w}_R\| = 1,$$

then, it is easy to see that, when  $\alpha \rightarrow -\infty$ , the summation is dominated by the largest  $|h_k|$ . Therefore, the proposed criterion reduces to the optimization of the best data-carrier.<sup>1</sup> Interestingly, in this case, the optimal beamformers can be obtained in closed-form as the left and right singular vectors associated to the largest eigenvalue of all the MIMO channels  $\mathbf{H}_k$  ( $k = 1, \dots, N_c$ ).

## 3.3.2 Main Properties

In this subsection, the main properties of the proposed beamforming criterion are summarized. Let us start by analyzing the performance of the proposed method in the low SNR regime.

**Property 1.** *In the low SNR regime ( $\gamma \rightarrow 0$ ), the proposed criterion reduces to the MaxSNR approach regardless of  $\alpha$ .*

*Proof.* The proof is based on the first order Taylor series approximation of  $f_\alpha(\mathbf{w}_T, \mathbf{w}_R)$  with respect to  $\gamma$

$$f_\alpha(\mathbf{w}_T, \mathbf{w}_R) \simeq -\gamma \sum_{k=1}^{N_c} |h_k|^2.$$

Thus, the minimization of  $f_\alpha(\mathbf{w}_T, \mathbf{w}_R)$  reduces to the maximization of the equivalent channel energy or received SNR.  $\square$

<sup>1</sup>This would be the optimal criterion for an adaptive power loading scheme with only one active subcarrier.

Obviously, the different criteria significantly differ for moderate or high SNRs. The following property ensures the Pareto optimality (or *efficiency*) [Boyd and Vandenberghe, 2004] of the obtained solutions. Specifically, a feasible pair of beamformers  $(\tilde{\mathbf{w}}_T, \tilde{\mathbf{w}}_R)$  is said to be Pareto optimal with respect to the individual channel energies  $(|h_k|^2)$  or MSEs ( $MSE_k$ ) iff there does not exist another feasible pair  $(\mathbf{w}_T, \mathbf{w}_R)$  satisfying

$$|\mathbf{w}_R^H \mathbf{H}_k \mathbf{w}_T|^2 \geq |\tilde{\mathbf{w}}_R^H \mathbf{H}_k \tilde{\mathbf{w}}_T|^2, \quad k = 1, \dots, N_c, \quad (3.3)$$

with at least one strict inequality.

**Property 2.** *The solutions  $(\tilde{\mathbf{w}}_T, \tilde{\mathbf{w}}_R)$  of the proposed beamforming criterion are Pareto optimal points of the vector optimization problem based on the individual channel energies  $(|h_k|^2)$  or MSEs ( $MSE_k$ ).*

*Proof.* The proof follows directly from the fact that  $f_\alpha(\mathbf{w}_T, \mathbf{w}_R)$  decreases with  $|h_k|^2$  ( $k = 1, \dots, N_c$ ). Thus, if a feasible point  $\mathbf{w}_T, \mathbf{w}_R$  satisfies the inequalities in (3.3), then  $f_\alpha(\mathbf{w}_T, \mathbf{w}_R) < f_\alpha(\tilde{\mathbf{w}}_T, \tilde{\mathbf{w}}_R)$ .  $\square$

Here, we must note that the converse of Property 2 is not true in general, i.e., not all the Pareto optimal points (with respect to the  $N_c$  channel energies  $|h_k|^2$  or MSEs) are solutions of the proposed criterion for some  $\alpha$ . This fact is illustrated by means of a toy example consisting of a SIMO system with  $N_c = 2$  data carriers,  $n_R = 2$  receive antennas, real beamformers, and subcarrier channels given by

$$\mathbf{H}_1 = \begin{bmatrix} 1 \\ 0 \end{bmatrix}, \quad \mathbf{H}_2 = \begin{bmatrix} 0.35 \\ -0.8 \end{bmatrix}.$$

Figure 3.2 shows the set of achievable points  $(|h_1|^2, |h_2|^2)$  with unit energy beamformers  $\mathbf{w}_R$ , where we can see that the solutions of the proposed criterion for different values of  $\alpha$  are only a subset of the Pareto optimal solutions. However, it should be pointed out that those points in the Pareto boundary that are not achievable by our criterion might not be of practical interest. As an example, consider the Pareto points in Figure 3.2 near  $|h_1|^2 = 0.4$ ,  $|h_2|^2 = 0.7$ . Clearly, these points are worse solutions than those near  $|h_1|^2 = 0.8$ ,  $|h_2|^2 = 0.4$ , which are solutions of the proposed criterion for some  $\alpha \simeq 0$ .

The above observation is a direct consequence of the fact that the ordering of the energies is irrelevant for the performance of the equivalent channel. A more sensible comparison between feasible pairs of beamformers can be established with the help of some standard majorization results [Marshall and Olkin, 1979, Palomar and Jiang, 2006].

**Property 3.** *Let us define  $P_\beta = \sum_{k=1}^{N_c} MSE_k^{\beta-1}$  and the vector  $\mathbf{p}_\beta(\mathbf{w}_T, \mathbf{w}_R) = [p_{\beta,1}, \dots, p_{\beta,N_c}]$  with elements<sup>2</sup>*

$$p_{\beta,k} = \frac{MSE_k^{\beta-1}}{P_\beta}, \quad k = 1, \dots, N_c.$$

*Then, the cost function  $f_\alpha(\mathbf{w}_T, \mathbf{w}_R)$  can be rewritten as*

$$f_\alpha(\mathbf{w}_T, \mathbf{w}_R) = f_\beta(\mathbf{w}_T, \mathbf{w}_R) + g_{\alpha,\beta}(\mathbf{p}_\beta(\mathbf{w}_T, \mathbf{w}_R)), \quad (3.4)$$

*where  $g_{\alpha,\beta}(\mathbf{p}_\beta(\mathbf{w}_T, \mathbf{w}_R))$  is a function satisfying the following properties:*

<sup>2</sup>Note that, since  $0 \leq p_{\beta,k} \leq 1$  and  $\sum_{k=1}^{N_c} p_{\beta,k} = 1$ ,  $\mathbf{p}_\beta(\mathbf{w}_T, \mathbf{w}_R)$  can be seen as the probability mass function of a discrete random variable.

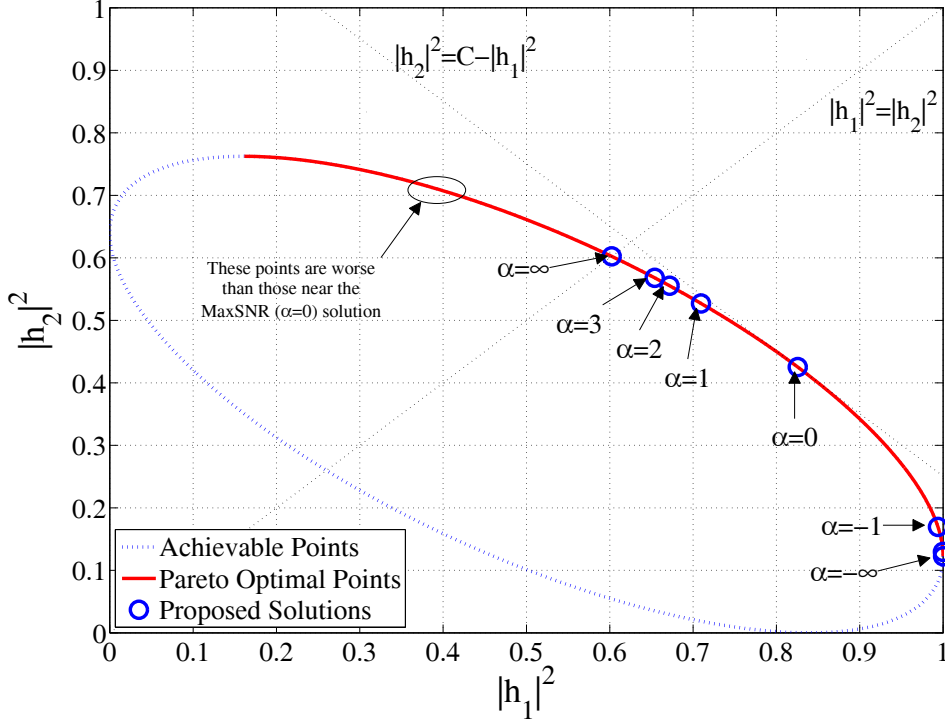


**Figure 3.2:** Toy example with a  $1 \times 2$  SIMO system with  $N_c = 2$  subcarriers. The figure shows the set of achievable points with  $\|\mathbf{w}_R\| = 1$  (dotted line), the Pareto optimal points (solid line), and the solutions associated to the proposed criterion (the section of the curve marked with circles).

1.  $g_{\alpha,\beta}(\mathbf{p}_\beta(\mathbf{w}_T, \mathbf{w}_R)) = -g_{\beta,\alpha}(\mathbf{p}_\alpha(\mathbf{w}_T, \mathbf{w}_R))$ .
2.  $g_{\alpha,\beta}(\mathbf{p}_\beta(\mathbf{w}_T, \mathbf{w}_R))$  increases with  $\alpha$ .
3. For  $\alpha > \beta$ :  $g_{\alpha,\beta}(\mathbf{p}_\beta(\mathbf{w}_T, \mathbf{w}_R))$  is a Schur-convex function [Marshall and Olkin, 1979, Palomar and Jiang, 2006], which attains its minimum  $g_{\alpha,\beta}(\mathbf{p}_\beta(\mathbf{w}_T, \mathbf{w}_R)) = 0$  iff  $p_{\beta,k} = 1/N_c$  ( $\forall k$ ).

*Proof.* See Appendix A. □

Property 3 allows us to shed light on the effect of the parameter  $\alpha$ . Firstly, we must note that  $P_\beta$  is a global performance measure directly related to the cost function

$$f_\beta(\mathbf{w}_T, \mathbf{w}_R) = \frac{1}{\beta - 1} \log \left( \frac{P_\beta}{N_c} \right),$$

whereas  $\mathbf{p}_\beta$  represents the distribution of  $P_\beta$  along the data carriers.

From eq. (3.4), we observe that  $f_\alpha(\mathbf{w}_T, \mathbf{w}_R)$  can be seen as a penalized version of the cost function  $f_\beta(\mathbf{w}_T, \mathbf{w}_R)$ . Furthermore, taking into account the Schur-convexity of the penalty term for  $\alpha > \beta$ , we can conclude that  $g_{\alpha,\beta}(\mathbf{p}_\beta(\mathbf{w}_T, \mathbf{w}_R))$  penalizes the *spreading* of the elements of  $\mathbf{p}_\beta(\mathbf{w}_T, \mathbf{w}_R)$ , i.e., it can be interpreted as an alternative measure of the spectral flatness of the equivalent channel [Gray and Markel, 1974, Marshall and Olkin, 1979, Palomar and Jiang, 2006]. On the other hand, since the penalty term  $g_{\alpha,\beta}(\mathbf{p}_\beta(\mathbf{w}_T, \mathbf{w}_R))$  increases

with  $\alpha$ , we can say that, when  $\alpha$  increases, the proposed beamforming criterion tends to flatten the equivalent channel, i.e., the critical data carriers (those with the smallest  $|h_k|$ ) are improved at the expense of a slight degradation of  $f_\beta(\mathbf{w}_T, \mathbf{w}_R)$ . Finally, taking into account that  $g_{\alpha,\beta}(\mathbf{p}_\beta(\mathbf{w}_T, \mathbf{w}_R)) = -g_{\beta,\alpha}(\mathbf{p}_\alpha(\mathbf{w}_T, \mathbf{w}_R))$ , we can obtain similar conclusions for the case  $\alpha < \beta$ . In particular, as  $\alpha$  decreases, the proposed criterion introduces a small increase in  $f_\beta(\mathbf{w}_T, \mathbf{w}_R)$  in order to obtain a higher spread of the terms in  $\mathbf{p}_\beta(\mathbf{w}_T, \mathbf{w}_R)$ .

As an example, consider the MaxSNR ( $\alpha = 0$ ), MaxCAP ( $\alpha = 1$ ), and MinMSE ( $\alpha = 2$ ) cases. Thus, when the parameter increases from  $\alpha = 1$  to  $\alpha = 2$ , the worst subcarriers are improved at the expense of a slight decrease of the equivalent channel capacity. On the other hand, when the design parameter decreases from  $\alpha = 1$  to  $\alpha = 0$ , the energy of the equivalent channel increases at the expense of a reduction in the spectral flatness as well as in capacity.

### 3.4 Optimization Problem and Proposed Algorithm

In this section, the optimization problem derived from the proposed beamforming criterion is analyzed. Although the optimization problem is in general non-convex, approximate solutions can be obtained by means of semidefinite relaxation (SDR) techniques for  $\alpha \geq 0$ . However, the computational cost associated to SDR techniques can be very high even for a moderate number of data subcarriers and antennas. For this reason, we propose a simple gradient search method, which is initialized using a closed-form approximation of the MaxSNR solution. As it will be shown in Section 3.5, this method provides very accurate results.

#### 3.4.1 Optimization Problem

Let us start by rewriting the optimization problem in (3.2) as

$$\begin{aligned} \underset{\mathbf{W}}{\text{minimize}} \quad & \frac{1}{\alpha - 1} \log \left( \frac{1}{N_c} \sum_{k=1}^{N_c} \left( 1 + \gamma |\text{Tr}(\mathbf{H}_k \mathbf{W})|^2 \right)^{1-\alpha} \right), \\ \text{subject to} \quad & \|\mathbf{W}\| = 1, \\ & \text{rank}(\mathbf{W}) = 1, \end{aligned} \quad (3.5)$$

where  $\mathbf{W} = \mathbf{w}_T \mathbf{w}_R^H$  is the rank-one transmit-receive beamforming matrix.<sup>3</sup> Although the solution of the above problem can be obtained in closed-form in some particular cases (see Table 3.1), in general, this is a very difficult problem due to the two following reasons. Firstly, the rank-one constraint on the beamforming matrix  $\mathbf{W}$  is not convex. Secondly, although the relaxation of the rank-one constraint will allow us to obtain good initialization points for the beamvectors, in general the cost function remains still non-convex for most values of  $\alpha$ ,<sup>4</sup> which precludes the application of standard convex optimization techniques [Boyd and Vandenberghe, 2004].

<sup>3</sup>Note that, given a solution  $\mathbf{W}$  of (3.5), the transmit and receive beamformers satisfying  $\|\mathbf{w}_T\| = \|\mathbf{w}_R\| = 1$  can be easily obtained as the singular vectors of  $\mathbf{W}$ .

<sup>4</sup>Specifically, the smoothness of the cost function decreases when  $|\alpha|$  increases.

Table 3.1: Particular cases with closed-form solutions.

System	$\mathbf{w}_T$	$\mathbf{w}_R$
SIMO with $\alpha = 0$ or $\gamma \simeq 0$	1	MRC
MISO with $\alpha = 0$ or $\gamma \simeq 0$	MRT	1
MIMO flat fading	MRT	MRC

### 3.4.2 Analysis of the Cost Function Minima

Although the non-convexity of the optimization problem precludes the obtention of a closed-form solution, we can gain some insight by applying the Lagrange multipliers method and, thus, finding conditions that must be satisfied by any local minima. In this subsection, we show that the local minima of our optimization problem are closely related to that of a weighted energy maximization problem. This relationship can be easily established by combining the two following lemmas.

**Lemma 3.1.** *The local minima of the optimization problem in (3.2) are solutions of the following coupled eigenvalue (EV) problems*

$$\mathbf{R}_{\text{MISO}_\alpha} \mathbf{w}_T = \lambda \mathbf{w}_T, \quad \mathbf{R}_{\text{SIMO}_\alpha} \mathbf{w}_R = \lambda \mathbf{w}_R, \quad (3.6)$$

where  $\lambda = \sum_{k=1}^{N_c} \text{MSE}_k^\alpha |h_k|^2$ ,

$$\mathbf{R}_{\text{MISO}_\alpha} = \sum_{k=1}^{N_c} \text{MSE}_k^\alpha \mathbf{h}_{\text{MISO}_k} \mathbf{h}_{\text{MISO}_k}^H, \quad (3.7)$$

$$\mathbf{R}_{\text{SIMO}_\alpha} = \sum_{k=1}^{N_c} \text{MSE}_k^\alpha \mathbf{h}_{\text{SIMO}_k} \mathbf{h}_{\text{SIMO}_k}^H, \quad (3.8)$$

can be seen as weighted covariance matrices and

$$\mathbf{h}_{\text{MISO}_k} = \mathbf{H}_k^H \mathbf{w}_R, \quad \mathbf{h}_{\text{SIMO}_k} = \mathbf{H}_k \mathbf{w}_T, \quad (3.9)$$

are the MISO (SIMO) channels after fixing the receive (transmit) beamformer.

*Proof.* Let us write the Lagrangian of (3.2) as

$$\mathcal{L}(\mathbf{w}_T, \mathbf{w}_R, \lambda_T, \lambda_R) = f_\alpha(\mathbf{w}_T, \mathbf{w}_R) + \lambda_T \left( \|\mathbf{w}_T\|^2 - 1 \right) + \lambda_R \left( \|\mathbf{w}_R\|^2 - 1 \right),$$

where  $\lambda_T$  and  $\lambda_R$  are the Lagrange multipliers. Solving with respect to  $\mathbf{w}_T$  and  $\mathbf{w}_R$ , we obtain

$$\nabla_{\mathbf{w}_T^*} f_\alpha(\mathbf{w}_T, \mathbf{w}_R) = -\lambda_T \mathbf{w}_T, \quad (3.10)$$

$$\nabla_{\mathbf{w}_R^*} f_\alpha(\mathbf{w}_T, \mathbf{w}_R) = -\lambda_R \mathbf{w}_R, \quad (3.11)$$

where the gradient of the cost function  $f_\alpha(\mathbf{w}_T, \mathbf{w}_R)$  with respect to the transmit and receive beamformers is given by

$$\nabla_{\mathbf{w}_T^*} f_\alpha(\mathbf{w}_T, \mathbf{w}_R) = -\frac{\gamma}{\sum_{k=1}^{N_c} \text{MSE}_k^{\alpha-1}} \mathbf{R}_{\text{MISO}_\alpha} \mathbf{w}_T,$$

$$\nabla_{\mathbf{w}_R^*} f_\alpha(\mathbf{w}_T, \mathbf{w}_R) = -\frac{\gamma}{\sum_{k=1}^{N_c} \text{MSE}_k^{\alpha-1}} \mathbf{R}_{\text{SIMO}_\alpha} \mathbf{w}_R.$$

Now, left-multiplying (3.10) and (3.11) by  $\mathbf{w}_T^H$  and  $\mathbf{w}_R^H$ , and taking into account the unit-energy constraint on the beamformers, we obtain

$$\lambda_T = \gamma \frac{\mathbf{w}_T^H \mathbf{R}_{\text{MISO}_\alpha} \mathbf{w}_T}{\sum_{k=1}^{N_c} \text{MSE}_k^{\alpha-1}}, \quad \lambda_R = \gamma \frac{\mathbf{w}_R^H \mathbf{R}_{\text{SIMO}_\alpha} \mathbf{w}_R}{\sum_{k=1}^{N_c} \text{MSE}_k^{\alpha-1}},$$

which combined with (3.10) and (3.11) yields

$$\begin{aligned} \mathbf{R}_{\text{MISO}_\alpha} \mathbf{w}_T &= \left( \mathbf{w}_T^H \mathbf{R}_{\text{MISO}_\alpha} \mathbf{w}_T \right) \mathbf{w}_T, \\ \mathbf{R}_{\text{SIMO}_\alpha} \mathbf{w}_R &= \left( \mathbf{w}_R^H \mathbf{R}_{\text{SIMO}_\alpha} \mathbf{w}_R \right) \mathbf{w}_R. \end{aligned}$$

Finally, from (3.7) and (3.8), it is easy to see that

$$\mathbf{w}_T^H \mathbf{R}_{\text{MISO}_\alpha} \mathbf{w}_T = \mathbf{w}_R^H \mathbf{R}_{\text{SIMO}_\alpha} \mathbf{w}_R = \sum_{k=1}^{N_c} \text{MSE}_k^\alpha |h_k|^2 = \lambda,$$

which implies  $\lambda_T = \lambda_R$  and proves (3.6).  $\square$

**Lemma 3.2.** Consider the following weighted energy maximization problem<sup>5</sup>

$$\underset{\mathbf{w}_T, \mathbf{w}_R}{\text{minimize}} \quad -\frac{1}{N_c} \sum_{k=1}^{N_c} c_k |h_k|^2 \quad \text{s. t.} \quad \|\mathbf{w}_T\| = \|\mathbf{w}_R\| = 1, \quad (3.12)$$

with  $\mathbf{c} = [c_1, \dots, c_{N_c}]^T \in \mathbb{R}^{N_c \times 1}$ . The local minima of (3.12) are also solutions of the coupled EV problems

$$\mathbf{R}_{\text{MISO}_c} \mathbf{w}_T = \lambda \mathbf{w}_T, \quad \mathbf{R}_{\text{SIMO}_c} \mathbf{w}_R = \lambda \mathbf{w}_R,$$

where  $\lambda = \sum_{k=1}^{N_c} c_k |h_k|^2$  and

$$\begin{aligned} \mathbf{R}_{\text{MISO}_c} &= \sum_{k=1}^{N_c} c_k \mathbf{h}_{\text{MISO}_k} \mathbf{h}_{\text{MISO}_k}^H, \\ \mathbf{R}_{\text{SIMO}_c} &= \sum_{k=1}^{N_c} c_k \mathbf{h}_{\text{SIMO}_k} \mathbf{h}_{\text{SIMO}_k}^H. \end{aligned}$$

*Proof.* The proof is analogous to that of Lemma 3.1.  $\square$

Combining the two previous lemmas, we can conclude that the local minima of the proposed optimization problem are also local minima of (3.12) with weights  $c_k = \text{MSE}_k^\alpha$ . This corroborates our previous finding about the proposed cost function, i.e., for  $\alpha > 0$ , the higher weights are given to the subcarriers with a worst response (larger  $\text{MSE}_k$ ). In other words, for  $\alpha > 0$ , part of the SNR is sacrificed in order to improve the worst data carriers, and the contrary happens for  $\alpha < 0$ .

In general, the EV problems in (3.6) cannot be easily solved due to the fact that the matrices  $\mathbf{R}_{\text{MISO}_\alpha}$  and  $\mathbf{R}_{\text{SIMO}_\alpha}$  depend on the beamformers. However, in the particular MaxSNR or

<sup>5</sup>Note that, in the case of equal weights ( $c_k = c, \forall k$ ), the weighted-energy maximization problem reduces to the MaxSNR criterion.

low-SNR cases<sup>6</sup> ( $\alpha = 0$  or  $\gamma \simeq 0$ , respectively) with MISO or SIMO systems, the optimal solution can be obtained in closed-form. Specifically, the transmit/receive beamformer [Okada and Komaki, 2001, Sandhu and Ho, 2003, Huang and Letaief, 2004b, Rahman et al., 2004, Li et al., 2007b, Wang et al., 2007, Wang et al., 2008] is given by the principal eigenvector of the matrices  $\mathbf{R}_{\text{MISO}_0}$  and  $\mathbf{R}_{\text{SIMO}_0}$  defined in (3.7) and (3.8), which resembles the maximum ratio transmission (MRT) or maximum ratio combining (MRC) technique [Proakis, 1988]. Finally, as summarized in Table 3.1, in the case of flat channels ( $\mathbf{H}_k = \mathbf{H}$ ,  $\forall k$ ), the optimal beamformers are given by the left and right singular vectors of  $\mathbf{H}$ , i.e., as expected, the optimal solution reduces to the MRT-MRC MIMO beamforming technique regardless of  $\alpha$ .

### 3.4.3 Approximated Solution based on Semidefinite Relaxation

An approximated solution to the non-convex optimization problem in (3.5) can be obtained by applying semidefinite relaxation (SDR) techniques. In [Vía et al., 2010a], we give a reformulation of (3.5) suitable for SDR.

Nevertheless, although this reformulation allows us to obtain an approximated solution to the original problem by means of SDR techniques, in general, the computational complexity of the overall algorithm can be prohibitive for practical applications. For these reasons, in this chapter, we focus on the solution given by a gradient search algorithm, which is presented in the next subsection.

### 3.4.4 Proposed Beamforming Algorithm

In order to avoid the computational cost associated to the SDR approach, we propose a simple iterative algorithm, which, equipped with an adequate initialization point that can be obtained in closed form, provides good results in most practical cases. Let us start by briefly describing the initialization method, which obtains an approximated MaxSNR solution in closed form. In particular, for  $\alpha = 0$  (or  $\gamma \simeq 0$ ), the optimization problem in (3.5) can be rewritten as

$$\begin{aligned} & \underset{\mathbf{W}, \mathbf{w}}{\text{maximize}} && \sum_{k=1}^{N_c} \mathbf{w}^H \tilde{\mathbf{H}}_k \mathbf{w}, \\ & \text{subject to} && \|\mathbf{w}\| = 1, \\ & && \text{vec}(\mathbf{W}) = \mathbf{w}, \\ & && \text{rank}(\mathbf{W}) = 1. \end{aligned}$$

Thus, defining  $\mathbf{R} = \sum_{k=1}^{N_c} \tilde{\mathbf{H}}_k$  and relaxing the rank-one constraint we obtain

$$\underset{\mathbf{w}}{\text{maximize}} \quad \mathbf{w}^H \mathbf{R} \mathbf{w}, \quad \text{subject to} \quad \|\mathbf{w}\| = 1,$$

whose solution is given by the principal eigenvector of  $\mathbf{R}$ . As previously pointed out, the matrix  $\mathbf{W}$  obtained from the solution  $\mathbf{w} = \mathbf{v}_{\max}(\mathbf{R})$  will not be rank-one in general, and we will have to apply a randomization step or a similar approach. Here, we propose a simpler alternative, which obtains the best (in the squared-norm sense) rank-one approximation of  $\mathbf{W}$ , i.e., we obtain the transmit and receive beamformers as the left and right singular vectors of  $\mathbf{W}$ .

<sup>6</sup>Property 1 ensures that in the low SNR regime the proposed criterion reduces to the MaxSNR approach regardless of  $\alpha$ .

**Algorithm 3.1** Proposed beamforming algorithm.

---

Select  $\mu$  and  $\alpha$ ; initialize  $\mathbf{w}_T$  and  $\mathbf{w}_R$ .

**repeat**

**Update of the transmit beamformer**

  Obtain the equivalent MISO channels  $\mathbf{h}_{\text{MISO}_k}$  with (3.9).

  Update  $h_k$  and  $\text{MSE}_k$  for  $k = 1, \dots, N_c$ .

  Obtain the matrix  $\mathbf{R}_{\text{MISO}_\alpha}$  with (3.7).

  Update the beamformer  $\mathbf{w}_T$  with (3.13).

  Normalize the solution:  $\mathbf{w}_T = \mathbf{w}_T / \|\mathbf{w}_T\|$ .

**Update of the receive beamformer**

  Obtain the equivalent SIMO channels  $\mathbf{h}_{\text{SIMO}_k}$  with (3.9).

  Update  $h_k$  and  $\text{MSE}_k$  for  $k = 1, \dots, N_c$ .

  Obtain the matrix  $\mathbf{R}_{\text{SIMO}_\alpha}$  with (3.8).

  Update the beamformer  $\mathbf{w}_R$  with (3.14).

  Normalize the solution:  $\mathbf{w}_R = \mathbf{w}_R / \|\mathbf{w}_R\|$ .

**until** Convergence

---

After obtaining the initialization point, the proposed iterative algorithm is based on the following updating rules

$$\mathbf{w}_T(t+1) = \mathbf{w}_T(t) + \mu \mathbf{R}_{\text{MISO}_\alpha}(t) \mathbf{w}_T(t), \quad (3.13)$$

$$\mathbf{w}_R(t+1) = \mathbf{w}_R(t) + \mu \mathbf{R}_{\text{SIMO}_\alpha}(t) \mathbf{w}_R(t), \quad (3.14)$$

where  $\mu$  is a step-size (or regularization parameter) and  $t$  denotes the iteration index. The above expressions, which can be seen as a simple gradient search algorithm, are inspired by the coupled EV problems in (3.6), and they can be interpreted as iterations of a power method for obtaining the solution of (3.6).<sup>7</sup> Specifically, the power method is applied to the regularized matrices  $\mathbf{I} + \mu \mathbf{R}_{\text{MISO}_\alpha}(t)$  and  $\mathbf{I} + \mu \mathbf{R}_{\text{SIMO}_\alpha}(t)$ , where the regularization factor avoids convergence problems due to large variations of the matrices between consecutive iterations. Thus, the overall technique, which includes a normalization step to force the unit energy constraint on the beamformers, is summarized in Algorithm 3.1.

Regarding the computational complexity, it is easy to find that the initialization step has a complexity of order  $\mathcal{O}(n_T^3 n_R^3 + N_c n_T^2 n_R^2)$ , whereas one iteration of the proposed method comes at a cost of approximately  $\mathcal{O}(N_c (n_T + n_R)^2)$ . Thus, 50 iterations of the proposed algorithm in the previous example ( $N_c = 64$  and  $n_T = n_R = 4$ ) would have a cost three orders of magnitude lower than that of the SDR approach previous to the randomization technique (see [Vía et al., 2010a] for more details).

Finally, analogously to other iterative techniques, the proposed algorithm can suffer from local minima. Nevertheless, we have verified by means of numerous simulations that, thanks to the initialization in the approximated MaxSNR solution, the proposed method provides very satisfactory results in most cases. Additionally, we must note that the convergence speed of the proposed algorithm could be further improved by adaptively changing the learning rate  $\mu$ , and that the algorithm can be easily modified to obtain a graduated nonconvexity technique [Blake and Zisserman, 1987]. In particular, we can make a smooth transition from the initialization point ( $\alpha = 0$  or  $\gamma \simeq 0$ ) to the desired value of  $\alpha$  and  $\gamma$  (see [Mohimani et al., 2009] for an application of this idea in the context of sparse representations).

<sup>7</sup>The proposed iterative approach is also closely related to alternating minimization methods [Stoica and Selen, 2004, Huang and Letaief, 2004b, Li et al., 2007b].

### 3.5 Simulation Results

The performance of the proposed technique is illustrated in this section by means of Monte Carlo simulations. In all the experiments, we consider a MIMO system with 64 subcarriers and  $n_T = n_R = 4$  transmit and receive antennas. An i.i.d. Rayleigh MIMO channel model with exponential power delay profile has been assumed. In particular, the total power associated to the  $l$ -th tap is

$$E \left[ \|\mathbf{H}[l]\|^2 \right] = (1 - \rho)\rho^l n_T n_R, \quad l = 0, \dots, L_c - 1,$$

where  $L_c$  is the length of the channel impulse response ( $L_c = 16$  in the simulations), and the exponential parameter  $\rho$  has been selected as  $\rho = 0.7$ . We have focused on the MaxSNR ( $\alpha = 0$ ) [Okada and Komaki, 2001, Sandhu and Ho, 2003, Huang and Letaief, 2004b, Rahman et al., 2004, Li et al., 2007b, Wang et al., 2007], MaxCAP ( $\alpha = 1$ ) and MinMSE ( $\alpha = 2$ ) approaches, which have been compared with a SISO system and with a full MIMO scheme applying maximum ratio transmission (MRT) and maximum ratio combining (MRC) per subcarrier (denoted as Full-MIMO), which can be seen as an upper bound for the performance of any analog antenna combining system.

Each Monte Carlo simulation consists of the generation of a channel realization, the obtention of the transmit and receive beamformers, and the evaluation of the system performance, which can be based on the analysis of the equivalent SISO channel or the transmission of one OFDM symbol. In all the examples, we have performed a minimum of 10,000 Monte Carlo simulations. However, in those experiments involving very low outage probabilities or BER values, the number of simulations has been increased to guarantee a minimum of 10 outage situations (or 10 incorrectly decoded OFDM symbols).

In all the experiments, the step-size has been fixed to  $\mu = 0.1$ , and the convergence criterion is based on the difference between the beamformers in two consecutive iterations. Specifically, the algorithm finishes when the Euclidian distance is lower than  $10^{-3}$ . With these values, the proposed algorithm has never<sup>8</sup> exceeded 50 iterations. As an example, the convergence of the MaxSNR, MaxCAP, and MinMSE algorithms for a SNR of 10 dB is illustrated in Figure 3.3. As seen in this figure, with the initialization in the approximated MaxSNR beamformers, the proposed algorithm converges very fast to the desired solution.

#### 3.5.1 Equivalent Channel Properties

In the first set of examples, we analyze the equivalent channel after beamforming for a fully loaded system ( $N_c = 64$ ). Figure 3.4 shows the frequency response of the equivalent channel for a random channel realization and a SNR  $\gamma = 10$  dB. As can be seen, the parameter  $\alpha$  establishes a tradeoff between the energy and the spectral flatness of the equivalent channel. Furthermore, as expected, the performance of the proposed analog combining schemes is between that of the SISO and Full-MIMO systems.

This effect can be seen more clearly in Figure 3.5, which shows the probability density function (obtained from 10000 random channel realizations) of the squared amplitude of the equivalent channel for a SNR of  $\gamma = 10$  dB. As can be seen, the MaxCAP and MinMSE

<sup>8</sup>Note that, in the cases of low BERs or outage probabilities, we have performed several millions of Monte Carlo simulations.

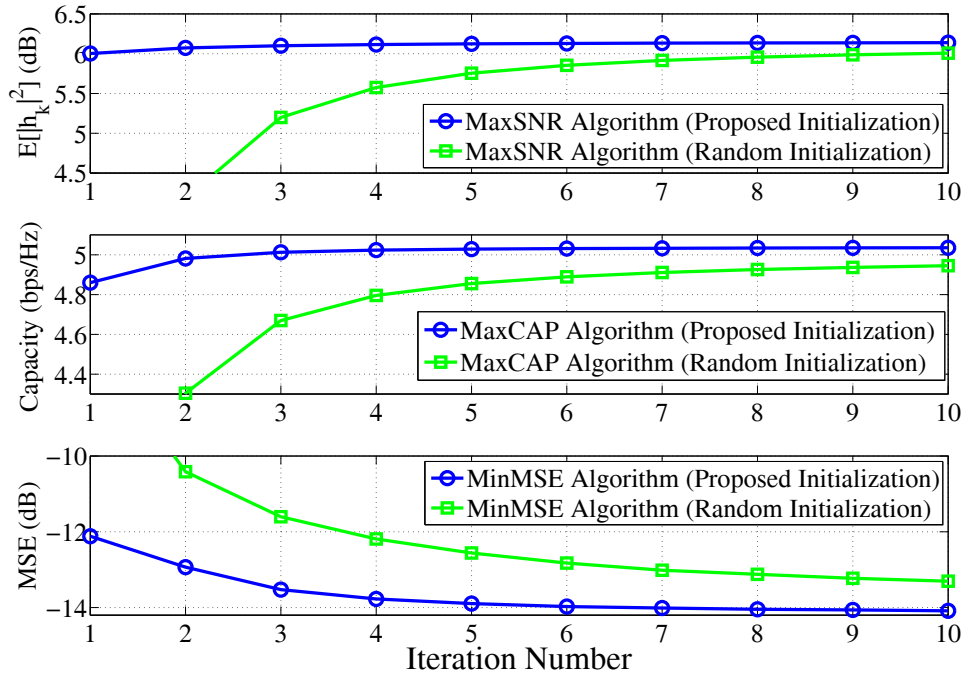


**Figure 3.3:** Convergence of the MaxSNR, MaxCAP, and MinMSE algorithms for SNR=10 dB. Initialization in the approximated MaxSNR solution or in a pair of unit-norm random vectors  $\mathbf{w}_T, \mathbf{w}_R$ .

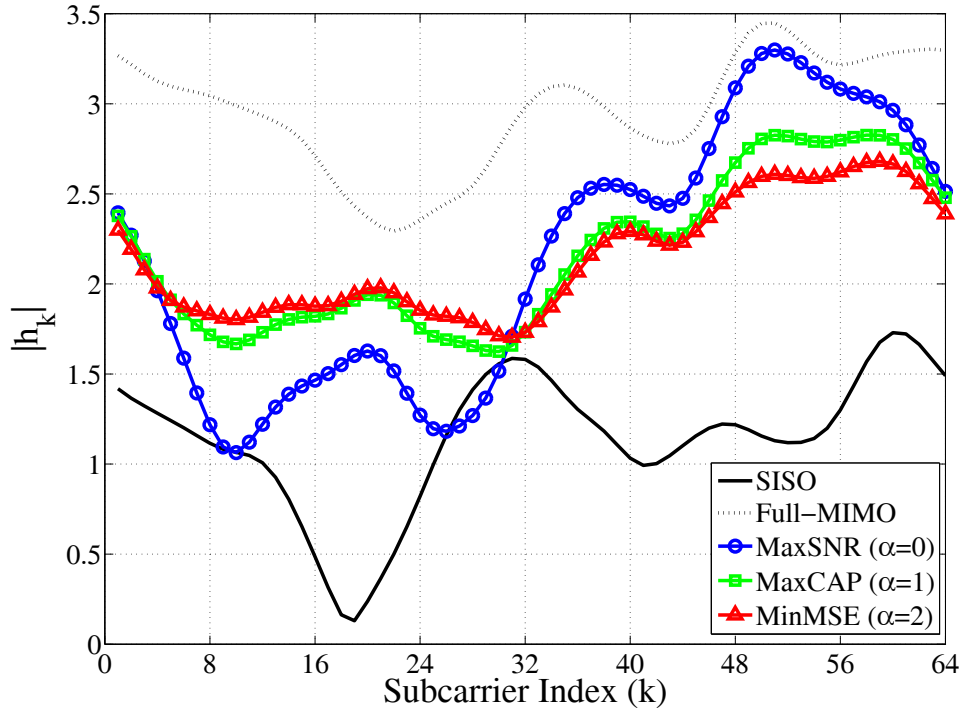


**Figure 3.4:** Channel response  $|h_k|$  after beamforming for a channel realization.

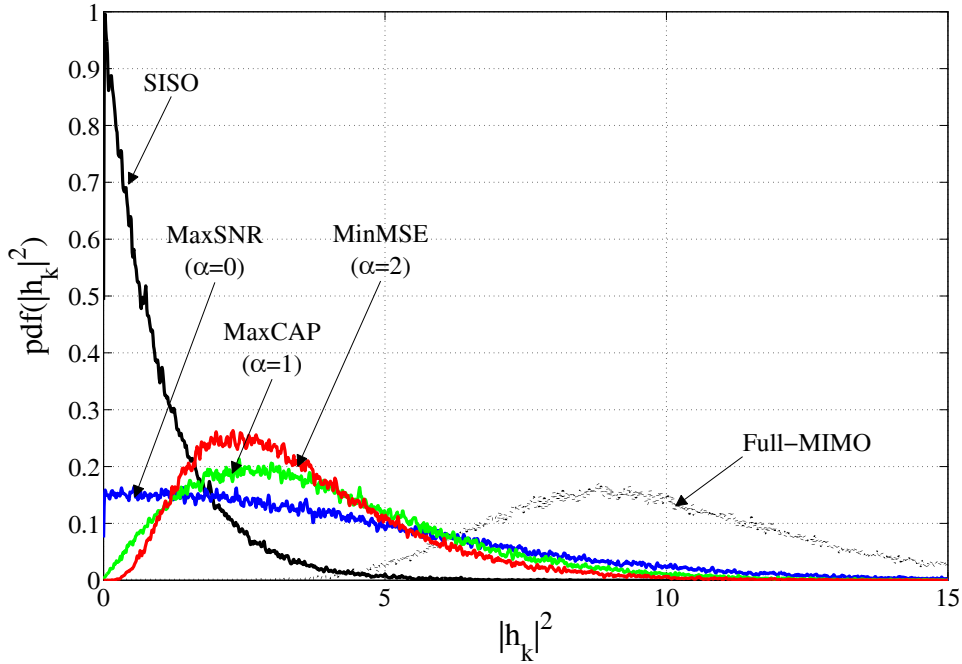


**Figure 3.5:** Probability density function (pdf) of the equivalent channel response  $|h_k|^2$ .  $\gamma = 10$  dB.

approaches avoid values close to zero at the expense of a slight degradation of the overall SNR. Finally, Figures 3.6 and 3.7 show the outage probability for a capacity of 5 bps/Hz and the evolution of the total MSE with the SNR. As expected, the best results are provided by the MaxCAP and MinMSE approaches, respectively, whereas the MaxSNR criterion suffers significant performance degradations.

### 3.5.2 Uncoded Transmissions

The advantage of the proposed MaxCAP and MinMSE criteria over the MaxSNR approach becomes clearer when the system performance is evaluated in terms of BER. Figure 3.8 shows the BER for uncoded QPSK transmissions with  $N_c = 64$  data carriers and LMMSE receivers. As can be seen, the MinMSE approach outperforms the remaining analog combining criteria, which is due to the fact that, for uncoded transmissions, the overall system performance is dominated by the worst data carriers. Therefore, since the MinMSE criterion assigns the highest weights ( $MSE_k^2$ ) to these critical carriers, it provides better results than those of the MaxCAP and MaxSNR approaches.

Finally, Figure 3.9 shows the BER when  $N_c = 64$  QPSK symbols are linearly precoded with the FFT matrix and the receiver is based on the LMMSE criterion. Again, as we will see in Chapter 3, the minimization of the BER is equivalent to the minimization of the MSE [Barbarossa, 2005, Palomar and Jiang, 2006], which explains the good performance of the MinMSE beamforming criterion in this case.

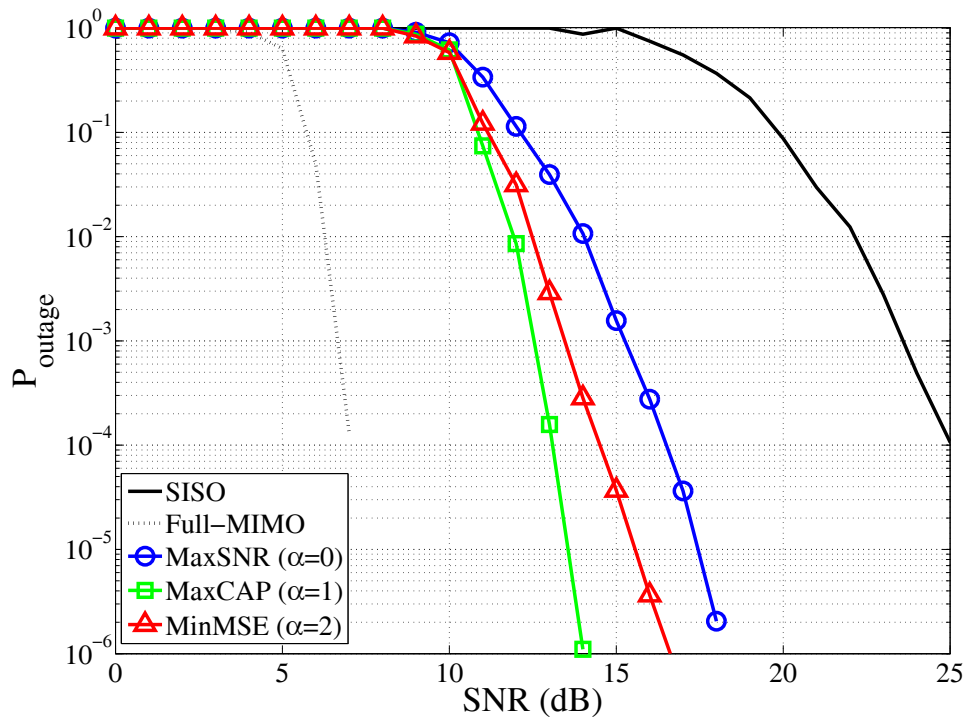


Figure 3.6: Outage probability for a transmission rate of 5 bps/Hz.

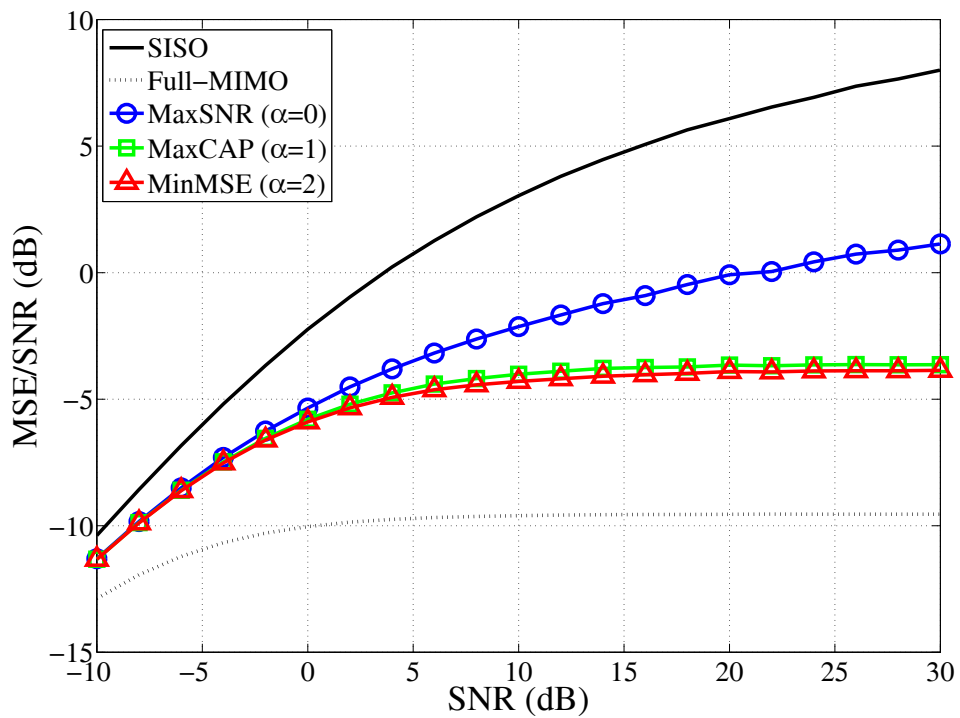


Figure 3.7: Evolution of the total MSE with the SNR.

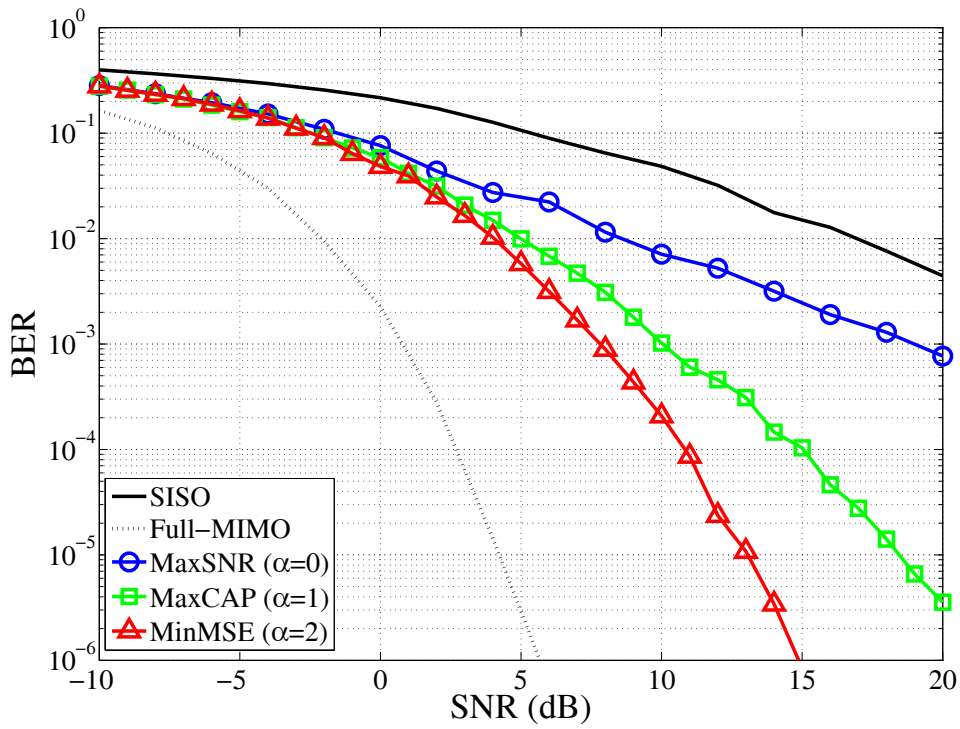


Figure 3.8: Bit error rate for the proposed criteria. Uncoded QPSK symbols.

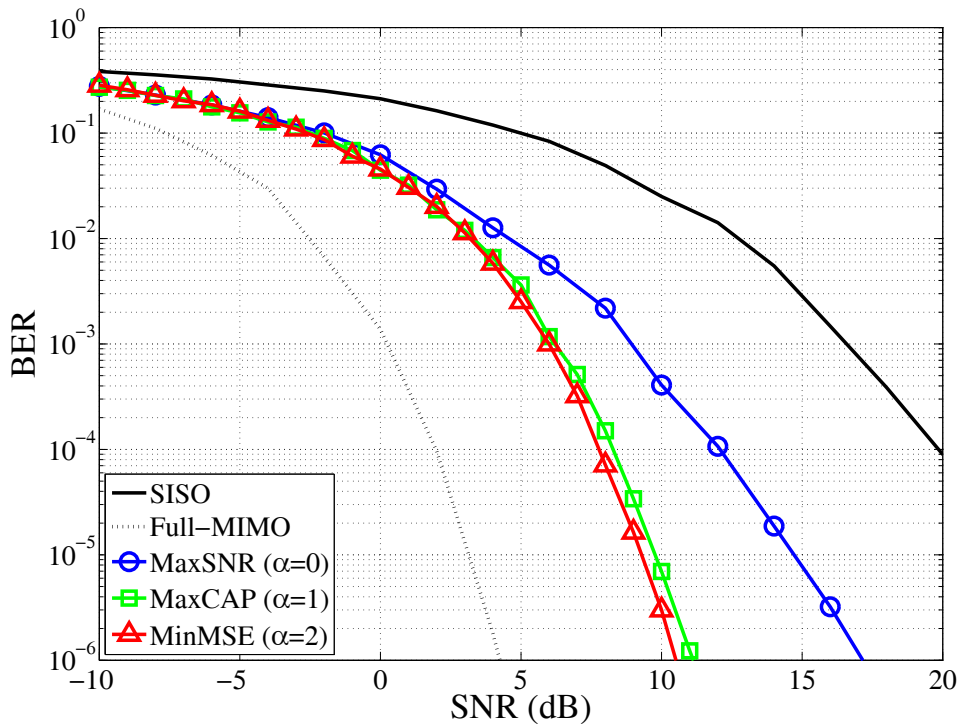
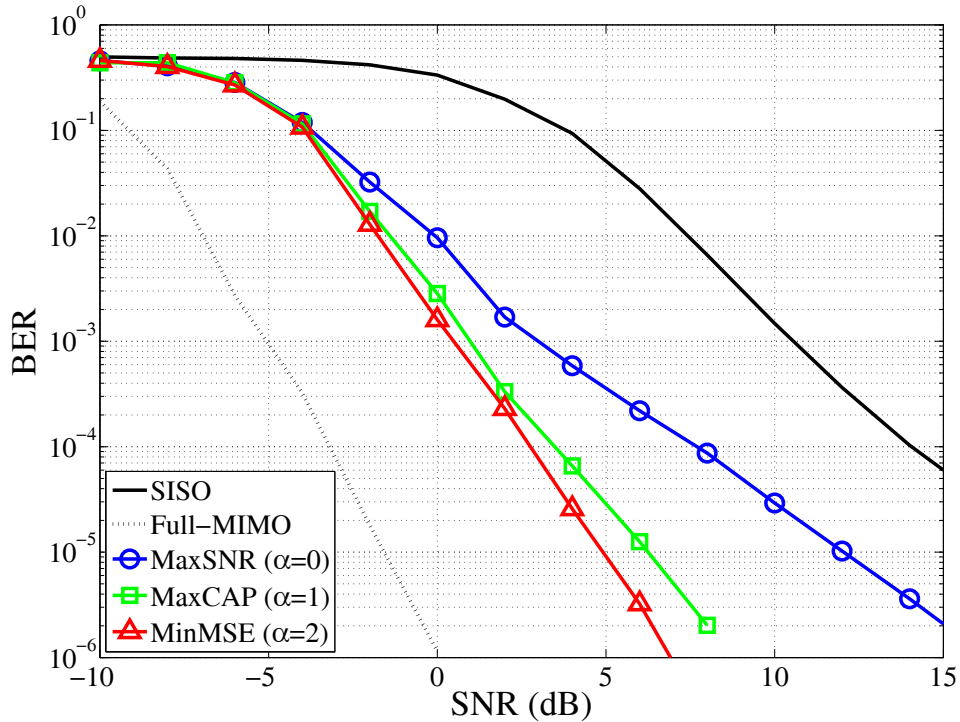


Figure 3.9: Bit error rate for the proposed criteria. QPSK symbols linearly precoded with the FFT matrix.



**Figure 3.10:** BER for a 802.11a based system with transmission rate of 12 Mbps. QPSK signaling and convolutional encoder of rate 1/2.

### 3.5.3 Coded Transmissions

In this pair of examples, the proposed schemes have been evaluated in a more practical situation. In particular, we have adopted the IEEE 802.11a standard [IEEE Std. 802.11a, 1999], because, as it will be shown in Chapter 5, MIMAX project is based on it. This standard uses  $N_c = 48$  out of 64 subcarriers for data transmission. The information bits are encoded with a convolutional code and block interleaved as specified in the standard. Finally, the receiver is based on a soft Viterbi decoder.

In the first example, we have selected a transmission rate of 12 Mbps, which implies QPSK signaling and a convolutional code of rate 1/2. Here, the introduction of a channel encoder could induce us to think that the MaxCAP criterion will outperform the remaining approaches. However, as can be seen in Figure 3.10, the best results are again provided by the MinMSE beamformers. This is due to the fact that we are not using an ideal channel encoder (note that the channel encoder operates on an OFDM symbol basis), which implies that a slight degradation in the capacity can be acceptable in order to obtain a less frequency selective equivalent channel. Finally, the same conclusions can be reached from the experiment with transmission rate of 54 Mbps (64-QAM signaling and 3/4 convolutional encoder), whose results are shown in Figure 3.11.

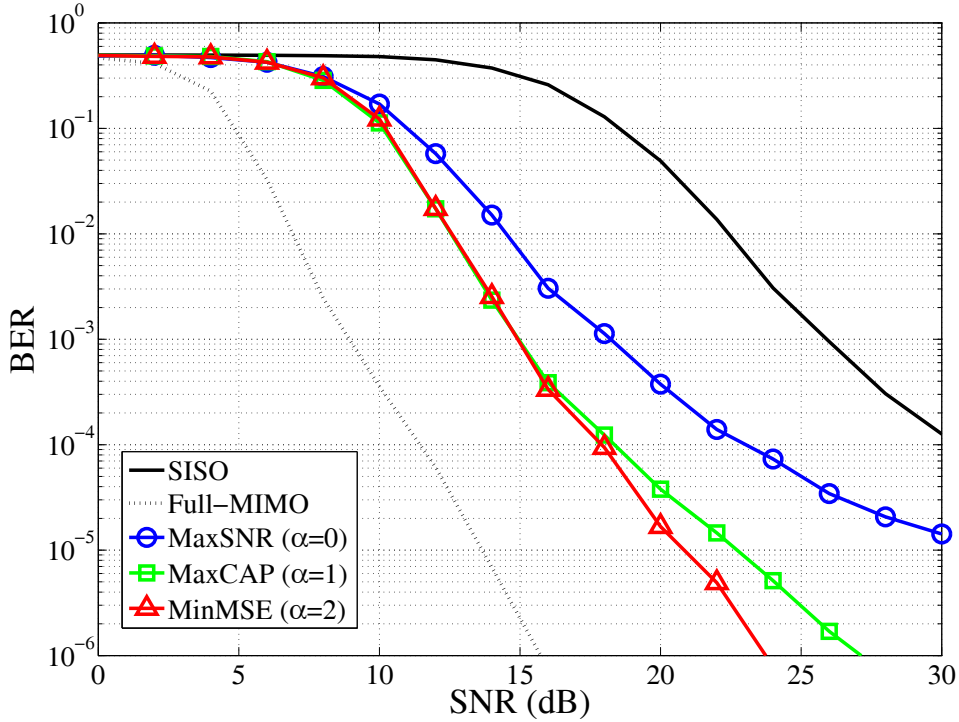


**Figure 3.11:** BER for a 802.11a based system with transmission rate of 54Mbps. 64-QAM signaling and convolutional encoder of rate 3/4.

### 3.5.4 Effects of RF Impairments and Channel Estimation Errors

In the final example, we have included RF impairments and channel estimation errors. In particular, we have obtained least squares (LS) estimates of  $\mathbf{H}_k$  ( $k = 1, \dots, N_c$ ) and  $\sigma^2$  by means of the sequential transmission (using different pairs of orthogonal transmit and receive beamformers) of  $n_T n_R = 16$  training OFDM symbols.<sup>9</sup> The estimated channel and noise variance have been used to obtain the transmit and receive beamformers, which are quantified with a resolution of 5 bits. Additionally, due to RF impairments, there exist a small difference between the quantized weights and the actual values applied in each antenna. This error is modeled as an i.i.d. uniform noise with the same range as that of the quantization error. The obtained results for the MinMSE ( $\alpha = 2$ ) case and 802.11a coded transmissions with a rate of 12Mbps are shown in Figure 3.12, where we can see that the realistic RF-combining system clearly outperforms the idealized SISO system. Furthermore, its performance degradation with respect to an idealized RF-combining system is of approximately 3 dB. Finally, we have verified by means of simulations that the 3 dB gap is mainly due to the effect of the channel estimation errors in the decoding process, and not to the small errors in the beamformers. Therefore, we can conclude that similar degradations would take place in a pre-FFT based system with channel estimation errors.

<sup>9</sup>The channel estimation algorithms and the channel estimation procedure are illustrated in detail in Chapter 5.

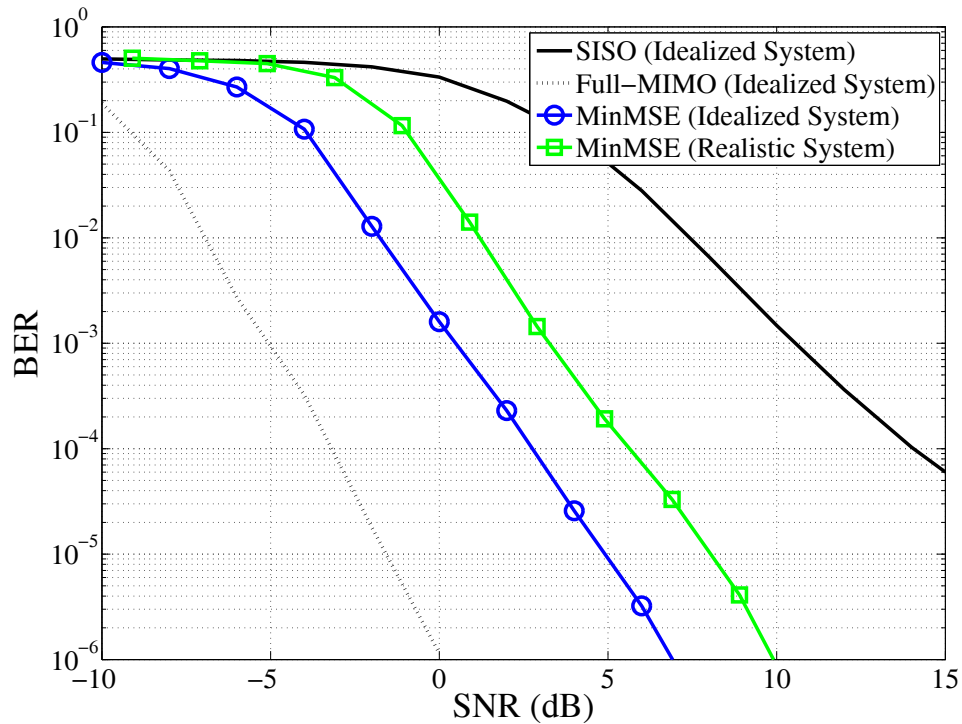


**Figure 3.12:** Performance of the MinMSE criterion in a 802.11a based system with transmission rate of 12 Mbps including the effect of channel estimation errors and RF impairments.

### 3.6 Conclusions

In this chapter, we have proposed a general beamforming criterion for a novel MIMO transceiver, which performs adaptive signal combining in the RF domain. With this new combining architecture and under multi-carrier transmissions, the same pair of transmit-receive beamformers must be applied to all the subcarriers and, due to this coupling, the beamforming design problem poses several new challenges in comparison to conventional MIMO schemes. Considering the case of perfect channel state information at the receiver where also the transmit beamformer is computed and sent to the transmitter, we have proposed a beamforming criterion which depends on a single parameter  $\alpha$ . This parameter establishes a tradeoff between the energy and spectral flatness of the equivalent channel, and allows us to obtain some interesting design criteria. Specifically, the proposed beamforming criterion can be reduced to the maximization of the received SNR (MaxSNR,  $\alpha = 0$ ), the maximization of the system capacity (MaxCAP,  $\alpha = 1$ ), and the minimization of the MSE (MinMSE,  $\alpha = 2$ ) of the optimal linear receiver. In general, the proposed criterion results in a non-convex optimization problem. We have proposed a simple and efficient algorithm, which, with a proper initialization, provides very good results in practical OFDM-based WLAN standards, such as 802.11a. Finally, the numerous simulation results allow us to conclude that, in general, it is a good idea to increase the spectral flatness of the equivalent SISO channel, even at the expense of a slight degradation in the overall SNR. In conclusion, we must note that the corresponding publications supporting the work within this chapter are [Santamaría et al., 2009a, Vía et al., 2010a, Vía et al., 2009c, Vía et al., 2009b, Vía et al., 2009, Vía et al., 2010b], and also the technical report [Santamaría et al., 2009b].



# Statistical Channel Knowledge at the Transmitter Side

## 4.1 Introduction

In the previous chapter, the design problem of the transmit and receive beamformers has been addressed for the novel analog antenna combining architecture. It has been assumed OFDM transmissions for the case of perfect channel state information at both transmitter and the receiver side (CSIT+CSIR). Starting from the results of Chapter 3, in this chapter, we focus on the same OFDM-based system and address the problem of designing the transmit and receive beamformers in the case of statistical channel state information at the transmitter side and perfect channel state information at the receiver side (CDIT+CSIR). The criterion for the design of the beamformers consists in the minimization of the bit error rate (BER) of the linear MMSE receiver. Thus, we firstly show that the optimal time and frequency precoders are given by the discrete Fourier transform (DFT) or the Walsh-Hadamard matrices, and reduce the problem to the design of the beamformers. The design of the receive beamformer follows along the lines of Chapter 3, which considers the problem of point-to-point channels with perfect channel knowledge at both sides of the link. On the other hand, the design of the transmit beamformers resembles the conventional problem of optimal precoding for correlated MIMO channels, and, in fact, the solution is rather similar: power waterfilling and transmission along the strongest modes of the transmit correlation matrix. However, a direct application of this solution to the analog combining architecture would require significant changes in the power of the RF transmit beamformers over time and, therefore, it is inadequate for practical implementation. To avoid this problem, an additional set of constraints to force transmit beamformers of constant energy must be introduced in the optimization problem. These new constraints are satisfied by mixing the strongest modes of the transmit correlation matrix, which is again achieved by the DFT or Walsh-Hadamard matrices. Finally, several simulation examples illustrate the great advantage of the proposed architecture over a conventional SISO system (its natural competitor), whereas the performance degradation with respect to conventional MIMO systems is justified by the reduction in the system cost and power consumption.

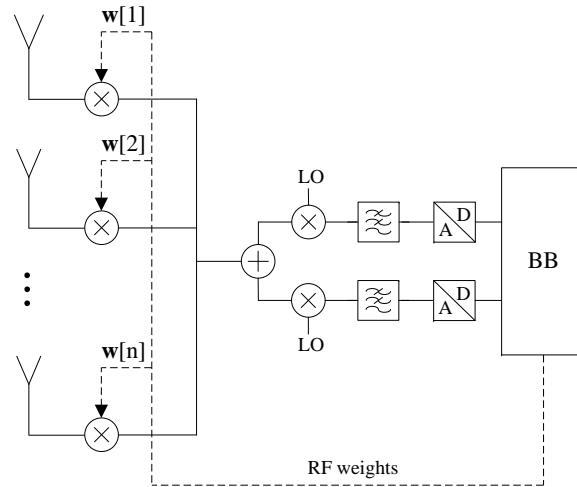


**Figure 4.1:** Analog antenna combining in the RF path for MIMO communications systems. Exemplarily shown for a direct-conversion receiver.

## 4.2 Preliminaries

### 4.2.1 Problem Statement

Conventional MIMO-OFDM baseband schemes have access to the signals at each one of the transmit/receive antennas and consequently can apply a different pair of beamformers in each subcarrier. However, as it can be seen in Figure 4.1, with the novel analog RF combining architecture, a per-carrier beamforming design is not possible since all the subcarriers are affected by the same pair of beamformers. Notice that, with the RF combining architecture, a single FFT must be computed after the analog beamforming (at the receiver side), which notably simplifies the hardware and the system computational complexity. However, this change also complicates the beamforming design problem due to the coupling among subcarriers. The difficulty in the calculation of the beamformers is the same as in the case of CSIT+CSIR studied in Chapter 3. This coupling among all the subcarriers imposes some tradeoffs and represents the main challenge for the design of the beamformers.

### 4.2.2 General System Model

Let us start by defining a transmission block as a set of  $M$  OFDM symbols with  $N_c$  subcarriers. These symbols will be sequentially transmitted and received using possibly  $M$  different pairs of beamformers, which are assumed to change synchronously. Due to technological reasons, the beamformer weights could have to remain fixed during the transmission of several OFDM symbols.<sup>1</sup> However, we must note that in that case the transmission blocks could be distributed among several beamformers as shown in Figure 4.2.

<sup>1</sup>In the case of the MIMAX project, the vector modulators have a settling time nearly 200 ns before the weights remain completely stable.

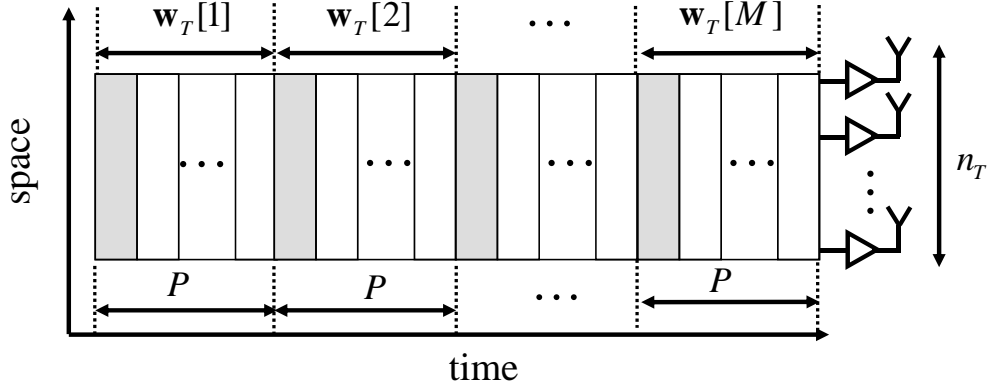


**Figure 4.2:** Distribution of a transmission block. The grey columns denote the  $M$  time and frequency precoded OFDM symbols of one block, which are transmitted using  $M$  different beamformers. In this example, the beamformers remain fixed during the transmission of  $P$  OFDM symbols. The minimum achievable  $P$  depends on the limitations of the RF implementation. On the other hand, the maximum allowable  $P$  is imposed by the temporal coherence of the channel.

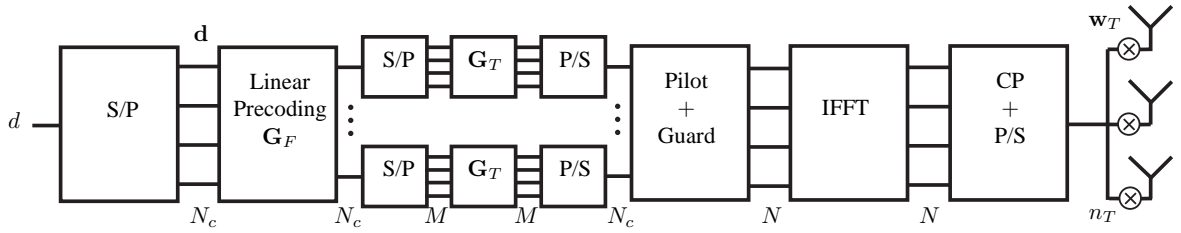


**Figure 4.3:** Block diagram of the OFDM-based transmitter with analog antenna combining. The receiver diagram is equivalent.

Now, considering a data matrix  $\mathbf{D} \in \mathbb{C}^{N_c \times M}$  containing  $N_c M$  information symbols, we can define the transmission matrix

$$\mathbf{S} = \mathbf{G}_F \mathbf{D} \mathbf{G}_T, \quad (4.1)$$

where  $\mathbf{G}_F \in \mathbb{C}^{N_c \times N_c}$  and  $\mathbf{G}_T \in \mathbb{C}^{M \times M}$  are, respectively, the frequency and time precoding matrices. Here, we must note that the total energy associated to a transmission block is

$$\|\mathbf{S}\|^2 = \|\mathbf{s}\|^2 = \|\mathbf{G}\mathbf{d}\|^2,$$

where  $\mathbf{s} = \text{vec}(\mathbf{S})$ ,  $\mathbf{d} = \text{vec}(\mathbf{D})$  and  $\mathbf{G} = \mathbf{G}_T \otimes \mathbf{G}_F$ . Therefore, in order to preserve the transmission energy, the precoding matrices should have a unitary Kronecker product, i.e.,  $\mathbf{G}^H \mathbf{G} = \mathbf{I}$ .

After linear precoding, each row of  $\mathbf{S}$  is associated to a subcarrier, whereas each column represents the linearly precoded data in one OFDM symbol. Thus, the  $n$ -th column of  $\mathbf{S}$  will be transmitted using the transmit and receive beamformers  $\mathbf{w}_T[n] \in \mathbb{C}^{n_T \times 1}$  and  $\mathbf{w}_R[n] \in \mathbb{C}^{n_R \times 1}$ , whose elements are given by the RF weights shown in Figure 4.1. Furthermore, as in Chapter 3, we will assume, without loss of generality, unit energy beamformers, i.e.,  $\|\mathbf{w}_T[n]\| = \|\mathbf{w}_R[n]\| = 1$ . Figure 4.3 shows this OFDM-based scheme at the transmitter side.

With the above definitions and the assumption of a cyclic prefix longer than the impulse response of the MIMO channel, the equivalent system model in the frequency domain for the  $n$ -th pair of beamformers ( $n = 1, \dots, M$ ) can be written as

$$y_k[n] = h_k[n]s_k[n] + n_k[n], \quad k = 1, \dots, N_c,$$

where  $y_k[n]$  denotes the observed signal at the  $k$ -th subcarrier,  $n_k[n]$  denotes the i.i.d. Gaussian noise with variance  $\sigma^2$ ,  $s_k[n]$  is the element in the  $k$ -th row and  $n$ -th column of  $\mathbf{S}$ , and the equivalent channel after transmit and receive beamforming is

$$h_k[n] = \mathbf{w}_R^H[n] \mathbf{H}_k \mathbf{w}_T[n], \quad k = 1, \dots, N_c,$$

where  $\mathbf{H}_k \in \mathbb{C}^{n_R \times n_T}$  represents the response of the MIMO channel at the  $k$ -th subcarrier.

### 4.3 General Analog Beamforming Criterion with Statistical CSIT and Perfect CSIR

In this section, as the main contribution of this chapter, we analyze in detail the case with perfect CSI at the receiver (CSIR) and only correlation CSI at the transmitter. We start by introducing the general problem under frequency selective channels with transmit antenna correlation. Our goal consists in designing the system parameters  $\mathbf{G}_F$ ,  $\mathbf{G}_T$ ,  $\mathbf{w}_T[n]$ , and  $\mathbf{w}_R[n]$  to minimize the average BER associated to the linear minimum mean square (MMSE) receiver, i.e., our optimization problem is

$$\begin{aligned} & \underset{\substack{\mathbf{G}, \mathbf{G}_T, \mathbf{G}_F, \\ \mathbf{w}_T[n], \mathbf{w}_R[n]}}{\text{minimize}} && \text{BER}(\mathbf{G}_T, \mathbf{G}_F, \mathbf{w}_T[n], \mathbf{w}_R[n]), \\ & \text{subject to} && \|\mathbf{w}_T[n]\| = \|\mathbf{w}_R[n]\| = 1, \quad n = 1, \dots, M, \\ & && \mathbf{G}^H \mathbf{G} = \mathbf{I}, \\ & && \mathbf{G} = \mathbf{G}_T \otimes \mathbf{G}_F. \end{aligned}$$

#### 4.3.1 Design of the Frequency and Time Precoders

The design of linear precoding schemes for OFDM systems has been addressed under different criteria in [Barbarossa, 2005, Ma and Giannakis, 2002, Xin et al., 2003]. Here, we follow the same principles applied on the matrix  $\mathbf{G}$ . In the case of linear receivers and QAM constellations, the basic idea consists in writing the average BER as a function of the MSE associated to the information symbols

$$\text{BER} = \frac{1}{N_c M} \sum_{k=1}^{N_c} \sum_{n=1}^M \text{BER}_k[n] = \frac{1}{N_c M} \sum_{k=1}^{N_c} \sum_{n=1}^M g(\text{MSE}_k[n]),$$

where  $\text{BER}_k[n]$  and  $\text{MSE}_k[n]$  represent, respectively, the BER and MSE associated to the information symbol in the  $k$ -th row and  $n$ -th column of  $\mathbf{D}$ , and  $g(\cdot)$  is an increasing convex function.<sup>2</sup>

<sup>2</sup>The convexity of  $g(\cdot)$  for practical BER values can be easily proven [Palomar and Jiang, 2006].

Interestingly, due to the unitarity of the precoding matrix  $\mathbf{G}$  and assuming unit power transmissions without loss of generality (i.e.,  $E[|s_k[n]|^2] = 1$ ), the mean MSE can be written as

$$\overline{\text{MSE}} = \frac{1}{NM} \sum_{k=1}^{N_c} \sum_{n=1}^M \text{MSE}_k[n] = \frac{1}{N_c M} \sum_{k=1}^{N_c} \sum_{n=1}^M \text{MSE}_{s_k}[n],$$

where

$$\text{MSE}_{s_k}[n] = \frac{1}{1 + \gamma |h_k[n]|^2},$$

denotes the MSE in the estimate of  $s_k[n]$ , and  $\gamma = 1/\sigma^2$  is the SNR. Thus, noting that  $\overline{\text{MSE}}$  does not depend on the specific unitary precoding matrix  $\mathbf{G}$ , and taking into account that the average BER is a Schur-convex function [Palomar and Jiang, 2006], we have

$$\text{BER} = \frac{1}{N_c M} \sum_{k=1}^{N_c} \sum_{n=1}^M g(\text{MSE}_k[n]) \geq g(\overline{\text{MSE}}),$$

and the lower bound is achieved when all the  $\text{MSE}_k[n]$  are equal [Barbarossa, 2005, Palomar and Jiang, 2006].

Finally, in order to ensure a uniform distribution of the total MSE among the information symbols, the optimal precoding matrix  $\mathbf{G}$  must be unitary with constant modulus entries, such as the DFT or Walsh-Hadamard matrices [Barbarossa, 2005, Palomar and Jiang, 2006]. However, we must note that, in our particular problem,  $\mathbf{G}$  must also satisfy the Kronecker structure  $\mathbf{G} = \mathbf{G}_T \otimes \mathbf{G}_F$ . Fortunately, the Kronecker product preserves the unitarity and constant modulus properties, i.e., given two unitary matrices  $\mathbf{G}_T$  and  $\mathbf{G}_F$  with constant modulus entries, the product  $\mathbf{G}_T \otimes \mathbf{G}_F$  is unitary with constant modulus elements. Thanks to this property, we can conclude that the separated time and frequency precoding is optimal. To summarize, we propose to independently choose the precoding matrices  $\mathbf{G}_T$  and  $\mathbf{G}_F$  as any DFT or Walsh-Hadamard matrices, which reduces the average BER to

$$\text{BER} = g(\overline{\text{MSE}}) = g\left(\frac{1}{N_c M} \sum_{k=1}^{N_c} \sum_{n=1}^M \frac{1}{1 + \gamma |h_k[n]|^2}\right). \quad (4.2)$$

### 4.3.2 Design of the Beamformers

In this subsection, the transmit and receive beamformers are designed in order to minimize the BER of the analog combining system. The proposed scheme assumes spatially correlated Rayleigh channels, and it is based on a set of  $M$  unit-energy transmit beamformers. At the receiver side, the channel and transmit beamformers are known, which reduces the problem to the minimization of the MSE, i.e., we can use the algorithm in the previous chapter. At the transmitter side, the beamformers would distribute the transmit power isotropically in the case without transmit correlation. Nevertheless, when the channels are spatially correlated at the transmitter side, the design of the optimal beamformers is more intricate.

#### Receive Beamformers

As we have previously shown, under the optimal precoding matrices  $\mathbf{G}_T$  and  $\mathbf{G}_F$ , the problem of minimizing the BER reduces to the minimization of the total MSE. Thus, taking (4.2) into

---

**Algorithm 4.1** Proposed algorithm for the obtention of the receive beamformers.

---

```

Select  $\mu$ .
for  $n = 1$  to  $M$  do
  Take  $\mathbf{w}_T[n]$  calculated in Subsection 4.3.2.
  repeat
    Update  $h_k$  and  $\text{MSE}_k$  for  $k = 1, \dots, N_c$ .
    Obtain the matrix  $\tilde{\mathbf{H}}[n]$  with (4.4).
    Update the beamformer  $\mathbf{w}_R[n]$  with (4.3).
    Normalize the solution:  $\mathbf{w}_R[n] = \mathbf{w}_R[n]/\|\mathbf{w}_R[n]\|$ .
  until Convergence
end for

```

---

account, the criterion for the design of the receive beamformers can be rewritten as the following uncoupled optimization problems

$$\underset{\mathbf{w}_R[n]}{\text{minimize}} \quad \sum_{k=1}^{N_c} \frac{1}{1 + \gamma|h_k[n]|^2}, \quad \text{s.t.} \quad \|\mathbf{w}_R[n]\| = 1,$$

for  $n = 1, \dots, M$ . Since the receiver knows the MIMO channel and the transmit beamformers, the above problems are equivalent to that of designing the minimum MSE (MinMSE) receive beamformer in an analog antenna combining SIMO system under OFDM transmissions. This problem, in the flat-fading case, reduces to the well known maximum ratio combining (MRC) receiver.

In Chapter 3, we have studied the general MIMO problem where the optimization problem (see (3.2)), depending on the real parameter  $\alpha$ , calculates the optimal transmit and receive beamformers for different criteria. In Subsection 3.3.1, we have seen that, for  $\alpha = 2$ , the proposed criterion minimizes the overall MSE. Therefore, we can apply the algorithm proposed in Chapter 3 but fixing the transmit beamformers to those calculated in the next subsection. As seen in Chapter 3, this algorithm rapidly converges to a satisfactory solution when it is initialized with the efficient method called approximated MaxSNR. Specifically, the updating rule is

$$\mathbf{w}_R[n] \leftarrow \mathbf{w}_R[n] + \mu \tilde{\mathbf{H}}[n] \mathbf{w}_R[n], \quad n = 1, \dots, M, \quad (4.3)$$

where

$$\tilde{\mathbf{H}}[n] = \sum_{k=1}^{N_c} \text{MSE}_k^2[n] \mathbf{h}_k[n] \mathbf{h}_k^H[n], \quad n = 1, \dots, M, \quad (4.4)$$

can be seen as a weighted correlation matrix, and

$$\mathbf{h}_k[n] = \mathbf{H}_k \mathbf{w}_T[n], \quad \begin{cases} n = 1, \dots, M, \\ k = 1, \dots, N_c, \end{cases}$$

defines the equivalent frequency selective SIMO channels after fixing the transmit beamformers. Algorithm 4.1 shows the pseudocode for the calculation of the optimal beamformers at the receiver.

### Transmit Beamformers

The design of the transmit beamformers is more involved due to the fact that only correlation CSI is available at the transmitter side. A simple alternative to design the transmit

beamformers consists in the minimization of the pairwise error probability (PEP). However, this is a very difficult problem in the analog antenna combining case, because the receive beamformer depends in a far from trivial way on the transmit beamformer. Here, in order to simplify our analysis, we focus on the case of having full access to the signals at all the receive antennas. Obviously, this can be seen as an upper bound for analog antenna combining schemes, and the bound is tight in the cases of flat-fading channels or only one receive antenna. However, this approximation allows us to obtain a neat formulation for the optimal transmit beamformers, and the bound is reasonably close to the performance of the proposed scheme.

The derivation of the PEP is based on the Chernoff bound [Tarokh et al., 1998]. Thus, the probability of decoding the codeword  $\hat{\mathbf{s}}$  when  $\mathbf{s}$  was transmitted is bounded by

$$P(\mathbf{s} \rightarrow \hat{\mathbf{s}} | \mathbf{H}) \leq \exp \left( -\frac{\gamma}{4} \sum_{k=1}^{N_c} \|\mathbf{H}_k \mathbf{W}_T \text{diag}(\mathbf{s}_k - \hat{\mathbf{s}}_k)\|^2 \right), \quad (4.5)$$

where  $\mathbf{s}_k$  is the  $k$ -th row of  $\mathbf{S}$ ,  $\hat{\mathbf{s}}_k$  is the  $k$ -th row of the matrix  $\hat{\mathbf{S}}$ ,  $\gamma$  is the signal to noise ratio and

$$\mathbf{W}_T = [\mathbf{w}_T[1] \quad \cdots \quad \mathbf{w}_T[M]].$$

Now, the average of (4.5) over the channel fading statistics yields [Jöngren et al., 2002]

$$P(\mathbf{s} \rightarrow \hat{\mathbf{s}}) \leq \left| \mathbf{I} + \frac{\gamma}{4} \sum_{k=1}^{N_c} \mathbf{R}_k^{1/2} \mathbf{E}_k(\mathbf{s} \rightarrow \hat{\mathbf{s}}) \mathbf{R}_k^{1/2} \right|^{-n_R}, \quad (4.6)$$

where  $\mathbf{R}_k$  is the transmit antenna correlation matrix at the  $k$ -th antenna, and  $\mathbf{E}_k(\mathbf{s} \rightarrow \hat{\mathbf{s}})$  is the codeword distance product matrix at the  $k$ -th subcarrier

$$\mathbf{E}_k(\mathbf{s} \rightarrow \hat{\mathbf{s}}) = \mathbf{W}_T \text{diag}(\mathbf{s}_k - \hat{\mathbf{s}}_k) \text{diag}(\mathbf{S}_k - \hat{\mathbf{S}}_k)^H \mathbf{W}_T^H.$$

Assuming that the transmit correlation is the same in all the subcarriers, which is true when the channel impulse response is uncorrelated in time domain [Choi et al., 2007], (4.6) can be rewritten as

$$P(\mathbf{s} \rightarrow \hat{\mathbf{s}}) \leq \left| \mathbf{I} + \frac{\gamma}{4} \mathbf{R}^{1/2} \sum_{k=1}^{N_c} \mathbf{E}_k(\mathbf{s} \rightarrow \hat{\mathbf{s}}) \mathbf{R}^{1/2} \right|^{-n_R}.$$

Obviously, the average PEP (and therefore the choice of  $\mathbf{W}_T$ ) depends on the specific pair of information vectors  $(\mathbf{s}, \hat{\mathbf{s}})$  considered. However, it seems reasonable to minimize the average PEP between the true information vector  $\mathbf{s}$  and its closest neighbor  $\hat{\mathbf{s}}$ , i.e., those vectors which only differ from  $\mathbf{s}$  by one element. With this choice and taking into account that the optimal  $\mathbf{G}_F$  and  $\mathbf{G}_T$  have constant modulus entries, the codeword distance product becomes independent of the transmitted vector, and its expression is reduced to

$$\mathbf{E}(\mathbf{s} \rightarrow \hat{\mathbf{s}}) = \frac{N_c d^2}{n_T} \mathbf{W}_T \mathbf{W}_T^H,$$

where  $d$  is the minimum Euclidean distance in the particular constellation. Thus, the optimization problem in (3.2) reduces to

$$\begin{aligned} & \underset{\mathbf{W}_T}{\text{maximize}} && \left| \mathbf{I} + \frac{\gamma N_c d^2}{4n_T} \mathbf{W}_T^H \mathbf{R} \mathbf{W}_T \right|, \\ & \text{subject to} && \|\mathbf{w}_T[n]\| = 1, \quad n = 1, \dots, n_T. \end{aligned} \quad (4.7)$$

which resembles the precoder design problem in conventional MIMO systems [Biglieri et al., 2007], with the additional constraint in the energy of the columns of  $\mathbf{W}_T$ .

Fortunately, the individual energy constraints can be easily satisfied. In particular, writing the singular value decomposition (SVD)

$$\mathbf{W}_T = \mathbf{U}_T \mathbf{\Lambda} \mathbf{V}_T^H,$$

where  $\mathbf{U}_T, \mathbf{V}_T$  are  $M \times M$  unitary matrices and

$$\mathbf{\Lambda} = \text{diag}([\lambda_1, \dots, \lambda_M]), \quad (4.8)$$

contains the singular values, it is easy to see that the determinant in (4.7) does not depend on the singular vectors  $\mathbf{V}_T$ . Therefore, we can choose  $\mathbf{V}_T$  as any unitary matrix with constant modulus elements, such as the DFT or the Walsh-Hadamard matrix, which ensures [Palomar and Jiang, 2006]

$$\|\mathbf{w}_T[n]\|^2 = \frac{\text{Tr}(\mathbf{\Lambda}^2)}{M} \quad n = 1, \dots, M.$$

With this choice of  $\mathbf{V}_T$ , (4.7) can be rewritten as

$$\underset{\mathbf{U}_T, \mathbf{\Lambda}}{\text{maximize}} \left| \mathbf{I} + \frac{\gamma N_c d^2}{4n_T} \mathbf{\Lambda}^2 \mathbf{U}_T^H \mathbf{R} \mathbf{U}_T \right| \quad \text{s.t.} \quad \text{Tr}(\mathbf{\Lambda}^2) = M,$$

and its solution is obtained from standard majorization results [Palomar and Jiang, 2006]. Specifically, writing the eigenvalue (EV) decomposition of  $\mathbf{R}$  as

$$\mathbf{R} = \mathbf{U}_R \mathbf{\Sigma}^2 \mathbf{U}_R^H, \quad (4.9)$$

the optimal beam directions are directly given by  $\mathbf{U}_T = \mathbf{U}_R$ , whereas the optimal power allocation is obtained from a standard waterfilling technique [Sampath and Paulraj, 2002]

$$\lambda_n^2 = \left( \kappa - \frac{4n_T}{\gamma N_c d^2 \sigma_n^2} \right)_+, \quad n = 1, \dots, M, \quad (4.10)$$

where  $\sigma_n^2$  are the eigenvalues of  $\mathbf{R}$ ,

$$(x)_+ = \begin{cases} 0 & x \leq 0, \\ x & x \geq 0, \end{cases}$$

and  $\kappa$  is the water level, which is chosen to satisfy

$$\text{Tr}(\mathbf{\Lambda}^2) = \sum_{n=1}^{n_T} \lambda_n^2 = M. \quad (4.11)$$

The obtention of the transmit beamformers is summarized in Algorithm 4.2.

---

**Algorithm 4.2** Proposed algorithm for the obtention of the transmit beamformers.

---

- Obtain  $\mathbf{V}_T$  as the  $M \times M$  DFT matrix.
  - Obtain  $\mathbf{U}_T = \mathbf{U}_R$  where  $\mathbf{U}_R$  comes from the EV decomposition of  $\mathbf{R}$  given in (4.9).
  - Obtain the optimal power allocation  $\lambda_n^2$  of the different directions with (4.10) and (4.11).
  - Build  $\mathbf{\Lambda}$  with (4.8).
  - Obtain  $\mathbf{W}_T = \mathbf{U}_T \mathbf{\Lambda} \mathbf{V}_T^H$
- 

### 4.3.3 Further Discussion

In the previous subsections, we have studied the design of the time and frequency precoders and the transmit and receive beamforming matrices in the case of statistical CSI at the transmitter side and perfect CSI at the receiver. For the initial design, we supposed a frequency selective channel with correlation at the transmitter side, but the design of the beamformers can be done in an easier way in some cases.

In the particular case of spatially uncorrelated channels, the design of the transmit beamformers becomes significantly easier. Specifically, the optimal solution is given by

$$\begin{aligned} \mathbf{W}_T^H \mathbf{W}_T &= \mathbf{I} & \text{for } n_T \geq M, \\ \mathbf{W}_T \mathbf{W}_T^H &= \mathbf{I} & \text{for } n_T \leq M, \end{aligned}$$

i.e., as one could expect, the available power has to be isotropically distributed, and the proposed beam-division multiplexing (BDM) scheme is reduced to the orthogonal BDM (OBDM) scheme [Santamaría et al., 2008, Elvira and Vía, 2009]. Furthermore, it is easy to prove that, for  $M \geq n_T$ , the beamformers in  $\mathbf{W}_T$  extract the spatial diversity at the transmitter side ( $n_T$ ) and maximize the coding gain. It is also easy to show that, at high SNRs, the OBDM scheme is optimal.

Note that when the channel is flat-fading the optimal receive beamformer is given by the maximum ratio combining (MRC) receiver

$$\mathbf{w}_R[n] = \frac{\mathbf{H} \mathbf{w}_T[n]}{\|\mathbf{H} \mathbf{w}_T[n]\|} \quad n = 1, \dots, M,$$

which maximizes the SNR and also minimizes the BER [Proakis, 1988]. In this case, the matrix  $\mathbf{G}_F$  is not necessary and the optimal matrix  $\mathbf{G}_T$  can be designed as the DFT matrix or the Walsh-Hadamard [Santamaría et al., 2008, Vía et al., 2009a].

In Chapter 3, the optimal selection of the beamformers has been addressed for the CSIT+CSIR case, while in this chapter we focused on the CDIT+CSIR case. The two remaining configurations are briefly discussed as follows:

- CSIT+CDIR case: When the channel state information is perfect at the transmitter, but only statistical information is available at the receiver, the system is complementary to the CDIT+CSIR discussed in throughout this chapter. Now, the receiver performs BDM, calculating the receive beamformers according to Algorithm 4.2. Once the receive beamformers have been obtained, the transmitter can calculate its transmit beamformers according to the pseudocode given in Algorithm 4.1. Obviously, in both algorithms,  $\mathbf{w}_T$  and  $\mathbf{w}_R$  must be interchanged.
- CDIT+CDIT case: When the channel state information is only statistical at both the transmitter and the receiver, BDM technique at both sides is optimal in order to minimize the BER. Particularly, if the MIMO channel is uncorrelated, or if the channel

correlation can be decomposed in transmit correlation and receive correlation,<sup>3</sup> then, the BDM technique can be independently applied at both sides. In other words, each side can calculate its own beamformers according to Algorithm 4.2.

## 4.4 Simulation Results

In this section, the performance of the proposed technique is evaluated by means of Monte Carlo simulations. In all experiments, we consider a block-fading model in which the channel response remains constant at least for a coherence interval of  $PM$  symbols (i.e., the frame duration seen in Figure 4.2). In all the experiments, we consider a  $4 \times 4$  MIMO system with 64 data subcarriers and QPSK information symbols, which are linearly precoded in frequency and time with the matrices proposed in the previous section. An i.i.d. Rayleigh MIMO channel model with exponential power delay profile has been assumed. In particular, the total power associated to the  $l$ -th tap is

$$E \left[ \|\mathbf{H}[l]\|^2 \right] = (1 - \rho)\rho^l n_T n_R, \quad l = 0, \dots, L_c - 1,$$

where  $L_c$  is the length of the channel impulse response ( $L_c = 20$  in all the simulations). The exponential parameter  $\rho$  has been selected as  $\rho = 0.4$  and  $\rho = 0.7$  to compare the performance of the techniques depending on the frequency selectivity. The transmit correlation matrix has been obtained from the Jakes model [Jakes, 1974] with antenna spacing of  $d_A = 0.1\lambda$  and  $d_A = 0.25\lambda$ , where  $\lambda$  is the wavelength.

### 4.4.1 Studied Schemes

The evaluated systems are summarized as follows:

- Full-MIMO: We consider a scheme performing MRT (Maximum Ratio Transmission) and MRC in each subcarrier. Obviously, this system implies perfect channel knowledge at both sides of the link, and, therefore, it can be seen as a non-tight upper bound for the performance of the proposed system and, in general, for the performance of any analog beamforming scheme.
- SISO: This scheme can be seen as the natural competitor of the proposed system, which provides better performance at the expense of a slight increase of complexity.
- MSE+MSE: MinMSE analog antenna beamforming at the transmitter and at the receiver. This is an upper bound for the performance of the proposed BDM+MSE scheme, since it assumes perfect channel knowledge (or feedback of the optimal beamformer) at the transmitter.
- BDM+MRC: BDM scheme at the transmitter and MRC in each subcarrier at the receiver. This scheme requires a conventional multi-antenna receiver with one down-conversion chain per antenna, and, therefore, it can be seen as an upper bound for the performance of the proposed architecture. Moreover, the PEP analysis in Subsection 4.3.2 provides a tight bound for this system.

<sup>3</sup>The model  $\mathbf{H} = \mathbf{R}_R^{1/2} \mathbf{H}_u \mathbf{R}_T^{1/2}$ , where  $\mathbf{H}_u$  is the i.i.d. Rayleigh MIMO channel matrix,  $\mathbf{R}_R$  is the receive antenna correlation matrix, and  $\mathbf{R}_T$  is the transmit antenna correlation matrix, is not the most general scenario. Nevertheless, this assumption is often done in order to simplify the design of the transceivers [A. Paulraj and Gore, 2003].

- BDM+MSE: The proposed analog antenna combining architecture with BDM at the transmitter and MinMSE beamforming at the receiver.

#### 4.4.2 Experiments

The spatial power distribution at the transmitter side is provided by the waterfilling technique. Figure 4.4 illustrates this power distribution among the different modes under two different scenarios. As it can be seen, the transmission scheme varies from pure beamforming for very low SNRs, which means using  $n_T$  identical beamformers, to isotropic radiation for high SNRs, which is equivalent to the OBDM scheme (i.e.,  $\mathbf{W}_T$  is unitary).

In the second experiment, we have evaluated the BER performance of the proposed scheme (OBDM+MSE) under different conditions. Figures 4.5 and 4.6 show the BER performance when there is not transmit correlation ( $d_A = \infty$ ). The noticeable decrease of BER in OBDM in comparison to the SISO system is due to the spreading of the information symbols along the  $n_T$  beamformers, as well as the optimal analog beamforming at the receiver side. The gap between OBDM and MSE+MSE in both cases is less than 5 dB in medium SNRs and represents the difference between having perfect CSIT or only statistical CSI at the transmitter side. Figures 4.7 and 4.8 show the performance when the transmit correlation is  $d_A = 0.25\lambda$ . In this case, all the curves remain similar except our proposed technique (OBDM+MSE), which improves its performance substantially by reducing the gap with respect to the MSE+MSE technique to 3 dB. Figures 4.9 and 4.10 go deeply into this idea and illustrate that, when the transmit correlation is higher ( $d_A = 0.1\lambda$ ), the difference between both techniques becomes lower, which results from the power being distributed in less modes when the correlation becomes higher. Furthermore, it can be observed that, when the correlation increases, pure beamforming becomes closer to optimal beamforming. We can also notice certain differences between the experiments with distinct frequency selectivity. It can be seen that, when the selectivity increases ( $\rho = 0.7$ ), the gap between the proposed OBDM+MSE and the Full-MIMO scheme also increases, which can be seen as a direct consequence of the fact that the proposed architecture applies the same pair of beamformers to all the subcarriers. Nevertheless, the increase of the selectivity has a greater impact on the MSE+MSE technique, which allows us to conclude that, as the frequency diversity increases, the gap between the optimal analog beamforming schemes with and without CSIT decreases.

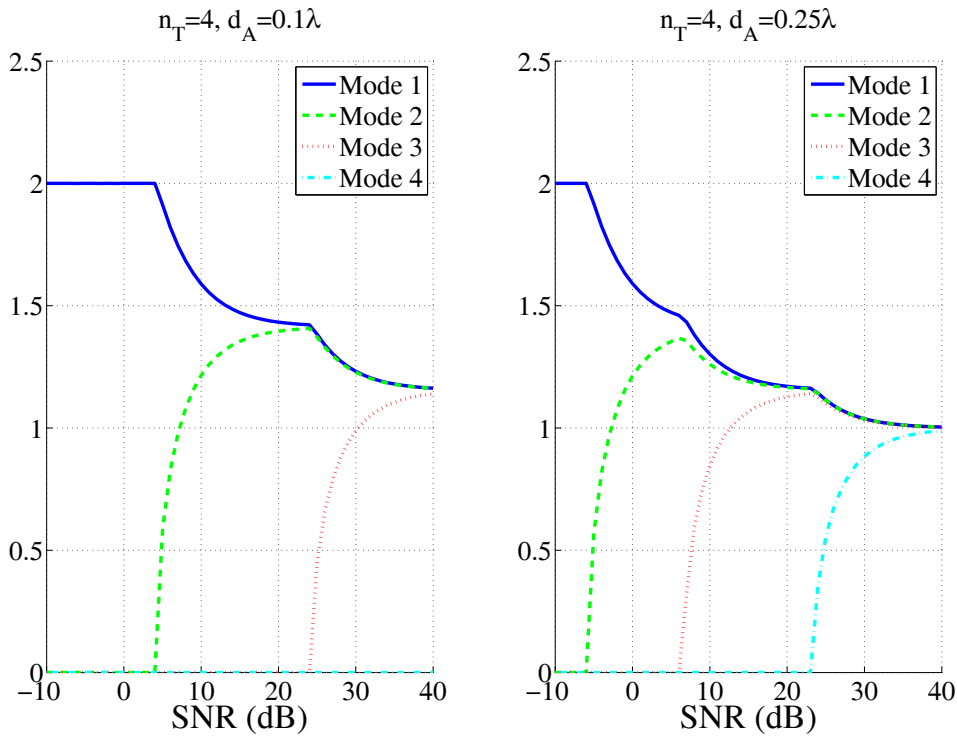


**Figure 4.4:** Spatial power distribution under different scenarios. a)  $n_T = 4, d_A = 0.1\lambda$ . b)  $n_T = 4, d_A = 0.25\lambda$ .

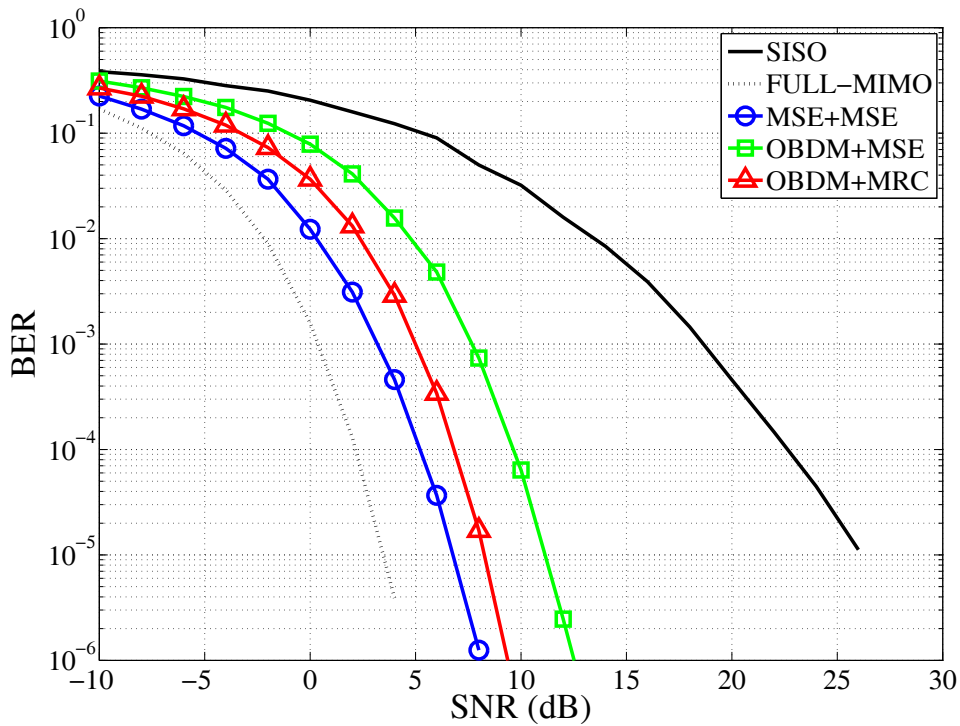


**Figure 4.5:** Bit error rate for the evaluated schemes ( $\rho = 0.4, d_A = \infty$ ).

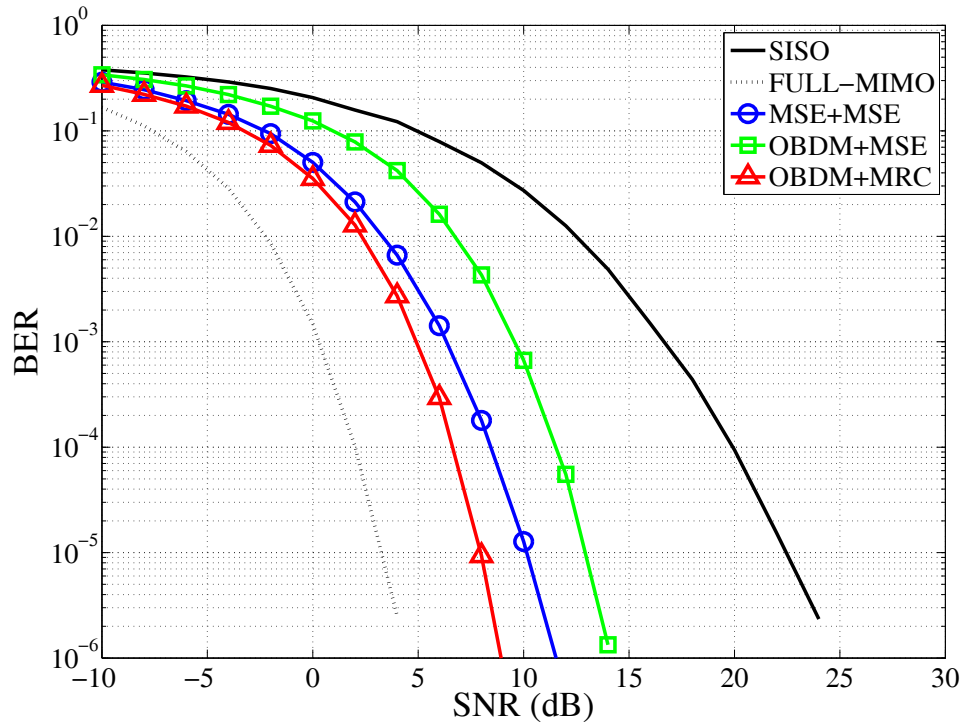


Figure 4.6: Bit error rate for the evaluated schemes ( $\rho = 0.7, d_A = \infty$ ).

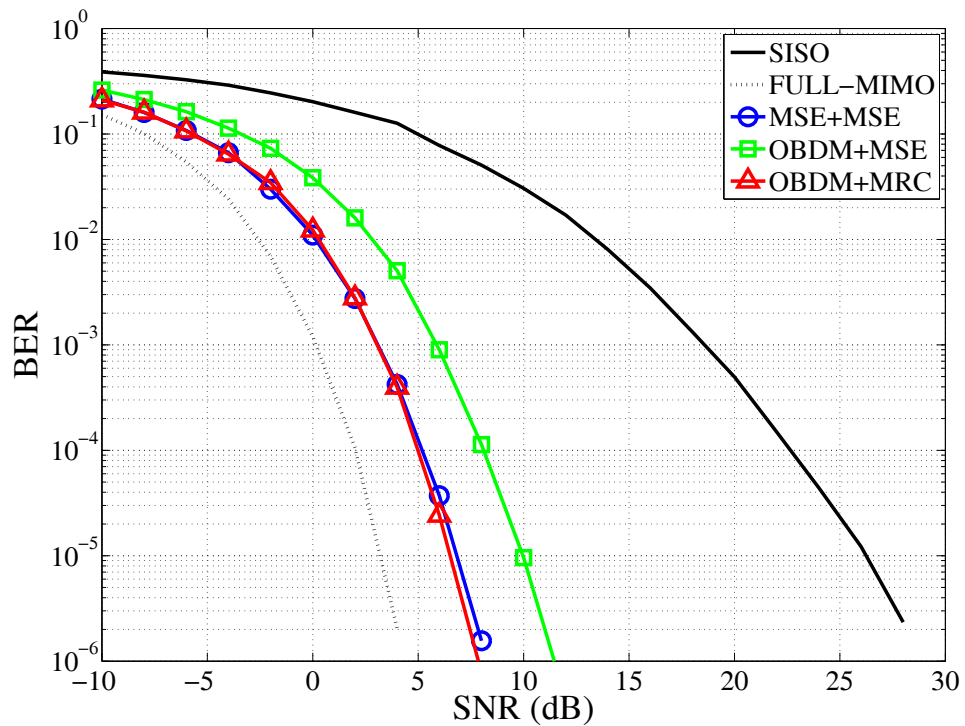


Figure 4.7: Bit error rate for the evaluated schemes ( $\rho = 0.4, d_A = 0.25\lambda$ ).

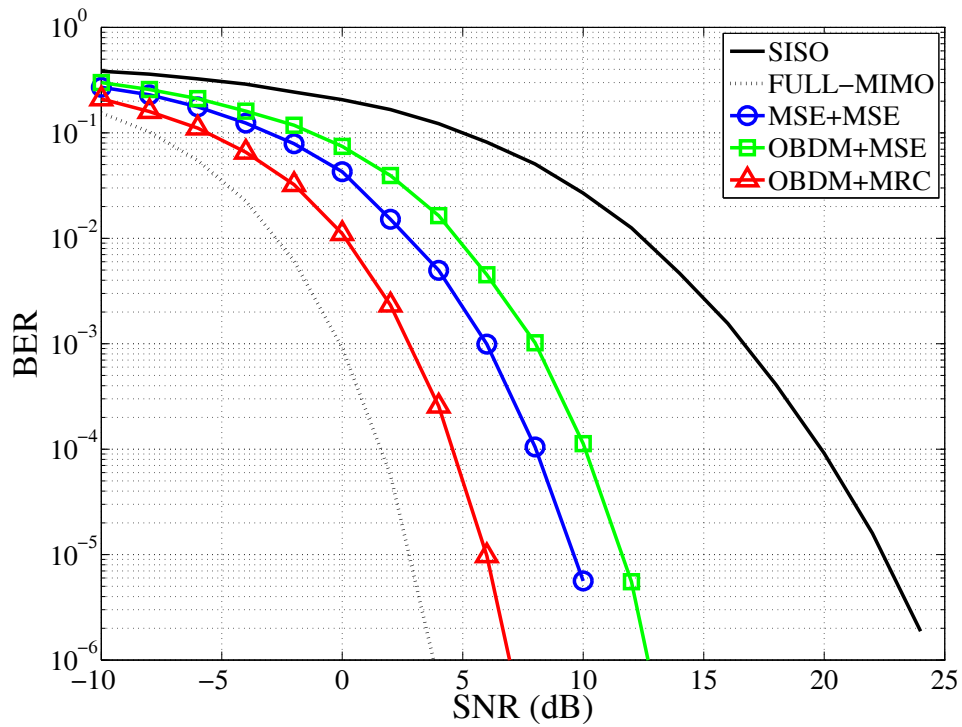


Figure 4.8: Bit error rate for the evaluated schemes ( $\rho = 0.7$ ,  $d_A = 0.25\lambda$ ).

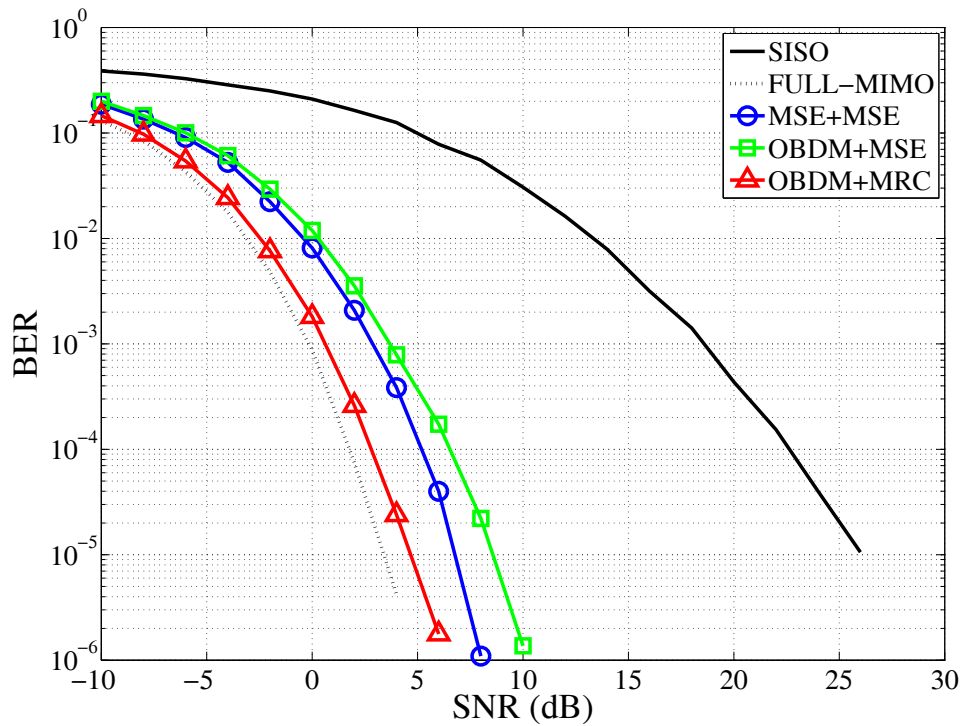


Figure 4.9: Bit error rate for the evaluated schemes ( $\rho = 0.4$ ,  $d_A = 0.1\lambda$ ).

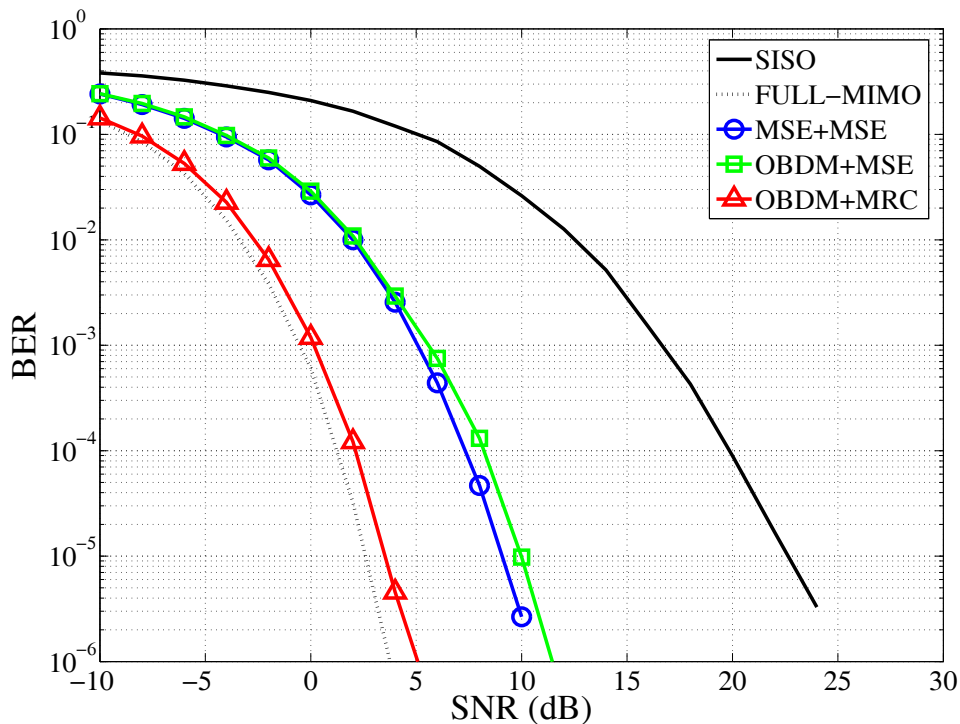


Figure 4.10: Bit error rate for the evaluated schemes ( $\rho = 0.7$ ,  $d_A = 0.1\lambda$ ).

## 4.5 Conclusions

In this chapter, we have addressed the problem of designing the transceiver for a novel architecture based on analog antenna combining. One of the main challenges of the design problem lies into the fact that the same pair of beamformers (RF weights) has to be applied to all the subcarriers, which introduces a coupling that is not present in conventional OFDM-based MIMO systems. Considering the case of perfect channel knowledge at the receiver side, and statistical channel state information at the transmitter, we have shown that the optimal scheme is based on the minimization of the MSE at the receiver (MinMSE receive beamforming), whereas the transmitter distributes the information symbols among different spatial directions, matched to the channel spatial correlation matrix. Interestingly, several simulation examples have shown that the performance of the proposed architecture is not very far from that of alternative schemes, such as the conventional MIMO systems, whereas the hardware and power consumption is closer to that of a conventional SISO system. Finally, notice that the publications that have contributed to this chapter are [Santamaría et al., 2009a, Santamaría et al., 2008, Vía et al., 2009a, Elvira and Vía, 2009, Vía et al., 2009, Elvira and Vía, 2011], and also the technical report [Santamaría et al., 2009b].



Part **II**

**New MIMAX Baseband: Design,  
Implementation, Integration, and  
Real-Time Testing**



# Chapter 5

## MIMAX Concept and Baseband Processor

### 5.1 Introduction

In the first part of this thesis, we introduced a novel MIMO wireless architecture that, based on analog antenna combining and maintaining some of the MIMO advantages, reduces the cost, size, and power consumption of the traditional MIMO transceivers. This novel architecture (also called MIMAX architecture) shifts the spatial processing of the signals, traditionally performed in the baseband processor, to the analog front-end (AFE) at the RF part, where all the branches are weighted by a different complex number and then combined. Therefore, a single RF branch, ADC, and baseband chain are needed at each wireless station.<sup>1</sup> This change of paradigm needs some baseband processing, mainly in order to select weights (or beamformers) that must be applied at the RF part. The algorithms that calculate the beamformers must work in real-time at the baseband processor of the receive station, taking into account the channel state at each moment.

This second part of the thesis is devoted to the design, implementation, and real-time testing of a new baseband processor that will be integrated within a prototype. This so-called MIMAX prototype will implement the novel analog antenna combining architecture and it is intended to demonstrate in real-time the benefits of the new paradigm. Therefore, our work will focus on the baseband processor of the prototype (also called MIMAX baseband processor), which is based on the IEEE 802.11a standard, and that must allow the features of novel architecture. For this purpose, some new blocks will be added to an existent 802.11a baseband processor, focusing on the block that computes the optimal weights. This block will perform one of the beamforming algorithms described in the first part of this thesis. Finally, the new MIMAX baseband processor will be integrated in a complete transceiver (MIMAX prototype), which is based on the analog antenna combining architecture. The final goal of this second part of the thesis is the real-time testing and validation of the MIMAX baseband processor, and we will also participate in a jointly demonstration of the complete integrated MIMAX prototype.

In this chapter, we start reviewing the MIMAX concept. Then, we present the MIMAX prototype (or demonstrator), describing all the substantial parts and introducing the IEEE 802.11a standard, which the MIMAX demonstrator is based on. We focus on the MIMAX baseband processor, describing the new blocks needed for allowing the MIMAX functional-

---

<sup>1</sup>For instance, in an OFDM-based system, a single FFT is needed at the baseband processor of each station

ties. These blocks will be designed, implemented, and tested in subsequent chapters. Finally, we also describe the channel estimation process as well as the new MIMAX frame that is required for training the channel.

## 5.2 MIMAX Project

MIMAX is a European Union funded project within the 7<sup>th</sup> Framework Programme that develops smart radio access in wireless communication networks. As seen in the introductory Chapter 2, the MIMAX architecture is based on an analog antenna combining architecture. In Section 2.5, we have introduced some of the basic characteristics of the project as well as the different partners. In this section, we start reviewing the MIMAX concept introducing the MIMAX demonstrator. Particularly, we will focus on the baseband processor of the demonstrator where our work will take place.

### 5.2.1 MIMAX Concept

Unlike conventional full MIMO systems, where combining and processing of the antenna signals is performed in the digital baseband (see Figure 5.1), the main novelty of a MIMAX transceiver consists in shifting the spatial processing of the signals to the analog RF front-end (see Figure 5.2). In the MIMAX receiver, only one path is needed after the combination of all branches in RF, which reduces notably the terminal cost and the power consumption.

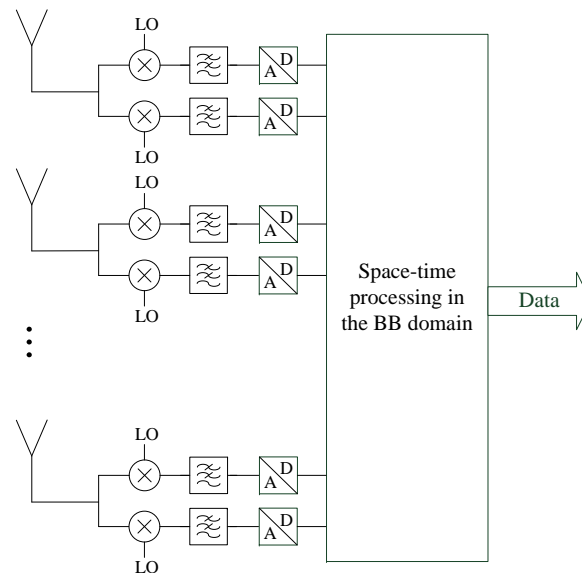


**Figure 5.1:** Full MIMO concept with space-time processing in the baseband.

### 5.2.2 MIMAX Demonstrator

In order to demonstrate the MIMAX capabilities within the context of the MIMAX project, a compact laptop-sized demonstrator (MIMAX prototype) has been developed and integrated.

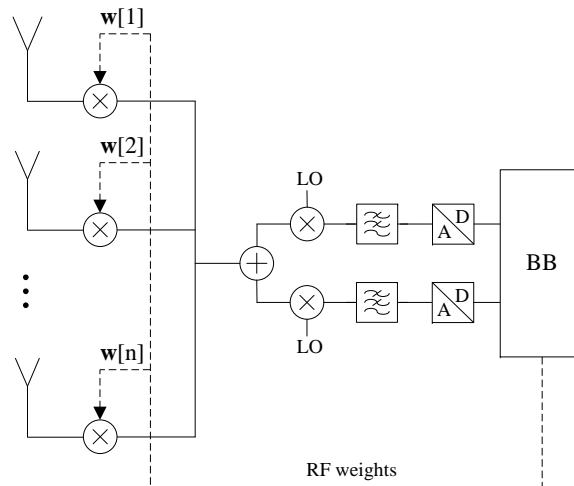


**Figure 5.2:** MIMAX concept: spatial processing in the AFE in the RF part and temporal digital processing in the baseband.

Most of the efforts of the project have been aimed at the development, integration, and testing of this demonstrator. In particular, our work has been directed to the development of some new parts to be included within an existing baseband processor.<sup>2</sup> In Subsection 5.3, we will give a first introduction to the work carried out within the existing baseband processor, and, in the following chapters, we will address the design, generation, integration, and real-time testing of the new baseband parts.

Figure 5.3 shows an overview of the MIMAX system architecture. Besides the antenna array, three different boards can be distinguished. The first board is a PCMCIA card that contains the MAC processor implemented in an FPGA. The second board consists of the baseband processor and the RF control unit (RFCU), both implemented in the same FPGA. The latter board contains the analog part of the transceiver, i.e., the analog front-end (AFE).

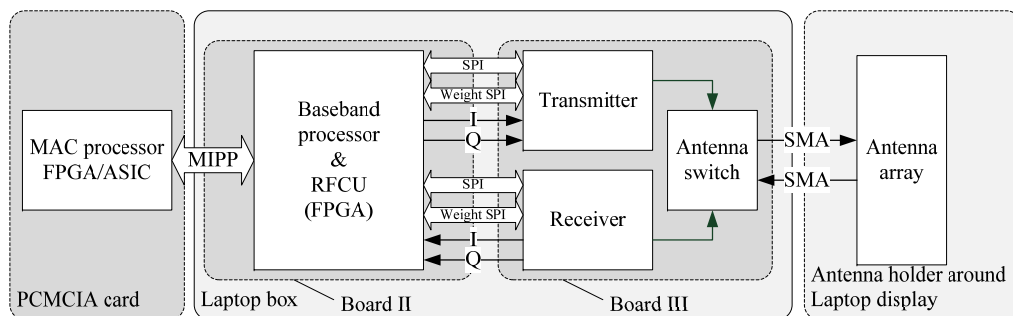


**Figure 5.3:** MIMAX system architecture.

The demonstrator contains all developed subsystems. A laptop has been chosen as a form factor, because it compromises between the users' acceptance and an optimal placement of four antennas with low correlation between the single elements. The demonstrator consists

<sup>2</sup>Throughout this chapter, we will see that the baseband processor of the MIMAX demonstrator is based on the IEEE 802.11a standard, which only allows SISO transmissions.

of a commercially available laptop, which has the ability to execute the applications and services for MIMAX. Beneath the laptop is installed a second box (called the MIMAX box), with same size and shape, which includes the developed subsystems, i.e., the MAC processor, the baseband processor, and the AFE. The antennas are mounted on the back of the laptop display or completely integrated in the display cover of the laptop. Figure 5.4 shows the front of the demonstrator, and, in Figure 5.5, its back is shown.

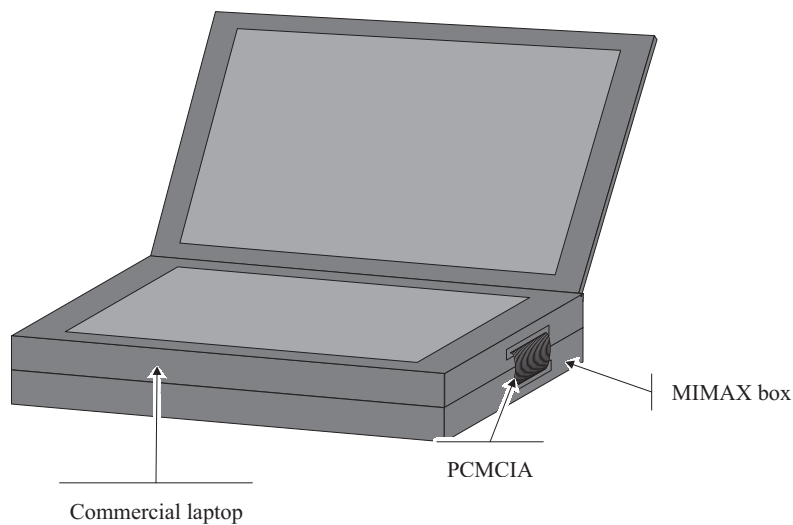


**Figure 5.4:** MIMAX demonstrator architecture (front).

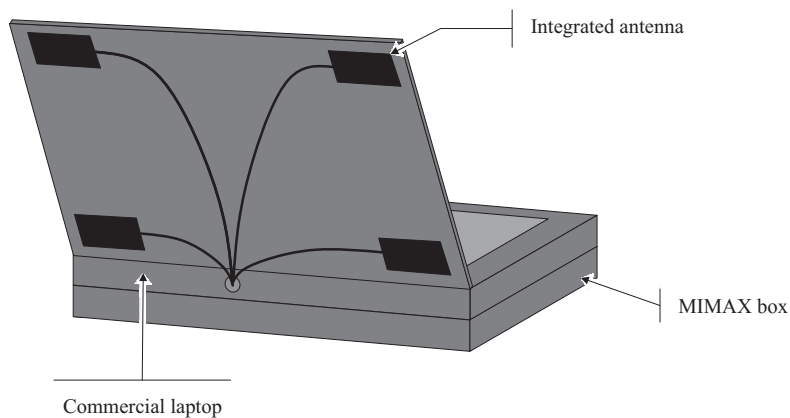


**Figure 5.5:** MIMAX demonstrator architecture (back).

### 5.2.3 Focusing on WLAN: IEEE 802.11a Standard

Although the MIMAX paradigm can be applied to any wireless technology, market and technology analysis within the MIMAX project revealed that wireless local area networks (WLAN) offer the biggest turnover potential. Especially, IEEE 802.11a standard provides promising market prospects for exploiting the benefits of spatial signal processing in RF because of

compact form factors, high revenues, and competitive system costs. Therefore, an integrated RF-MIMO transceiver, which features enhanced 802.11a MIMO modes but still supports backward compatibility to the wireless technology, has been developed as a hardware prototype.

The choice of the IEEE 802.11a standard as a reference technology was also made in order to reduce developing time, effort, and risks, implementing the new MIMAX concept on basis of an already existing WLAN standard. Moreover, the chosen 802.11a standard works at an unlicensed frequency band that allows a good compromise between the application demands and the technological constraints.

The IEEE 802.11a standard is an amendment to the original IEEE 802.11 specification and is also widely used today, along with the 802.11b, 802.11g, and 802.11n, as a wireless networking transmission method commonly known as *Wi-Fi*. The IEEE 802.11 standard allows the transmission by frequency-hopping spread spectrum (FHSS), direct sequence spread spectrum (DSSS), or orthogonal frequency-division multiplexing (OFDM), with all of them in the Industrial Scientific Medical (ISM) frequency band at 2.4 GHz. Nevertheless, IEEE 802.11a standard operates in the 5 GHz band, which is less used than the 2.4 GHz band. The developed demonstrator works in this 5 GHz band where 802.11a specifies an OFDM physical layer (PHY).

#### 5.2.4 MIMAX Compatibility with Legacy 802.11a Devices

The MIMAX devices are intended to communicate also with legacy 802.11a devices. Nevertheless, as we will show in next section, a special MIMAX frame (called MIMAX frame II or training frame) is needed to allow the estimation of the MIMO channel, which is necessary for calculating the optimal weights in MIMAX. Therefore, the use of the RTS/CTS MAC procedure, described in the 802.11 standard family, has been proposed in order to prevent a legacy 802.11a terminal from receiving these non-standard frames. Furthermore, even if the special MIMAX frame was detected and processed by a legacy 802.11a terminal, it would be discarded by the baseband processor after decoding the SIGNAL field.

The RTS/CTS procedure is also needed in the case that all the terminals in the network implement MIMAX. A station in an IEEE 802.11a network under distributed coordination function (DCF) does not normally know from which peer station it will receive the next frame. This precludes benefiting from the MIMAX architecture, because a station cannot set in advance the optimal weights. A solution is to use the short frame exchange sequence RTS/CTS (Request-to-send / Clear-to-send) defined in [IEEE Std. 802.11a, 1999] before any data frame transfer begins. This allows the identification of the peer station from the RTS frame and to set the weights accordingly. Typically, after the RTS/CTS exchange, the channel is estimated within a training process (see Section 5.4 for more details), and then several data frames are transmitted. Further information about the application of the RTS/CTS procedure can be found in [Kraemer et al., 2008, Santamaría et al., 2009b].

### 5.3 Baseband Processor

This section is of particular importance, because we address the main contribution of this second part of the thesis, which is the development of the new MIMAX baseband processor. Throughout this section, we briefly overview this MIMAX baseband processor, which, as the MAC layer, is based on the IEEE 802.11a standard. We propose some of the changes that have been performed in the legacy 802.11a baseband processor, including the new MIMAX

baseband blocks whose development will be addressed in the next chapters. Notice, that the main work done on this MIMAX demonstrator consists of the design, implementation, and real-time testing of these new baseband blocks, which have been inserted into the conventional 802.11a baseband processor. Refer [Kraemer et al., 2008] for further discussion about the MIMAX baseband specifications.

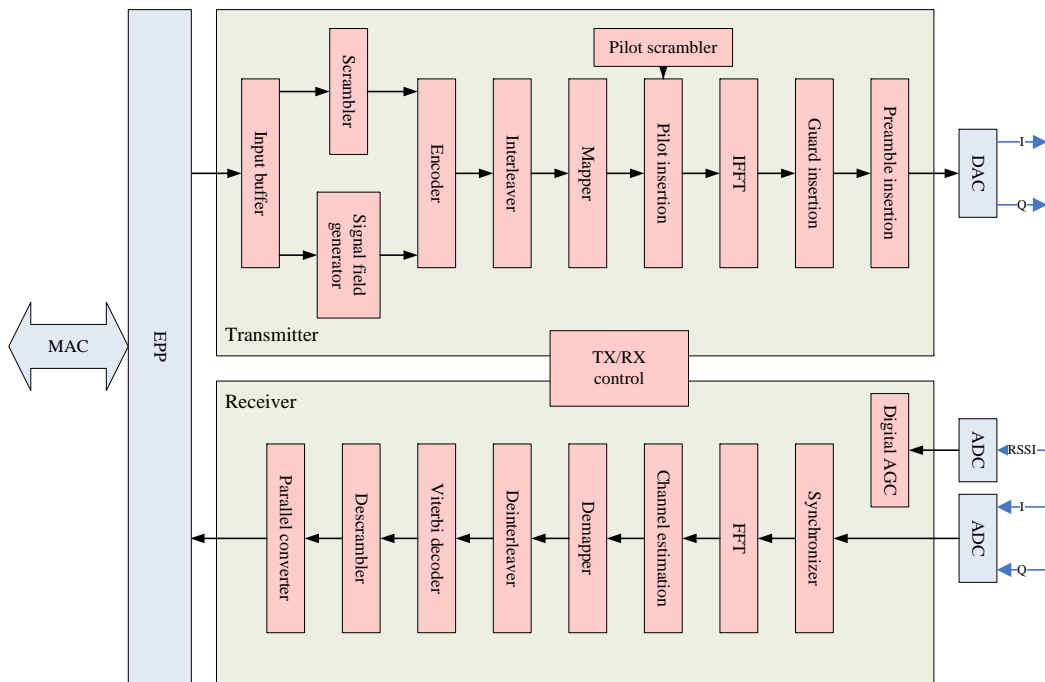


Figure 5.6: Block diagram of the IEEE802.11a baseband processor.

### 5.3.1 802.11a PHY Layer: A Technical Overview

Figure 5.6 shows the block diagram of the conventional 802.11a baseband processor. Although it is not the objective of this work to go into detail about the technical description of the IEEE 802.11a standard, we present a short summary of the main points of this standard:<sup>3</sup>

- Information data rate: 6, 9, 12, 18, 24, 36, 48, and 54 Mbps
- Error correcting code:  $K = 7$  (64 states) convolutional code
- Coding rate:  $1/2, 2/3, 3/4$
- Number of subcarriers: 52 (4 for pilots and 48 for data)
- OFDM symbol duration:  $4 \mu s$
- Guard interval:  $0.8 \mu s$
- Occupied bandwidth: 16.6 MHz

<sup>3</sup>All the details about the physical and MAC layers of this standard can be found in [IEEE Std. 802.11a, 1999]

### 5.3.2 Types of Frames

In order to satisfy the requirements of the new architecture, it has been proposed that the MIMAX PHY-layer uses two different frame types, both being compliant with the IEEE standard. The first frame is identical to the legacy frame defined in [IEEE Std. 802.11a, 1999], and, therefore, it is completely compatible with a legacy 802.11a terminal. In the second frame, specific controls and formats of MIMAX have been introduced in order to permit the estimation of the MIMO channel between two MIMAX terminals.

#### MIMAX Frame I (Legacy 802.11a Frame)

Figure 5.7a shows the MIMAX frame I, which is identical to the IEEE 802.11a frame. The MIMAX frame I is utilized to allow compatibility with 802.11a terminals for data communications, and also to transmit data between MIMAX transceivers. The MIMAX frame I, also called the legacy frame, is used for transmitting data, beacons, and RTS/CTS frames. This ensures the compatibility with legacy 802.11a devices. The SIGNAL field of the legacy frame is also shown in Figure 5.8a.

#### MIMAX Frame II (Training Frame)

This frame is introduced to allow MIMO channel estimation and the subsequent calculation of the optimal beamformers. For this reason, this frame is also called the training frame. Figure 5.7b shows the MIMAX frame II, which includes a modified SIGNAL field (the so-called MIMAX SIGNAL field). The rest of the frame is the same as the standard frame except stuffing and training symbols are used in place of DATA symbols. As shown in Figure 5.7b, after the MIMAX SIGNAL field, there are a number of stuffing or dummy symbols. These stuffing symbols provide the time required by the TX/RX Control Block to recognize the incoming frame as a training frame and then settling adequately the RF weights in every training symbol. After the stuffing symbols, the frame includes a variable number of OFDM training symbols for MIMO channel estimation.<sup>4</sup> Each pair of transmit and receive beamformers changes from training symbol to training symbol during the transmission/reception of the frame. The number of these training symbols is determined in the MIMAX SIGNAL field and agrees with the number of equivalent SISO channels to be estimated. A more detailed discussion about the channel estimation process is given in Section 5.4.

The MIMAX SIGNAL field occupies a single OFDM symbol and must use BPSK modulation without scrambling, convolutional coding at  $R=1/2$ , interleaving, and pilot insertion (the same encoding procedure as the SIGNAL field of the MIMAX frame I). The MIMAX SIGNAL field is composed of 24 bits, as illustrated in Figure 5.8b. The bits 0 to 3 encode the MIMAX configuration. Bit 4 is always set to one to identify the MIMAX frame II; otherwise, the baseband processor identifies the frame as a MIMAX frame I.<sup>5</sup> Bits 6 and 7 ( $N_{TX}$  field) indicate the number of active transmitter antennas  $n_T$ , and bits 9 and 10 ( $N_{RX}$ ) correspond to the number of receive antennas  $n_R$ . For WLAN indoor applications, a maximum number of four antennas is considered; however, bits 5 and 8 of the SIGNAL field are reserved and can be used to define a higher number antennas (up to eight antennas). Bits 12 to 16 encode

<sup>4</sup>A training symbol is identical to the long training symbol of the standard, i.e., it is an OFDM symbol of 4  $\mu$ s duration where all the subcarriers are modulated by  $\pm 1$ . The predefined sequence of  $\pm 1$  symbols can be found in [IEEE Std. 802.11a, 1999].

<sup>5</sup>A conventional 802.11a receiver discards the MIMAX frame II due to this bit.

the number of training symbols,  $N_T$  (up to maximum number of 32 training symbols). Bit 11 is also reserved and allows for an increase of this number up to 64 training symbols, which could be of interest if a higher number of antennas is used. Bits 18 to 23 are the signal tail bits and must be set to zero to finish the signal SIGNAL decoding properly.

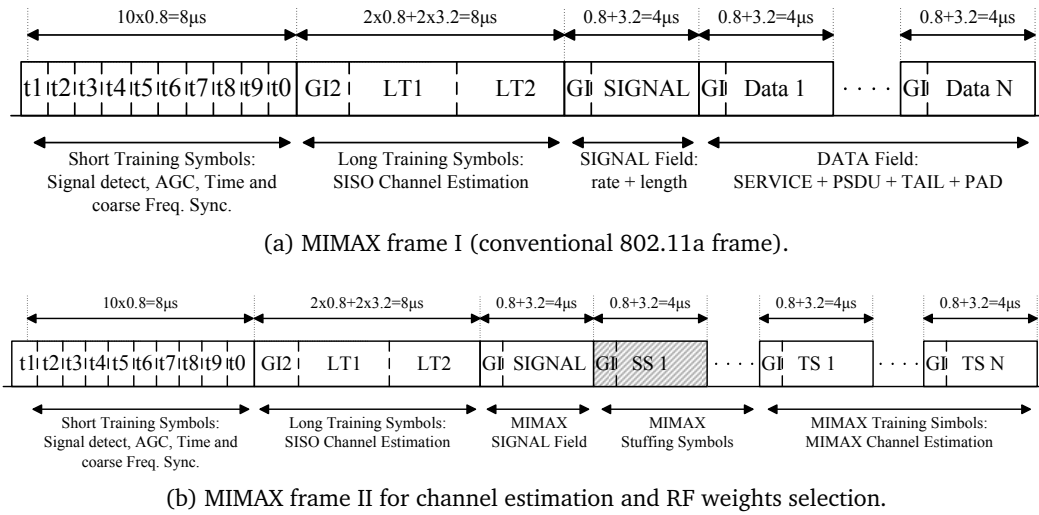


Figure 5.7: Types of frames in MIMAX.

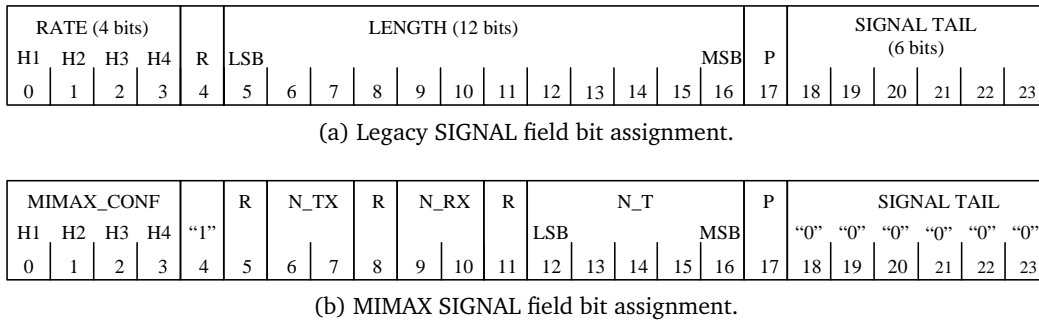


Figure 5.8: SIGNAL field bit assignments for both types of frames in MIMAX.

### 5.3.3 Required Baseband Processor Changes

According to the new needs of the physical layer, some changes in the 802.11a baseband processor architecture have been proposed. Figure 5.9 shows the MIMAX baseband with the new proposed baseband blocks, where the following parts can be distinguished:

- The blocks of the **legacy 802.11a baseband processor** with the transmitter, the receiver, and the TX/RX Control Block (pink color).
- The **MIMAX modules** (orange color) and RF control unit (dark blue color)

- The different interfaces with the MAC processor and with the AFE (light blue color)

Therefore, these changes consist of some modifications within the legacy 802.11a baseband processor plus the addition of the new baseband modules, which are introduced in the next subsection.

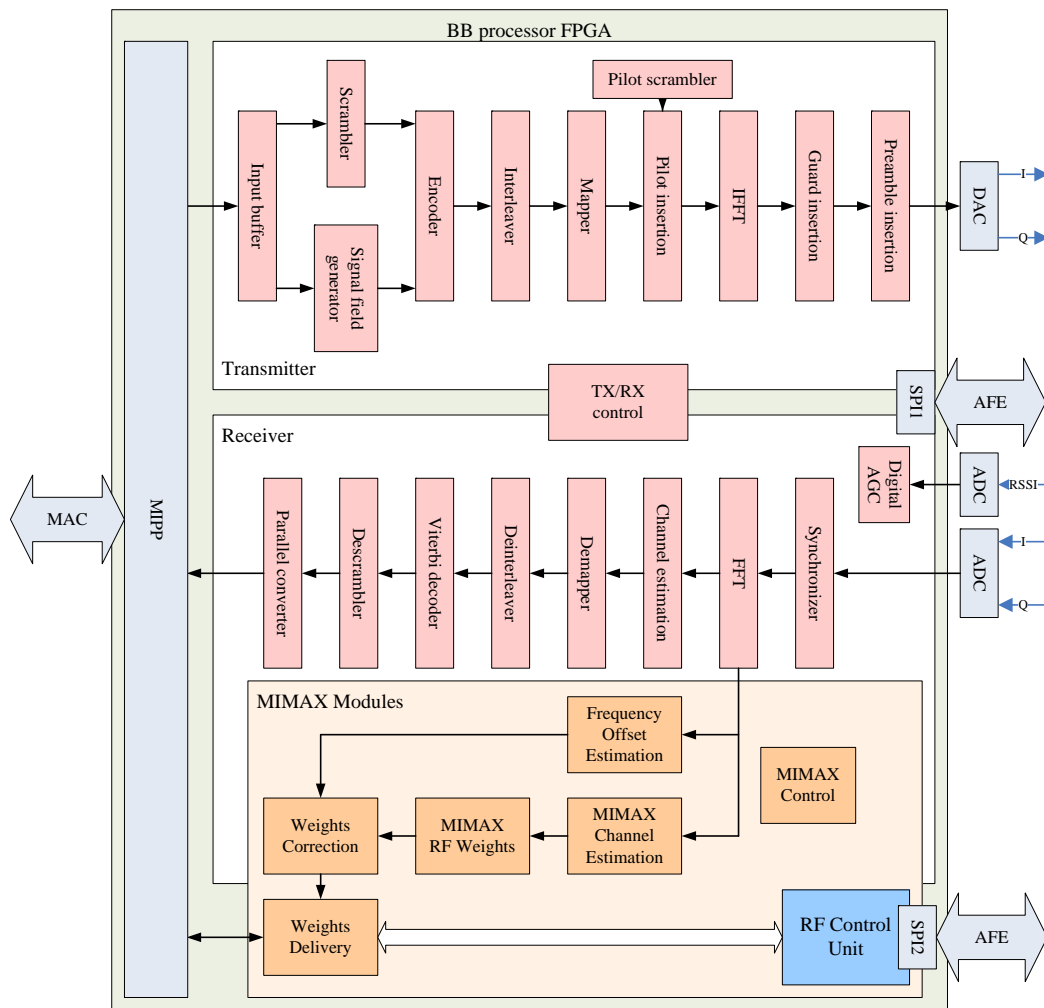


Figure 5.9: Block diagram of the MIMAX baseband processor architecture.

### 5.3.4 New MIMAX Baseband Blocks

The main change in the MIMAX baseband processor consists in the addition of some new blocks. In Chapter 6, we will address the design of each block, and, therefore, a detailed description will be also given. Most of these blocks (except the RF control unit block and the Weights Delivery Block) are only activated when a training frame is received, i.e., they work during an insignificant portion of the total time. This means that the power consumption of the MIMAX baseband processor is practically identical to that of the legacy 802.11a.

In this subsection, we present these new baseband modules with a brief explanation of their functionality.

### MIMAX Channel Estimator

This module estimates the  $n_R \times n_T$  MIMO channel based on the  $n_R n_T$  training OFDM symbols of the received training frame. It works in the frequency domain by taking the FFT signal provided by the IEEE 802.11a processor as input.

### RF Weights

The MIMAX RF Weights Block takes the estimated MIMO channel as input and computes the optimal transmit/receive beamforming weights using an algorithm among those explored in the first part of this thesis. It is the most important block in terms of complexity and FPGA resources, and it has also been the most challenging block during the design process, as we will see in the next chapter.

### Frequency Offset Estimation

At the output of the conventional IEEE 802.11a Synchronizer, there is always a residual frequency error. Moreover, when the channel must be estimated through the training frame, the pilots of the OFDM symbols cannot be used for the correction of this frequency error.<sup>6</sup> As a consequence of these two facts, it is recommended to include a Frequency Offset Estimation working in parallel with the MIMAX Channel Estimator and RF weights modules in order to reduce the residual frequency error. To estimate the frequency offset, it would be necessary to transmit an additional OFDM symbol after the last OFDM training symbol. This symbol must be transmitted and received under the same pair of beamformers as a previous OFDM symbol taken as a reference.<sup>7</sup> The inclusion of the Frequency Offset Estimation Block within the MIMAX baseband processor is optional. In Chapter 7, we will discuss whether this block is included or not. The decision will depend on the observed frequency error at the output of the Synchronizer and the degradation of the system performance due to an incorrect calculation of the optimal weights.

### Weights Correction

This module rotates the optimal weights (calculated by the RF Weights Block) in order to compensate the effects of the residual frequency offset after the Synchronizer. It also rotates the optimal weights depending on the specific transmit/receive beamformers used during training (see Subsection 5.4.2).

### Weights Delivery

It transfers the calculated optimal weights to the MAC processor when they are ready (the weight updating). In addition, it allows the application (from the baseband) of the predefined set of weights during training (the weight setting) and transferring (from MAC to the analog front-end through the RF control unit) the optimal or default weights during data transmission or reception (the weight uploading).

<sup>6</sup>Note that every training symbols is transmitted and received under a different pair of beamformers.

<sup>7</sup>The reference OFDM symbol could be one of the two long training symbols, transmitted and received with the default weights, in order to ensure that the signal level is adequate. Otherwise, the signal level could be too low or too high to ensure a good frequency offset estimation.

### MIMAX Control

This module controls the signal and data flow among all MIMAX blocks. It receives from the Tx/Rx Control Block information included in the MIMAX SIGNAL field (the number of transmit/receive antennas and the number of training symbols), as well as some activation and synchronization signals.

### RF Control Unit

This is a control interface between the baseband processor and the MIMAX functionalities of the analog front-end (AFE). This block is intended to compensate the RF impairments (mainly correlation between the real and the imaginary part of the weights), which is achieved by calibration. It is an integrated part of the baseband processor and is the only new baseband block, whose development has not been carried out by the Advanced Signal Processing Group (GTAS).

#### 5.3.5 New MIMAX Blocks Interfaces

In the previous subsection, we have introduced the new MIMAX baseband blocks, which are also shown in Figure 5.9 in an orange color. Hereafter, we present the interfaces within the 802.11a baseband processor.

#### Inputs

- **Reset signal:** The new MIMAX blocks are reset when the whole baseband processor is reset and also after the reception of a training frame. This signal is generated by the TX/RX Control Block of the baseband processor.
- **FFT output signals:** They are the two (I/Q) data outputs of the FFT Block. Each one has a 16-bit representation. They represent serially the 52 samples of all the OFDM symbols including the two long training symbols and the SIGNAL field.
- **FFT output valid signal:** It is the boolean signal, coming from the FFT Block, which enables the FFT output signals.
- **N\_TX and N\_RX:** These 2-bit signals represent the number of transmit and receive antennas, respectively, i.e., they can represent a number up to four antennas. As we will see in Subsection 6.8, the RF Weights Block can calculate the optimal weights, for a system where the transmit and receive antennas are at most four. This block needs to know both number antennas to perform the algorithms. This information is coded in the MIMAX SIGNAL field as shown in Figure 5.8b.
- **Incoming training frame signal:** The new MIMAX blocks must know whether the incoming frame is a training frame or not. Note that the output of the FFT is active for both kinds of frames (legacy and training frame). This boolean signal enables the MIMAX blocks when receiving a training frame. Specifically, it is activated by the TX/RX Control Block four cycles before the FFT Block delivers the first sample of the first training symbol (see Figure 5.7b).

## Outputs

- **Optimal weight signals:** Once the MIMAX blocks have calculated the optimal weights, they are delivered to the MAC processor through the MIMAX Parallel Port (MIPP) shown in Figure 5.9, which is a 16-bit version of the standard enhanced parallel port (EPP) interface. There are four 16-bit signals (one per antenna), which represent the value of the optimal weights calculated by the MIMAX blocks. The 8 LSBs of each weight represent the real part and the 8 MSBs are the imaginary part.
- **Valid optimal weights signal:** It is the boolean signal that, through the MIMAX parallel port (MIPP) interface, notifies the MAC processor when the optimal weights are already calculated.

## 5.4 Channel Estimation in MIMAX

One substantial part of the baseband work has focused on the study and development of the most appropriate techniques for MIMO channel estimation. The novel MIMAX architecture also poses several design challenges to the MIMAX Channel Estimation Block. In essence, the main problem arises from the fact that the RF transmit and receive beamformers project the MIMO channel onto an equivalent SISO channel. Therefore, the  $n_R \times n_T$  frequency-selective MIMO channel has to be estimated from a number of MIMO channel projections (equivalent SISO channels) under different transmit-receive beamformers. Consequently, these beamformers have to be carefully chosen.

Similarly to the transmit-receive schemes developed in the first part of the thesis, the channel estimation algorithms presented in this section also have to take into account the specifications of OFDM-based 802.11a transmissions, and that we should keep backwards compatibility whenever possible. Specifically, a time-division duplex (TDD) operation mode and channel reciprocity are assumed. These assumptions avoid the requirement for a continuous feedback of the channel estimate, while still allowing to make use of the CSIT to optimize the beamforming algorithms as described in the first part of this work. Finally, we assume that the typical MIMAX operating condition for deployment and benchmarking is a low mobility (e.g., 0-3 m/s) indoor scenario with moderate delay spreads ( $\ll 0.8 \mu\text{s}$ ).<sup>8</sup> These low mobility channels are typical in offices, industrial buildings, exhibition halls, or even home environments.

In order to have a complexity-constrained and efficient channel estimation algorithm, once we have defined the special MIMAX frame (training frame or MIMAX frame II) in Sub-section 5.3.2, several key aspects must be solved throughout this section:

- defining the channel estimation procedure (also called training process),
- selecting the optimal transmit-receive beamformers to be used during training, and
- finding the most adequate MIMO channel estimation algorithm.

<sup>8</sup>Note that, since  $0.8 \mu\text{s}$  is the duration of the cyclic prefix of each OFDM symbol in 802.11a, these values of delay spreads (associated to the multipath channel) are too low to provoke inter-carrier interference (ICI).

### 5.4.1 Channel Estimation Procedure and Frames

Let us consider two terminals, which are denoted by T1 and T2 and equipped with  $n_1$  and  $n_2$  antennas, respectively. The channel estimation procedure to acquire CSIT+CSIR comprises the two following phases:

- The equipment that initiates the transmission, T1, sends a training frame with  $n_1 n_2$  OFDM training symbols to T2. These symbols are transmitted and received using different combinations of orthogonal transmit-receive beamformers. Any set of orthogonal beamforming vectors can be used for this purpose, as we will see in Subsection 5.4.2. Once T2 receives the OFDM symbols, it estimates the frequency-selective  $n_2 \times n_1$  MIMO channel and computes its optimal beamformers using any of the criteria described in Chapter 3. The discussion of the selection of the beamforming algorithm will be held in Chapter 6. Note that, due to the channel reciprocity, these are the optimal beamformers to be applied by T2 when either transmitting or receiving data.
- Once the optimal beamformer has been fixed at T2, it transmits a training frame to T1 with  $n_1 n_2$  OFDM training symbols through  $n_2$  orthogonal beamforming vectors. T1 receives these OFDM symbols through  $n_1$  orthogonal beamformers, estimates the frequency-selective MIMO channel, and computes its optimal weights. The optimal beamforming vectors at each side must be transferred to the MAC processor through the MIMAX parallel port (MIPP) for storage. They remain fixed, while the quality of the equivalent SISO channel, measured through the channel quality indicator (CQI) or the frame error rate (FER), is higher than a prescribed level (to be determined); otherwise, the procedure starts again. This re-estimation process is controlled by the MAC layer.

The channel estimation procedure requires the use of the new training frame (MIMAX frame II). The differences between MIMAX frame I (legacy) and II (training) are that after the SIGNAL field, in the MIMAX frame I, there is a set of  $N$  OFDM data symbols (see Figure 5.7a), whereas in the MIMAX frame II, there is a set of  $N$  OFDM training symbols for channel estimation (denoted by TS 1 to TS  $N$  in Figure 5.7b).

#### Further Discussion

The second phase of the channel estimation procedure could be done in at least two different ways.

- On one hand, taking advantage of the fact that T2 has already calculated its own optimal beamformer, it could send a training frame with only  $n_1$  OFDM training symbols. In this case, T2 would transmit the frame under its optimal beamformer, and T1 would use its set of  $n_1$  orthogonal beamformers to receive the frame (one different OFDM training symbol under one different training beamformer).
- On the other hand, since after the first step T2 knows the complete MIMO channel, it could calculate also the optimal beamformer of T1 and send it to T1. This alternative would reduce the feedback notably compared to the case when the whole estimated channel is sent.

Nevertheless, for the sake of simplicity in the final MIMAX system, the channel estimation procedure is always done by sending a training frame with  $n_1 n_2$  OFDM training symbols.

### 5.4.2 Beamformers for Channel Estimation

As described in the previous subsection, any set of orthogonal beamformers can be used for channel estimation. The first proposal is to use the columns of the DFT matrix. This selection makes it possible to keep fixed the amplitudes in each RF combiner and change only the phases. Other valid examples of orthogonal matrices are the identity matrix (in this case only a pair of transmit/receive antennas is active during the transmission/reception of each training symbol) or the Hadamard matrix, whose elements are either  $+1$  or  $-1$ . However, we should stress that any set of orthogonal beamformers can be used without any performance degradation. In other words, theoretically, any set of orthogonal beamformers performs identically in terms of MSE or BER.

Finally, we have decided to use the identity matrix as the training beamformer matrix at the transmitter and also at the receiver due to two main reasons.

- Firstly, since a single pair of transmit/receive antennas is active during the transmission/reception of each training symbol, the application of the weights is easier for the AFE.
- Secondly, with this set of beamformers, the estimated channel is the MIMO channel without any rotation. As we will see in Subsection 5.4.3, the weight calculation algorithms can obtain the optimal weights starting from any rotated version of the MIMO channel (see (5.5)). Although in this case, it is necessary to derotate the optimal weights once they have been calculated. Nevertheless, if we estimate the MIMO channel without any rotation (as it is the case when using the beamformers of the identity matrix), the final derotation is not needed. This derotation, along with the frequency offset correction, is originally done by the Weights Correction Block. Therefore with the selection of the identity matrix as a training beamformer matrix, this block could be avoided in a final implementation.

As we have seen, the channel estimation procedure consists of the transmission of a training frame with  $n_1 n_2$  training symbols where each one is transmitted/received under a different combination of transmit/receive beamformers. These beamformers are the columns of the identity matrix, i.e., each OFDM training symbol is used for the estimation of a different equivalent SISO channel between two different antennas.

Figure 5.10 shows an example of a channel estimation procedure where the transmitter has  $n_1 = 2$  antennas and the receiver has  $n_2 = 3$ . As seen in the figure, the short training symbols, long training symbols, the SIGNAL field, and the stuffing symbols are transmitted under some default weights (every antenna weight is set to 1 in this example). Then,  $n_1 n_2 = 6$  training symbols are sent, and each one is affected by a different and unique combination of transmit and receive beamformers. Note that the first transmit beamformer  $w_T[1]$  remains  $n_2 = 3$  OFDM symbols in order to set the three different beamformers at the receiver. Therefore, the first OFDM training symbol is transmitted by the antenna 1 and received by the antenna 1, the second is transmitted by the antenna 1 and received by the antenna 2, etc. In the fourth training symbol, the transmitter applies its second beamformer  $w_T[2]$ , which remains set, while the receiver applies again its three different beamformers to the remaining training symbols. It can be seen that, at the end, a different OFDM symbol has been sent through all the possible equivalent SISO channels.

TX Weights	$\mathbf{w}_{\text{DEFAULT}}$		$\mathbf{w}_{\text{DEFAULT}}$		$\mathbf{w}_T[1]$		$\mathbf{w}_T[2]$								
	1	1	1	1	1	0	0	1							
	1	1	1	1	0	1	1	0							
Training Frame	STS <sub>1</sub>	...	STS <sub>10</sub>	LTS <sub>1</sub>	LTS <sub>2</sub>	SF	SS <sub>1</sub>	SS <sub>2</sub>	SS <sub>3</sub>	TS <sub>1</sub>	TS <sub>2</sub>	TS <sub>3</sub>	TS <sub>4</sub>	TS <sub>5</sub>	TS <sub>6</sub>
RX Weights	1		1		1	0	0	1	0	0					
	1		1		0	1	0	0	1	0					
	1		1		0	0	1	0	0	1					
	$\mathbf{w}_{\text{DEFAULT}}$		$\mathbf{w}_{\text{DEFAULT}}$		$\mathbf{w}_R[1]$	$\mathbf{w}_R[2]$	$\mathbf{w}_R[3]$	$\mathbf{w}_R[1]$	$\mathbf{w}_R[2]$	$\mathbf{w}_R[3]$					

Figure 5.10: Transmit and receive beamformers for a training frame in a  $2 \times 3$  system.

### 5.4.3 Channel Estimation Algorithms

Regarding the MIMO channel estimation algorithms, we have conducted a complete theoretical and simulation study, which has included the following estimators:

- Least squares (LS) estimator is the simplest solution, which does not require any prior information about the frequency-selectivity or statistics of the channel.
- Minimum mean-square error (MMSE) estimator exploits the frequency correlation properties of the channel. This Bayesian estimator requires knowledge about the channel power delay profile and the noise variance.
- To further explore the tradeoff between performance versus complexity, a number of different versions of the LS estimator have also been evaluated. They would mainly be scaled versions that exploit the SNR information and filtered versions of the LS that assume a maximum length of the channel impulse response equal to the cyclic prefix.

#### Channel Estimation Algorithms in Frequency Domain

Each OFDM training symbol in the MIMAX frame II has  $N_c = 52$  data subcarriers available for channel estimation. Each pair of transmit and receive beamformers changes from symbol to symbol during the transmission/reception of the training frame. The  $N_c \times 1$  vectors  $\mathbf{x}$  and  $\mathbf{v}_n$  represent the transmitted and received OFDM symbols, respectively. Since the same OFDM training symbol is repeatedly transmitted, we have dropped the subindex  $n$  in the transmitted signal. The input/output relationship can be expressed as

$$\mathbf{v}_n = \mathbf{X}\mathbf{H}\boldsymbol{\Theta}_n + \mathbf{n},$$

where  $\mathbf{X} = \text{diag}(\mathbf{x})$ ,  $\mathbf{n}$  is a noise vector whose entries are samples of independent and identically distributed zero-mean circularly symmetric complex Gaussian (ZMCSCG) random variables,  $\boldsymbol{\Theta}_n = \mathbf{w}_T[n] \otimes \mathbf{w}_R[n]$  is the Kronecker product of the receive and transmit weight vectors

for the  $n$ -th OFDM symbol, and  $\mathbf{H}$  is a  $N_c \times n_T n_R$  matrix containing the MIMO channel responses at each subcarrier

$$\mathbf{H} = [\text{vec}(\mathbf{H}_1) \dots \text{vec}(\mathbf{H}_{N_c})]^T.$$

Grouping the  $n_T n_R$  received OFDM symbols, the input/output relationship can be expressed as

$$\mathbf{V} = \mathbf{X}\mathbf{H}\mathbf{\Theta} + \mathbf{N}, \quad (5.1)$$

where

$$\mathbf{\Theta} = [\mathbf{\Theta}_1 \dots \mathbf{\Theta}_{n_R n_T}].$$

As we mentioned in Subsection 5.4.2, the beamformers used for the training process must form an orthogonal set. This means that  $\mathbf{\Theta}$  should be chosen as an unitary matrix of dimensions  $n_T n_R \times n_T n_R$  preserving the Kronecker structure. On the other hand, the measurement noise matrix contains  $\mathbf{N}$  samples of independent and identically distributed ZMCSCG random variables. Therefore, the MIMO channel estimation problem stated in the frequency domain consists of estimating  $\mathbf{H}$  in (5.1), given  $\mathbf{V}$  (observations),  $\mathbf{X}$  (known training sequence), and  $\mathbf{\Theta}$  (beamformers used during training).

**LS Estimation:** The LS estimate [Kay, 1993] of the frequency domain MIMO channel matrix is given by

$$\hat{\mathbf{H}}_{\text{LS}} = \mathbf{X}^{-1} \mathbf{V} \mathbf{\Theta}^{-1}. \quad (5.2)$$

Note that both  $\mathbf{X}$  and  $\mathbf{\Theta}$  are known; therefore, their inverses can be computed and stored in advance. Moreover, since  $\mathbf{\Theta}$  is unitary,  $\mathbf{\Theta}^{-1} = \mathbf{\Theta}^H$ , and since  $\mathbf{X}$  is a diagonal, its inverse is trivial to compute. The LS estimate does not need any knowledge of the statistics of the channel, but it suffers from a high mean-square error in the low SNR-regime. The LS estimation can be refined if some information about the channel is known.

**Scaled LS Estimation:** The LS estimate does not necessarily lead to the channel estimate with the lowest MSE. In fact, it is well-known in the statistical literature that biasing the LS estimator can be beneficial in terms of MSE [Mayer and Willke, 1973]. Therefore, one can argue that, by properly scaling (and thus biasing the estimator) the LS estimate it is possible to further reduce the channel estimation error. Specifically, the scaled LS estimator (SLS) is given by [Biguesh and Gershman, March 2006]

$$\hat{\mathbf{H}}_{\text{SLS}} = \gamma \hat{\mathbf{H}}_{\text{LS}}, \quad (5.3)$$

where

$$\gamma = \frac{\text{SNR} \cdot \text{tr}(\mathbf{R}_{\mathbf{H}})}{\text{SNR} \cdot \text{tr}(\mathbf{R}_{\mathbf{H}}) + N_c}$$

and  $\mathbf{R}_{\mathbf{H}}$  is the channel frequency correlation matrix, which is assumed to be identical for all spatial subchannels. Note that the knowledge of the frequency correlation matrix is equivalent to the knowledge of the channel PDP. It can be shown that the scale factor  $\gamma$  minimizes the MSE among all possible scale factors [Mayer and Willke, 1973, Biguesh and Gershman, March 2006]. Regarding (5.3), it is clear that the SLS method requires knowledge about

the average SNR (or the noise power) as well as about the trace of the frequency correlation matrix, which is the total channel energy that is the sum of the variances of the channel at the subcarriers or, equivalently, the total energy of the PDP. Obviously, the requirement of knowing  $\text{tr}(\mathbf{R}_H)$  is less restrictive than the knowledge of the full correlation matrix.

The necessity to know the trace of the frequency correlation matrix can be avoided by using a LS-based sample estimate of the trace. This leads to the following approximated SLS (referred to as aSLS) estimator

$$\hat{\mathbf{H}}_{\text{aSLS}} = \gamma_a \hat{\mathbf{H}}_{\text{LS}},$$

where

$$\gamma_a = \frac{\text{SNR} \cdot \text{tr}(\hat{\mathbf{H}}_{\text{LS}}^H \hat{\mathbf{H}}_{\text{LS}})}{\text{SNR} \cdot \text{tr}(\hat{\mathbf{H}}_{\text{LS}}^H \hat{\mathbf{H}}_{\text{LS}}) + N_c}.$$

It is finally interesting to mention that, although SLS and aSLS estimators can improve the performance of LS in terms of MSE, all of them have identical performance in terms of BER (i.e., the scaling of the channel estimate does not affect the BER). They are included in this study only for comparative purposes.

**Filtered LS Estimation (fLS):** In the IEEE 802.11a standard, the length of the cyclic prefix (CP) is  $L_{\text{CP}} = 16$  samples, because it assumes that the channel length is equal or lower than 16 samples. This assumption can also be used to further refine the LS estimates by filtering them in the frequency domain as follows:

$$\hat{\mathbf{H}}_{\text{fLS}} = \mathbf{F}\mathbf{F}^+ \hat{\mathbf{H}}_{\text{LS}},$$

where the superscript  $+$  denotes the Moore-Penrose pseudoinverse and  $\mathbf{F}$  is the  $N_c \times L_{\text{CP}}$  Fourier matrix whose entries are given by

$$[\mathbf{F}]_{i,j} = \frac{1}{\sqrt{N_c}} \exp\left(-j \frac{2\pi}{N_c} (i-1)(j-1)\right), 1 \leq i \leq N_c, 1 \leq j \leq L_{\text{CP}}.$$

Note that this frequency domain filter is constructed only from the knowledge of the maximum channel length  $L_{\text{CP}}$ . In other words, it does not need any statistical knowledge about the channel or SNR. On the other hand, this estimator is not optimal in terms of MSE, because it does not fully exploit the frequency correlation characteristics of the channel.

**MMSE Estimation:** The linear MMSE estimator [Kay, 1993] [Biguesh and Gershman, March 2006] is the optimal one in terms of MSE. It fully exploits the frequency correlation characteristics of the channel. On the other hand, it requires full knowledge of the frequency correlation matrix and the average SNR. The MMSE estimate is given by

$$\hat{\mathbf{H}}_{\text{MMSE}} = \mathbf{R}_H \left( \mathbf{R}_H + \frac{(\mathbf{X}\mathbf{X}^H)^{-1}}{\text{SNR}} \right)^{-1} \hat{\mathbf{H}}_{\text{LS}}.$$

Figure 5.11 compares the performance of the above estimators in terms of MSE as a function of the average SNR. Within these simulations, a frequency-selective  $4 \times 4$  spatially uncorrelated MIMO Rayleigh channel is considered. The channel has a truncated exponential

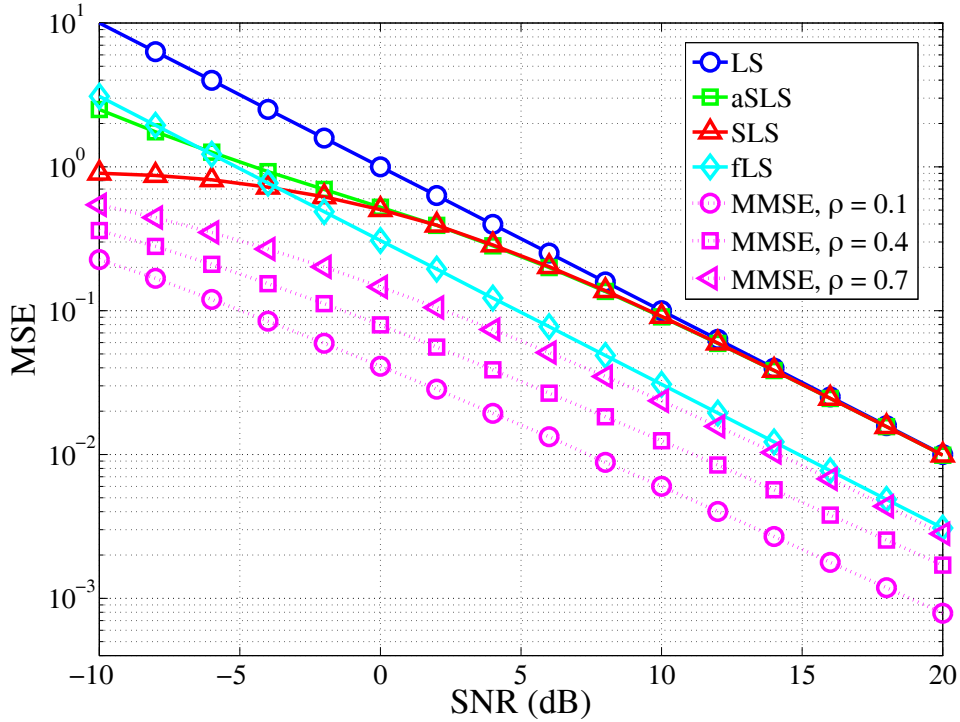


**Figure 5.11:** MSE of the channel estimates as a function of the average SNR.

PDP with decay factor  $\rho$  and length  $L = L_{CP} = 16$ . For channel estimation, we have used the  $N_c = 52$  subcarriers available in the IEEE 802.11a standard.

Note that the LS-based estimates do not depend on the specific shape of the PDP; hence, they are identical for all values of  $\rho$  assuming, of course, that the PDP is normalized. On the other hand, the performance of the MMSE estimator is highly dependent on the shape of the PDP, because it is able to fully exploit the frequency correlation characteristics of the channel. The figure shows curves of the MMSE estimates for the following values of  $\rho = 0.1, 0.4,$  and  $0.7$ , which correspond to the following values of the channel root mean squared (RMS) delay spread: 17 ns, 53 ns, and 132 ns, respectively. One can observe that, in highly correlated channels (low values of  $\rho$ ), the gap between the MMSE estimator and the LS-based estimators is significant. However, when the frequency correlation is low (high values of  $\rho$ ), the MMSE estimator has little room for improvement. Among the LS-based estimators, the filtered-LS is clearly the best choice for moderate and high SNRs. The scaled-LS estimators are better only for unrealistic values of SNR.

### Noise Variance Estimation

The MMSE, SLS, and aSLS estimators require previous knowledge of the average SNR or, equivalently, of the noise variance. In this subsection, we present a simple method to estimate the noise variance from the LS and fLS estimates. From (5.2), the matrix of the received training symbols can be expressed in terms of the LS estimate as

$$\mathbf{V} = \mathbf{X}\hat{\mathbf{H}}_{LS}\Theta.$$

Considering (5.1), the noise matrix  $\mathbf{N}$  is given by

$$\mathbf{N} = \mathbf{X} \left( \hat{\mathbf{H}}_{\text{LS}} - \hat{\mathbf{H}}_{\text{fLS}} \right) \Theta,$$

substituting now the channel response  $\mathbf{H}$  by its fLS estimate, we obtain the following approximation for the noise matrix

$$\mathbf{N} = \mathbf{X} \left( \hat{\mathbf{H}}_{\text{LS}} - \hat{\mathbf{H}}_{\text{fLS}} \right) \Theta.$$

Assuming that the entries of the noise matrix are i.i.d. zero-mean Gaussian samples, the maximum likelihood estimator of the noise variance is given by

$$\hat{\sigma}^2 = \frac{1}{N_c n_T n_R} \sum_{i=1}^{N_c} \sum_{j=1}^{n_R n_T} \left[ \hat{\mathbf{N}} \right]_{ij}^2, \quad (5.4)$$

that is, we simply add the squared entries of the noise matrix.

If we showed a log-log representation of the MSE of the noise variance estimate given by (5.4) versus the SNR, we would see that the MSE decreases linearly with the SNR. It also implies that the noise variance estimate with LS and fLS is very accurate even for low SNRs.

### Channel Estimation Algorithms for the Rotated MIMO Channel

In Chapters 3 and 4, we have seen that the equivalent SISO channel of the  $k$ -th subcarrier after beamforming is given by  $h_k = \mathbf{w}_R^H \mathbf{H}_k \mathbf{w}_T$ . This equation can be rewritten as

$$h_k = \mathbf{w}_R^H \mathbf{H}_k \mathbf{w}_T = \underbrace{\mathbf{w}_R^H \mathbf{Q}_R}_{\mathbf{w}_{\text{rot},R}^H} \underbrace{\mathbf{Q}_R^H \mathbf{H}_k \mathbf{Q}_T}_{\mathbf{H}_{\text{rot},k}} \underbrace{\mathbf{Q}_T^H \mathbf{w}_T}_{\mathbf{w}_{\text{rot},T}}, \quad k = 1, \dots, N_c, \quad (5.5)$$

where  $\mathbf{Q}_R$  and  $\mathbf{Q}_T$  are the receive and transmit rotation matrices of the channel, respectively.

Therefore, the optimal selection of the beamformers is invariant to rotations of the MIMO channel. In other words, the beamforming algorithms can work with a rotated version of the real MIMO channel and, once the optimal beamformers are calculated, they can be derotated.

As shown in Subsection 5.4.2, this invariance allows us to simplify the channel estimation problem, since now only a rotated version of the MIMO channel needs to be estimated. To show the implications of this property, let us stack the orthogonal beamformers used during the channel estimation into the following unitary matrices

$$\mathbf{Q}_R = \left( \mathbf{w}_{R,1} \dots \mathbf{w}_{R,n_R} \right),$$

$$\mathbf{Q}_T = \left( \mathbf{w}_{T,1} \dots \mathbf{w}_{T,n_T} \right).$$

The key point is that we can now estimate the rotated MIMO channel

$$\mathbf{H}_{\text{rot},k} = \mathbf{Q}_R^H \mathbf{H}_k \mathbf{Q}_T, \quad k = 1, \dots, N_c,$$

sequentially on a symbol-by-symbol basis.<sup>9</sup> That is, the OFDM training symbol that is received when both the  $i$ -th receive beamformer ( $i$ -th column of  $\mathbf{Q}_R$ ) and the  $j$ -th transmit beamformer ( $j$ -th column of  $\mathbf{Q}_T$ ) are active, is used to estimate the  $ij$ -th element of  $\mathbf{H}_{\text{rot},k}$ .

<sup>9</sup>This is of particular importance from the point of view of the implementation, because it allows for the reduction of the hardware resources and the whole latency of the process.

More precisely, let the  $N_c \times 1$  vectors  $\mathbf{x}$  and  $\mathbf{v}$  represent one transmitted and received OFDM symbol in the frequency domain, respectively. If  $\mathbf{x}$  is transmitted using the  $j$ -th column of  $\mathbf{Q}_T$  as RF weights and  $\mathbf{v}$  is received using the  $i$ -th column of  $\mathbf{Q}_R$  as receive beamforming, then the input-output relation can be expressed as follows

$$\mathbf{v} = \mathbf{X}\tilde{\mathbf{h}}^{i,j} + \mathbf{n},$$

where  $\mathbf{X} = \text{diag}(\mathbf{x})$ ,  $\mathbf{n}$  is a noise vector, whose entries are independent and identically distributed ZMCSG random variables, and  $\tilde{\mathbf{h}}^{i,j}$  is a  $N_c \times 1$  vector, whose entries are the  $ij$ -th elements of the rotated channel matrices for all the subcarriers, i.e.,

$$\tilde{\mathbf{h}}^{i,j} = \left[ [\mathbf{H}_{\text{rot},1}]_{i,j} \quad [\mathbf{H}_{\text{rot},2}]_{i,j} \cdots [\mathbf{H}_{\text{rot},N_c}]_{i,j} \right]^T = \left[ \mathbf{w}_{R,i}^H \mathbf{H}_1 \mathbf{w}_{T,j} \mathbf{w}_{R,i}^H \mathbf{H}_2 \mathbf{w}_{T,j} \cdots \mathbf{w}_{R,i}^H \mathbf{H}_{N_c} \mathbf{w}_{T,j} \right]^T.$$

Then, the LS-based estimates of  $\tilde{\mathbf{h}}^{i,j}$  will be:

$$\text{LS:} \quad \hat{\mathbf{h}}_{LS}^{i,j} = \mathbf{X}^{-1} \mathbf{v}.$$

$$\text{SLS:} \quad \hat{\mathbf{h}}_{SLS}^{i,j} = \gamma \hat{\mathbf{h}}_{LS}^{i,j}, \text{ where} \quad \gamma = \frac{\text{SNR} \quad \text{tr}(\mathbf{R}_H)}{\text{SNR} \quad \text{tr}(\mathbf{R}_H) + N_c}.$$

$$\text{aSLS:} \quad \hat{\mathbf{h}}_{aSLS}^{i,j} = \gamma_a \hat{\mathbf{h}}_{LS}^{i,j}, \text{ where} \quad \gamma_a = \frac{\text{SNR} \quad \text{tr} \left( \left( \hat{\mathbf{h}}_{LS}^{i,j} \right)^H \hat{\mathbf{h}}_{LS}^{i,j} \right)}{\text{SNR} \quad \text{tr} \left( \left( \hat{\mathbf{h}}_{LS}^{i,j} \right)^H \hat{\mathbf{h}}_{LS}^{i,j} \right) + N_c}.$$

$$\text{fLS:} \quad \hat{\mathbf{h}}_{fLS}^{i,j} = \mathbf{F}\mathbf{F}^+ \hat{\mathbf{h}}_{LS}^{i,j}.$$

Finally, the MMSE estimate is given by

$$\hat{\mathbf{h}}_{MMSE}^{i,j} = \mathbf{R}_H \left( \mathbf{R}_H + \frac{(\mathbf{X}\mathbf{X}^H)^{-1}}{\text{SNR}} \right)^{-1} \hat{\mathbf{h}}_{LS}^{i,j}.$$

The performance of the estimators for the rotated MIMO channel is the same as the performance of the estimators for the true (de-rotated) channel (see Figure 5.11); therefore, the results are not repeated here.

#### 5.4.4 Simulation Results for 802.11a Transmissions

The selection of the MIMO channel estimator establishes a tradeoff between the performance and the computational complexity of the estimator. Additionally, the benefits of higher complexity estimators, such as the MMSE are revealed in channels with large coherence bandwidth. In other words, the MMSE is optimum in terms of MSE for all channel conditions, but, only in highly correlated channels, the gains with respect to simpler estimators, such as the LS, are relevant (see Figure 5.11). On the other hand, MMSE needs prior estimates of the frequency correlation matrix and noise power. In practice, this prior information has to be acquired and handled by the MAC and BB processors in an adequate manner. The second estimator in terms of MSE performance is the filtered LS. Its main advantage is the lack of requirements for information about the channel or noise power. Other LS-based estimators do not improve the performance of fLS in the normal range of average SNR values.

In this subsection, we present some simulation results that compare the different MIMO channel estimators in terms of BER for 802.11a transmissions when the MinMSE beamforming algorithm described in Chapter 3 has been applied (under a CSIT+CSIR scenario). Specifically, Figure 5.12 shows the BER obtained using the MMSE, LS, and fLS channel estimators for a frequency-selective  $4 \times 4$  spatially uncorrelated Rayleigh channel. The channel has a truncated exponential PDP with decay factor  $\rho = 0.7$  and length  $L = L_{CP} = 16$ . For channel estimation, we have used the  $N_c = 52$  subcarriers available in the IEEE 802.11a standard. The channel coding rate was 54 Mbps. In order to obtain the transmit-receive beamformers, the MinMSE criterion, assuming CSIT+CSIR (see Chapter 3) has been applied. In addition to the BER curves obtained for the MMSE, LS and fLS estimators, we also have included the BER curve obtained when perfect CSIT-CSIR is used (the light-blue curve denoted as MSE in the figure). Also, the BER curves for a conventional SISO system and a conventional MIMO system with independent MRC at each subcarrier are included as a lower and upper bound in performance, respectively. For the SISO and full MIMO cases, perfect channel knowledge has been assumed.

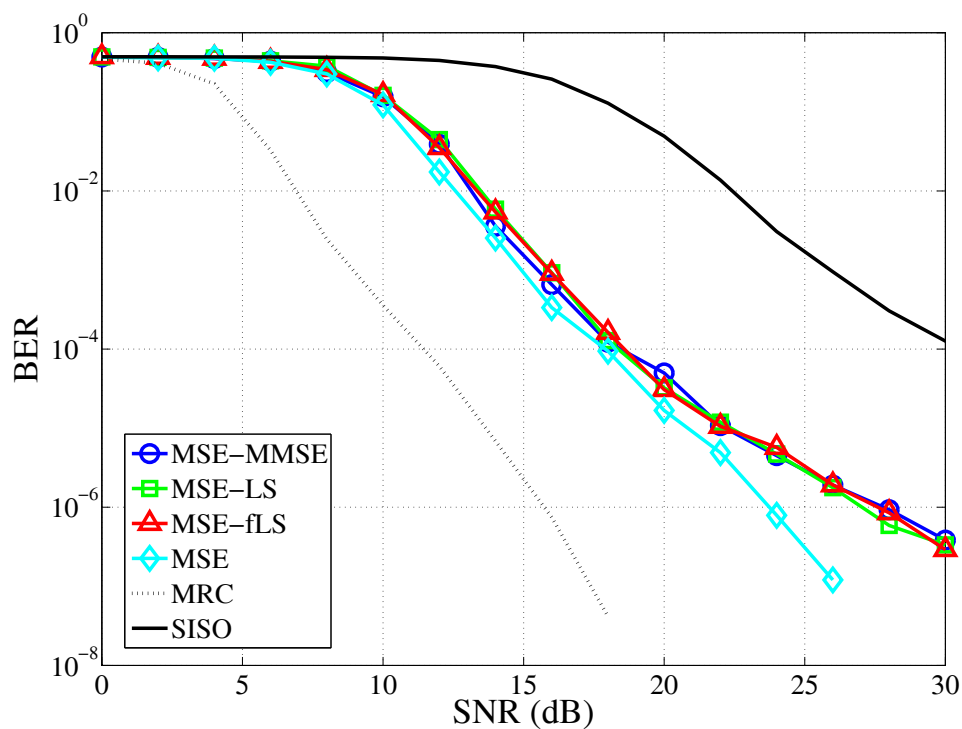


**Figure 5.12:** Simulated BER of MIMAX systems using different MIMO channel estimators.

From the results shown in Figure 5.12, it can be concluded that, when the beamforming stage is included, the BER performance of the complete baseband processor for the different channel estimators is quite similar. In other words, the MinMSE beamforming criterion is rather robust against channel estimation errors. This suggests that it is advisable to use a simple LS-based estimator instead of the more complex MMSE estimate. Similar conclusions are obtained from other simulations considering other channel conditions, coding rates, and beamforming selection algorithms. Consequently, we have selected the LS channel estimation algorithm for the implementation in the final MIMAX prototype. More details about the

selection of the MIMAX channel estimation algorithms and procedures can be found in [Santamaría et al., 2009b].

## 5.5 Conclusions

In this chapter, the MIMAX concept has been reviewed. Then we have presented the MIMAX demonstrator describing all the principal parts and introducing the standard IEEE 802.11a, which the MIMAX demonstrator is based on. Particularly, we have focused on the MIMAX baseband processor, describing its new blocks. All the novelties incorporated to the conventional 802.11a baseband processor have been depicted, including the channel estimation procedure. Moreover, certain channel estimation algorithms have also been proposed and compared by means of intensive simulations. Finally, the LS channel estimation algorithm has been selected to be implemented in the MIMAX demonstrator.

This chapter opens the second part of the thesis, where we will focus on the design, implementation, and testing of the new baseband blocks. These modules will be integrated into the 802.11a MIMAX processor of the MIMAX demonstrator. This MIMAX demonstrator has been developed by the whole consortium of the MIMAX project, in order to show the benefits of the MIMAX concept in a real prototype. Finally, notice that certain contributions to this chapter were made by [Eickhoff et al., 2009, Kraemer et al., 2010, Stamenkovic et al., 2010, Elvira et al., 2010, Eickhoff et al., 2011], and also by the technical reports [Santamaría et al., 2009b, Ibañez et al., 2009a].

# Chapter 6

## FPGA Design of the New MIMAX Blocks

### 6.1 Introduction

In the previous chapter, we have introduced the MIMAX architecture, and, more precisely, the new baseband processor, which is based on the IEEE 802.11a standard. Some changes within this baseband processor and the addition of some new blocks have been proposed in order to exploit the new capabilities of the system. Figure 6.1 shows again the baseband processor of the new MIMAX transceiver with the incorporated blocks (in orange). In the previous chapter, we have already listed all the new blocks as well their brief descriptions.

In this chapter, we focus on the design of the new MIMAX baseband blocks. Although all the MIMAX blocks have been successfully designed, simulated, implemented, and tested, some of these blocks, such as the MIMAX Control Block or the Weights Delivery Block, are quite simple, and their functions are synchronizing or controlling the rest of the blocks. Therefore, in this chapter, we will focus on the design of the most challenging blocks, which are:

- MIMAX Channel Estimation Block
- Frequency Offset Estimation Block
- MIMAX RF Weights Block (transmit-receive beamforming block)

In particular, the most consuming block in terms of FPGA resources and design efforts is the RF Weights Block, and, therefore, we will dedicate a detailed section to discuss its design. A further description of the design of all the MIMAX blocks can be found in [Ibañez et al., 2009b, Ibañez et al., 2009a] and they are also reviewed in [Gonzalez et al., 2009].

All these blocks without exception have been successfully designed, which is the starting point for the work of the following chapters. The new blocks along with the 802.11a VHDL design will be further integrated into a common Xilinx ISE project to get a final FPGA implementation. The whole integration procedure and its details will be addressed in Chapter 7.

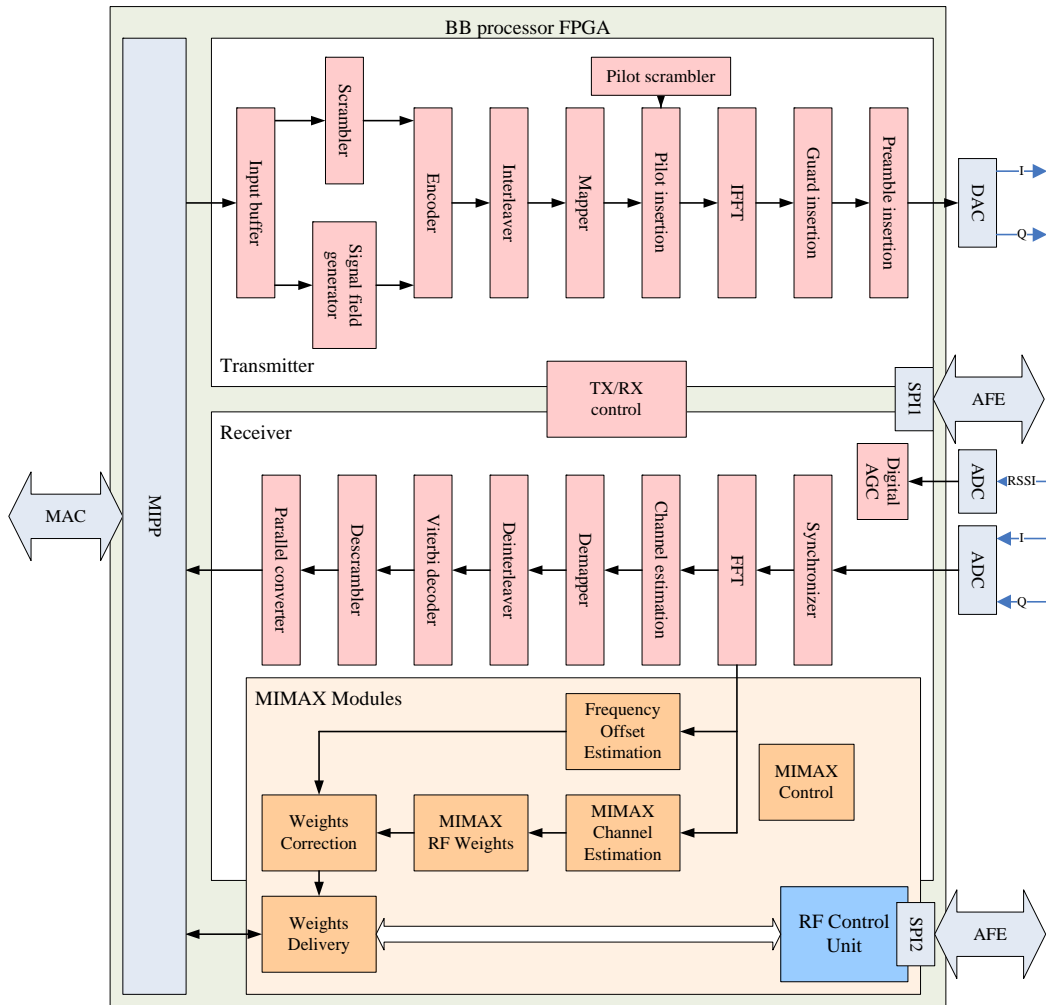


Figure 6.1: Block diagram of the MIMAX baseband processor architecture.

## 6.2 Tools

In this section, we describe the software tools that have been used throughout the design, implementation, simulation, and integration processes, which comprises the material of this chapter and also Chapter 7. Note that, although all the tools have been employed, System Generator for DSP has been the reference tool due to its features to design blocks that can be easily synthesized to produce FPGA implementations.

### 6.2.1 MATLAB and Simulink

MATLAB is an high-level language and interactive environment that enables to perform computationally intensive tasks faster and easier than with traditional programming languages such as C, C++, and Fortran. Developed by MathWorks, MATLAB allows matrix manipulations, implementation of algorithms, plotting of functions and data, creation of user interfaces, and interfacing with programs written in other languages.

MATLAB can be used in a wide range of applications, including signal processing, which is particularly useful for programming and simulating the algorithms that have been proposed throughout this thesis.

Simulink, also developed by MathWorks, is an environment for multidomain simulation and model-based design for dynamic and embedded systems. It provides an interactive graphical environment and a customizable set of block libraries that permit the design, simulation, implementation, and testing of a variety of time-varying systems, including communications, controls, signal processing, video processing, and image processing.

Simulink is integrated into MATLAB, providing immediate access to an extensive range of tools that permits the development of algorithms, analysis and visualization of simulations, creation of batch processing scripts, customization of the modeling environment, and definition of signal, parameter, and test data.

### 6.2.2 System Generator for DSP

System Generator for DSP is a Xilinx toolbox of graphical simulation blocks for simulating and generating VHDL designs. System Generator is integrated in MATLAB/Simulink environment. On one hand, this program allows us to create some blocks and simulate their behavior, feeding their inputs with MATLAB signals or Simulink blocks and analyzing their outputs in MATLAB. Therefore, the behavior of a System Generator-based design can be compared with its equivalent MATLAB algorithm. On the other hand, the blocks created with System Generator can be synthesized to produce VHDL code and netlist files. This code can be integrated into a common Xilinx ISE project to get a final FPGA implementation, which is useful for our purposes.

As we will see in this section, System Generator has been the most useful tool in the design of the new baseband modules, because the use of MATLAB/Simulink can make validation of FPGA algorithms more flexible and simple by avoiding the generation of traditional testbenches and extensive ModelSim simulations. Moreover, the use of System Generator requires few skills related to VHDL programming, which makes the design process friendlier.

### 6.2.3 ModelSim

ModelSim is a widespread tool for HDL simulation. With ModelSim, it is possible to apply stimulus to a VHDL design, run the simulation, and analyze the results. There are two kinds of simulations. A functional simulation is used to check that the logic of a design is correct. A timing simulation also takes into account the timing properties of the logic and the FPGA. In ModelSim, the behavior of the new MIMAX blocks can be tested and debugged, both stand-alone or within the whole baseband processor.

### 6.2.4 Xilinx ISE Foundation

ISE Foundation suite is an integrated graphical environment that provides a design, synthesis, implementation, and programming interface for Xilinx logic designs. It is the chosen tool to synthesize the baseband VHDL design and generate the FPGA configuration file.

### 6.2.5 Chipscope Pro

This program allows us to evaluate the behavior of a VHDL design in-circuit, as a logic analyzer does, analyzing real-time signals stored when a trigger condition occurs. It consists of two main modules: Chipscope Analyzer, which is a logic analyzer that shows the evolution of signals inside the FPGA, and Chipscope Core Inserter, which creates the logic structure that is necessary to generate the trigger conditions and to store the captured signals.

### 6.2.6 AccelDSP

AccelDSP of Xilinx is an automatic MATLAB to VHDL translator, which can also generate System Generator models. It is specially suited for DSP application and matrix-based operations, which are very common in MIMO scenarios. This solution is considered interesting for complex matrix operations, such as the singular value decomposition (SVD), which is extensively used in the MIMAX algorithms described in the first part of this thesis.

## 6.3 Design Procedure

Initially, we chose the Xilinx tools AccelDSP and System Generator for the implementation of the algorithms. Although AccelDSP provides the largest flexibility and some features that would have made our work easier, finally, the possibility of its use has had to be discarded. Unfortunately, as stated in the previous section, AccelDSP is also limited in its capability to generate synthesizable code when designing blocks that manage huge amount of data and with a large number of inputs/outputs. For this reason, System Generator was finally chosen for the implementation of the new MIMAX blocks.

### 6.3.1 MATLAB Floating-Point Model

A complete MATLAB toolbox that implements the whole baseband processor, including the MIMO algorithms specifically designed for MIMAX and described in Chapters 3 and 4, has been developed within our group (GTAS group). It is composed of ten MATLAB functions and one script specifying the main model parameters. The principal features of the floating-point model of the MIMAX baseband processor are the following:

- It implements the channel estimation procedure described in Section 5.4, which includes the sequential transmission of  $n_{Tn_R}$  OFDM training symbols and applies the filtered LS channel algorithm at both sides of the link.
- It implements the MaxSNR and MinMSE algorithms described in Chapters 3 and 4 to obtain the beamformers from the estimated channel. They can be calculated also from the rotated channel (see Subsection 5.4.2). In this case, the beamformers must be derotated to obtain the true beamformers.
- It includes the Frequency Offset Estimation Block and the Weights Correction Block.
- The model also includes the effect of quantization of the RF weights, which are also affected by a random uniform noise of the same range as the quantization errors.
- The baseband processor model includes the LS estimation of the equivalent SISO channel after fixing the transmit-receive beamformers.

- It implements the transmission rates defined in the 802.11a standard and applies a soft Viterbi decoder.
- The model can be used to perform Monte Carlo simulations obtaining bit and frame error rate (FER) curves. This model has been used to obtain the simulations in Chapters 3 and 4.

The structure of this MATLAB-based MIMAX baseband model is shown in Figure 6.2. In this figure, the orange blocks denote the main scripts, yellow blocks are specific MIMAX operations, and green blocks represent the IEEE802.11a processing (legacy baseband processor in Figure 5.6). Also, grey blocks denote simulation and measurement operations. Finally, the MATLAB functions of each step of the process are shown in blue tags.

### 6.3.2 MATLAB Fixed-Point Model

The MATLAB-based baseband processor model, previously described, uses floating-point operations to implement all the baseband blocks. Floating-point allows values to be represented with a large dynamic range and high precision but requires more FPGA resources (area and power) compared to a fixed-point representation. Therefore, the floating-point toolbox of Section 6.3.1 can be useful to obtain an upper bound on the expected performance of the baseband processor, but it cannot be used in an FPGA-based implementation.

As illustrated in the design flow diagram of Figure 6.3, in parallel with the design and implementation of the different MIMAX blocks, we have created a fixed-point model, which must replicate bit-to-bit the behavior of these blocks.<sup>1</sup> For this purpose, the MATLAB fixed-point toolbox has been used, which operates with fixed-point variables and operations. This toolbox allows us to set some parameters of the fixed-point variables (e.g., number length, fraction length) and the fixed-point operations (e.g., overflow mode, round mode).

The developed model is useful from two points of view. On one hand, this model can be integrated within the floating-point MATLAB model of the complete baseband, presented in Subsection 6.3.1. Therefore, this fixed-point model allows us to evaluate in a flexible manner the impact of changing the precision of the variables, some parameters of the proposed algorithm, etc. Consequently, design decisions may be taken using the model. On the other hand, the fixed-point beamforming MATLAB model can be used to debug and verify the System Generator FPGA design, following the iterative procedure illustrated in Figure 6.3.

### 6.3.3 System Generator Model

In principle, the new MIMAX baseband blocks were supposed to be implemented with the AccelDSP tool, but, as described in Subsection 6.2.6, its use was discarded. Therefore, the design of these blocks has been entirely done with System Generator, which uses Xilinx blocks that are directly synthesizable. Thus, it avoids the problems encountered with AccelDSP described above. On the contrary, using System Generator, part of the flexibility provided by AccelDSP is lost, because System Generator blocks are basic entities like simple multipliers, delayers, RAMs, etc. Therefore the design decisions are linked to the architecture decisions.

<sup>1</sup>Note that this fixed-point model has been made for the new MIMAX blocks and not for the whole baseband processor.

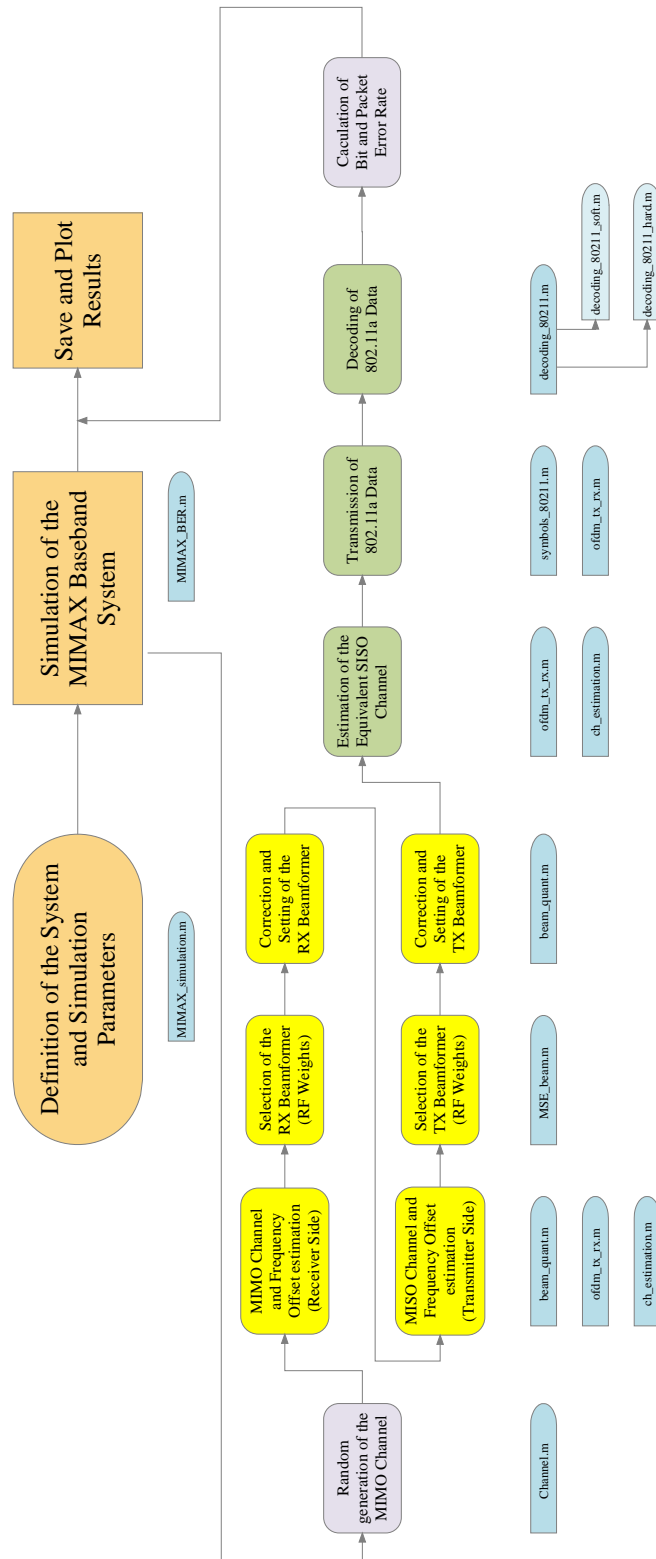
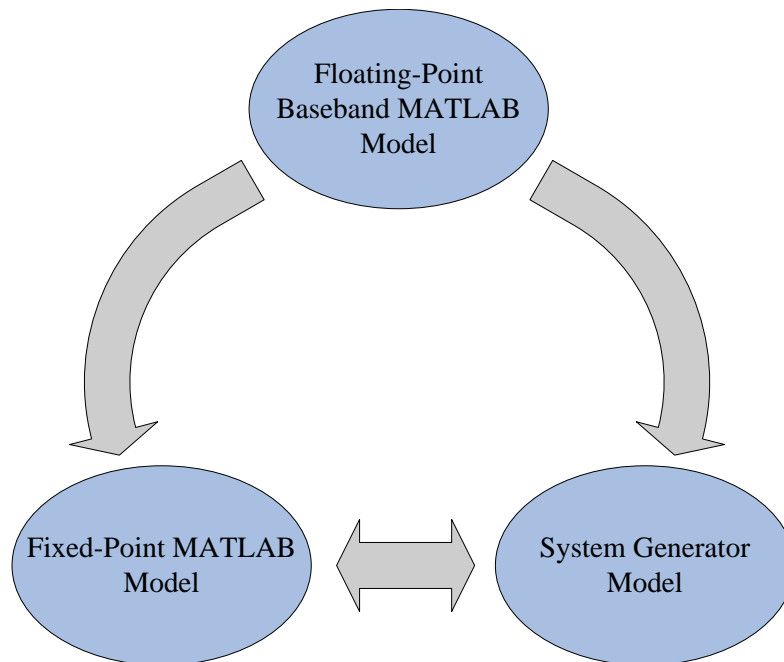


Figure 6.2: Block diagram of the MATLAB-based MIMAX baseband model.



**Figure 6.3:** Design flow of the new MIMAX baseband blocks.

Figure 6.3 illustrates the design procedure followed within this work, which starts from a MATLAB-based floating-point version of the algorithm and then iterates back and forth between a fixed-point MATLAB version and the System Generator model (final FPGA design).

In the next sections, we detail the design/implementation of the new MIMAX blocks. Note that, by using System Generator, the terms "design" and "implementation" are closely related, and we will use them interchangeably.

## 6.4 MIMAX Channel Estimation Block

In this section, we describe the design process of the MIMAX Channel Estimation Block and its final architecture. In Section 5.4, we have carried out a thorough study of the performance of different techniques for the MIMO channel estimation. According to the obtained results by means of simulations, it has been decided to implement a simple least squares (LS) algorithm in the frequency domain.

Once we chose the LS estimator to be designed and then implemented, a possible post-filtering technique was also explored as discussed in Section 5.4. Nevertheless, the improvement of the system performance with the post-filtering technique is negligible and did not compensate for the extra computational cost. In this way, no prior channel information is required.

As previously presented in Section 5.4, the algorithm estimates the MIMO channel between two terminals T1 and T2 in two steps. In the first step, T1 sends a training frame to T2 with  $n_1 n_2$  OFDM training symbols. In this manner, T1 estimates the frequency-selective  $n_1 \times n_2$  MIMO channel and calculates the optimal beamformers. In the second step, T2 transmits a training frame to T1 with  $n_1 n_2$  OFDM training symbols, and T1 estimates the MIMO channel in the same way. Note that, at each station, once the optimal beamformer is calculated, it is unique for both transmitting and receiving.

A schematic view of the block implemented with System Generator is shown in Figure 6.4. The inputs of the block, except the reset signal, come from the output of the FFT Block. The reset signal is activated by the baseband control (TX/RX block in Figure 6.1). The outputs of the MIMAX Channel Estimation Block feed the inputs of the RF Weights Block (see Figure 6.1). At the output of the MIMAX Channel Estimation Block, the block delivers all the estimated SISO channels serially.

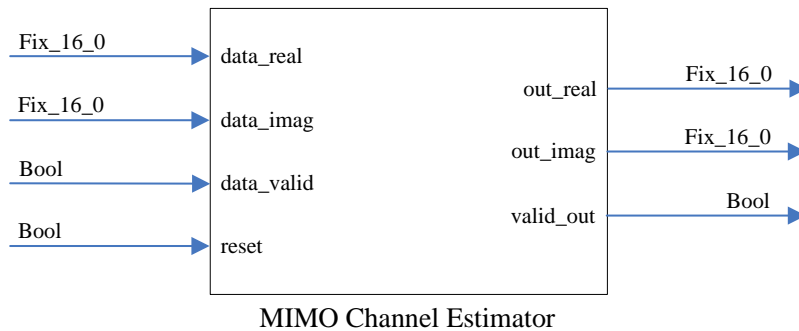


**Figure 6.4:** System Generator diagram of the MIMAX Channel Estimation Block.

The OFDM training symbols used during the training process are identical to the long training symbols. They consist of 52 subcarriers, which are modulated by  $\pm 1$  [IEEE Std. 802.11a, 1999], i.e., some subcarriers are inverted and some other remain without modulation.<sup>2</sup> Since the chosen channel estimation algorithm is the simple Least Squares (see Subsection 5.4.3), the MIMAX Channel Estimation Block must invert the symbols associated to the inverted subcarriers. This means that no divisions nor products are required but only sign changes. Therefore, from the point of view of the final FPGA implementation, the design of this block is quite simple, and it requires very few resources.

## 6.5 Frequency Offset Estimation Block

Besides the conventional IEEE802.11a Synchronizer detecting the incoming frame, it also estimates and corrects the frequency offset between the transmit and the receive stations. Nevertheless, at the output of the Synchronizer provided by one of the project partners [Troya et al., 2002, Krstic et al., 2003], there is a residual frequency error. For this reason, it could be necessary to include a Frequency Offset Estimation Block, working in parallel with the MIMAX channel estimation and the RF weights modules, in order to reduce this frequency offset.

The frequency offset estimation of this new block is done in the frequency domain (post-FFT) and is connected to the FFT output as illustrated in Figure 6.1. The outputs of this block feed the Weights Correction Block, indicating the phase correction (due to the estimated frequency offset) that must be applied to the calculated optimal weights. As explained in Subsection 5.3.4, this block uses an additional training symbol in the training frame. This symbol is transmitted and received with the same pair of beamformers as another different symbol taken as a reference. The frequency offset is assumed to be lower than the subcarrier

<sup>2</sup>The sequence of inverted subcarriers can be also found in [IEEE Std. 802.11a, 1999].

spacing after the correction done by the 802.11a Synchronizer. Specifically, the frequency offset estimate is given, in Hertz, by

$$\hat{\Delta}f_{ML} = \frac{1}{2\pi\Delta t} \text{angle} \left( \sum_{k=1}^{N_c} s_1[k]s_2^*[k] \right),$$

where  $N_c$  is the number of active (pilot and data) subcarriers (52 subcarriers in the 802.11a standard),  $s_1$  and  $s_2$  are the OFDM training symbols used for the frequency estimation, and  $\Delta t$  is the time, in seconds, between symbols  $s_1$  and  $s_2$ . The implementation of the frequency estimator block is depicted in Figure 6.5.

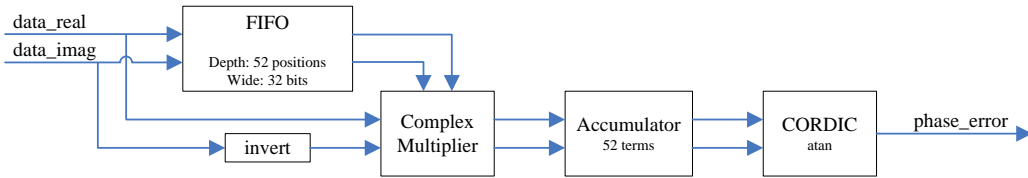


**Figure 6.5:** Schematic diagram of the Frequency Offset Estimation Block.

The design of this block requires the following resources: a FIFO memory of with 52 positions of 32 bits, a complex multiplier, two accumulators, and a CORDIC atan block. The final System Generator block indicating the input and output lines is shown in Figure 6.6.

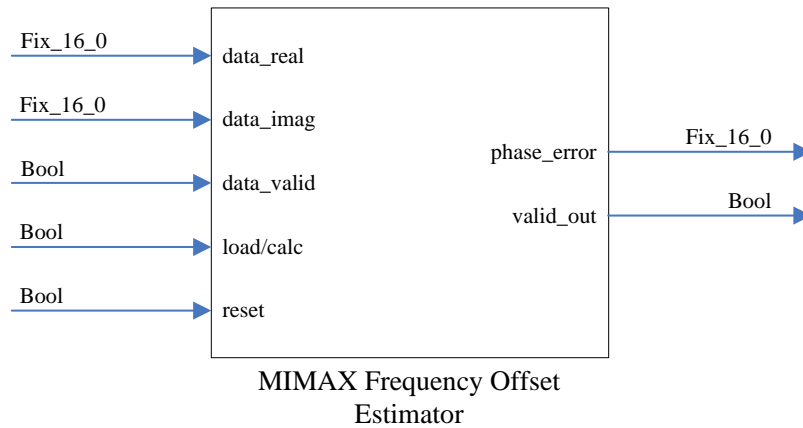


**Figure 6.6:** System Generator Frequency Offset Estimation Block.

## 6.6 Weights Correction Block

As shown in Figure 6.1, this block works at the output of the RF Weights Block and the Frequency Offset Estimation Block; it operates once the optimal weights are calculated. The Weights Correction Block rotates the obtained weights for two different purposes:

- If the training beamformers are not taken from the identity matrix, the estimated MIMO channel is a rotated version of the MIMO channel (see Subsection 5.4.2). The optimal

weights can be calculated from the rotated channel, but then, once the weights have been obtained, they must be derotated.

- As seen in Section 6.4, at the output of the conventional 802.11a Synchronizer, there is a residual frequency error estimated by the Frequency Offset Estimation Block. In the case that this error is sufficiently large, it affects the MIMO channel estimation, and, therefore, it should be corrected by rotating the obtained RF weights.

Both rotations can be applied with a multiplication block of a  $4 \times 4$  complex matrix by a  $4 \times 1$  complex vector. Only a multiplication block is needed, because both rotations can be applied serially. Although this block has been implemented, it has not been ultimately integrated in the final demonstrator due to two reasons.<sup>3</sup> Firstly, the selected training beamformers belong to the identity matrix. Secondly, in practice, the residual frequency error of the Synchronizer hardly affects the system performance. An intensive study was done in this direction by measuring the frequency error in real-time at the output of the Synchronizer. We also carried out a set of simulations of the system performance in terms of BER in order to check the effect of the frequency error. The slight degradation of the performance suggested not to include this block.

## 6.7 MIMAX RF Weights Block (Transmit-Receive Beamforming Block)

In this section, we describe the design procedure and the proposed architecture of the RF Weights Block. The algorithm for the weights calculation is based on those studied in Chapter 3 for the case of channel state information at both sides of the link. Throughout this section, we discuss which algorithm should be chosen for implementation, highlighting the required changes within it to obtain a version amenable to FPGA implementation. This block is the most difficult to be designed and implemented due to its complexity and the amount of data that must be processed to obtain the optimal transmit-receive beamformers.

### 6.7.1 Criterion, Algorithm, and Pseudocode

In the first part of this thesis, we have performed a thorough study of the design of the analog transmit-receive beamformers under different assumptions of the channel state information available at the transmitter and the receiver side. For the different assumptions, some criteria of optimization have been introduced and the algorithms to calculate the optimal beamformers have been also proposed. Now, we review them in order to choose the most appropriate for the nature of the MIMAX prototype.

#### Criterion and Algorithm

Once a complete study of the different criteria and algorithms for the selection of the beamformers has been done in Chapters 3 and 4, the next goal is the selection of the most appropriate criterion for the MIMAX project characteristics. Note that, due to the training process described in the previous chapter, the designed transceivers at the MIMAX project have access to the channel state information before each data transmission at the transmitter and at

<sup>3</sup>Its implementation consists in reusing the second part of Step C of the RF Weights Block. In Subsection 6.7.2, we analyze in detail the implementation of this  $4 \times 4$  by  $4 \times 1$  complex multiplication block.

the receiver side. Therefore, the RF Weights Block will be designed starting from the study carried out in Chapter 3 for the case of channel state information at both sides (CSIT+CSIR). The general criterion proposed for the case of CSIT+CSIR consists in the minimization of the following cost function:

$$f_{\alpha}(\mathbf{w}_T, \mathbf{w}_R) = \frac{1}{\alpha - 1} \log \left( \frac{1}{N_c} \sum_{k=1}^{N_c} \text{MSE}_k^{\alpha-1} \right),$$

where  $\alpha$  is a real parameter, which controls the overall system performance. The optimization problem can be written as

$$\arg \min_{\mathbf{w}_T, \mathbf{w}_R} f_{\alpha}(\mathbf{w}_T, \mathbf{w}_R) \quad \text{s. t.} \quad \|\mathbf{w}_T\|^2 = \|\mathbf{w}_R\|^2 = 1.$$

In Subsection 3.3.1, some interesting values of  $\alpha$  have been analyzed in more detail. Specifically the key cases are the maximization of the received SNR with  $\alpha = 0$  (MaxSNR) and the minimization of the overall MSE with  $\alpha = 1$  (MinMSE).

Two main points have been taken into account for the choice of the criterion, and, consequently, the algorithm to be developed. Firstly, the performance of the different algorithms has been evaluated in Section 3.5. Figures 3.10 and 3.11 illustrate the BER performance of both MinMSE and MaxSNR algorithms, under 802.11a transmissions and in i.i.d. Rayleigh channels with exponential parameter  $\rho = 0.7$ . The MinMSE algorithm obviously obtain better BER results than the MaxSNR approach, being the gap between them 3 or 4 dB for moderate SNRs. Note that, with  $\rho = 0.7$ , the channel is highly frequency-selective, and this fact benefits the performance of the MinMSE algorithm. However, the channels measurements obtained in our laboratory have shown a much lower frequency-selectivity, and, therefore, we would not expect high differences between the performances of MinMSE and MaxSNR algorithms in practical situations. Secondly, the estimated resources of the implementation of all the different algorithms have been also analyzed. Although the MinMSE algorithm shows the best performance, its fixed-point implementation would need a high number of SVDs, divisions, and some other complex operations. Therefore, since the performance of the MinMSE is not much better than that of the MaxSNR, the former algorithm has been discarded.

Moreover, since both MinMSE and MaxSNR criteria are initialized using a common starting point, which turns out to be the approximated version of the MaxSNR solution, our work has been focused on the implementation of this approximated MaxSNR solution. It is important to mention that this initial point is a very accurate approximation of the final MaxSNR solution (see Figure 3.3) by using much less resources, and then it provides very good results even without any further refinement.

### Pseudocode

A pseudocode for the approximated MaxSNR algorithm amenable to implementation has been developed and is shown in Algorithm 6.1. For the sake of simplicity, we have divided the algorithm into the following three steps (see Figure 6.7). Step A includes the "For" loop, Step B performs the line 7, and Step C the lines 8, and 9.

---

**Algorithm 6.1** Pseudocode of the approximated MaxSNR algorithm.

---

- 1: Initialize  $\mathbf{Y}$  to a  $16 \times 16$  zero matrix.
  - 2: **for**  $k = 0$  to 52 **do**
  - 3:   Create  $\mathbf{x}_k$  ( $16 \times 1$ ) where the  $i$ -th element of  $\mathbf{x}_k$  is the sample of the  $k$ -th subcarrier for the  $i$ -th equivalent SISO channel.
  - 4:    $\mathbf{X}_k = \mathbf{x}_k * \mathbf{x}_k^*$
  - 5:    $\mathbf{Y} = \mathbf{Y} + \mathbf{X}_k$
  - 6: **end for**
  - 7: Calculate the dominant eigenvector  $\mathbf{z}$  of the matrix  $\mathbf{Y}$ .
  - 8: Resize  $\mathbf{z}$  as the  $4 \times 4$  matrix  $\mathbf{Z}$ .
  - 9: Obtain  $\mathbf{w}_R$  as the first column of the matrix  $\mathbf{U}$  resultant of the SVD of  $\mathbf{Z}$ .
- 

The first challenge we face is that Step B requires the obtention of the dominant eigenvector of a  $16 \times 16$  complex matrix. Note that, since we do not need to extract all the eigenvectors of the matrix, the full eigendecomposition is not required. To this end, we have chosen the power method (also called vector iteration method), which is probably the simplest technique for finding the largest eigenvector of a matrix. In its basic form, the power method is applied as follows:

1. Assign to the candidate matrix an arbitrary normalized eigenvector with at least one element being nonzero.
2. Multiply the original matrix by the normalized eigenvector to calculate a new eigenvector.
3. Normalize this eigenvector.
4. Repeat the entire process from point 2, multiplying by the previous normalized eigenvector until the absolute relative error between successive eigenvalues satisfies an arbitrary tolerance (threshold) value.

Therefore, the power method needs to perform several matrix-vector multiplications. Nevertheless, regarding the design and implementation, it requires a single matrix-vector entity, because, independently of the number of iterations performed in the method, the eigenvector calculated in the previous iteration is the input to the next iteration. Therefore, the architecture cannot be parallelized. The normalization is also intended to avoid overflows and underflows and is performed by bit shifting, which is very low consuming in terms of resources. The number of iterations must be determined before the implementation process, but, at this point, it can be set as a parameter. A further study, in Subsection 6.7.3, will determine a suitable number of iterations.

The next challenge is Step C of the pseudocode. It consists of calculating the first column of the  $\mathbf{U}$  matrix resultant of the singular value decomposition (SVD) of a  $4 \times 4$  matrix. Initially, we contemplated the use of some IP blocks (the so called AccelWare Cores) of AccelDSP, because one of them performs the whole SVD. Nevertheless, it is not necessary to calculate the complete SVD, because only the first column vector of the  $\mathbf{U}$  matrix is needed. Furthermore, the resources and the time required for obtaining the SVD are quite high; therefore, it is better to find a simplified solution for obtaining this vector. This solution is again the power method described in this section. It is easy to check that the first column vector of  $\mathbf{U}$  is the dominant eigenvector of the matrix  $\mathbf{Z}\mathbf{Z}^H$ . Then, the design of this step can be done with a

multiplication block of two  $4 \times 4$  complex matrices and then the application of the power method to the resultant matrix.

### 6.7.2 Design and Architecture

The first approach to the RF Weights Block architecture comes from Algorithm 6.1 and, as stated above, the block has been divided into the three steps shown in Figure 6.7. This block has been initially designed for the case of  $n_1 = n_2 = 4$  antennas. Afterwards, we have made some changes in order to allow for some reconfigurability in the sense that we have considered up to four transmit/receive antennas. This design is reconfigurable by using the information provided in the SIGNAL field of the training frame, therefore, it can also operate with a smaller number of antennas (from one up to four). For the sake of simplicity, we start explaining the block design for the case of  $n_1 = n_2 = 4$  antennas and, then, in Section 6.8, the changes needed to allow reconfigurability are described.

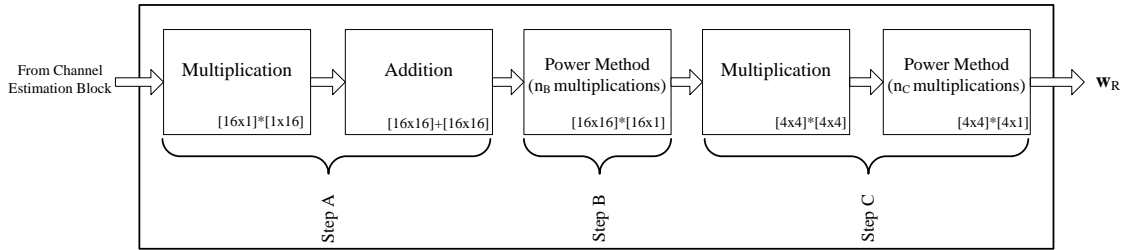


Figure 6.7: Steps of MaxSNR algorithm implementation.

#### Step A Block

During the training process, the RF Weights Block uses the the  $4 \times 4$  MIMO channel estimates of the received training frame from the MIMAX Channel Estimation Block. These estimates are relative to the 52 data subcarriers of the 16 equivalent SISO channels. Thus, at the beginning of Step A, they are stored in 52 dual-port RAMs with 16 words per RAM. We consider these 52 RAMs as 52  $16 \times 1$  vectors  $\mathbf{x}_k$ . Each word has 32-bit precision and contains the 16 bits of the real and imaginary part of the signal delivered at the output of the MIMAX Channel Estimation Block. At the output of the MIMAX Channel Estimation Block, we have created an entity whose purpose is to scale and truncate adequately the channel estimates in order to reduce the number of bits that Step A must manage. Once all the samples are stored (line 3 of Algorithm 6.1), we must create 52  $16 \times 16$  matrices  $\mathbf{X}_k = \mathbf{x}_k * \mathbf{x}_k^*$  (line 4). Afterwards, these matrices are added to obtain  $\mathbf{Y}$  (line 5), which will be the starting point of Step B.

The proposed architecture for Step A includes the following operations. Firstly, note that the  $\mathbf{X}_k$  are Hermitian matrices, i.e.,  $\mathbf{X}_k = \mathbf{X}_k^H$ , because  $\mathbf{X}_k(i, j) = \mathbf{x}_k(i) * \mathbf{x}_k(j)^*$  and  $\mathbf{X}_k(j, i) = \mathbf{x}_k(j) * \mathbf{x}_k(i)^* = \mathbf{X}_k(i, j)^*$ . Then, the  $\mathbf{X}_k$  matrices are calculated in parallel with 52 complex multipliers, but, instead of calculating the 256 elements of each matrix, we calculate only the 136 corresponding to the lower triangular matrix. For each  $\mathbf{X}_k$  matrix, the 136 elements are calculated sequentially and, since the  $\mathbf{X}_k$  calculation is parallelized in  $k$ , while the

**Algorithm 6.2** Pseudocode of Step A block.

```

1: for  $i = 1$  to 16 do
2:   for  $j = 1$  to  $i$  do
3:     Calculate in parallel  $\mathbf{X}_k(i, j) = \mathbf{x}_k(i) * \mathbf{x}_k(j)^*$  for  $k = 1$  to 52.
4:      $\mathbf{Y}(i, j) = \sum_{k=1}^{52} \mathbf{X}_k(i, j)$ 
5:   end for
6: end for
7: Normalization and truncation.

```

$\mathbf{X}_k$  entries are being calculated, they are added as  $\mathbf{Y}(i, j) = \sum_{k=1}^{52} \mathbf{X}_k(i, j)$ . The Algorithm 6.2 clarifies the design of Step A.

For the creation of a complex multiplication, we have implemented a complex multiplier by using four simple multipliers and two adders. By using the Gauss's complex multiplication algorithm, it would be possible to reduce the number of simple multipliers to three by increasing the number of adders to five. Figure 6.8 shows the architecture of the complex multiplication block.<sup>4</sup>

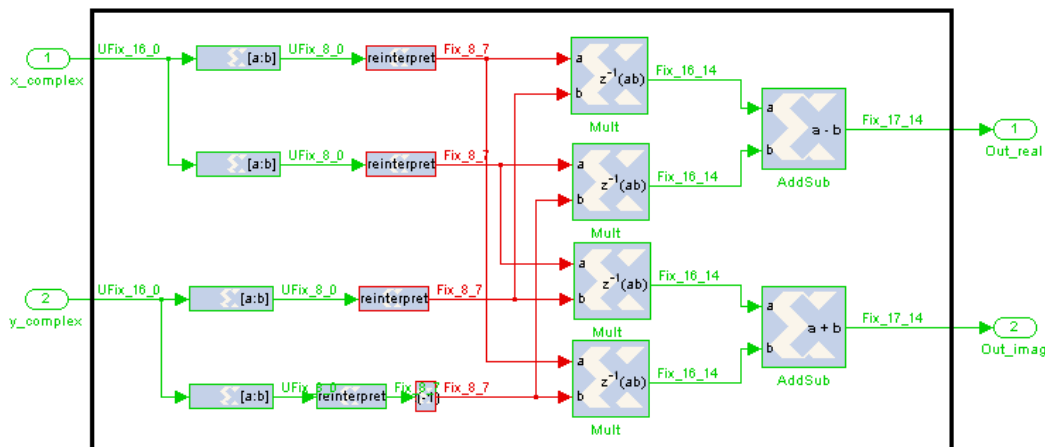


**Figure 6.8:** Architecture of the complex multiplication block.

Note that each element of  $\mathbf{Y}$  is obtained from the addition of 52 elements. Nevertheless, System Generator only provides simple adders with two inputs. Therefore, we need to cascade the additions, which must be done for the real and imaginary parts. Therefore, 104 simple adders have been required.

In line 7 of Algorithm 6.2, the  $\mathbf{Y}$  matrix is finally normalized and truncated. Observe that, when operating with fixed-point variables, the resolution of the resultant variables becomes higher. Thus, it is needed to reduce the number of bits of the signals. This process will be described in detail in Section 6.7.2.

<sup>4</sup>As we will see in the next chapters, the occupancy of the MIMAX baseband blocks is not an element to be optimized. The target FPGA is big enough for all these designs and the MIMAX prototype purpose does not include the optimization of the used resources.

### Step B Block

The block corresponding to Step B has been the most complex in terms of time required for completion, and it is also the one which uses more resources. Each column of the matrix  $\mathbf{Y}$  obtained after Step A is stored in a different RAM: 16 RAMs in total each one with a depth of 16 complex values. This RAM with the 256 complex elements of  $\mathbf{Y}$  is placed between Step A and Step B as seen in Figure 6.9.

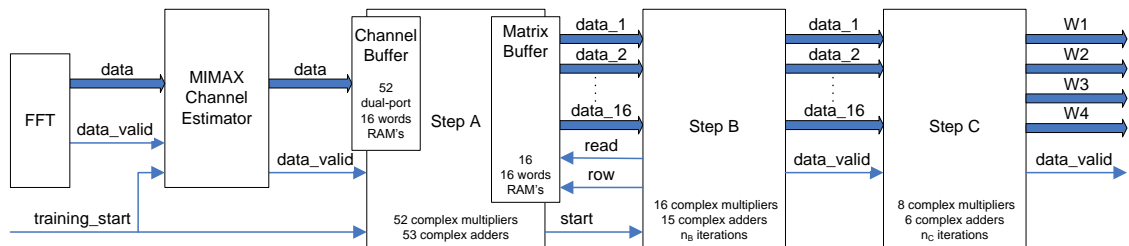


Figure 6.9: MIMAX blocks control and data flow diagram.

As Algorithm 6.3 depicts, Step B executes the first power method to obtain the largest eigenvector of  $\mathbf{Y}$ . This power method is performed for  $n_B$  iterations. In each iteration, a complex  $16 \times 16$  matrix is multiplied by a complex  $16 \times 1$  vector. For this purpose, we have designed the  $16 \times 16$  matrix RAM in such a way that the 16 elements of each matrix row can be read in the same cycle and can be multiplied by the vector. To perform these multiplications, we have implemented the inner product of two  $16 \times 1$  complex vectors. It uses 16 complex multipliers, as the one displayed in Figure 6.8, and 30 simple adders in cascade.

In the first iteration of the power method, an arbitrary vector with at least one element being nonzero is used. When the  $k$ -th matrix row is multiplied by the vector, the new value is stored at the  $k$ -th position of the new vector (using flip-flops). When all the matrix rows have been multiplied by the current vector, the dominant eigenvector has been completely updated. This vector is normalized in order to avoid underflows and overflows. Afterwards, the vector is also truncated in order to avoid a huge, meaningless increase of the bit precision of the signal. Then, the process starts again, but, now, each matrix row is multiplied by the normalized vector obtained in the previous iteration. After a fixed number of iterations, the resultant vector is forwarded to block C.

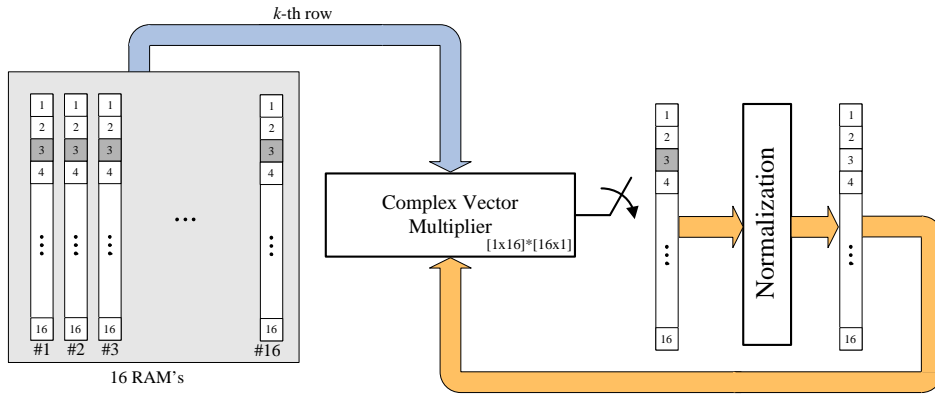
The reading of the  $k$ -th matrix row and the multiplication is performed at the clock rate, whereas the normalization and the beamformer updating at the input of multiplier block is carried out at a slower rate, because it is necessary to wait until the 16 sample of the vector is computed. Each iteration takes 16 cycles plus some latency cycles. The final decisions about the number of iterations as well as the bit resolution of each signal will be made using the fixed-point model and it will be discussed in Subsection 6.7.3. Figure 6.10 shows the proposed design for this block, and Algorithm 6.3 clarifies its pseudocode.

### Step C Block

The block relative to Step C is the last one of the RF Weights Block and delivers at the end the calculated optimal weights at the receiver. As shown in Algorithm 6.1, this block calculates

**Algorithm 6.3** Pseudocode of Step B block.

- 1: Initialize  $\mathbf{z}_0 = (0.5 + 0.5j)$  ones (1, 16)
- 2: **for**  $i = 1$  to  $n_B$  **do**
- 3:   **for**  $j = 1$  to 16 **do**
- 4:      $\mathbf{z}_i(j) = \mathbf{y}_j \mathbf{z}_{i-1}$ , where  $\mathbf{y}_j$  is the  $j$ -th row of  $\mathbf{Y}$ .
- 5:   **end for**
- 6:   Normalization and truncation of  $\mathbf{z}_i$ .
- 7: **end for**

**Figure 6.10:** System Generator architecture for Block B.

the optimal weight  $\mathbf{w}_R$  as the first column of the matrix  $\mathbf{U}$  resultant of the SVD of  $\mathbf{Z}$ , which is the resized version of the vector  $\mathbf{z}$  obtained in Step B. As explained in Subsection 6.7.1, the design of this step can be done with a multiplication block of two  $4 \times 4$  matrices ( $\mathbf{Z}$  and  $\mathbf{Z}^*$ ) and the application of the power method to the resultant matrix.

Algorithm 6.4 describes in detail the design of this step. The obtained vector  $\mathbf{z}$  in Step B is resized as the matrix  $\mathbf{Z}$ , and each column is stored in a different RAM, i.e., the matrix occupies four RAMs of four complex values. For the sake of simplicity, the  $\mathbf{Z}$  and  $\mathbf{Z}^*$  needed for the matrix multiplication have been stored in two different memories (each row of  $\mathbf{Z}^*$  is stored in a different RAM).

Once the matrix  $\mathbf{C}$  has been calculated as  $\mathbf{C} = \mathbf{Z}\mathbf{Z}^H$ , the block performs a power method on it in the same way as in Step B. Note that, in this case, the complex matrix size is  $4 \times 4$ . After the last iteration of the power method the resultant vector is the calculated optimal weight. In this moment, a valid signal is activated to indicate that the output of the RF weights are already available.

Regarding the resources employed in this block, the first part uses four complex multipliers and six adders, and the power method also needs four complex multipliers and six adders.

**Normalization and Truncation**

The RF Weights Block calculates the optimal weights  $\mathbf{w}_R$  that must be applied in the antennas to maximize the SNR of the equivalent SISO channel. Note that any scaled or rotated version of  $\mathbf{w}_R$  is equivalent, thus, taking into account the nature of the pseudocode depicted

---

**Algorithm 6.4** Pseudocode of Step C block.

---

```

1: for  $i = 1$  to 4 do
2:   for  $j = 1$  to 4 do
3:      $C(i, j) = \mathbf{z}_i * \mathbf{z}_j^*$ , where  $\mathbf{z}_i$  is the  $i$ -th row of  $\mathbf{Z}$ .
4:   end for
5:   Normalization and truncation of  $\mathbf{C}$ .
6: end for
7: Initialize  $\mathbf{w}_0 = (0.5 + 0.5j)$  ones (1, 4)
8: for  $i = 1$  to  $n_C$  do
9:   for  $j = 1$  to 4 do
10:     $\mathbf{w}_i(j) = \mathbf{c}_j \mathbf{w}_{i-1}$ , where  $\mathbf{c}_j$  is the  $j$ -th row of  $\mathbf{C}$ .
11:   end for
12:   Normalization and truncation of  $\mathbf{w}_i$ .
13: end for

```

---

in Algorithm 6.1, we can scale the result at any point along the calculation process. Note also that we are working with fixed-point arithmetic, which means that the bit precision of an operation result is always higher than the bit precision of the operands. For instance, the result of fixed-point multiplication of two 8-bit operands should be represented with 16 bits in order to avoid overflow. Therefore, we must limit the bit precision at some points of the algorithm, because, otherwise, the bit precision would increase dramatically after each step, and the necessary FPGA resources would increase accordingly. Moreover, the project consortium agreed that the applied beamformer in the AFE would have 8-bit precision for each component (real and imaginary part). This decision was supported by different simulations of the RF impairments effect on the performance of the floating-point baseband model. Therefore, the precision of the final calculated  $\mathbf{w}_R$  has been set to 8 bits too. Consequently, it is highly recommended not to work with a higher bit resolution between the different steps. A study to determine a suitable bit resolution between the different blocks is carried out below in Section 6.7.3. As we will see, we have also decided to truncate the signals at the input of each block to 8 bits without significant performance degradation.

### Data Flow

The control and data flow diagram of the RF Weights Block is depicted in Figure 6.9. The samples from the MIMAX Channel Estimation Block are stored in 52 dual-port RAMs. Step A calculates the  $16 \times 16$  complex matrix  $\mathbf{Y}$  and activates the start signal at the end of the process. Step B applies the power method to the matrix  $\mathbf{Y}$  and then feeds the resultant vector to Step C. Step C reorders the vector from Step B as a matrix and multiplies it by its Hermitian matrix (transpose and conjugate) to obtain matrix  $\mathbf{C}$ . Finally, it applies the power method and obtains the receive beamformer  $\mathbf{w}_R$ .

A timing diagram of the RF Weights Block is shown in Figure 6.11. The  $16 \times 16$  Hermitian matrix  $\mathbf{Y}$  is constructed in Step A. As stated before, due to its symmetry, it is only necessary to calculate 136 entries of this matrix, specifically those along the diagonal and on the lower triangular block. Considering that one clock cycle is required per addition and per multiplication, the total time,  $t_A$ , needed for calculating each entry is seven cycles. As it can be seen in Figure 6.11, this step is pipelined, and the associated latency  $\tau_A$  is only one clock cycle. Therefore, Step A takes  $135 * 1 + 7 = 142$  clock cycles. In Step B, the time  $t_B$  for each iteration

is 21 clock cycles, considering again one cycle per addition and per multiplication and one cycle for the normalization block. Then, Step B takes a total of  $21 * n_B$  clock cycles, where  $n_B$  is the number of iterations. Finally, in Step C,  $t_{mult}$  is four clock cycles, the latency  $\tau_{mult}$  is one clock cycles, and the time  $t_C$  for each iteration is six clock cycles. Therefore, the total time taken by this step is  $15 * 1 + 4 + 6 * n_C = 19 + 6 * n_C$ , where  $n_C$  is the number of iterations carried out in this step.

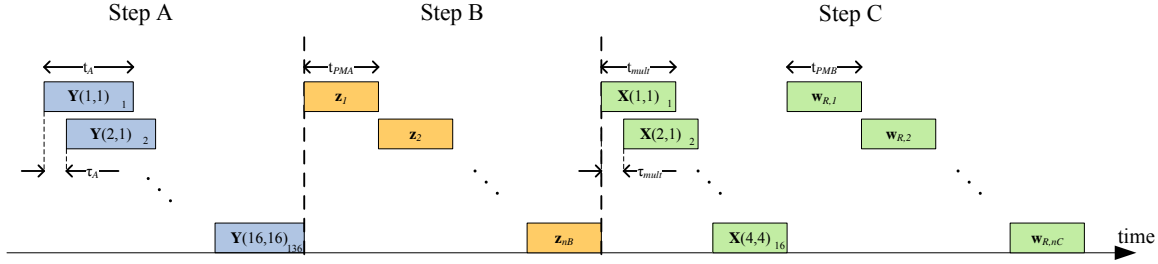


**Figure 6.11:** Timing diagram for the MIMAX beamforming block.

Taking into account the time needed by each step, a first estimation of the total time required by the RF Weights Block would be  $t_{MaxSNR} = t_{StepA} + t_{StepB} + t_{StepC} = 142 + 21 * n_B + 19 + 6 * n_C = 161 + 21 * n_B + 6 * n_C$  clock cycles. Although the final values for  $n_B$  and  $n_C$  are determined below in Section 6.7.3, we anticipate that we will perform five iterations for each power method. This means that the complete block takes 296 clock cycles.

At this point, we have not yet determined the clock that will drive the new MIMAX modules. In Chapter 7, we will see that the selected clock frequency to drive the block will be 20 MHz. An OFDM symbol has a duration of 80 cycles at 20 MHz. Therefore, we can conclude that the time required for the beamforming calculation is approximately the equivalent to four OFDM symbols, which is  $16 \mu s$ . This time is acceptable for an adequate behavior of the baseband and the MAC processor of the MIMAX transceiver.

### 6.7.3 Design Decisions

As discussed in Subsection 6.3, the fixed-point model is a useful tool for making the main design decisions, especially those related to the RF Weights Block. This MATLAB model limits the bit precision at the inputs of the different blocks (Steps A, B and C) and is equivalent bit-to-bit to the final implementation.

Now, we present some Monte Carlo simulation results to evaluate the impact on the BER performance of the fixed-point model in comparison with the floating-point model. We have integrated the fixed-point model into the MATLAB-based baseband processor model, described in Subsection 6.3.1. The simulation results are obtained for a frequency-selective  $4 \times 4$  spatially uncorrelated Rayleigh channel. The channel has a truncated exponential power delay profile (PDP) with decay factor  $\rho = 0.4$  and 16 taps length. For channel estimation, we have used the  $N_c = 52$  subcarriers available in the 802.11a standard. The binary rate was 54 Mbps, which corresponds to 64-QAM and coding rate  $3/4$ . The MaxSNR transmit-receive beamformers for both the floating-point and the fixed-point implementations have been applied.

In Section 6.7.2, we have explained the importance of reducing the bit resolution of the signals between the different blocks. Figure 6.12 shows the effect of a finite resolution at

a given interface between two blocks of the algorithm (except the interface under study all other interfaces use floating-point signals and operations). The values  $p_0$ ,  $p_A$ , and  $p_B$  are the number of bits used at the inputs of block A, block B, and block C, respectively (see Figure 6.7). As can be seen in the figure, the effect of using 8-bit signals at any interface is negligible, and the BER curves are indistinguishable.

In the second example, the simulation aims at evaluating the impact of applying a fixed number of iterations in the power method of the blocks B ( $n_B$ ) and C ( $n_C$ ). Figure 6.13 shows the results obtained for some different systems, where one of the power methods performs a limited number of iterations. It can be seen that the BER performance with five iterations is very close to that of the floating-point system. When the number of iterations is lowered to two or one, the system performance shows a clear degradation. We also observe that applying a low number of iterations is more critical in Step B than in Step C. Finally, Figure 6.14 shows the BER curves, when the RF Weights Block uses finite precision signals and both power methods apply a fixed number of iterations. We can conclude that the system with 8-bit interfaces and five iterations in both power methods performs similarly to the floating-point system (less than 0.5 dB of loss in the simulated SNR range). To summarize, the important design decisions made throughout this section are the following:

- Precision at the input of the steps ( $p_0, p_A$  and  $p_B$ ): 8-bit
- Number of iterations for both power methods: 5

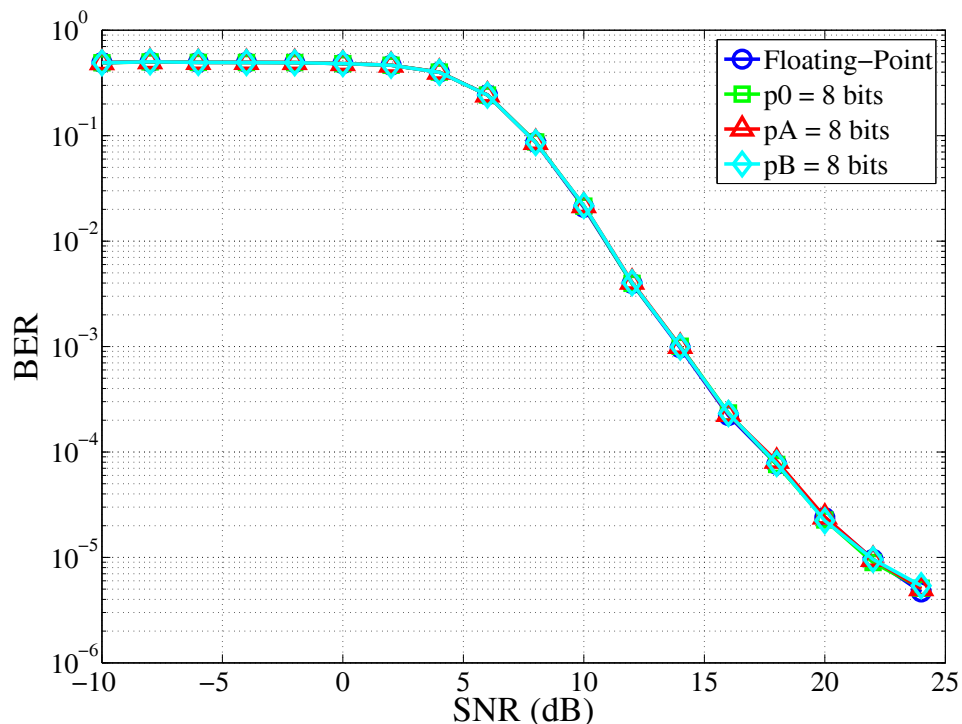


Figure 6.12: Performance of the MaxSNR Block with finite-precision signals.

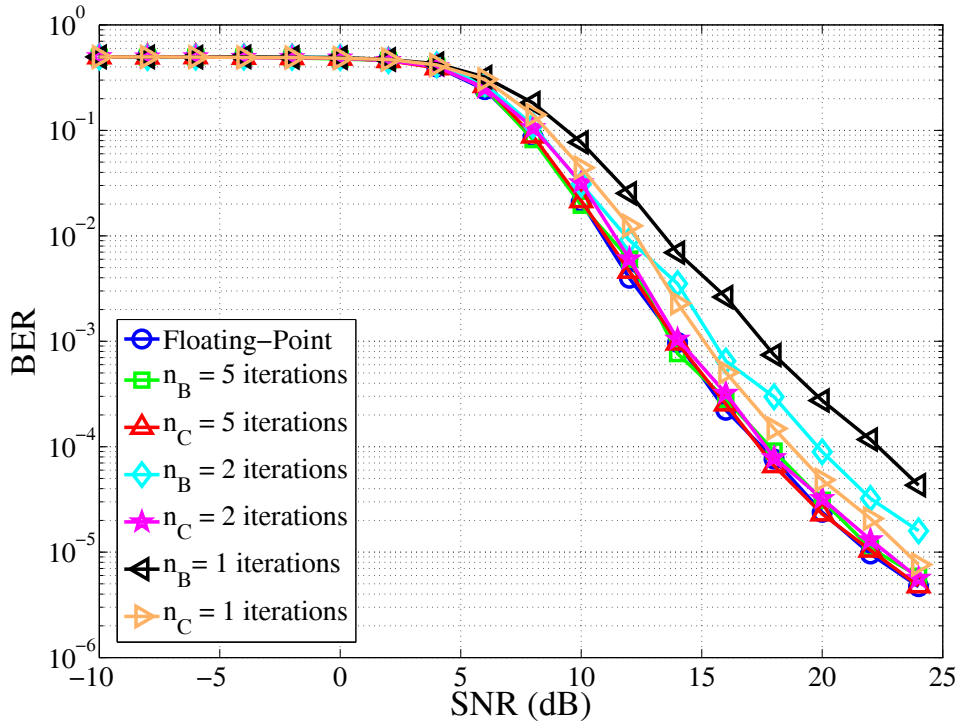


Figure 6.13: MaxSNR Block performance with a fixed number of iterations in Steps B and C.

## 6.8 Reconfigurability

Up to this point, all the new MIMAX blocks have been designed for a system where both the transmitter and the receiver have fixed number of antennas ( $n_T = n_R = 4$ ). Nevertheless, the flexibility of the design flow allow us to introduce some reconfigurability, in the sense that each transceiver can have up to four antennas. This new design is reconfigurable by using the information provided in the SIGNAL field of the incoming training frame. Figure 5.8b shows that in the SIGNAL field of the training frame, there are two fields for representing the number of transmit and receive antennas, with 2 bits for each one. Therefore, after enhancing the design with reconfigurability, each terminal can also operate with a smaller number of antennas (one to four).

All the blocks, except the RF Weights Block, can operate with the existing design with a different number of transmit and receive antennas. Thus, no change is needed for them. The RF Weights Block, designed for a  $4 \times 4$  system, must be adapted to permit some reconfigurability (different  $n_T$  and  $n_R$ ).

The  $4 \times 4$  RF Weights Block, at the beginning of Step A, stores the 52 samples relative to the 16 training symbols from the MIMAX Channel Estimation Block within the matrix memory. Note that these 16 symbols correspond to all possible SISO channels in a  $4 \times 4$  system. When the system has different  $n_T$  or  $n_R$ , the number of training symbols is  $n_T n_R$ . After a first study of the algorithms, we have determined that, if the training symbols are allocated in the appropriate columns of that initial matrix, it is possible to maintain almost all the block design, remaining with the other columns set to zero.

The way we have approached the incorporation of the reconfigurability feature is not optimal in terms of computing time when the number of transmit or receive antennas is lower

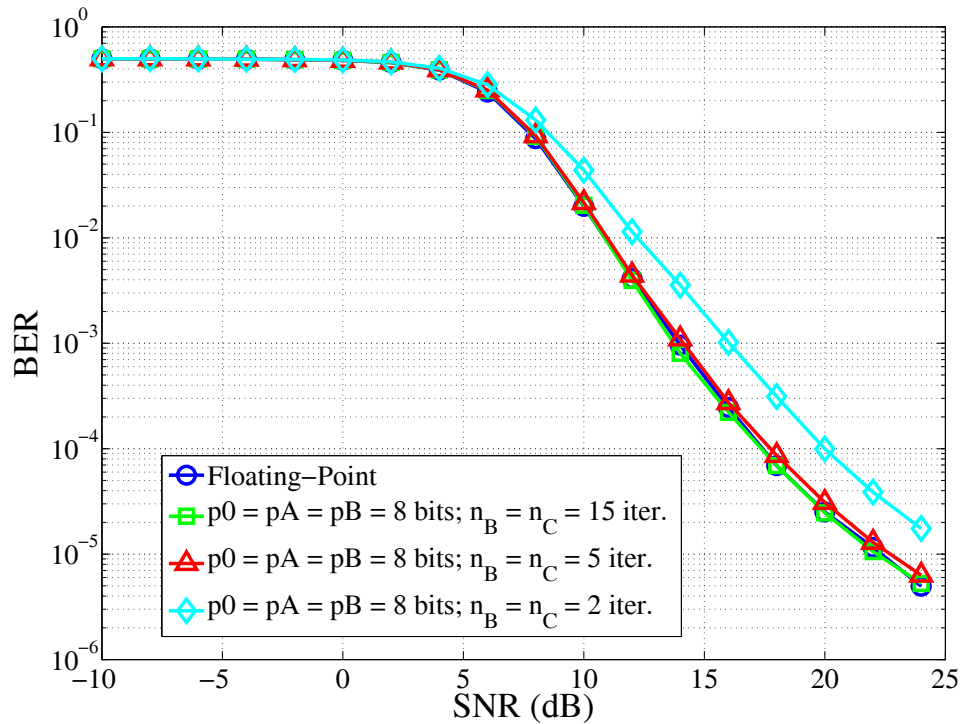


**Figure 6.14:** MaxSNR Block performance with finite-precision signals and a fixed number of iterations.

than four, in the sense that with less than four antennas at any station, the weights could be obtained faster than for a  $4 \times 4$  system. Although, with this design, the block takes the same time to obtain the weights regardless the number of transmit antennas, the necessary FPGA resources are not increased with the addition of this reconfigurability.

Figure 6.15 illustrates two examples that clarify the allocation of training symbols with reconfigurability. The row in each example represents the matrix memory, where each of the 16 squares is a block that contains the 52 samples of a MIMAX training symbol, i.e., the 16 training symbols of the  $4 \times 4$  system. Gray squares contain the appropriate MIMAX training symbol, while white squares have all the samples set to zero. Figure 6.15a depicts the samples' allocation of the training process of a  $4 \times 1$  system. Thus, its training frame contains four training symbols which are allocated in columns 1, 5, 9, and 13. Figure 6.15b represents the analogous process in a  $3 \times 2$  system. The six incoming training symbols are allocated in columns 1, 2, 5, 6, 9, and 10.

## 6.9 Conclusions

In this chapter, we have introduced the tools and the design procedure in order to implement the new MIMAX baseband blocks. We have exposed the three different models (floating-point, fixed-point, and System Generator), which have allowed us to move from a theoretical algorithm to an FPGA-based implementation.

As the main contribution of this chapter, we have given a detailed description of the design of all of the new MIMAX baseband blocks. Particularly, we have focused on the RF

(a)  $4 \times 1$  scheme.(b)  $3 \times 2$  scheme.

**Figure 6.15:** Allocation of the MIMAX training symbols in the  $52 \times 16$  matrix memory of the RF Weights Block. Each square represent the 52-sample memory relative to a MIMAX training symbol.

weights calculation block, whose design has been based on an adapted version of the proposed algorithm for the case CSIT+CSIR given in Chapter 3. Finally, taking into account that the whole first design was done for a  $4 \times 4$  MIMO system, we have added some reconfigurability in the sense that each terminal can have up to four different number of antennas. The publications that have contributed to this chapter are [Kraemer et al., 2010, Stamenkovic et al., 2010, Elvira et al., 2010, Eickhoff et al., 2011]. Certain contributions have also been made by the following technical reports [Ibañez et al., 2009b, Ibañez et al., 2009a]

# 7

Chapter

## Simulation, Generation, and Integration

### 7.1 Introduction

In this chapter, the new MIMAX baseband blocks are validated by means of different types of simulations. The System Generator design tool also allow us to test the blocks designs in a stand-alone manner or within a reduced model with some extra blocks of the receiver baseband processor. On the other hand, ModelSim tool permits a reliable simulation of the blocks within the whole MIMAX baseband processor. Several campaigns of simulations are carried out utilizing both tools with successful results.

Once the simulations validate the design of the new MIMAX baseband blocks, they are generated with System Generator into NGC files. These files are netlists that provide the instances to Xilinx blocksets (which are directly synthesizable), interconnections, and some attributes of the blocksets. Finally, we focus on the integration of the new MIMAX baseband blocks within the whole baseband processor by merging the generated netlist files into the ISE project of the modified 802.11a baseband processor.

### 7.2 Simulation of the New MIMAX Baseband Blocks

This section deals with the simulation of the new baseband blocks. Firstly, the System Generator simulations are presented, distinguishing between the stand-alone tests of each block and the final set of simulations that have validated the correct behavior of all the new blocks within a reduced version of the baseband processor at the receiver. Secondly, the set of simulations carried out in ModelSim environment is also depicted.

#### 7.2.1 System Generator Simulation

As earlier stated, System Generator designs can be simulated within Simulink environment of MATLAB. Therefore, with Simulink/System Generator, we can generate the stimulus to be applied to the design and analyze in MATLAB the outputs of the design. System Generator also allows us to integrate VHDL entities within the Simulink environment for simulation purposes. This is particularly interesting, because the new MIMAX baseband blocks can be tested along with some other existing blocks described in VHDL, such as those of the legacy 802.11a baseband processor.

### First Set of Simulations

It is quite complicated to separate the design process and the basic simulations of the blocks in a stand-alone manner, because both procedures have been somehow executed in parallel. Nevertheless, for the sake of simplicity, we have presented them separately. In the previous chapter, we have addressed the design process of the new MIMAX baseband blocks. Along the design process, some different fixed-point programs have been made for each block. As seen in Section 6.3.2, where the fixed-point model of the RF Weights Block is described, these models must be bit-to-bit identical to the final design. Thus, they are particularly useful to debug and verify the designs by comparing the fixed-point models with the simulation of the designed blocks.

The design process and these first simulations have been carried out in parallel in order to test the basic behavior of each new MIMAX baseband block in a stand-alone mode. In this initial phase, the new blocks have been fed with signals generated in MATLAB. These input signals have been also used to feed the fixed-point models. Each block has been independently validated by comparing the outputs of its System Generator design simulation with the outputs of its fixed-point model.

### Second Set of Simulations

The second set of simulations has particularly focused on intensive test of the RF Weights Block, the most intricate module, and also the MIMAX Channel Estimation Block. For this purpose, a Simulink model with some legacy 802.11a baseband blocks has been generated. Note that the RF Weights Block, as well as all the new baseband blocks, works exclusively when receiving a training frame (MIMAX frame II). Thus, we have only included in the model the blocks that are between the ADCs and the new MIMAX baseband blocks. Figure 6.1 illustrates the baseband processor and shows that the only necessary legacy blocks are the Synchronizer and FFT. The VHDL description of the whole legacy 802.11a baseband has been provided by the project partner, IHP. As mentioned above, System Generator allows us to include blocks, described in VHDL within Simulink environment, therefore, the VHDL descriptions of both the Synchronizer and the FFT Block have been translated into System Generator blocks.

Figure 7.1 shows the baseband Simulink model built for the simulation of the reception of a training frame. As shown, it includes the Synchronizer and the FFT Block as legacy blocks, and the Channel Estimation Block and the RF Weights Block as MIMAX blocks. The model is fed by an emulated received training frame and delivers as an output the calculated optimal weights. It can be seen that the interconnections of this model agree with the interfaces of the new MIMAX baseband blocks within the legacy 802.11a baseband processor that were introduced in Subsection 5.3.5.

Nevertheless, the model created for this second set of simulations does not include the whole baseband receiver, which means that not all the MIMAX blocks interfaces are available (see Subsection 5.3.5 for more details). For this reason, certain essential signals that should be generated by some baseband blocks, such as the TX/RX Control Block of the legacy baseband processor, have been emulated. These signals, that must be synchronized with the incoming training frame, are:

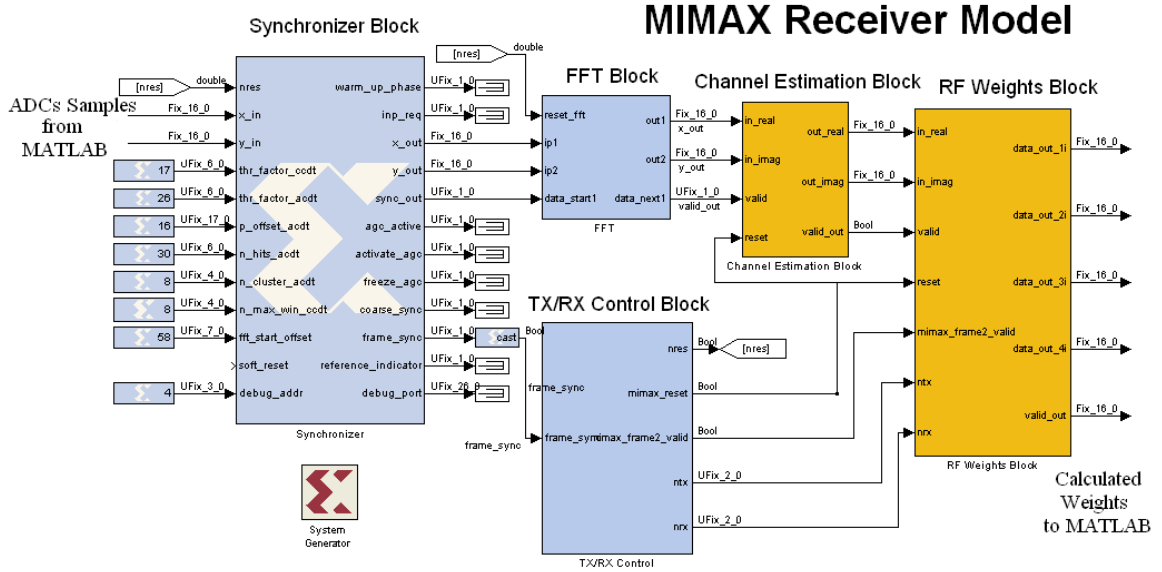


**Figure 7.1:** Baseband Simulink model for the simulation of the reception of a training frame (MIMAX frame II).

- **reset:** The reset signal of the new baseband blocks is enabled with the hard reset of the baseband board and also before receiving a training frame. It is generated by the Tx/Rx Control Block.
- **mimax\_frame2\_valid:** This signal is activated when the baseband processor receives a training frame. The baseband processor takes some time to decode the SIGNAL field before it knows that the received frame is a training frame (for this purpose there are three stuffing symbols before the MIMAX training symbols as shown in Figure 5.7b)
- **nrTX** and **nrRX:** After decoding the SIGNAL field (see Figure 5.8b), the baseband control informs the RF Weights Block of the number of antennas available at the transmitter and receiver.

The model shown in Figure 7.1 is fed by the emulated received I/Q signals of the training frames that are supposed to come through the baseband processor ADCs. A function in MATLAB for the generation of these kind of frames has been programmed. The generated frames are based on the standard training frame (see Figure 5.7b), but taking into account two peculiarities:

- For an appropriate MIMO channel estimation, each training symbol of the training frame is affected by a specific pair of transmit and receive beamformers, i.e., by a different equivalent SISO channel. Thus, the MATLAB function distorts the training frame by a known MIMO channel.

An i.i.d. Rayleigh MIMO channel model with exponential power delay profile has been assumed. In particular, the total power associated to the  $l$ -th tap is

$$E \left[ \|\mathbf{H}[l]\|^2 \right] = (1 - \rho) \rho^l n_T n_R, \quad l = 0, \dots, L_c - 1,$$

where  $L_c$  is the length of the channel impulse response ( $L_c = 20$  in all the cases),  $n_T$  the number of transmit antennas, and  $n_R$  the number of receive antennas. The exponential

parameter  $\rho$  has been selected as  $\rho = 0.4$  and  $\rho = 0.7$  to compare the performance of weights calculation design depending on the frequency selectivity.

In the particular case when the MIMO channel is flat, this distortion consists solely in the multiplication of each training symbol by a different element of the MIMO channel matrix (i.e., a complex number). An example of a received training frame through a flat  $2 \times 3$  MIMO channel is shown in Figure 7.2. It is possible to identify the different OFDM symbols of the frame: the ten short training symbols (ST1 to ST10), the double guard interval (GI) relative to the subsequent two long training symbols (LT1 and LT2), the SIGNAL field (SF), three stuffing symbols (SS), and, finally, the six ( $n_T n_R$ ) training symbols (TS1 to TS6) corresponding to the six SISO equivalent channels. It can be observed that each training symbols has a different amplitude.

- The frame must be scaled in order to have an adequate range at the inputs of the Synchronizer. In this model, no AGC is used. Therefore, the signal must be as high as possible to ensure the frame detection at the Synchronizer but avoiding an overflow at its input. The data inputs of the Synchronizer are signed and have 16-bit precision. Hence, the input values must be between  $-32,768$  and  $32,767$ . We have also observed that, when the incoming frame has its maximum value under around 2,000, the Synchronizer cannot detect the frame.

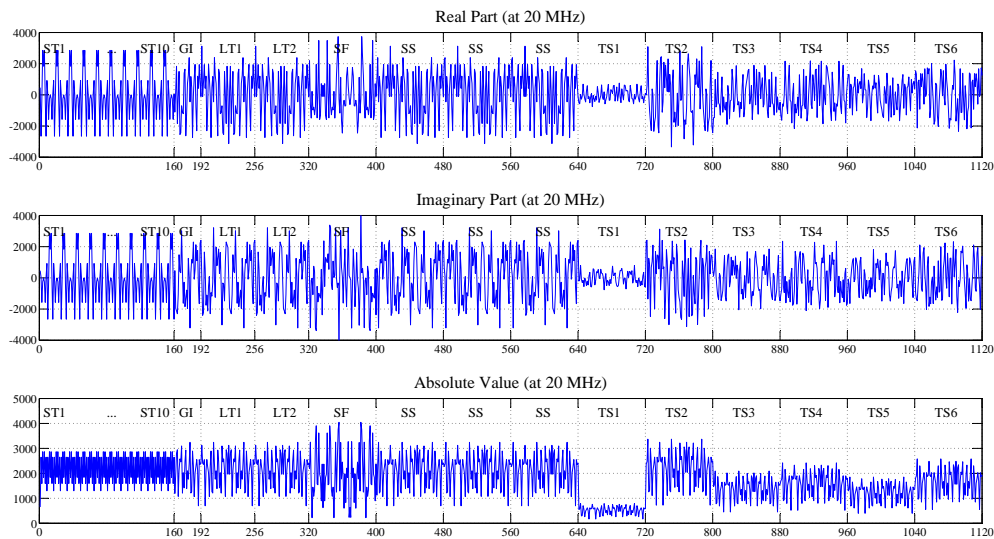


**Figure 7.2:** Received training frame (MIMAX frame II) through a  $2 \times 3$  flat MIMO channel.

Therefore, the second set of tests has been carried out as follows: different emulated received training frames have been generated (each one affected by a different MIMO channel), the Simulink/System Generator baseband receiver model has been fed with these frames, and the optimal weights have been finally calculated by the RF Weights Block for each different training frame. For every different received training frame, the calculated weights have been compared with those obtained with the fixed-point model, checking that they are bit-to-bit identical. The Simulink and the fixed-point model results have been also compared with the weights obtained through the floating-point model of the approximated MaxSNR algorithm.

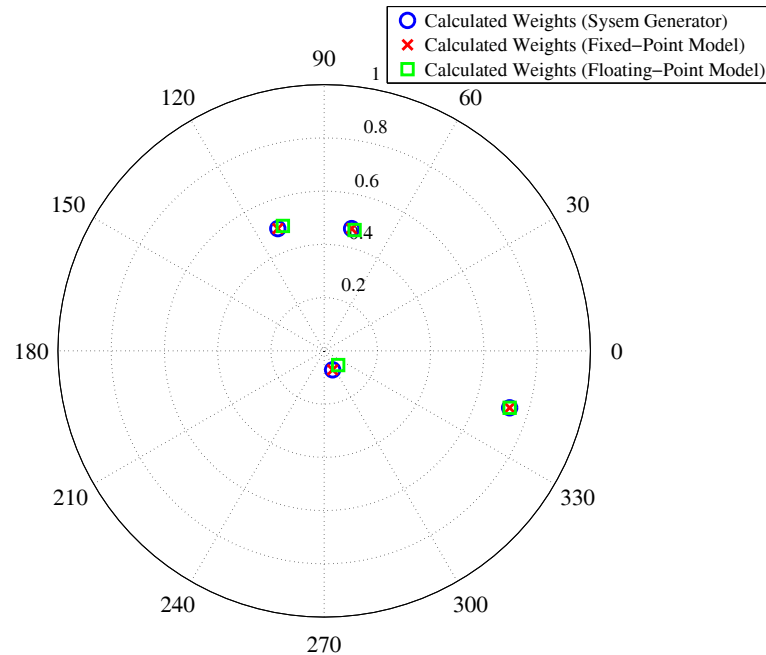


**Figure 7.3:** Comparison among the RF weights calculated in System Generator model, fixed-point model, and floating-point simulation.

Figure 7.3 shows a first example of the comparison among different simulations that have been carried out for a particular flat-fading  $4 \times 4$  Rayleigh channel. For this first example, Table 7.1 shows the values of the calculated weights under the different models (after scaling and rotation, and rounded to four decimal digits). As expected, it can be observed that the fixed-point model replicates bit-to-bit the weights obtained in the Simulink simulation. The weights calculated with the floating-point model show very slight differences due to the limited precision of the fixed-point model and the System Generator design. In fact, the norm of the distance between the fixed-point vector and the floating-point vector is  $\|\mathbf{w}_{\text{fixed}} - \mathbf{w}_{\text{float}}\| \simeq 0.037$ , thus, we can consider less than a 4% of error in this example. In practice, this tiny difference has a negligible effect on the BER performance of the whole system.

**Table 7.1:** Optimal weights obtained under different models for a particular MIMO channel (after rotation and scaling).

Model	Simulink/System Generator Model	Fixed-point model	Floating-point model
Weight 1	0.0317 - 0.0713i	0.0317 - 0.0713i	0.0526 - 0.0533i
Weight 2	0.6968 - 0.2138i	0.6968 - 0.2138i	0.6967 - 0.2137i
Weight 3	-0.1742 + 0.4592i	-0.1742 + 0.4592i	-0.1551 + 0.4693i
Weight 4	0.1029 + 0.4592i	0.1029 + 0.4592i	0.1144 + 0.4538i

The same procedure has been repeated for more than 20 different frames, i.e., the transmission of several training frames has been emulated through different MIMO channels. The MIMAX blocks have estimated the channels and calculated the optimal weights for every

case. In all the cases, the result has been satisfactory, showing a perfect concordance between the Simulink/System Generator model and the fixed-point model. Figure 7.4 shows this concordance for four frames distorted by different  $4 \times 4$  MIMO channels.

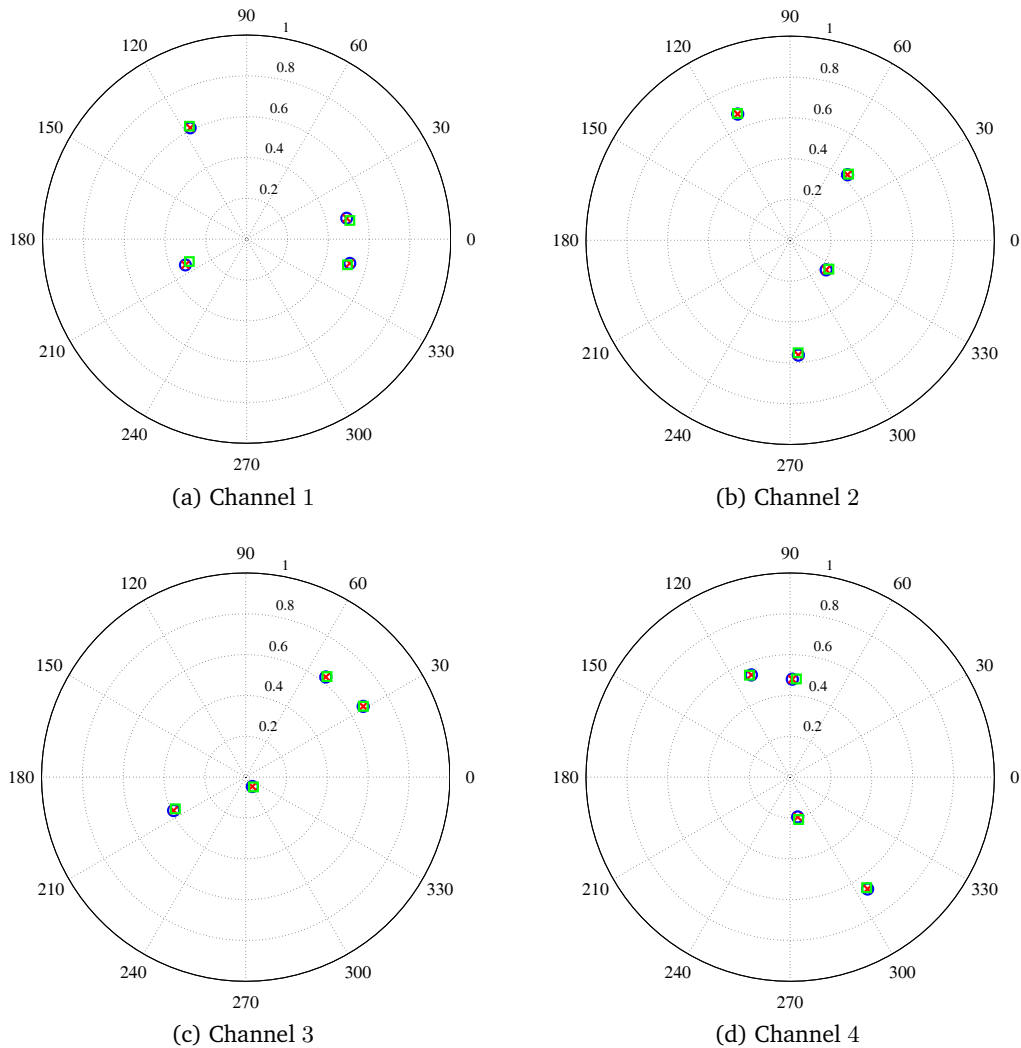


**Figure 7.4:** Comparison among the RF weights calculated in System Generator model (blue circles), fixed-point model (red crosses), and floating-point simulation (green squares).

### Reconfigurability

Prior to this point, all simulations have been conducted for the case when four antennas are present at the transmitter and the receiver side. The same type of simulations has been carried out for other numbers of transmit and receive antennas in order to test the performance of the reconfigurability. Figure 7.5 shows the weights calculated with all the models for a  $3 \times 3$  system. Again, the design behavior is identical bit-to-bit to the fixed-point model, and

also its behavior is almost the same as the floating-point model. Figure 7.6 shows some other configurations where all the models fit as expected.

Note that, in most of the polar representations with reconfigurability (Figures 7.5 and 7.6), there are some weights set to zero (in the center of the polar representation). The reasoning is that, regardless the number of receive antennas  $n_R$  of the wireless station, the RF Weights Block computes the four weights. In the cases where  $n_R < 4$ , there must exist at least  $4 - n_R$  weights set to zero corresponding to the non-existent antennas. For instance, Figure 7.6b and 7.6d have two weights set to zero, because both systems dispose  $n_R = 2$ .

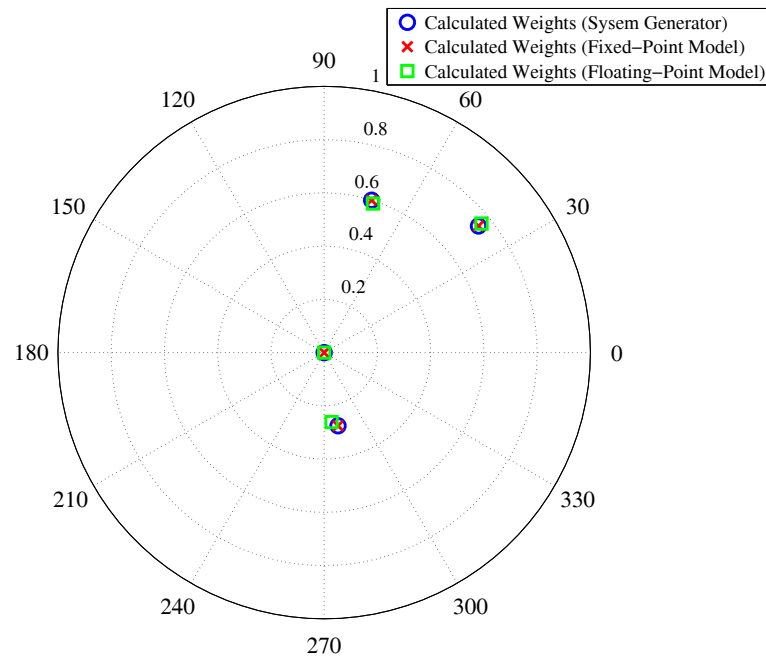


**Figure 7.5:** Comparison among the RF weights calculated in System Generator model, fixed-point model, and floating-point simulation for a  $3 \times 3$  system.

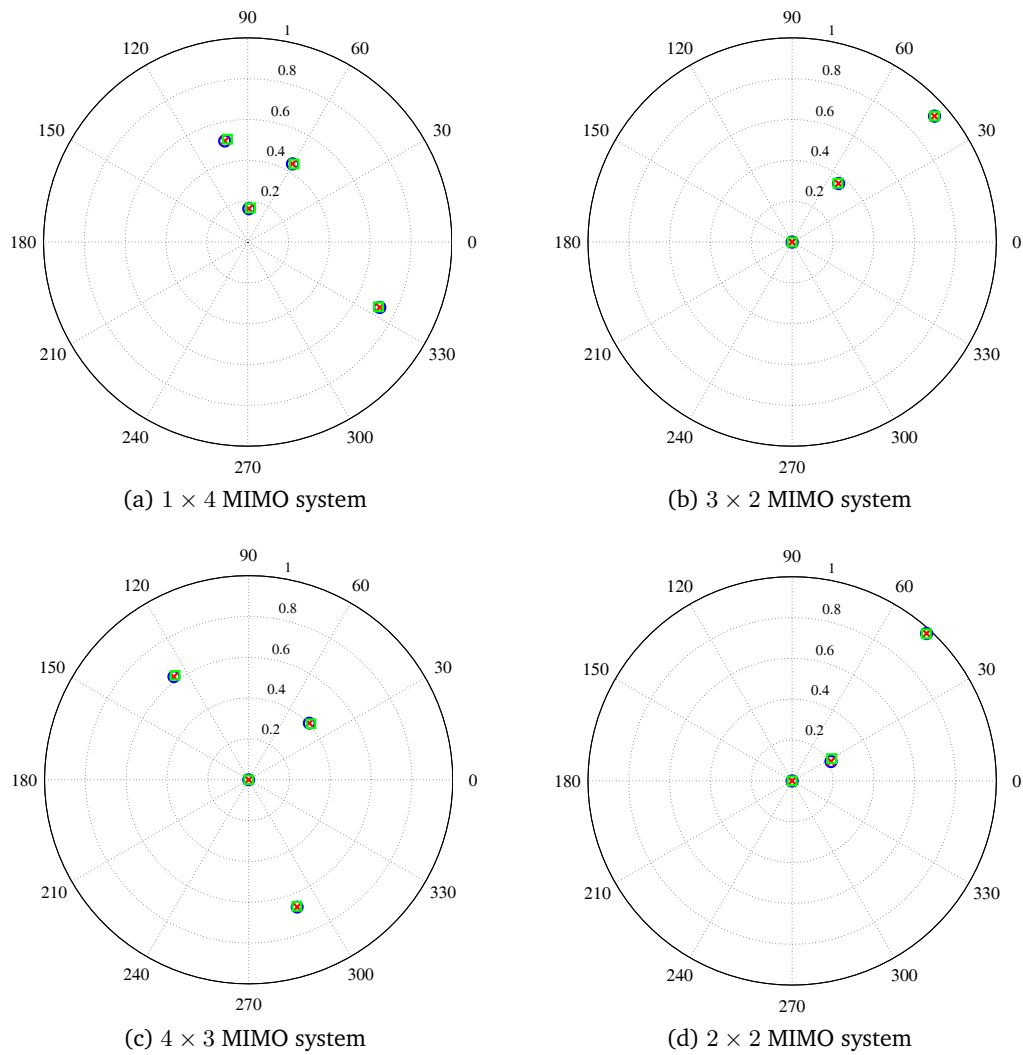


**Figure 7.6:** Comparison among the RF weights calculated in System Generator model (blue circles), fixed-point model (red crosses), and floating-point simulation (green squares).

### 7.2.2 ModelSim Simulation

After performing several simulations with System Generator, as described in the previous subsection, we have carried out some new simulations with ModelSim in order to test the behavior of the new MIMAX blocks. ModelSim is a verification and simulation tool for VHDL. As introduced in Chapter 6, System Generator designs can generate VHDL code, which can be integrated within some other VHDL projects. Therefore, a VHDL code generation from System Generator design has been done. Section 7.3 will enter into this subject in more detail.

Figure 7.7 shows the procedure to perform the ModelSim simulation of the new baseband blocks. One of the MIMAX partners, IHP, has provided the whole functional description in VHDL of the 802.11a baseband processor, and, in a joint development, new MIMAX functionalities have been added to it. These changes within the legacy 802.11a baseband allows the integration of the new MIMAX baseband blocks.

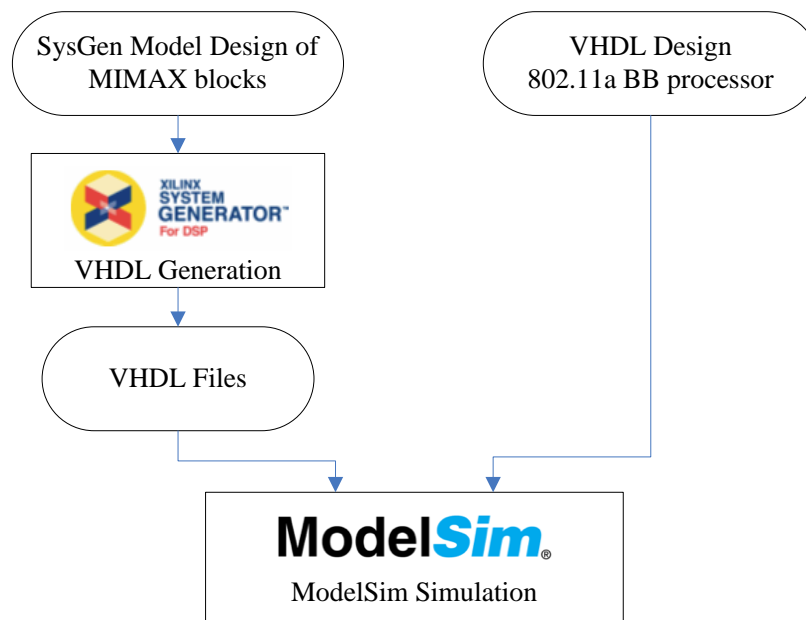


**Figure 7.7:** VHDL simulation flow: mixing VHDL and System Generator designs.

The legacy baseband processor model had been previously tested in ModelSim for the reception and transmission of different beacon and legacy frames.<sup>1</sup> Afterwards, several simulations of the whole MIMAX baseband processor have been performed in the reception of some training frames by using ModelSim testbench. The emulated received training frames used for these experiments are the same as those generated in Subsection 7.2.1 for the System Generator experiments.

Figure 7.8a represents an example in which the I and Q temporal samples of the incoming training frame (the two upper signals), the I and Q outputs of the FFT (the two signals in the middle) and the four weights, and valid signals (the lower ones) are shown. Figure 7.8b shows a zoomed version of the previous capture at cursor time, when the beamforming block provides the calculated optimal weights.

<sup>1</sup>This work was done by the MIMAX partner IHP institute.



## 7.3 Generation Process

As seen in Chapter 6, all the new baseband blocks were designed with System Generator. With this tool, the design process and the implementation are deeply interrelated in the sense that the design decisions are linked to the final architecture and, therefore, to the implementation. Some of those design decisions were made in Section 6.7.3, and some remaining decisions are still open at this point. Here, we summarize the final settings before generating the new baseband blocks:

- Signal precision at the input/output of the RF Weights Block: 8-bit
- Signal precision between the different steps of the RF Weights Block: 8-bit
- Number of power methods iterations: 5 iterations
- Number of delay cycles in adders and multipliers: 1 clock cycle

We have also added some delays in the data flow between the different new baseband blocks. The purpose of these extra delays consists in ensuring a correct routing and mapping in the generation process. This increases the time that the new baseband blocks take to calculate the optimal weights around a 5%, but this increment is not critical for the correct timing of the transceiver.

The ultimate goal of this section consists in the development of the complete MIMAX baseband processor merging the VHDL design of the conventional baseband processor with the new MIMAX blocks. Figure 7.9 shows the design flow followed to accomplish this goal. Further information about the generation process can also be found in [Santamaría et al., 2011].

The first part of the generation process consists in the generation of VHDL files, used for the ModelSim simulation (see Section 7.2.2), and the NGC files required for a further compilation. These NGC files are netlist files generated by the XST synthesis tool of Xilinx. Those netlist files provide the instances to Xilinx blocksets, interconnections, and some attributes of the blocksets.

The generation of the NGC and VHDL files is done through the System Generator Setting token within the Simulink environment. Figure 7.10 shows the dialog box for the files generation, where the relevant parameters are:

- **Compilation:** Specifies the type of compilation result that should be produced when the code generator is invoked. In our case, we would choose NGC Netlist or HDL Netlist.
- **Part:** Defines the FPGA type to be used. As seen in the next section, the FPGA model is the Virtex-5 LX330.
- **Hardware Description Language:** Specifies the HDL language to be used for the compilation of the design. The possibilities are VHDL and Verilog, and the former has been chosen.
- **Synthesis tool:** Specifies the tool to be used to synthesize the design. Xilinx's XST is selected.

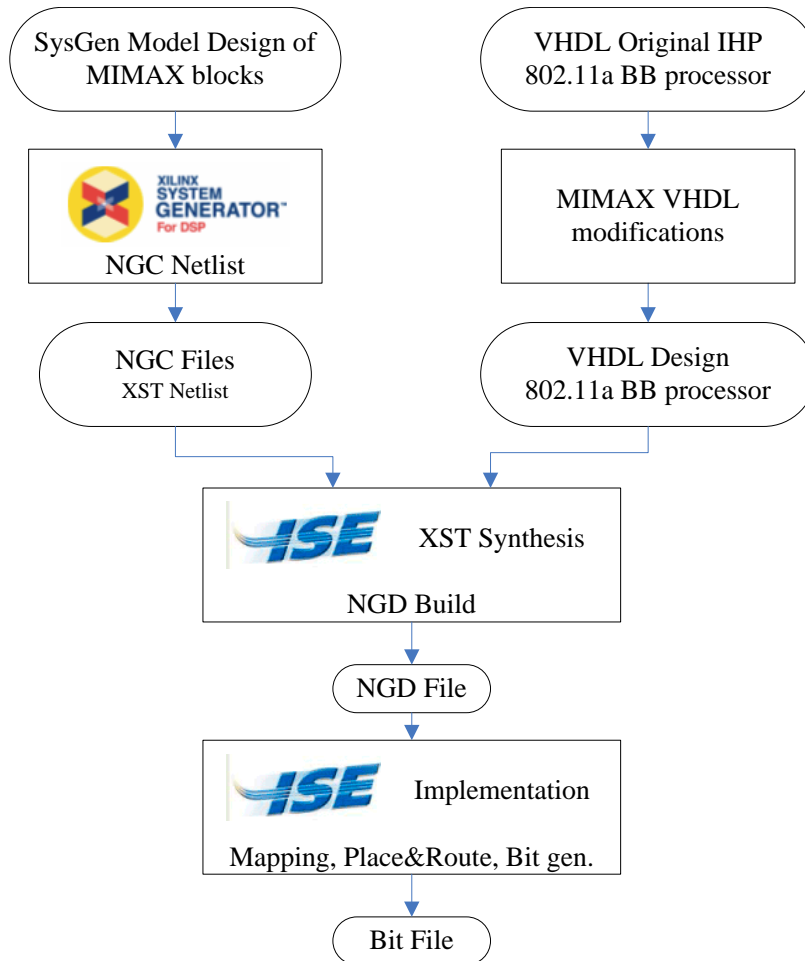


**Figure 7.9:** FPGA design flow: mixing VHDL and System Generator designs.

- FPGA clock period (ns): Defines the period in nanoseconds of the hardware clock as a constraint. We discuss this parameter in Subsection 7.3.3.

Note that the generation of the new MIMAX baseband blocks has been a single joint generation process for all the blocks, which means that a single entity (from now on, the MIMAX entity) containing all the MIMAX blocks has been created. This MIMAX entity is shown in Figure 7.11, and it has the interfaces that we have listed in Subsection 5.3.5. The architectural body of the new baseband blocks is thus included into the NGC file. This file contains all the information about the behavior and the structure of the new MIMAX blocks. In the following, several key aspects of the generation process are discussed.

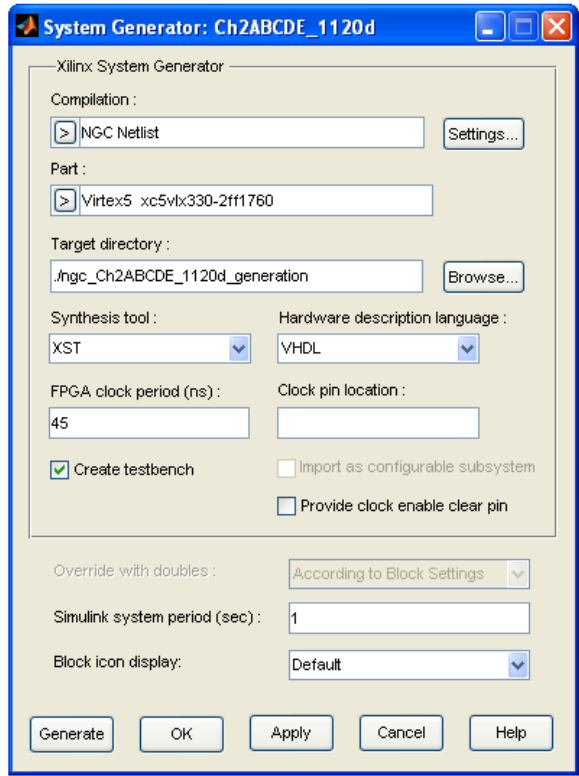


Figure 7.10: Dialog box for the generation of the NGC and VHDL files.

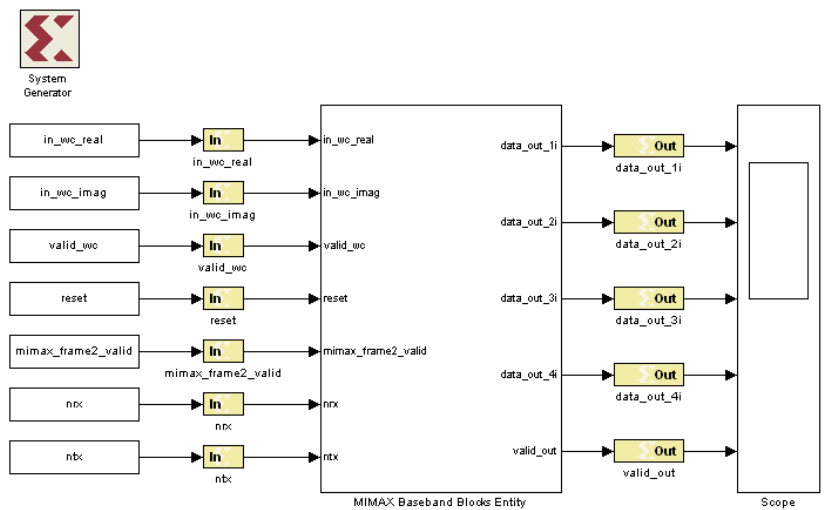


Figure 7.11: MIMAX entity generated with System Generator.

### 7.3.1 Target FPGA

Some preliminary studies about the final FPGA target were carried out at the beginning of the project, and they showed that the Virtex-5 LX220 could be a sufficient basis for the baseband MIMAX design. This baseband MIMAX processor includes the legacy 802.11a baseband processor, the new baseband blocks, and the RF control unit. Nevertheless, it was hard to estimate precisely the required resources before designing all the new MIMAX baseband blocks. For this reason, it was decided to consider a larger FPGA in order to minimize risks. Table 7.2 shows some of the most relevant features of both FPGA models. Finally, as we will see in the next chapter, the Virtex-5 LX330 FPGA was chosen for developing the MIMAX baseband prototype and for being mounted in the final baseband board.

**Table 7.2:** Most relevant features of XC5VLX220 and XC5VLX330 FPGAs of Virtex-5 family.

Resources	XC5VLX220	XC5VLX330
Virtex 5 Slices	34,560	51,840
Max Distributed RAM (Kb)	2,280	3,420
DSP48E Slices	128	192

### 7.3.2 First Generation Results

Once the generation process is finished (see Figure 7.10), many different files, including the NGC and VHDL ones, have been generated. Also, System Generator gives a report with statistics of the predicted FPGA utilization of the new baseband blocks. Table 7.3 shows the most relevant parameters.

**Table 7.3:** Slice logic utilization of the MIMAX blocks for XC5VLX330 FPGA.

Resources	XC5VLX330
Number of Slice Registers:	6%
Number of Slice LUTs:	19%
Number of Block RAM/FIFO:	25%
Number of DSP48Es:	16%

System Generator also makes an estimation of some timing constraints, such as the maximum achievable frequency. As shown in Table 7.4, the driving clock of the MIMAX blocks could not be higher than 53.35 MHz.

### 7.3.3 New Baseband Blocks Frequency Clock

In Subsection 6.7.2, we concluded that the RF Weights Block takes around 300 clock cycles to obtain the optimal weights. The objective now consists in selecting the frequency of the

**Table 7.4:** Summary of timing constrains.

Parameters	Time
Minimum period:	18.744 ns
Maximum clock frequency:	53.35 MHz
Minimum input arrival time before clock:	9.292 ns
Maximum output required time after clock:	0.396 ns
Maximum combinational path delay:	No path found

clock to drive the new baseband blocks. The sampling of the analog I/Q signals at the ADCs of the legacy 802.11a baseband board is done at 80 MHz. Nevertheless, these signals are oversampled in order to improve the performance of the Synchronizer, which decimates the signals by a factor of four. Thus, the FFT Block works at 20 MHz, and the input of the MIMAX Channel Estimation Block, the first new baseband block, is also at 20 MHz.

As seen above, the report after the generation of the NGC files shows that the maximum achievable frequency is 53.35 MHz. Then, it would be possible to drive the new blocks at 40 MHz, and they would take around 8  $\mu$ s to obtain the optimal weights. Nevertheless, as stated before, this time is not critical, and the increase of the clock frequency would involve an extra risk for the correct prototype working. Therefore, we have decided to minimize risks and to drive the new baseband blocks at 20 MHz.

## 7.4 FPGA Integration

Following the FPGA design flow diagram of Figure 7.9, in this section, we focus on the integration of the new baseband blocks (in form of the NGC files) within the updated legacy 802.11a baseband processor. This part has been done with Xilinx ISE Foundation. This program is an integrated design environment that consists of a set of programs to create, simulate, and implement digital designs in an FPGA. In this case, we take advantage of the synthesis and implementation feature for merging the whole MIMAX baseband processor.

### 7.4.1 First Integration Tests

The first integration tests of the System Generator compilation results were made for a simple design with a reduced ISE project. In this simple project, the whole baseband processor was not present but only the MIMAX entity. The success of this first test illustrated the feasibility of the integration between the new baseband blocks and the Xilinx ISE project of the modified legacy 802.11a baseband processor. It also allowed us to find out the real occupancy results of the MIMAX baseband blocks.<sup>2</sup> Table 7.5 shows the occupancy of the new MIMAX baseband blocks for the Xilinx FPGA model Virtex-5 XC5VLX220 and also for the Virtex-5 XC5VLX330.

<sup>2</sup>Note that the occupancy results given by System Generator in the generation report and shown in Table 7.3 are simply an estimation.

**Table 7.5:** FPGA resources of MIMAX beamforming block generation.

Resources	XC5VLX220	XC5VLX330
Slice registers	13%	8%
Slice LUTs	29%	19%
Occupied slices	33%	22%

### 7.4.2 Integration of the New MIMAX Blocks within the Legacy 802.11a Baseband Processor

Once the feasibility of the integration process has been proven, the next step consists in merging the resultant NGC files of the MIMAX entity with the whole baseband processor ISE project (see Figure 6.1).

Starting from the existent ISE project of the baseband processor, the MIMAX entity must be firstly declared. This represents the external interface to the design entity, and it agrees with the inputs and the outputs of the System Generator block as shown in Figure 7.12 that represents the declaration in VHDL of the entity as a component of the ISE project.

```

component ch2abcde_1120d_cw
port (
  ce: in std_logic := '1';
  clk: in std_logic;
  in_wc_imag: in std_logic_vector(15 downto 0);
  in_wc_real: in std_logic_vector(15 downto 0);
  mimax_frame2_valid: in std_logic;
  nrx: in std_logic_vector(1 downto 0);
  ntx: in std_logic_vector(1 downto 0);
  reset: in std_logic;          -- high active
  valid_wc: in std_logic;
  data_out_1i: out std_logic_vector(15 downto 0);
  data_out_2i: out std_logic_vector(15 downto 0);
  data_out_3i: out std_logic_vector(15 downto 0);
  data_out_4i: out std_logic_vector(15 downto 0);
  valid_out: out std_logic);
end component;

ATTRIBUTE syn_black_box : BOOLEAN;
ATTRIBUTE syn_black_box OF ch2abcde_1120d_cw : COMPONENT IS
true;
ATTRIBUTE box_type : STRING;
ATTRIBUTE box_type OF ch2abcde_1120d_cw : COMPONENT IS
"black_box";

```

**Figure 7.12:** VHDL declaration of the entity within the ISE project.

The next step of the integration of the new baseband blocks consists in the instantiation of the block, i.e., the location of the block within the baseband processor, defining the port mapping of the entity as shown in Figure 7.13.

The NGC file must be added to the ISE project in order to be merged with the VHDL description of the rest of the baseband processor. Figure 7.14 displays the ISE project environment, where the MIMAX entity is included.

```

ich2: ch2abcde_1120d_cw PORT MAP
  (clk => clk20,
   reset => ch2abcde_rst,
   ce => ce,
   mimax_frame2_valid => mimax_frame2_valid,
   nrx => N_RX,
   ntx => N_TX,
   in_wc_real => FFTout1,
   in_wc_imag => FFTout2,
   valid_wc => FFTvalid,
   data_out_1i => OptWght0,
   data_out_2i => OptWght1,
   data_out_3i => OptWght2,
   data_out_4i => OptWght3,
   valid_out => OptwReady0);

```

Figure 7.13: VHDL instantiation of the entity within the ISE project.

The screenshot displays the ISE Project Navigator interface. The main window shows the Design Summary for the project 'MimaxBB\_USB'. The summary table is as follows:

MimaxBB_USB Project Status (03/31/2011 - 16:24:53)			
<b>Project File:</b>	MimaxBB_USB.isc	<b>Implementation State:</b>	Programming File Generated
<b>Module Name:</b>	MimaxBB_USB	<b>Errors:</b>	No Errors
<b>Target Device:</b>	xc5v1x330-1ff1760	<b>Warnings:</b>	5387 Warnings
<b>Product Version:</b>	ISE 11.1	<b>Routing Results:</b>	All Signals Completely Routed
<b>Design Goal:</b>	Balanced	<b>Timing Constraints:</b>	All Constraints Met
<b>Design Strategy:</b>	Xilinx Default (unlocked)	<b>Final Timing Score:</b>	0 (Setup: 0, Hold: 0, Component Switching Limit: 0) (Timing Report)

Below the summary table, there is a 'Device Utilization Summary' section with a table that has columns for 'Slice Logic Utilization', 'Used', 'Available', 'Utilization', and 'Note(s)'. The 'Design Summary (Programming File Generated)' window is active at the bottom.

Figure 7.14: ISE project.

The final steps of the FPGA design flows, shown in Figure 7.9, consist of the synthesis (with XST synthesis tool of Xilinx) and the implementation of the whole baseband processor. ISE project completed those steps successfully and provided the statistics of the process. Table 7.6 shows the resources occupied by this first MIMAX baseband processor when implemented in a Xilinx Virtex-5 XC5VLX220 FPGA and into a XC5VLX330. This is an important milestone in the baseband development, and it is remarkable that the first complete FPGA version of the baseband processor would even fit in a cheaper FPGA, such as the Virtex-5 XC5VLX220. The outcome of the ISE implementation process is a .bit file that can configure the FPGA of the baseband board. The configuration of the baseband board FPGA as well as some real-time test campaigns will be discussed in Chapter 8.

**Table 7.6:** FPGA resources of complete MIMAX baseband processor generation.

Resources	XC5VLX220	XC5VLX330
Slice registers	33%	22%
Slice LUT's	61%	40%
Occupied slices	71%	47%

## 7.5 Conclusions

In this chapter, starting from the the design of the new MIMAX blocks proposed in the previous chapter, the behavior of these blocks has been tested by means of different simulations. The design of each block has been successfully evaluated as well as the behavior of all the blocks within the receiver part of the legacy 802.11a baseband processor by means of different simulations conducted in System Generator and in ModelSim.

Once the blocks have been validated in simulation, the NGC generation of the blocks has been performed with System Generator, obtaining at the end the MIMAX entity. A first estimate of the needed resources of the new MIMAX blocks has been given by the generation report of System Generator. Finally, the new MIMAX blocks have been successfully integrated within the ISE project of the whole baseband processor. The project has been synthesized and implemented, and first results of the occupancy of the MIMAX baseband processor have been obtained. It has been shown that the MIMAX baseband processor fits in the Virtex-5 XC5VLX330 FPGA, which is the FPGA model mounted in the baseband board that will allow us to test in real-time the behavior of the designed MIMAX blocks as will be shown in the next chapter. As a final point, the publications that have contributed to this chapter are [Kraemer et al., 2010, Stamenkovic et al., 2010, Elvira et al., 2010, Eickhoff et al., 2011], and also the technical report [Ibañez et al., 2009b].

## 8.1 Introduction

The ISE project of the whole baseband processor, including the new blocks, has been synthesized and implemented in the previous chapter to obtain a `.bit` file, which programs the FPGA of the MIMAX baseband board. In this chapter, the MIMAX baseband board has allowed us to test in real-time the synthesized blocks within the whole MIMAX baseband processor. A simple setup with the baseband board and a vector signal generator is firstly proposed in order to test the behavior of the new MIMAX blocks within the baseband processor. The computed weights are compared with those expected in simulation, checking the correct operation of the new MIMAX blocks within the FPGA. A different setup for the physical layer tests of the MIMAX demonstrator (or prototype) is also presented. These tests have been carried out through a wireless channel between two stations, each one with the whole MIMAX physical layer (i.e., the MIMAX antenna array, the MIMAX analog front-end, and the MIMAX baseband processor). Finally, certain user-level tests are briefly reviewed, where the complete MIMAX prototype has been employed for some services of the triple play, such as Internet Protocol Television (IPTV) or High Definition (HD) video conference over Skype.

## 8.2 MIMAX Baseband Board

According to the MIMAX system architecture shown in Figure 5.3 and regarding the required functionalities, the MIMAX baseband board has been jointly designed by IHP and the GTAS group. Figure 8.1 shows the picture of this MIMAX baseband board that has been manufactured and mounted by IHP.

The baseband board integrates the baseband processor, i.e., signal processing chain of the conventional SISO IEEE 802.11a and the new MIMAX blocks with the RF control unit inside a single FPGA. In particular, the baseband modules are integrated within this board featuring communication with the MAC and the AFE. For this purpose, the baseband board incorporates a flexible FPGA and all required interfaces. The main component of the baseband board is the FPGA, which is the Xilinx Virtex-5 LX330 selected in previous chapters. Nevertheless, a smaller and cheaper FPGA, such as LX220, LX155, or LX110, could be soldered, if they were sufficient for further MIMAX prototypes (see Section 7.3 about the FPGA occupancy of the MIMAX baseband processor). Other components are digital-to-analog (DACs) and analog-to-digital converters (ADCs) for baseband and Q transmit/receive signals and RSSI



**Figure 8.1:** MIMAX baseband board (135 mm × 225 mm).

signal, programmable flash memories, power and clock circuitries, and connectors. A detailed description of the main components and connectors of the baseband board is given as follows:

- FPGA:
  - Component: Xilinx Virtex-V LX330.
  - Function: MIMAX baseband processor and RF control unit.
- Dual digital to analog converter:
  - Component: AD9763.
  - Function: Generation of I- and Q-baseband transmitted signals.
  - Specifications:
    - \* Sampling frequency: 80 Msps.
    - \* Resolution: 10 bit.
- Dual analog to digital converter
  - Component: AD9218.
  - Function: Acquisition of I- and Q-baseband received signals.
  - Specifications:
    - \* Sampling frequency: 80 Msps.
    - \* Resolution: 14 bit.<sup>1</sup>
- RSSI analog to digital converter:
  - Component: AD9200.

<sup>1</sup> Note that this additional range allows a proper AGC operation when receiving training frames (MIMAX frames II). Notice that all the training symbols are distorted by a different equivalent SISO channel (unknown when the AGC is frozen), and, therefore, the signal level of one of them could largely exceed the signal level of the frame preamble.

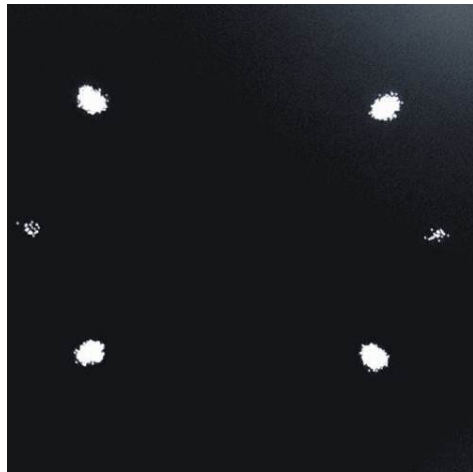
- Function: Acquisition of RSSI signal.
- Specifications:
  - \* Sampling frequency: 20 Msps.
  - \* Resolution: 10 bit.
- Main Interfaces:
  - MAC connector (MIPP).
  - AFE connector.

The baseband board supplies three debug ports of 16-bit width plus one clock each. By modifying the VHDL code of the baseband processor, any internal signal of the baseband could be available for debugging purposes. A connector for a normal computer monitor is also provided for debugging purposes. It operates in super video graphics array (SVGA) mode  $800 \times 600$  at 75Hz and permits the showing of the constellation diagram of all OFDM data symbols (except preamble) in every received frame and, the screen is cleared before every new frame. Then, for each subcarrier in every payload OFDM symbol, one pixel is switched on to show the constellation. The emerging picture depends on the modulation scheme and noise. It is overlaid with the two dots originating from the SIGNAL field (always BPSK modulated). As an example, Figure 8.2 shows different constellation diagrams of different received legacy data frame at the baseband processor. It can be appreciated that the constellations for wireless channels suffer certain performance degradation, especially the constellation shown in Figure 8.2d, which represents the reception of a BPSK frame under a noisy channel.

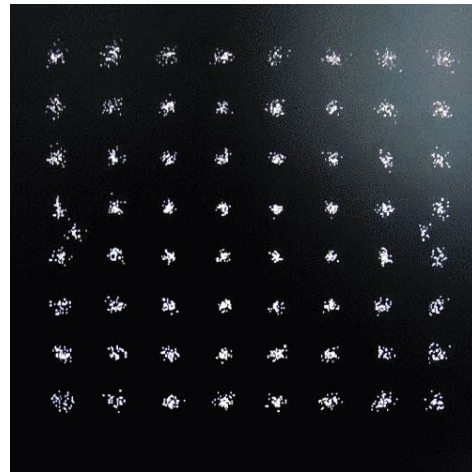
The developed board has one 8-bit dual in-line packet (DIP) switch to select which internal signals are routed to the three debug output ports mentioned above. Also, the transmitter test modes are enabled with certain switch settings. Additionally, the baseband board provides three push buttons and two rows of eight LEDs each. The six green LEDs of the lower row indicate good levels of power supply at different parts baseband board. The 7<sup>th</sup> LED is not utilized. The 8<sup>th</sup> LED lights red while the FPGA is being programmed. The LEDs in the upper row are user-programmable. The push buttons "TA1" and "TA2" are currently connected to the "reset" outputs to the analog front-end. When pressing the "PROG" button, the FPGA is re-booted from the flash. Figure 8.3 shows the LEDs, switches, and buttons panel.

For FPGA programming, a Xilinx programming unit (Xilinx Platform Cable USB II) must be connected to the JTAG connector. One can either directly program the FPGA or the code flashes (PROMS). The latter is permanent while the former is volatile, i.e., the program is lost when the board is switched off. The FPGA program is contained within the `.bit` file generated with ISE project navigator as depicted in Chapter 7.

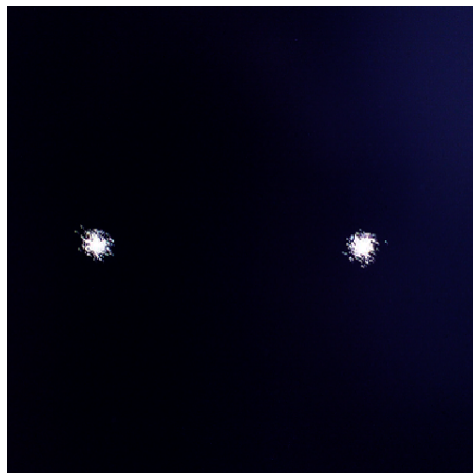
While the powering-up of the baseband board, the content of the code flashes is loaded into the FPGA. For this reason, we decided to program the code flashes, thus, we do not need to program manually the baseband processor every time we operate with it. The code flashes are three Xilinx xcf32p PROM chips, each having 32 Mbit of capacity (see Figure 8.1). The three PROM files must be generated from the `.bit` file with the Xilinx Impact tool. This program divides the `.bit` file and program the code flashes.



(a) Constellation plot for a wired transmission of a QPSK data frame.



(b) Constellation plot for a wired transmission of a 64-QAM data frame.



(c) Constellation plot for a wireless transmission of a BPSK data frame (high SNR).



(d) Constellation plot for a wireless transmission of a BPSK data frame (low SNR).

**Figure 8.2:** Different constellations observed in a monitor through the VGA monitor connector of the baseband board.

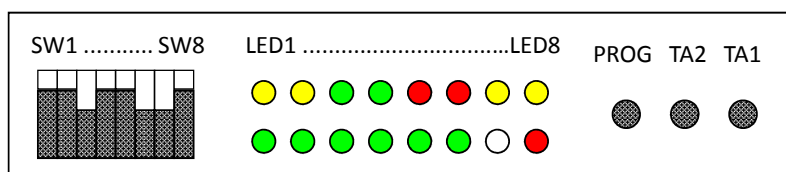


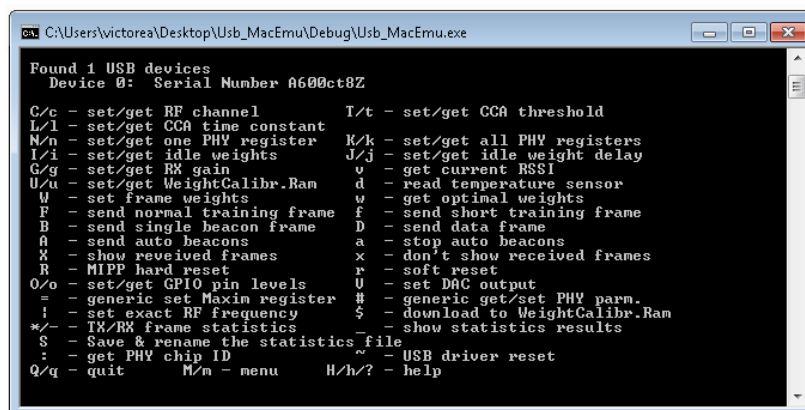
**Figure 8.3:** Switches, LEDs, and push buttons on the baseband board.

## 8.3 MAC Emulator

The MAC emulator, developed by the MIMAX partner IHP, is a program that runs on a PC. It has been used for the tests, because it provides more flexibility and control over the setup than the final MAC board, and it also allows to test the baseband processor isolated from the MAC processor.<sup>2</sup>

The USB terminal program USB\_MacEmu (also called MAC emulator user interface) is an interactive terminal program to send and receive control commands as well as frame data directly from the PC to the MIMAX baseband board without the need for a MAC. It requires a special USB adapter board, which must be connected to the MIMAX baseband board at the MIPP connector. The executable program USB\_MacEmu must be started in a terminal under Linux or from the DOS prompt under Windows.<sup>3</sup>

The MIMAX baseband board including USB converter board is powered on before starting USB\_MacEmu. As seen in Figure 8.4, the USB program displays a menu of available commands. A command is executed by pressing the respective key. Generally, lower case letters are for reading parameters, while upper case letters are for setting them. The user is prompted for the required parameters or values. In most cases, the currently used parameter value is displayed. When no change is intended, the user can simply press <Enter>. Otherwise, simply type the new value. The old value is automatically cleared.



```

C:\Users\victorea\Desktop\Usb_MacEmu\Debug\Usb_MacEmu.exe
Found 1 USB devices
Device 0: Serial Number A600ct8Z

C/c - set/get RF channel          T/t - set/get CCA threshold
L/l - set/get CCA time constant   K/k - set/get all PHY registers
N/n - set/get one PHY register    J/j - set/get idle weight delay
I/i - set/get idle weights        v - get current RSSI
G/g - set/get RG gain             d - read temperature sensor
U/u - set/get WeightCalibr.Ram    w - get optimal weights
W - set frame weights             f - send short training frame
F - send normal training frame    D - send data frame
B - send single beacon frame      a - stop auto beacons
A - send auto beacons             x - don't show received frames
K - show received frames          r - soft reset
R - MIPP hard reset               U - set DAC output
O/o - set/get GPIO pin levels     # - generic get/set PHY parm.
- - generic set Maxin register    $ - download to WeightCalibr.Ram
! - set exact RF frequency        ~ - show statistics results
*/- - TX/RX frame statistics
S - Save & rename the statistics file
: - get PHY chip ID               ~ - USB driver reset
Q/q - quit                        M/m - menu      H/h/? - help

```

Figure 8.4: MAC emulator user interface (Usb\_MacEmu program).

Here, we present some of the most important commands of the USB\_MacEmu and a brief description of them:

- "R": board hard reset (resets almost everything on the baseband board)
- "~": USB interface reset
- "N": read PHY ID from board, shall return 240 if the baseband board is operative
- "T/t": set/get the CCA threshold

<sup>2</sup>Refer to [Ibañez et al., 2009b] for more details about the MIMAX MAC processor and its features with respect to the legacy 802.11a MAC processor

<sup>3</sup>It is console application and not a graphical user interface (GUI)

- "c": read current RF channel number, which default value in decimal is 52
- "C": change current RF channel number. Bit 2 of the RF channel number is connected to the rightmost yellow LED 8 (see Figure 8.3), which shall be on or off, depending on channel number (e.g. on for default channel 52, off for channel 48 or 56)
- "q" or "Ctrl-C": terminate the MAC emulator
- "D": send a data frame
- "F": send a training frame
- "w": get the optimal weights calculated for the last received training frame

The received frames (beacon, data, or training frames) are automatically shown in the USB terminal program, i.e., the baseband processor is always in reception mode except when it transmits a frame or when the hard reset signal is activated. The MAC emulator program has been also modified at the GTAS group in order to add some other functionalities for further experiments as we will see in Section 8.5.

## 8.4 First Real-Time Testing of the MIMAX Blocks

In order to test the implementation of the new baseband blocks, a first setup without the AFE and the MAC processor has been developed. In this way, the baseband processor has been isolated.

### 8.4.1 Setup

In the first part of the real-time experiments, an exhaustive battery of tests of the baseband board has been conducted. To this end, we have used the setup shown in Figure 8.5, where the following elements can be identified:

- **Baseband board:** Its main component is the FPGA which contains the MIMAX baseband processor.
- **MAC emulator:** It allows emulating some basic MAC functions (such as data and training frame transfers) by means of a USB terminal program.
- **Xilinx Platform Cable USB II:** It programs the FPGA using the JTAG port of the board.
- **Oscilloscope:** Connected to the DAC outputs for testing the frame transmissions of the board.
- **Vector signal generator:** Used to transmit different data and training frames feeding the ADC inputs of the board, i.e., it replaces the AFE.

The baseband version uploaded on the FPGA includes the full 802.11a compliant baseband (with the required changes for the adaptation to MIMAX), the RFCU, and the new MIMAX blocks.

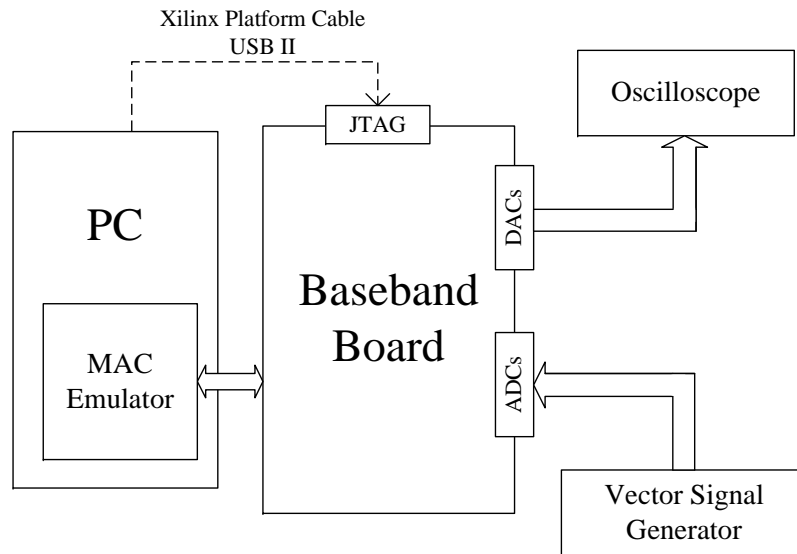


Figure 8.5: Setup for the first real-time tests.

#### 8.4.2 Preliminary Basic Tests

With the aim of verifying the basic operation of the baseband board, we have performed some preliminary, basic experiments. In order to test that the baseband board was operative and also that the MAC emulator was working as expected, we have verified the correct reading, changing, and re-reading of a few configuration parameters. We have experimented with these parameters, specifically with the RF channel and the CCA threshold parameters, because, as seen in Section 8.3, LED 8 and LED 1 of the board are enabled/disabled depending on the values of these parameters. Figure 8.6 shows the MAC emulator user interface while performing these basic tests.

```

C:\Users\victorea\Desktop\Usb_MacEmu\Debug\Usb_MacEmu.exe
M/m - set/get one PHY register      K/k - set/get all PHY registers
I/i - set/get idle weights         J/j - set/get idle weight delay
G/g - set/get RX gain              v - get current RSSI
U/u - set/get WeightCalibr.Ram     d - read temperature sensor
W - set frame weights              w - get optimal weights
F - send normal training frame     f - send short training frame
B - send single beacon frame       D - send data frame
A - send auto beacons              a - stop auto beacons
X - show received frames           x - don't show received frames
R - MIPF hard reset                r - soft reset
O/o - set/get GPIO pin levels      U - set DAC output
= - generic set Maxim register     # - generic get/set PHY parm.
! - set exact RF frequency         $ - download to WeightCalibr.Ram
*/ - TX/RX frame statistics        - show statistics results
$ - Save & rename the statistics file
: - get PHY chip ID                ~ - USB driver reset
Q/q - quit                          M/m - menu      H/h/? - help

c curr. RF channel = 52 [5260 MHz]
C new RF channel (36 [5180MHz] - 64 [5320MHz]): 50
c curr. RF channel = 50 [5250 MHz]
t curr. CCA threshold = 35
I new CCA threshold: 5
t curr. CCA threshold = 5
  
```

Figure 8.6: Preliminary basic tests consisting in reading, changing, and re-reading some configuration parameters.

### 8.4.3 Basic Transmission and Reception Tests

New MIMAX baseband blocks do not operate on the transmission of beacon and data frames. Nevertheless, we have carried out some basic tests for the transmission and reception of these legacy 802.11a frames in order to test the fine behavior of the baseband board. Note that none of the changes performed on the legacy 802.11a frames should be involved when transmitting and receiving legacy frames.

First of all, a few beacon and data frames have been transmitted using the USB program terminal. Figure 8.7 shows the transmission of a data frame with a payload of 44 bytes at rate 6 Mbps. The generated I/Q signals at the DAC have been analyzed in order to verify a correct transmission of the different frames.

```

C:\Users\victorea\Desktop\Usb_MacEmu\Debug\Usb_MacEmu.exe
N/n - set/get one PHY register      K/k - set/get all PHY registers
I/i - set/get idle weights         J/j - set/get idle weight delay
G/g - set/get RX gain              v - get current RSSI
U/u - set/get WeightCalibr.Ran     d - read temperature sensor
W - set frame weights              w - get optimal weights
F - send normal training frame     f - send short training frame
B - send single beacon frame       D - send data frame
a - send auto beacons              a - stop auto beacons
X - show received frames           x - don't show received frames
R - MIPP hard reset                r - soft reset
O/o - set/get GPIO pin levels      U - set DAC output
= - generic set Maxim register     # - generic get/set PHY parm.
! - set exact RF frequency         $ - download to WeightCalibr.Ran
*/- - TX/RX frame statistics       - - show statistics results
$ - Save & rename the statistics file
+ - get PHY chip ID                * - USB driver reset
Q/q - quit                          H/h/? - help

D send one data frame at <6/9/12/18..Mbit/s>: 6
payload length: 16 dest. address (last byte): A2
TX 44 bytes @ rate B
08 00 00 02 00 50 C2 61 21 A2 00 50 C2 61 21 AA
22 44 66 88 AA CC 00 00 00 01 02 03 04 05 06 07
08 09 0A 0B 0C 0D 0E 0F 24 4D E2 40

```

Figure 8.7: MAC emulator user interface when transmitting a data frame.

Afterwards, some different 802.11a data frames have been generated in MATLAB (off-line) with a function programmed to create configurable 802.11a frames. The generated frames have been downloaded to the vector signal generator (Agilent E4438C). The I/Q signals generated with the vector signal generator have been used to feed the ADCs of the MIMAX baseband board as depicted in Figure 8.5.

Once the baseband processor has detected an incoming frame and has processed the data, it delivers the data payload to the MAC layer (the MAC emulator in our case). Figure 8.8 shows the correct reception of a data frame (indicated by the "Good CRC") and the data bytes of the payload delivered to the MAC emulator.

### 8.4.4 Reception of Training Frames

In this section, we describe the most important test aimed at checking the adequate real-time behavior of the developed blocks. Note that the new baseband blocks, studied, designed, and implemented in the previous chapters, only work when receiving a training frame (MIMAX frame II). These blocks are responsible mainly for the correct MIMO channel estimation and the calculation of the optimal weights that must be applied at the analog front-end.

In order to check the real-time behavior of the MIMAX blocks, some training frames have been created in MATLAB (off-line). The generation of the incoming training frames has been done analogously to the generation in Section 7.2.1. Therefore, a training frame for a  $4 \times 4$  MIMO system has been generated, where each of the 16 training symbols is affected by a

```

C:\Users\victorea\Desktop\Usb_MacEmu\Debug\Usb_MacEmu.exe
L/l - set/get CCA time constant      K/k - set/get all PHY registers
N/n - set/get one PHY register      J/j - set/get idle weight delay
I/i - set/get idle weights          v - get current RSSI
G/g - set/get RX gain               d - read temperature sensor
U/u - set/get WeightCalibr.Ram      w - get optimal weights
W - set frame weights               f - send short training frame
F - send normal training frame      D - send data frame
B - send single beacon frame        a - stop auto beacons
A - send auto beacons               x - don't show received frames
X - show received frames            r - soft reset
R - MIPP hard reset                 U - set DAC output
O/o - set/get GPIO pin levels        # - generic get/set PHY parm.
= - generic set Maxim register       $ - download to WeightCalibr.Ram
i - set exact RF frequency          ~ - show statistics results
w/- TM/RX frame statistics           ~ - USB driver reset
S - Save & rename the statistics file
: - get PHY chip ID
Q/q - quit                          M/m - menu      H/h/? - help

RX 52 bytes @ rate B
00 00 00 02 FF FF FF FF FF 00 50 C2 61 21 AA
22 44 66 88 AA CC 03 00 05 00 00 00 00 00 00
00 04 02 00 00 05 4D 69 6D 61 78 01 01 8C 06 02
00 00 5C 86 02 34 <Good CRC>

```

Figure 8.8: MAC emulator user interface when receiving a data frames.

different SISO channel, i.e., a training frame distorted by a known MIMO channel. In this manner, we have then generated several training frames affected by different MIMO channels. Specifically, we have generated flat-fading channels and frequency-selective channels with different delay profiles (see Section 7.2 for more details).

For these tests, the same baseband processor setup shown in Figure 8.5 has been used. The different training frames have been then downloaded and transmitted with the vector signal generator. For each received MIMAX training frame, the procedure has been as follows: the Synchronizer detects the incoming frame, the transmit/receive baseband block identifies the frames as training frames, and it activates the new baseband blocks. These blocks estimate the MIMO channel and calculate the optimal weights. Finally, when the optimal weights are available, they are sent to the MAC emulator. Then, the USB program terminal notifies the reception of a training frame as well as the calculated optimal weights. Figure 8.9 shows a capture of the USB program terminal after the reception of the training frame. It can be seen that the calculated optimal weights are the following four words of 16-bit precision given in hexadecimal: "05FA EB45 EE2E 0A2D". Each word represents one of the four entries of the weights vector  $\mathbf{w}_R$ . The first and the second bytes of the word are, respectively, the signed representation of the Q (imaginary) and I (real) part of the optimal weight. For this example, "FA" is the I (real) part of the first weight (applied to the first antenna), and "05" is the Q (imaginary) part of the same first weight. For each different received training frame, we have converted the hexadecimal value of the weights to signed value in order to represent them in a graphical polar plot. Following the same example, the obtained weights in Figure 8.9 are  $\mathbf{w}_R = [0.0391 - 0.0469i; 0.5391 - 0.1641i; -0.1406 + 0.3594i; 0.0781 + 0.3516i]^T$ .

Note that, as stated in the previous chapters, any scaled or rotated version of  $\mathbf{w}_R$  is equivalent; hence, within all the polar figures, we have scaled the weights to a unitary norm and rotated them to align the largest weight in order to appreciate the graphical comparison between the obtained values in the real-time test and the expected ones. The expected values have been taken from simulations made in System Generator or ModelSim, as described in Section 7.2 (both types of simulations provide identical bit-to-bit results).

Figure 8.10 shows a first comparison in polar representation between the weights provided by the new baseband blocks to the MAC emulator in real-time and the weights obtained in simulation. We have also added the weights calculated with the floating-point algorithm of the approximated MaxSNR solution. Firstly, we can see that the agreement between the real-

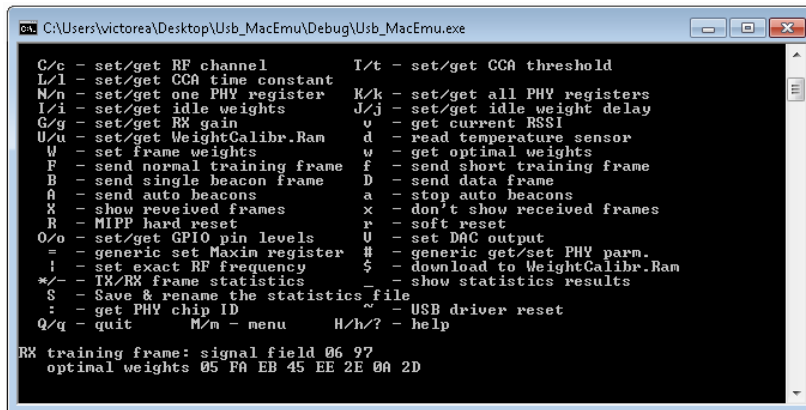


Figure 8.9: MAC emulator user interface when receiving a training frame.

time and the fixed-point simulation is almost perfect. The tiny differences can be blamed on the fact that the MATLAB digital signals are converted to analog domain by the vector signal generator, transmitted, and finally reconverted to digital at the baseband board ADCs.

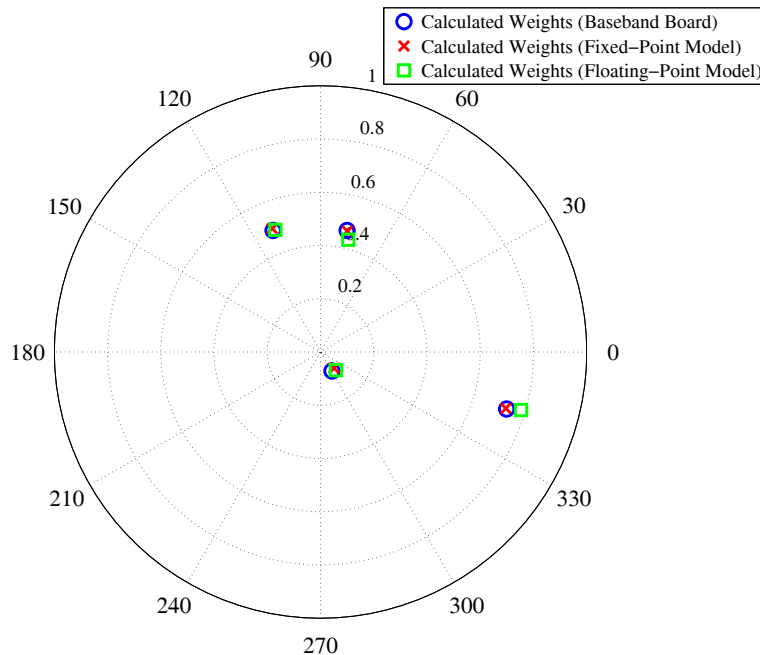
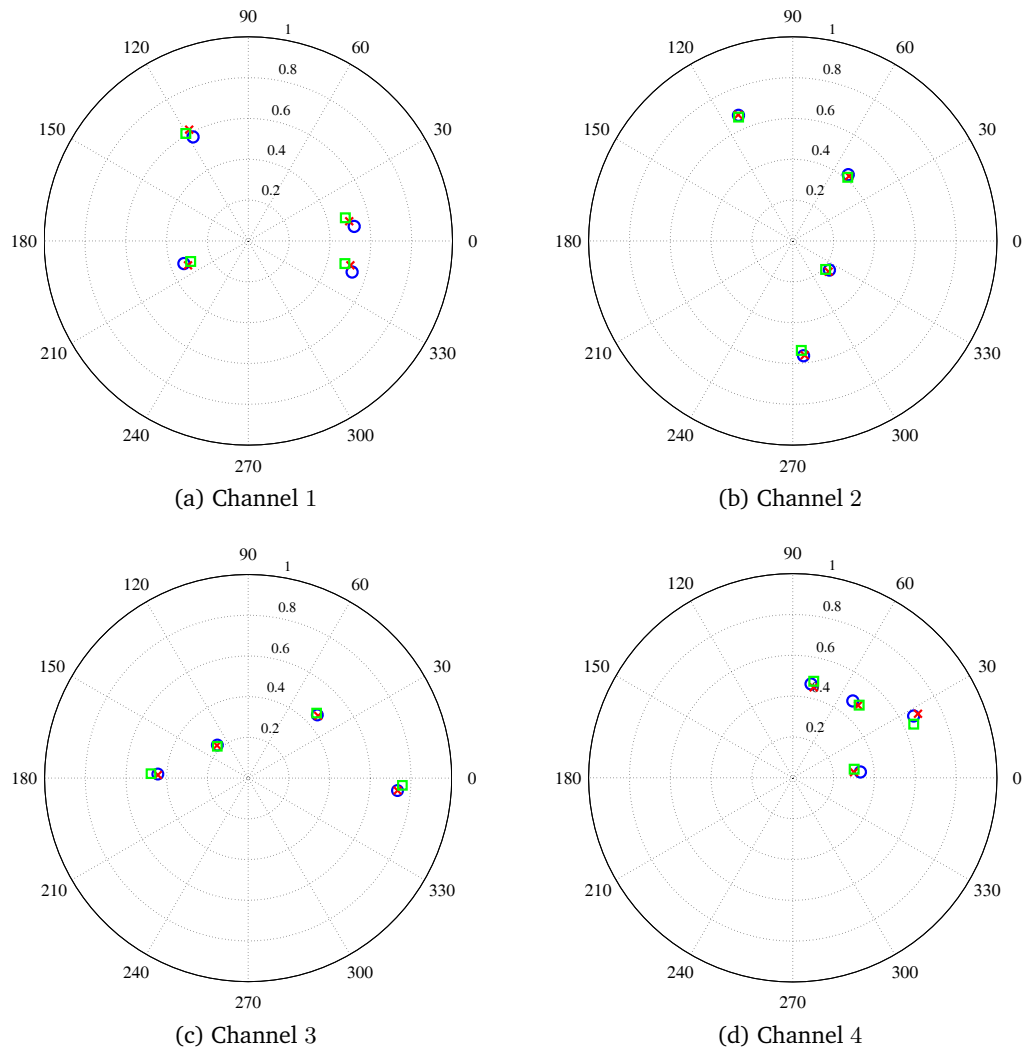


Figure 8.10: Comparison among the RF weights obtained in real-time, in fixed-point design simulation, and in floating-point simulation.

This procedure has been performed for several training frames affected by different MIMO channels: flat channel, frequency-selective channels with different delay profiles, etc. In all examples, a very good agreement between the weights obtained in simulation and those provided by the board was obtained. Figure 8.11 illustrates four examples of different MIMO channels, where the successful behavior of the new baseband blocks in real-time is shown.



**Figure 8.11:** Comparison among the RF weights calculated in real-time (blue circles), fixed-point design simulation (red crosses), and floating-point simulation (green squares) for four different channels.

## Reconfigurability

Previous to this point, we have tested in real-time the implementation of the new baseband blocks for the reception of training frames in a simulated  $4 \times 4$  system. This means that the incoming training frames have 16 training symbols and indicate in its MIMAX SIGNAL field a number of 4 transmit and receive antennas. In Section 6.8, we have added some reconfigurability to the design, in the sense that the transceivers could have a different number of antennas (up to four). The proper behavior of the new baseband blocks with this reconfigurability was successfully simulated in Section 7.2.1.

In this section, we study the real-time test of the new baseband blocks, when the baseband processor receives training frames in a different configuration than a  $4 \times 4$ . The testing procedure has been exactly the same as in the previous subsection, i.e., the comparison between the real-time weights provided by the MAC emulator user interface (the console application) and the weights obtained in simulation with System Generator or ModelSim. All the 16 possible configurations ( $1 \times 1$ ,  $1 \times 2$ , ...,  $4 \times 3$ , and  $4 \times 4$ ) have been successfully tested. Figure 8.12 shows that, for a  $3 \times 3$  system, the agreement between the real-time and the fixed-point simulation weights is again almost perfect. Note that one of the four weights is set to zero in all the simulations. This weight corresponds to the weight of the non-existent antenna.<sup>4</sup> Figure 8.13 also shows the comparison between the real-time and fixed-point simulation results for the MIMO systems  $1 \times 4$ ,  $3 \times 2$ ,  $4 \times 3$ , and  $2 \times 2$ .

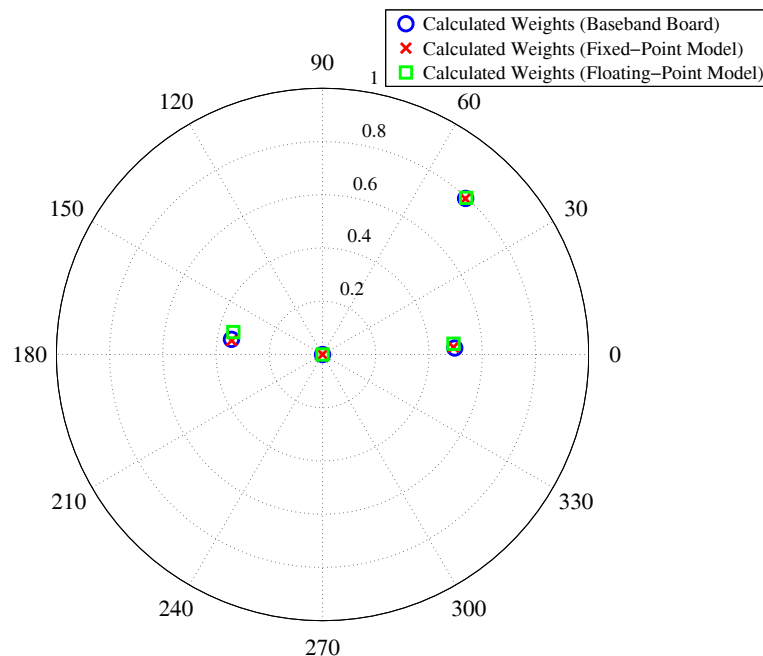


**Figure 8.12:** Comparison among the RF weights obtained in real-time, in fixed-point design simulation, and in floating-point simulation for a  $3 \times 3$  system.

<sup>4</sup>As stated in Subsection 6.8, the RF Weights Block calculate four optimal weights regardless the number of receive antennas. Obviously, if the station has  $n_R < 4$ , only  $n_R$  weights are non-zero.

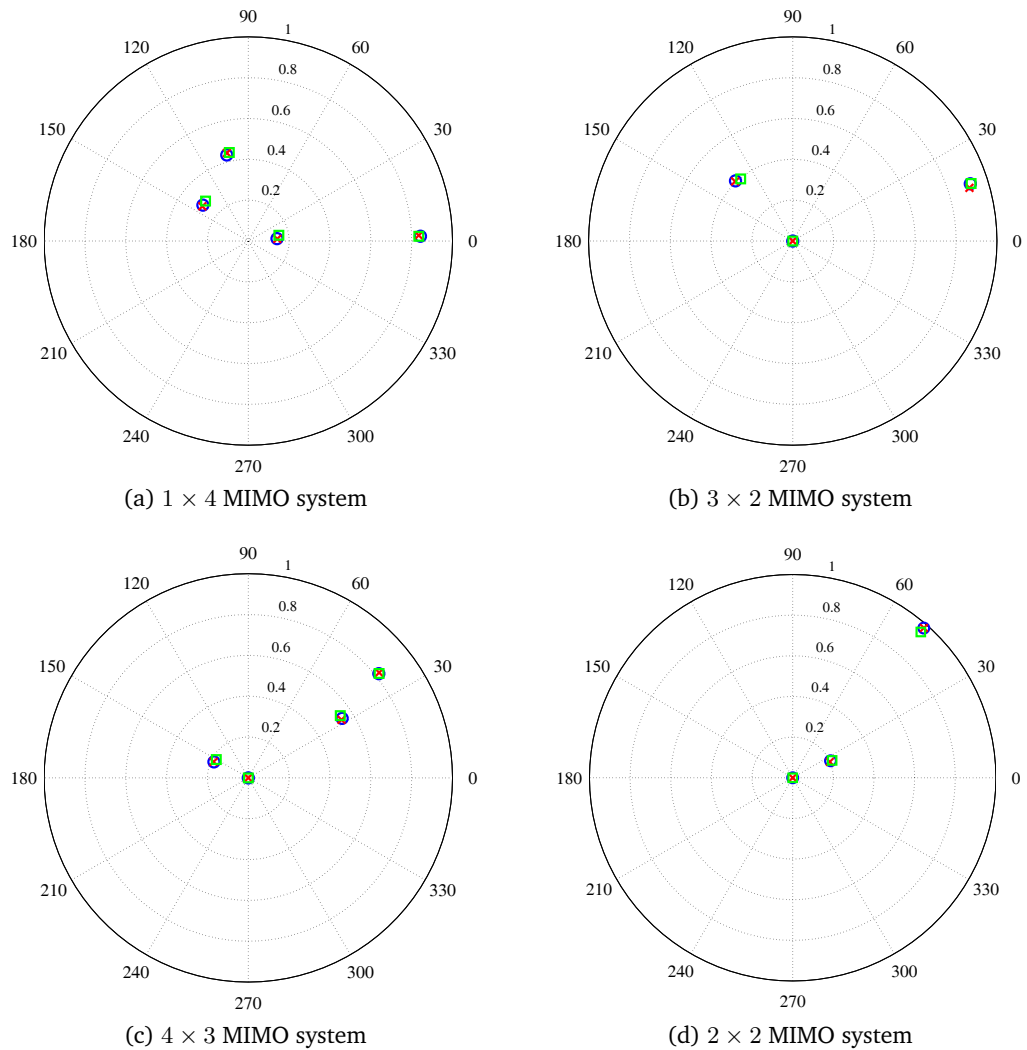


**Figure 8.13:** Comparison among the RF weights calculated in real-time (blue circles), fixed-point design simulation (red crosses), and floating-point simulation (green squares).

## 8.5 Physical Layer Tests in MIMAX

In Chapters 3 and 4, the improvement of the MIMAX architecture with respect to the SISO system has been illustrated through different Monte Carlo simulations. The results of these experiments, especially those obtained in Chapter 3 for the case of CSIT+CSIR, have allowed us to validate the MIMAX concept, as well as to have a quantitative idea about the expected improvements of MIMAX in comparison to SISO in terms of SNR gain or BER improvement.

In this section, we evaluate the complete physical layer of the MIMAX demonstrator (from now on, the MIMAX prototype), presented in Chapter 5, i.e., the setup includes the MIMAX baseband processor, the MIMAX analog front-end, and the MIMAX antenna array (the last two will be briefly overviewed within the subsequent subsections).

Several indoor and outdoor experiments have been conducted by varying the signal constellation and the frame length. A physical layer characterization of the system has been performed using, as figures of merit, the frame error rate (FER), the RSSI level after combining (power of the received signal after combining), and the SNR gain. These values can easily be translated into coverage improvement, link reliability, or increased rate in comparison to SISO system.

### 8.5.1 MIMAX Analog Front-End

The MIMAX analog front-end has been developed by one of the partners of the MIMAX project, the Chair for Circuit Design and Network Theory at the Dresden University of Technology. It is designed to support transmit and receive signal weighting in the analog RF domain. Most of the analog-front end is designed in a SiGe BiCMOS technology with a 250 nm CMOS option [Ellinger, 2007]. The architecture of the MIMAX analog front-end is depicted in Figure 8.14.

The incoming standard-conform signals from the antennas have a signal power each of  $-82$  to  $-30$  dBm, are filtered by a bandpass filter (BPF), and are amplified by a low noise amplifier (LNA), before they are eventually led into the weighting module, namely a vector modulator. This module alters phase and amplitude of the incoming RF signals in a way that, after adding them up, the resultant signal has an improved signal quality leading to higher data rates and/or higher link quality. Because the MIMAX receiver is intended to be

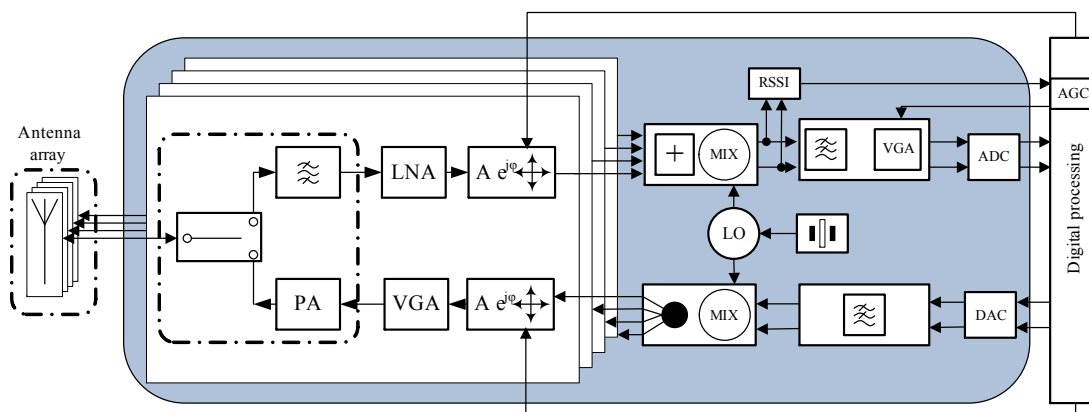
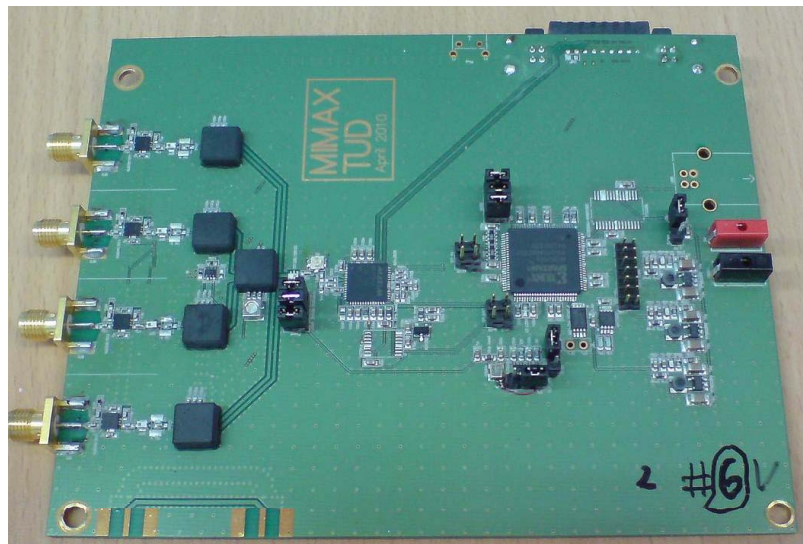


Figure 8.14: MIMAX analog front-end.

fully backwards compatible to 802.11a and to enable a fair comparison with existing WLAN receivers, it is possible to switch off complete branches and let the front-end operate as a single-input single-output (SISO) device.

The last analog stages incorporate variable gain and low pass filtering features to set up optimal signal conditions for the receive analog to digital converter (ADC). The design of the transmit path (Tx) makes use of components from the receive path (Rx), such as parts from the baseband variable gain amplifier (VGA) and filter. Furthermore, an identical weighting module is used, which consequently means that, in total, two vector modulators are employed per antenna branch, one for transmitter and one for receiver. The transmit power control required by the authorities is done by a VGA before the power amplifier (PA). The active up-conversion mixer driven by the PLL feeds its output signal to the individual transmit branches by means of splitting amplifiers. The PA and the antenna switch are off-chip components and form the last part of the transmit branch. The image of the manufactured analog front-end board is illustrated in Figure 8.15. More details about the analog-front end and its technology can be found in [Ellinger et al., 2001, Ellinger, 2007, Ellinger et al., 2010] and in the technical reports [Kraemer et al., 2008, Santamaría et al., 2010, Mayer et al., 2009, Mayer et al., 2010].



**Figure 8.15:** Picture of the MIMAX analog front-end board manufactured at the Dresden University of Technology.

### 8.5.2 MIMAX Antenna Array

The MIMAX antenna array has been developed by the TTI company, partner of the MIMAX project. This MIMAX antenna array consists of four multiband radiating elements, and its form factor is determined by a mechanical antenna holder for a laptop of 14" in size. The multiband antenna is based on a microstrip-fed planar F-shaped monopole, printed on a FR4 substrate of thickness  $h = 0.5$  mm. The overall size of the antenna is  $35.9 \text{ mm} \times 11.17 \text{ mm}$ . In particular, the lower branch of the F-shaped antenna controls the resonance at 5.6 GHz, while the upper part determines the antenna resonance at 2.4 GHz. More information about the MIMAX antenna array can be found in the publications [Gago et al., 2009a, Gago et al.,

2009b] and the technical reports [Gonzalez et al., 2009, Gago et al., 2009c]. Figure 8.16 shows the antenna array PCB directly stuck to the laptop cover.

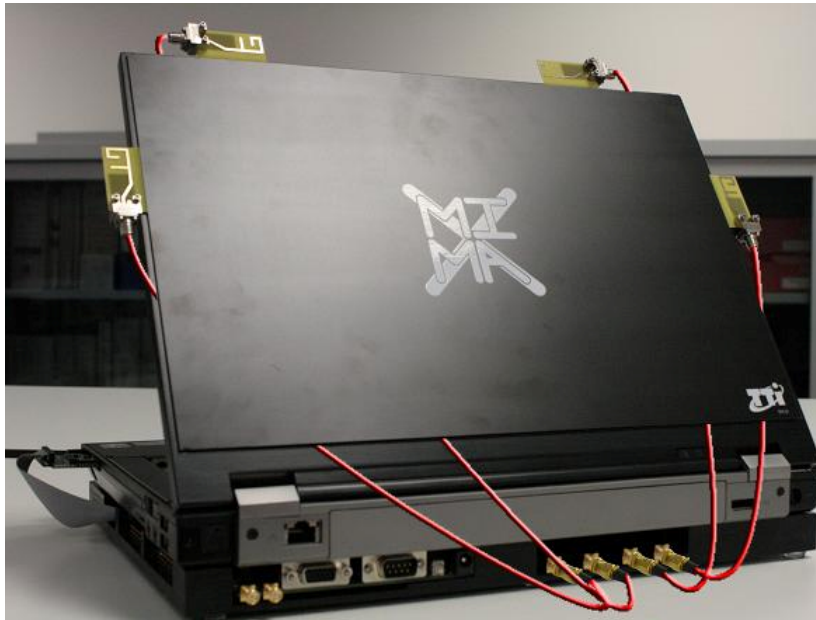


Figure 8.16: MIMAX Antenna Array integrated with the laptop.

### 8.5.3 Setup

Now, we describe the setup used to benchmark the performance of the MIMAX prototype at the physical layer level. The considered setup integrates the antenna array, the analog front-end, and the baseband processor as shown in Figure 8.17. The MAC emulator was used for these tests, because it provides more flexibility and control over the setup than the final MAC boards. It runs on a PC and is connected to the baseband through a USB port as shown in Subsection 8.3.

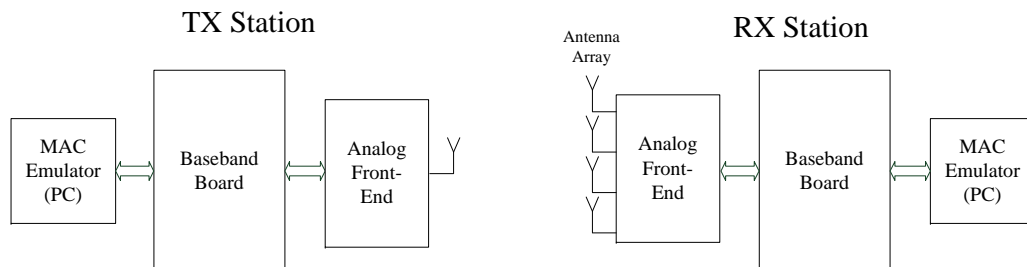


Figure 8.17: Setup of the physical layer tests.

Two stations have been used to carry out the experiments. At this point, we must note that, due to some problems at the implementation process of the analog front-end, the transmitter part of the AFEs could only use a single branch when the experiments took place.

Thus, the physical layer tests have been performed for a  $1 \times 4$  SIMO channel with an associated decrease of the MIMAX performance. Note that, in this case, the transmission is performed by only one antenna, which is chosen randomly. Nevertheless, this reduced  $1 \times 4$  SIMO system is still enough to show the capabilities of the MIMAX architecture.

### 8.5.4 Figures of Merit and Testing Procedure

#### Figures of Merit

As figures of merit to assess the performance of MIMAX in comparison to SISO, the FER and the RSSI level provided by the MAC emulator are used. The FER accounts for the error rate due to transmission errors (bad CRC) or lost packets (e.g., undetected frames). On the other hand, the RSSI level gives a measure of the received signal power after combining the RF signals weighted by the vector modulators (VM). Differences in the RSSI level between MIMAX and SISO transmission can be used as estimates of the power gain provided by MIMAX under different circumstances, i.e., the RSSI differences can directly be translated into actual SNR gain in dB. The parameters used during the benchmarking are as follows:

- Central frequency: 5.26 GHz
- Number of transmit antennas:  $n_T = 1$
- Number of receive antennas:  $n_R = 4$
- Number of OFDM symbols per transmitted frame: 10 symbols (short frames) or 20 symbols (long frames)
- Constellation and data rate: BPSK (9 Mbps), QPSK (18 Mbps), 16-QAM (36 Mbps), 64-QAM (54 Mbps)

#### Testing Procedure

The testing procedure is graphically depicted in Figure 8.18. Basically, it consists of two evaluation stages. The SISO system is evaluated in the first stage (i.e., the MIMAX prototype using default weights), and the MIMAX system is evaluated in the second stage (using optimal weights). In each measurement, 100 frames are transmitted for both schemes under the same channel conditions (assuming a low mobility scenario). More precisely, the testing procedure for each measure is as follows:

- The SISO evaluation stage comprises the transmission of the first set of 100 data frames. During the signal reception, the default weights are applied, which means that the same weights are applied to all the antennas.
- The MIMAX evaluation stage requires a more sophisticated procedure, which is controlled by the MAC emulator. This MAC emulator (USB\_MacEmu program) has been modified for this purpose.
  - Firstly, a training frame is transmitted, and the baseband board computes the optimal weights.
  - Secondly, the optimal weights are applied by the AFE.

- Finally, the second set of 100 data frames is received with the optimal weights. The results obtained from these 100 frames are compared to those obtained during the SISO evaluation stage.

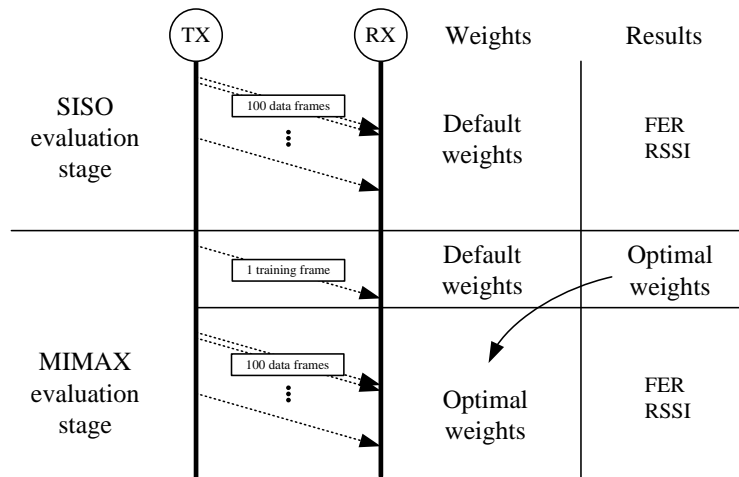


Figure 8.18: Timing diagram of the testing procedure.

### 8.5.5 Experiments

An intensive campaign has been carried out at GTAS group in order to test jointly the different parts of the MIMAX prototype in the physical layer tests. The MIMAX architecture, in comparison with SISO, has been evaluated in diverse indoor and outdoor locations for different constellations and frame lengths. Although the main purpose of this thesis is not the validation of the whole MIMAX prototype and we will not go deeply into all the results, we give an example of a single experiment in an indoor scenario in order to show the improvement of MIMAX with respect to SISO.

In this experiment, the transmitter and receiver were placed approximately 12 meters apart (locations Tx and Rx in Figure 8.19) and separated by office furniture and bookshelves at the GTAS laboratory. In this location, the receiver has been moved to 25 different close positions within a small local area (around 0.9 m<sup>2</sup>) in order to transmit under 25 different channels, and, therefore, to obtain valid statistical results. In each of the 25 positions, the testing procedure described in Subsection 8.5.4 has been performed, i.e., the transmission of 100 frames with default weights (SISO system) and other 100 frames with the optimal weights (MIMAX system). The experimental results obtained in this indoor scenario have statistical relevance and are summarized in Table 8.1.

For instance, the MIMAX FER when transmitting data frames with 10 OFDM symbols at 36 Mbps is 2.3%, whereas, for the SISO system (using default weights in the MIMAX prototype), the FER increases to 41.8%. In this case, using 64-QAM, the MIMAX FER is close to 24%, and, for SISO, it goes up to 85%. From a practical point of view, this means that, in SISO, we are limited to 18 Mbps, while MIMAX allows us to double the rate and transmit at 36 Mbps with a FER five times lower. For this location, MIMAX can even work at 54 Mbps,



**Figure 8.19:** Transmitter and receiver locations used for the experiments.

where SISO can only work at 18 Mbps. In terms of power, the gain of MIMAX versus SISO is close to 5.5 dB, which roughly means that MIMAX increases the coverage by a factor of two.

### 8.5.6 Conclusion of the Physical Layer Tests

I has been verified by the indoor test scenarios that MIMAX achieves lower FER in comparison to its SISO competitor 802.11a. Consequently, at the same range, the system can switch to a higher-order modulation scheme, and, therefore, the wireless link achieves higher data rates. Nevertheless, we have to mention that the maximum achievable rate cannot exceed the defined 54 Mbps, because the designed system must be compatible to the 802.11a and its legacy devices.

**Table 8.1:** Performance comparison between SISO and MIMAX systems. Rates: 9, 18, 36, and 54 Mbps. Data frame length: 10 OFDM symbols.

	Rate: 9 Mbps (BPSK)		18 Mbps (QPSK)		36 Mbps (16-QAM)		54 Mbps (64-QAM)	
	MIMAX	SISO	MIMAX	SISO	MIMAX	SISO	MIMAX	SISO
FER (%)	0	1.3	0.1	11	2.3	41.8	23.9	85.8
RSSI (dBm)	-53.8	-57.8	-52.8	-59.0	-52.9	-58.5	-53.7	-59.1
Power Gain (dB)	5.5							

Furthermore, MIMAX increases the coverage range for this indoor test scenario, and the system is able to double the distance at the same data rate. Therefore, our concept outperforms legacy 802.11a devices in terms of link distances at the same data rates. We must remember that these experiments have been carried out for a  $1 \times 4$  SIMO channel due to some final problems at the manufacturing of the transmitter part in the AFEs. The expected improvement in a  $4 \times 4$  MIMO channel in comparison with SISO would be higher than what was observed in these tests. To conclude this section, note that a thorough benchmarking of the MIMAX physical layer can be found in [Santamaría et al., 2011], where several experiments for different indoor and outdoor scenarios are described. In all of them, the MIMAX performance largely exceeds that of the SISO system.

## 8.6 User-Level Tests in MIMAX

Some final tests have been conducted to evaluate the whole MIMAX architecture. Particularly the MIMAX partner PrimeTel, has developed an Internet Protocol Television (IPTV), which is one of the triple play services (telephony, Internet, and television services). The MIMAX prototype has been tested with IPTV as a service level, as well as some other video services, such as HD video conference over Skype.

This user-level benchmarking is far from the scope of this second part of the thesis, which aims the design, implementation, and testing of the new blocks needed in the baseband processor of the MIMAX system. Nevertheless, we can assign an important part of the success of these user-level tests to the improvement obtained by the new MIMAX baseband blocks in the calculation of the optimal beamformers. A deep study of this type of tests can be found in [Santamaría et al., 2011].

## 8.7 Conclusions

In this chapter, we have introduced the MIMAX baseband board, jointly designed within the MIMAX consortium and manufactured by one of the MIMAX partners. With this MIMAX baseband board, the real-time behavior of the new MIMAX baseband blocks has been tested. Then, a simple setup has been proposed in order to isolate the baseband processor and test the performance of the new MIMAX blocks, mainly in the reception of training frames. For several training frames, the obtained weights have been compared with those expected in simulation, checking the successful behavior of the blocks within the FPGA.

Once the behavior of the stand-alone MIMAX baseband processor has been tested, a new setup has been proposed for more general experiments, the physical layer tests. These tests have been carried out through a wireless channel between stations, each one comprising the MIMAX antenna array, the MIMAX analog front-end, and the MIMAX baseband processor. We have seen that, due to some technical problems at the manufacture of the analog front-end at the Dresden University of Technology, these tests have been conducted for a  $1 \times 4$  SIMO channel. Nevertheless, a considerable improvement of MIMAX in terms of SNR improvement and FER decreasing has been shown. Specifically, it has been seen that MIMAX increases the coverage range for an indoor test scenario, and the system is able to double the distance at the same data rate. Therefore, it has been also shown that our concept outperforms legacy 802.11a devices in terms of link distances at the same data rates. It has been shown that, in this scenario, MIMAX has allowed us to double or even quadruplicate the rate in comparison with the SISO system, even with a substantial reduction of the FER in many cases.

To conclude this chapter, we have briefly reviewed some user-level tests of the complete MIMAX prototype, where it is used for some services of the triple play, such as IPTV, or HD video conference over Skype. Finally, note that the publications that have contributed to this chapter are [Kraemer et al., 2010, Stamenkovic et al., 2010, Elvira et al., 2010, Eickhoff et al., 2011].



Part **III**

**Conclusions and Future Directions**



# 9

Chapter

## Conclusion and Future Directions

### 9.1 Conclusions

In this work, within the context of an European Union funded project, called MIMAX, a novel architecture for a MIMO transceiver (MIMAX transceiver) based on analog antenna combining in the RF domain has been proposed. With this architecture, some of the MIMO benefits can be extracted avoiding the costs associated with the traditional MIMO architectures. The new architecture of this transceiver has been the consistent thread of this work from the baseband algorithm design to the final integration of the MIMAX transceiver.

#### 9.1.1 Part I: Design of the Transmit and Receive Beamformers

In the first part of this thesis, we have studied the optimization of the beamformers (RF weights) for the novel MIMO transceiver under OFDM transmissions. The novel architecture of the transceiver poses several challenges in comparison with the conventional MIMO system. In particular, the selection of the optimal beamforming to be applied in RF is an intricate problem, because the same pair of transmit-receive beamformers must be applied to all the subcarriers. We have proposed a general beamforming criterion to select these beamformers for the channel state information (CSI) at the transmitter (CSIT) and the receiver (CSIR) side. Because of the coupling of the subcarriers, a parameter of the general criterion establishes a tradeoff between the energy and spectral flatness of the equivalent channel. Depending on this parameter, some interesting criteria, such as the maximization of the received SNR or the minimization of the MSE, have been proposed. In order to solve this non-convex optimization problem, a simple and efficient gradient search algorithm has been proposed, which, in practice, provides satisfactory solutions with a moderate computational cost.

The same problem abovementioned has been also tackled for the case when perfect CSI is available at the receiver but only statistical CSI is available at the transmitter. The selection of the beamformers at the receiver is analogous to the CSIT+CSIR case. To obtain the optimal beamformers at the transmitter under the assumption of transmit correlated channel, we have proposed the beam-division multiplexing (BDM) transmission scheme. This method translates the MIMO spatial diversity into a time diversity by transmitting through different directions. In the particular case without spatial correlation, the optimal transmit beamform-

ers consist of a set of orthogonal vectors (such as the columns DFT matrix), and the method is called orthogonal BDM (OBDM).

The results of several Monte Carlo simulations have shown the good performance of the proposed algorithms for both schemes (CSIT+CSIR and CDIT+CSIR). The numerous simulation results allow us to conclude that, in general, it is a good idea to increase the spectral flatness of the equivalent SISO channel, even at the expense of a slight degradation in the overall SNR (MinMSE method). Nevertheless, the BER performance of MinMSE method, which minimizes the BER with linear receivers and QAM constellations, exceeds but not largely the performance of MaxSNR, whose computational cost is lower. Supported by means of simulations, we have decided to implement an approximated version of the MaxSNR algorithm for an FPGA development of a baseband processor.

In summary, in this first part, we have studied the optimization of the beamformers for a new analog antenna combining architecture based on OFDM transmissions. It has also shown the benefits of the novel MIMO architecture and its wide improvement over the SISO performance.

### 9.1.2 Part II: New MIMAX Baseband: Design, Baseband Integration, and Real-Time Testing

The joint development of the MIMAX transceiver within the MIMAX project has been the central topic in this second part of the thesis. Based on the standard IEEE 802.11a, the development of the MIMAX baseband processor has been carried out, focusing on the new functionalities required by the MIMAX transceiver. These functionalities have been translated into some slight changes in an existing 802.11a baseband processor but mainly into the addition of new baseband blocks. These blocks, fully developed by the author of this work, have been designed in order to make possible the MIMO channel estimation and the optimal calculation of the RF weights. In order to obtain these weights, the algorithm that maximizes the SNR, proposed in the first part of this thesis, has been adapted to be implemented into an FPGA. All the new MIMAX blocks have been designed, implemented, and merged with the the legacy 802.11a baseband processor. The behavior of the designed blocks has been tested firstly by means of simulations and then in real-time. Finally, within a complete setup containing the AFE, the antenna array, and the baseband processor, several campaigns of experiments have been carried out, not only for testing the adequate behavior of the new MIMAX baseband blocks, but also for illustrating the advantages provided by MIMAX in comparison with a conventional SISO scheme in a real system.

## 9.2 Future Directions

### 9.2.1 Theoretical Work

In the first part of the thesis, we have addressed the selection of the optimal transmit-receive beamformers in the communication of two station with the proposed novel architecture. On this vein, we can list some future guidelines:

- In the analog antenna combining architecture, we only consider one RF chain at the transmitter and receiver. The extension of the results in Chapters 3 and 4 to the case of multiple data streams using multiple analog beamformers in parallel, each one followed by the corresponding RF chain and FFT Block, would follow in the lines of [Huang and

Letaief, 2004a, Li et al., 2007a] for the pre-FFT MaxSNR case, and could be considered in the future.

- In a broadcast channel, where there is a transmitting base station and several users as receivers, some strategies and algorithms of joint beamforming calculation could be studied. Note that, in this case, many criteria could be proposed, such as maximizing the total data throughput, improving the equivalent SISO channel of the users with worst channels, reducing the interferences between user for broadcast transmissions, etc.
- The proposed architecture, based on analog antenna combining, multiplies the different RF branches by a complex number, which implies that the analog front-end needs to implement VGA and phase shifters or vector modulators (as in the case of the MIMAX AFE). The complexity of the AFE could be reduced, if this complex number were limited to unit norm (like in equal gain combining (EGC), where only a phase shifter is needed), to a real number (two VGA would be needed) or some other simplifications. Several of these problems have been already addressed within the GTAS group [Lameiro et al., 2011, Gholam et al., 2011].
- In Chapter 3, we have analyzed the calculation of the beamformers under CSIT+CSIR. Nevertheless, we have imposed unit-norm transmit beamformers due to technical reasons. This fact precludes performing adaptive power loading techniques at the transmitter side. The design of the beamformers under channel knowledge at the transmitter side with adaptive power loading constitutes an interesting topic for future research.
- In Chapters 3 and 4, the design of the beamformers has been presented under the assumptions of no RF impairments neither channel estimator errors. It would be interesting to extend the algorithms for the robust design of the transceiver when some information is available about the impairments or errors in the channel estimates.

### 9.2.2 Practical Work

The work carried out in the second part of the thesis has been directed to develop the baseband processor of the MIMAX prototype in order to show the MIMAX capabilities within a real environment. We have focused on fulfilling the MIMAX functionalities within the shortest time possible regardless the resources used by the new MIMAX baseband blocks (a large enough FPGA was available). There would be many ways to reduce the occupancy of the MIMAX baseband blocks, such as by reducing the bit precision of all the internal signals and the calculated beamformers,<sup>1</sup> implementing the Gauss's multiplication for the complex multipliers, reusing some blocks to perform different parts of the algorithm, etc. It would be also possible to address the implementation of some other algorithms of those studied in the first part, such as that associated to the MinMSE criterion. Moreover, the first stage of this algorithm would be the approximated version of the MaxSNR, which has been already implemented throughout the second part of this thesis.

As a future line of work, if MIMAX architecture emerges and a mass fabrication of MIMAX transceivers is needed, most of the MIMAX prototype should be redesigned. Similarly,

<sup>1</sup>Although the AFE stores the beamformers in 8-bit registers before setting them, in practice, the precision of the applied weights is around 5 bits. This fact is not critical, because, we have performed some studies (similar to those of Chapter 6), which show that the system performance with 5-bit weights is similar to that with floating-point calculations.

also the MIMAX baseband processor should be reconsidered and redesigned for an ASIC (application-specific integrated circuit) implementation due to the lower unit costs, lower power consumption, and smaller form factor.

The second part of this thesis has concluded favorably with the successful application of the analog antenna combining scheme and the theoretical concepts, proposed within the first part of the thesis, to a real system IEEE 802.11a (WiFi). It is apparent that it would be of great interest to extend the MIMAX scheme to other systems, which might possibly be car to car (C2C) communications (where link reliability is of chief importance), MIMO RFID (where the size, cost, and consumption are critical), and other wireless systems at high data throughput (in the range of various Gbps) and/or with high frequency (e.g., in the 60 GHz band), where the technological restrictions could impede the application of conventional MIMO schemes.

# Rewriting and Analyzing the Beamforming Function

## A.1 Rewriting the Cost Function

Let us start by writing  $\text{MSE}_k = (P_\beta p_{\beta,k})^{\frac{1}{\beta-1}}$ . Thus, the cost function  $f_\alpha(\mathbf{w}_T, \mathbf{w}_R)$  can be rewritten as

$$f_\alpha(\mathbf{w}_T, \mathbf{w}_R) = \frac{1}{\alpha - 1} \log \left( \frac{1}{N_c} \sum_{k=1}^{N_c} (P_\beta p_{\beta,k})^{\frac{\alpha-1}{\beta-1}} \right),$$

and, after a straightforward manipulation, we obtain

$$f_\alpha(\mathbf{w}_T, \mathbf{w}_R) = f_\beta(\mathbf{w}_T, \mathbf{w}_R) + g_{\alpha,\beta}(\mathbf{p}_\beta(\mathbf{w}_T, \mathbf{w}_R)), \quad (\text{A.1})$$

with

$$g_{\alpha,\beta}(\mathbf{p}_\beta(\mathbf{w}_T, \mathbf{w}_R)) = \frac{\alpha - \beta}{(\alpha - 1)(\beta - 1)} \log(N_c) + \frac{1}{\alpha - 1} \log \left( \sum_{k=1}^{N_c} p_{\beta,k}^{\frac{\alpha-1}{\beta-1}} \right).$$

Eq. (A.1) shows that the cost function for a given parameter  $\alpha$  can be written as the cost function for a different parameter  $\beta$ , plus a penalty term that depends on  $\alpha$ ,  $\beta$ , and  $p_{\beta,k}$ .

## A.2 Analysis of the Penalty Term

### A.2.1 Antisymmetry

From eq. (A.1), and interchanging the values  $\alpha$  and  $\beta$ , we can directly conclude that

$$g_{\alpha,\beta}(\mathbf{p}_\beta) = -g_{\beta,\alpha}(\mathbf{p}_\alpha),$$

where, for notational simplicity, we have omitted the dependency with the beamformers. Thus, we can restrict our study to the case  $\alpha > \beta$ .

### A.2.2 Monotonicity

In order to prove that  $g_{\alpha,\beta}(\mathbf{p}_\beta)$  increases with  $\alpha$  we evaluate its derivative

$$\frac{\partial g_{\alpha,\beta}(\mathbf{p}_\beta)}{\partial \alpha} = \frac{\log(N_c)}{(\alpha-1)^2} + \frac{\sum_{k=1}^{N_c} p_{\beta,k}^{\frac{\alpha-1}{\beta-1}} \log\left(p_{\beta,k}^{\frac{\alpha-1}{\beta-1}}\right)}{(\alpha-1)^2 \sum_{k=1}^{N_c} p_{\beta,k}^{\frac{\alpha-1}{\beta-1}}} - \frac{\log\left(\sum_{k=1}^{N_c} p_{\beta,k}^{\frac{\alpha-1}{\beta-1}}\right)}{(\alpha-1)^2},$$

which, after defining  $A = \sum_{k=1}^{N_c} p_{\beta,k}^{\frac{\alpha-1}{\beta-1}}$  and  $a_k = \frac{p_{\beta,k}^{\frac{\alpha-1}{\beta-1}}}{A}$ , can be rewritten as

$$\frac{\partial g_{\alpha,\beta}(\mathbf{p}_\beta)}{\partial \alpha} = \frac{1}{(\alpha-1)^2} \sum_{k=1}^{N_c} a_k \log(a_k N_c).$$

Thus, taking into account that  $\sum_{k=1}^{N_c} a_k = 1$  (i.e.,  $a_k$  can be seen as the probability mass function of a discrete random variable), it is easy to prove that the above function is Schur-convex with respect to  $a_k$  ( $k = 1, \dots, N_c$ ) [Marshall and Olkin, 1979, Palomar and Jiang, 2006], i.e., it attains its minimum value for  $a_k = \frac{1}{N_c}$ , which yields  $\frac{\partial g_{\alpha,\beta}(\mathbf{p}_\beta)}{\partial \alpha} = 0$ . Therefore, we can conclude that the derivative is non-negative and the function  $g_{\alpha,\beta}(\mathbf{p}_\beta)$  increases with  $\alpha$ .

### A.2.3 Schur-Convexity of $g_{\alpha,\beta}(\mathbf{p}_\beta)$

The proof is based on the two following observations. Firstly, for  $\alpha > \beta$ , the function

$$\sum_{k=1}^{N_c} p_{\beta,k}^{\frac{\alpha-1}{\beta-1}},$$

is Schur-convex if  $\alpha > 1$  and Schur-concave if  $\alpha < 1$  [Marshall and Olkin, 1979, Palomar and Jiang, 2006]. Secondly, the function  $\frac{1}{\alpha-1} \log(\cdot)$  is increasing for  $\alpha > 1$  and decreasing for  $\alpha < 1$ . Thus,  $\forall \alpha > \beta$ , the composite function  $g_{\alpha,\beta}(\mathbf{p}_\beta)$  is Schur-convex [Marshall and Olkin, 1979, Palomar and Jiang, 2006], which implies that it attains its minimum when

$$p_{\beta,k} = \frac{1}{N_c}, \quad \text{for } k = 1, \dots, N_c.$$

Finally, when all the  $p_{\beta,k}$  are equal we have that  $g_{\alpha,\beta}(\mathbf{p}_\beta) = 0$ , which implies that  $g_{\alpha,\beta}(\mathbf{p}_\beta)$  is non-negative for  $\alpha > \beta$ .

# Appendix **B**

## Publications

Here, we provide the entire listing of the publications of this work.

### **B.1 Book Chapter**

- I. Santamaría, J. Vía, V. Elvira, J. Ibáñez, J. Pérez, R. Eickhoff, and U. Mayer. *Handbook of Smart Antennas for RFID Systems*, chapter Low cost and compact RF-MIMO transceivers. Wiley, 2009.

### **B.2 International Journals**

- J. Vía, I. Santamaría, V. Elvira, and R. Eickhoff. "A general criterion for analog Tx-Rx beamforming under OFDM transmissions". *IEEE Transactions on Signal Processing*, volume 58, no. 4, pages 2155-2167, 2010.
- V. Elvira and J. Vía. "Analog antenna combining in transmit correlated channels: Transceiver design and performance evaluation". *Submitted to Signal Processing (Second Review)*. 2011.

### **B.3 International Conferences**

- I. Santamaría, V. Elvira, J. Vía, D. Ramírez, J. Pérez, J. Ibáñez, R. Eickhoff, and F. Ellinger. "Optimal MIMO transmission schemes with adaptive antenna combining in the RF path". In *16th European Signal Processing Conference (EUSIPCO 2008)*. Lausanne, Switzerland, 2008.
- J. Vía, V. Elvira, I. Santamaría, and R. Eickhoff. "Minimum BER beamforming in the RF domain for OFDM transmissions and linear receivers". In *IEEE International Conference on Acoustics, Speech, and Signal Processing (ICASSP 2009)*. Taipei, Taiwan, 2009.
- J. Vía, V. Elvira, J. Ibáñez, and I. Santamaría. "Optimal precoding for a novel RF-MIMO scheme in transmit correlated rayleigh channels". In *IEEE Workshop on Signal Processing Advances in Wireless Communications (SPAWC 2009)*. Perugia, Italy, 2009.

- J. Vía, V. Elvira, I. Santamaría, and R. Eickhoff. "Analog antenna combining for maximum capacity under OFDM transmissions". In *IEEE International Conference on Communications (ICC 2009)*. Dresden, Germany, 2009.
- V. Elvira and J. Vía, "Diversity techniques for analog combining schemes: design and performance evaluation". In *Proceedings of the 17th European Signal Processing Conference (EUSIPCO 2009)*. Glasgow, Scotland. 2009.
- R. Eickhoff, U. Mayer, M. Wickert, F. Ellinger, I. Santamaría, V. Elvira, J. Ibáñez, and J. Vía. "Fully integrated MIMO transceiver with pre-FFT processing for 802.11a". In *FP7 Workshop on Advanced MIMO and Cooperative Communications*. Brussels, Belgium. 2009.
- J. Vía, I. Santamaría, V. Elvira, J. Ibáñez, and R. Eickhoff. "OFDM system with pre-FFT processing for MIMO systems". In *FP7 Workshop on Advanced MIMO and Cooperative Communications*. Brussels, Belgium. 2009.
- J. Vía, I. Santamaría, V. Elvira, and R. Eickhoff. "A general pre-FFT criterion for MIMO-OFDM beamforming". In *IEEE International Conference on Communications (ICC 2010)*. Cape Town, South Africa. 2010.
- R. Kraemer, Z. Stamenkovic, K. Tittelbach-Helmrich, L. González, S. Ruiz, O. Gago, J. Ibáñez, V. Elvira, M. Wickert, and R. Eickhoff. "RF-MIMO WLAN modem demonstrator". In *25th Wireless World Research Forum WWRF Meeting*. London, UK. 2010.
- Z. Stamenkovic, K. Tittelbach-Helmrich, M. Krstic, J. Ibáñez, V. Elvira, and I. Santamaría. "Mac and baseband hardware platforms for RF-MIMO WLAN". In *Proceedings of the 5th European Conference on Circuits and Systems for Communications*. Belgrade, Serbia. 2010.
- V. Elvira, J. Ibáñez, I. Santamaria, M. Krstic, K. Tittelbach- Helmrich, and Z. Stamenkovic. "Baseband processor for RF-MIMO WLAN". In *17th IEEE International Conference on Electronics, Circuits, and Systems (ICECS 2010)*. Athens, Greece. 2010.
- R. Eickhoff, K. Tittelbach-Helmrich, M. Wickert, J. Wagner, U. Mayer, V. Elvira, , and J. Ibáñez. "Physical layer amendments for MIMO features in 802.11a". In *Proceedings of the Future Network and MobileSummit*. Warsaw, Poland. 2011.

# List of Figures

2.1	Effect of diversity on the SER performance in Rayleigh channel. . . . .	11
2.2	SER performance depending on the array gain, coding gain, and diversity gain. . . . .	12
2.3	Achievable diversity-multiplexing curves for a $4 \times 4$ system with full MIMO and SISO. . . . .	13
2.4	Full MIMO transceiver. Exemplarily shown for a direct-conversion receiver. . . . .	16
2.5	Conventional approach performing adaptive combining. . . . .	17
2.6	Comparison among the different MIMO combining algorithms. . . . .	20
2.7	Analog antenna combining in the RF path for MIMO communications systems. Exemplarily shown for a direct-conversion receiver. . . . .	21
2.8	Achievable diversity-multiplexing curves for a $4 \times 4$ system with full MIMO, MIMAX, and SISO. . . . .	25
3.1	Analog antenna combining in the RF path for MIMO communications systems. Exemplarily shown for a direct-conversion receiver. . . . .	32
3.2	Toy example with a $1 \times 2$ SIMO system with $N_c = 2$ subcarriers. The figure shows the set of achievable points with $\ \mathbf{w}_R\  = 1$ (dotted line), the Pareto optimal points (solid line), and the solutions associated to the proposed criterion (the section of the curve marked with circles). . . . .	38
3.3	Convergence of the MaxSNR, MaxCAP, and MinMSE algorithms for SNR=10 dB. Initialization in the approximated MaxSNR solution or in a pair of unit-norm random vectors $\mathbf{w}_T, \mathbf{w}_R$ . . . . .	45
3.4	Channel response $ h_k $ after beamforming for a channel realization. . . . .	45
3.5	Probability density function (pdf) of the equivalent channel response $ h_k ^2$ . $\gamma = 10$ dB. . . . .	46
3.6	Outage probability for a transmission rate of 5 bps/Hz. . . . .	47
3.7	Evolution of the total MSE with the SNR. . . . .	47
3.8	Bit error rate for the proposed criteria. Uncoded QPSK symbols. . . . .	48
3.9	Bit error rate for the proposed criteria. QPSK symbols linearly precoded with the FFT matrix. . . . .	48
3.10	BER for a 802.11a based system with transmission rate of 12 Mbps. QPSK signaling and convolutional encoder of rate 1/2. . . . .	49
3.11	BER for a 802.11a based system with transmission rate of 54 Mbps. 64-QAM signaling and convolutional encoder of rate 3/4. . . . .	50
3.12	Performance of the MinMSE criterion in a 802.11a based system with transmission rate of 12 Mbps including the effect of channel estimation errors and RF impairments. . . . .	51
4.1	Analog antenna combining in the RF path for MIMO communications systems. Exemplarily shown for a direct-conversion receiver. . . . .	54

4.2	Distribution of a transmission block. The grey columns denote the $M$ time and frequency precoded OFDM symbols of one block, which are transmitted using $M$ different beamformers. In this example, the beamformers remain fixed during the transmission of $P$ OFDM symbols. The minimum achievable $P$ depends on the limitations of the RF implementation. On the other hand, the maximum allowable $P$ is imposed by the temporal coherence of the channel.	55
4.3	Block diagram of the OFDM-based transmitter with analog antenna combining. The receiver diagram is equivalent.	55
4.4	Spatial power distribution under different scenarios. a) $n_T = 4, d_A = 0.1\lambda$ . b) $n_T = 4, d_A = 0.25\lambda$ .	64
4.5	Bit error rate for the evaluated schemes ( $\rho = 0.4, d_A = \infty$ ).	64
4.6	Bit error rate for the evaluated schemes ( $\rho = 0.7, d_A = \infty$ ).	65
4.7	Bit error rate for the evaluated schemes ( $\rho = 0.4, d_A = 0.25\lambda$ ).	65
4.8	Bit error rate for the evaluated schemes ( $\rho = 0.7, d_A = 0.25\lambda$ ).	66
4.9	Bit error rate for the evaluated schemes ( $\rho = 0.4, d_A = 0.1\lambda$ ).	66
4.10	Bit error rate for the evaluated schemes ( $\rho = 0.7, d_A = 0.1\lambda$ ).	67
5.1	Full MIMO concept with space-time processing in the baseband.	72
5.2	MIMAX concept: spatial processing in the AFE in the RF part and temporal digital processing in the baseband.	73
5.3	MIMAX system architecture.	73
5.4	MIMAX demonstrator architecture (front).	74
5.5	MIMAX demonstrator architecture (back).	74
5.6	Block diagram of the IEEE802.11a baseband processor.	76
5.7	Types of frames in MIMAX.	78
5.8	SIGNAL field bit assignments for both types of frames in MIMAX.	78
5.9	Block diagram of the MIMAX baseband processor architecture.	79
5.10	Transmit and receive beamformers for a training frame in a $2 \times 3$ system.	85
5.11	MSE of the channel estimates as a function of the average SNR.	88
5.12	Simulated BER of MIMAX systems using different MIMO channel estimators.	91
6.1	Block diagram of the MIMAX baseband processor architecture.	94
6.2	Block diagram of the MATLAB-based MIMAX baseband model.	98
6.3	Design flow of the new MIMAX baseband blocks.	99
6.4	System Generator diagram of the MIMAX Channel Estimation Block.	100
6.5	Schematic diagram of the Frequency Offset Estimation Block.	101
6.6	System Generator Frequency Offset Estimation Block.	101
6.7	Steps of MaxSNR algorithm implementation.	105
6.8	Architecture of the complex multiplication block.	106
6.9	MIMAX blocks control and data flow diagram.	107
6.10	System Generator architecture for Block B.	108
6.11	Timing diagram for the MIMAX beamforming block.	110
6.12	Performance of the MaxSNR Block with finite-precision signals.	111
6.13	MaxSNR Block performance with a fixed number of iterations in Steps B and C.	112
6.14	MaxSNR Block performance with finite-precision signals and a fixed number of iterations.	113

6.15	Allocation of the MIMAX training symbols in the $52 \times 16$ matrix memory of the RF Weights Block. Each square represent the 52-sample memory relative to a MIMAX training symbol. . . . .	114
7.1	Baseband Simulink model for the simulation of the reception of a training frame (MIMAX frame II). . . . .	117
7.2	Received training frame (MIMAX frame II) through a $2 \times 3$ flat MIMO channel. . . . .	118
7.3	Comparison among the RF weights calculated in System Generator model, fixed-point model, and floating-point simulation. . . . .	119
7.4	Comparison among the RF weights calculated in System Generator model (blue circles), fixed-point model (red crosses), and floating-point simulation (green squares). . . . .	120
7.5	Comparison among the RF weights calculated in System Generator model, fixed-point model, and floating-point simulation for a $3 \times 3$ system. . . . .	121
7.6	Comparison among the RF weights calculated in System Generator model (blue circles), fixed-point model (red crosses), and floating-point simulation (green squares). . . . .	122
7.7	VHDL simulation flow: mixing VHDL and System Generator designs. . . . .	123
7.8	Captures of ModelSim simulations of the whole MIMAX baseband processor for a received training frame. . . . .	124
7.9	FPGA design flow: mixing VHDL and System Generator designs. . . . .	126
7.10	Dialog box for the generation of the NGC and VHDL files. . . . .	127
7.11	MIMAX entity generated with System Generator. . . . .	127
7.12	VHDL declaration of the entity within the ISE project. . . . .	130
7.13	VHDL instantiation of the entity within the ISE project. . . . .	131
7.14	ISE project. . . . .	131
8.1	MIMAX baseband board ( $135 \text{ mm} \times 225 \text{ mm}$ ). . . . .	134
8.2	Different constellations observed in a monitor through the VGA monitor connector of the baseband board. . . . .	136
8.3	Switches, LEDs, and push buttons on the baseband board. . . . .	136
8.4	MAC emulator user interface (Usb_MacEmu program). . . . .	137
8.5	Setup for the first real-time tests. . . . .	139
8.6	Preliminary basic tests consisting in reading, changing, and re-reading some configuration parameters. . . . .	139
8.7	MAC emulator user interface when transmitting a data frame. . . . .	140
8.8	MAC emulator user interface when receiving a data frames. . . . .	141
8.9	MAC emulator user interface when receiving a training frame. . . . .	142
8.10	Comparison among the RF weights obtained in real-time, in fixed-point design simulation, and in floating-point simulation. . . . .	142
8.11	Comparison among the RF weights calculated in real-time (blue circles), fixed-point design simulation (red crosses), and floating-point simulation (green squares) for four different channels. . . . .	143
8.12	Comparison among the RF weights obtained in real-time, in fixed-point design simulation, and in floating-point simulation for a $3 \times 3$ system. . . . .	144
8.13	Comparison among the RF weights calculated in real-time (blue circles), fixed-point design simulation (red crosses), and floating-point simulation (green squares). . . . .	145

8.14 MIMAX analog front-end. . . . .	146
8.15 Picture of the MIMAX analog front-end board manufactured at the Dresden University of Technology. . . . .	147
8.16 MIMAX Antenna Array integrated with the laptop. . . . .	148
8.17 Setup of the physical layer tests. . . . .	148
8.18 Timing diagram of the testing procedure. . . . .	150
8.19 Transmitter and receiver locations used for the experiments. . . . .	151

# List of Tables

2.1	Transmission schemes under different scenarios. . . . .	15
2.2	Transmission schemes under different scenarios. . . . .	22
2.3	Maximum achievable diversity, multiplexing, and array gains for full MIMO, MIMAX, and SISO systems. . . . .	24
3.1	Particular cases with closed-form solutions. . . . .	40
7.1	Optimal weights obtained under different models for a particular MIMO channel (after rotation and scaling). . . . .	119
7.2	Most relevant features of XC5VLX220 and XC5VLX330 FPGAs of Virtex-5 family.	128
7.3	Slice logic utilization of the MIMAX blocks for XC5VLX330 FPGA. . . . .	128
7.4	Summary of timing constrains. . . . .	129
7.5	FPGA resources of MIMAX beamforming block generation. . . . .	130
7.6	FPGA resources of complete MIMAX baseband processor generation. . . . .	132
8.1	Performance comparison between SISO and MIMAX systems. Rates: 9, 18, 36, and 54 Mbps. Data frame length: 10 OFDM symbols. . . . .	151



# List of Algorithms

3.1	Proposed beamforming algorithm. . . . .	43
4.1	Proposed algorithm for the obtention of the receive beamformers. . . . .	58
4.2	Proposed algorithm for the obtention of the transmit beamformers. . . . .	61
6.1	Pseudocode of the approximated MaxSNR algorithm. . . . .	104
6.2	Pseudocode of Step A block. . . . .	106
6.3	Pseudocode of Step B block. . . . .	108
6.4	Pseudocode of Step C block. . . . .	109



# Bibliography

- [A. Paulraj and Gore, 2003] R. N. A. Paulraj and D. Gore. *Introduction to Space-Time Wireless Communication*. Cambridge University Press, 2003.
- [Alamouti, 1998] S. Alamouti. “A simple transmit diversity technique for wireless communications”. *IEEE Journal on Selected Areas in Communications*, volume 45, no. 9, pages 1451–1458, 1998.
- [Andrews et al., 2007] J. Andrews, A. Ghosh, and R. Muhamed. *Fundamentals of WiMAX: Understanding Broadband Wireless Networking*. Prentice Hall, 2007.
- [Barbarossa, 2005] S. Barbarossa. *Multiantenna Wireless Communication Systems*. Artech House Publishers, Boston, MA, 2005.
- [Biglieri et al., 2007] E. Biglieri, R. Calderbank, A. Constantinides, A. Goldsmith, A. Paulraj, and H. V. Poor. *MIMO Wireless Communications*. Cambridge University Press, New York, NY, USA, 2007.
- [Biguesh and Gershman, March 2006] M. Biguesh and A. Gershman. “Training based mimo channel estimation: a study of tradeoffs and optimal training signals”. *IEEE Transactions on Signal Processing*, volume 54-3, pages 884–893, March 2006.
- [Blake and Zisserman, 1987] A. Blake and A. Zisserman. *Visual reconstruction*. MIT Press, Cambridge, MA, USA, 1987.
- [Boyd and Vandenberghe, 2004] S. Boyd and L. Vandenberghe. *Convex Optimization*. Cambridge University Press, 2004.
- [Choi et al., 2007] J. Choi, S. Kim, and I. Choi. “Statistical eigen-beamforming with selection diversity for spatially correlated OFDM downlink.”. *IEEE Transactions on Vehicular Technology*, volume 56-5, pages 2931–2940, 2007.
- [Cover and Thomas, 1991] T. M. Cover and J. A. Thomas. *Elements of information theory*. Wiley-Interscience, New York, NY, USA, 1991.
- [E. Dahlman and Bemming, 2007] J. S. E. Dahlman, S. Parkvall and P. Bemming. *3G Evolution: HSPA and LTE for Mobile Broadband*. Academic Press, Oxford, 2007.
- [Eickhoff et al., 2008] R. Eickhoff, F. Ellinger, U. Mayer, M. Wickert, I. Santamaría, R. Kraemer, L. González, P. Sperandio, and T. Theodosiou. “MIMAX: Exploiting the maximum performance and minimum system costs of wireless MIMO systems”. In *17th ICT Mobile and Wireless Summit, Stockholm, Sweden*. 2008.

- [Eickhoff et al., 2009] R. Eickhoff, U. Mayer, M. Wickert, F. Ellinger, I. Santamaría, V. Elvira, J. Ibáñez, and J. Vía. “Fully integrated MIMO transceiver with pre-FFT processing for 802.11a”. In *FP7 Workshop on Advanced MIMO and Cooperative Communications*. EU Commission, EU Commission, Brussels, Belgium, 2009.
- [Eickhoff et al., 2011] R. Eickhoff, K. Tittelbach-Helmrich, M. Wickert, J. Wagner, U. Mayer, V. Elvira, and J. Ibañez. “Physical layer amendments for MIMO features in 802.11a”. In *Proceedings of the Future Network and Mobile Summit*. Warsaw, Poland, 2011.
- [Ellinger, 2007] F. Ellinger. *Radio Frequency Integrated Circuits and Technologies*. Springer-Verlag, Berlin, 2007.
- [Ellinger et al., 2001] F. Ellinger, U. Lott, and W. Bachtold. “An antenna diversity MMIC vector modulator for HIPERLAN with low power consumption and calibration capability”. *IEEE Trans. on Microwave Theory and Techniques*, volume 49, no. 5, pages 964–969, 2001.
- [Ellinger et al., 2010] F. Ellinger, U. Mayer, M. Wickert, N. Joram, J. Wagner, R. Eickhoff, I. Santamaria, C. Scheytt, and R. Kraemer. “Integrated adjustable phase shifters”. *IEEE Microwave Magazine*, volume 11, no. 6, pages 97–108, 2010.
- [Elvira et al., 2010] V. Elvira, J. Ibáñez, I. Santamaria, M. Krstic, K. Tittelbach-Helmrich, and Z. Stamenkovic. “Baseband processor for RF-MIMO WLAN”. In *17th IEEE International Conference on Electronics, Circuits, and Systems (ICECS 2010)*. Athens, Greece, 2010.
- [Elvira and Vía, 2011] V. Elvira and J. Vía. “Analog antenna combining in transmit correlated channels: Transceiver design and performance evaluation”. *Submitted to Signal Processing (Second Review)*, 2011.
- [Elvira and Vía, 2009] V. Elvira and J. Vía. “Diversity techniques for analog combining schemes: Design and performance evaluation.”. In *17th European Signal Processing Conference (EUSIPCO 2009)*. Glasgow, Scotland, 2009.
- [Erdogmus et al., 2004] D. Erdogmus, K. E. H. II, J. C. Príncipe, M. Lázaro, and I. Santamaría. “Adaptive blind deconvolution of linear channels using Renyi entropy with Parzen windowing estimation”. *IEEE Transactions on Signal Processing*, volume 52, no. 6, pages 1489–1498, 2004.
- [Foschini and Gans, 1998] G. Foschini and M. Gans. “On limits of wireless communications in a fading environment when using multiple antennas”. *Wireless Personal Communications*, volume 6, pages 311–335, 1998.
- [Foschini, 1996] G. J. Foschini. “Layered space-time architecture for wireless communication in a fading environment when using multiple antennas”. *Bell Labs Technical Journal*, volume 1, pages 41–59, 1996.
- [Gago et al., 2009a] O. Gago, L. González, and R. Eickhoff. “Study of the optimum number of radiating elements for different portable devices operating in a mimo system”. In *Proc. 15th European Wireless Conference*. 2009.
- [Gago et al., 2009b] O. Gago, L. González, R. Eickhoff, and I. Santamaría. “Mifa: Modified ifa radiating element for small handheld devices”. In *Proc. ICT Mobile Summit*,. 2009.

- [Gago et al., 2009c] O. Gago, S. Ruiz, and L. González. “D4.3 - Design of antenna array”. Deliverable D4.3, MIMAX Project, Santander, Spain, 2009.
- [Gholam et al., 2011] F. Gholam, J. Vía, and I. Santamaría. “Beamforming design for simplified analog antenna combining architectures”. *IEEE Transactions on Vehicular Technology*, , no. 0, 2011.
- [Goldsmith, 2005] A. Goldsmith. *Wireless Communications*. Cambridge University Press, New York, NY, USA, 2005.
- [Gonzalez et al., 2009] L. Gonzalez, Z. Stamenkovic, M. Wickert, I. Santamaria, and R. Eickhoff. “D6.1 - First system integration and test”. Technical report, MIMAX Project, 2009.
- [Gray and Markel, 1974] A. Gray and J. Markel. “A spectral-flatness measure for studying the autocorrelation method of linear prediction of speech analysis”. *IEEE Transactions on Acoustics, Speech and Signal Processing*, volume 22, no. 3, pages 207–217, 1974.
- [Huang and Letaief, 2004a] D. Huang and K. Letaief. “Pre-DFT processing using eigenanalysis for coded OFDM with multiple receive antennas”. *IEEE Transactions on Communications*, volume 52, no. 11, pages 2019–2027, 2004.
- [Huang and Letaief, 2004b] D. Huang and K. B. Letaief. “Symbol-based space diversity for coded OFDM systems”. *IEEE Transactions on Wireless Communications*, volume 3, no. 1, pages 117–127, 2004.
- [Ibañez et al., 2009a] J. Ibañez, V. Elvira, O. González, J. Gutiérrez, and I. Santamaría. “D5.2 - Integration and testing of MIMO algorithms”. Technical report, MIMAX Project, 2009.
- [Ibañez et al., 2009b] J. Ibañez, J. Vía, M. Kritic, V. Elvira, K. Tittelbach-Helmrich, I. Santamaría, and Z. Stamenkovic. “D3.2 - Design of a reconfigurable baseband and MAC processor”. Technical report, MIMAX Project, 2009.
- [IEEE Standard 802.11n, 2007] IEEE Standard 802.11n. “Ieee standard 802.11n, wireless lan medium access control (mac) and physical layer (phy) specifications, draft 2.0”. 2007.
- [IEEE Std. 802.11a, 1999] IEEE Std. 802.11a. *Supplement to Part 11: Wireless LAN Medium Access Control (MAC) and Physical Layer (PHY) specifications: High-speed Physical Layer in the 5 GHz Band*. IEEE., 1999.
- [Jakes, 1974] W. Jakes. *Microwave Mobile Communications*. John Wiley & Sons In, 1974.
- [Jöngren et al., 2002] G. Jöngren, M. Skoglund, and B. Ottersten. “Combining beamforming and orthogonal space-time block coding”. *IEEE Transactions on Information Theory*, volume 48, no. 3, pages 611–627, 2002.
- [Kay, 1993] S. M. Kay. *Fundamentals of Statistical Signal Processing, Volume 1: Estimation Theory*. Prentice Hall, NJ, 1993.
- [Kraemer et al., 2008] R. Kraemer, I. Santamaría, L. Gonzalez, and R. Eickhoff. “D3.1 - System requirements, architecture and specifications”. Technical report, MIMAX Project, 2008.

- [Kraemer et al., 2010] R. Kraemer, Z. Stamenkovic, K. Tittelbach-Helmrich, L. González, S. Ruiz, O. Gago, J. Ibañez, V. Elvira, M. Wickert, and R. Eickhoff. “RF-MIMO WLAN modem demonstrator”. In *Wireless World Research Forum WWRF Meeting 25, Wireless World Research Forum*. London, UK., 2010.
- [Krstic et al., 2003] M. Krstic, A. Troya, K. Maharatna, and E. Grass. “Optimized low-power synchronizer design for the IEEE 802.11a standard”. In *IEEE International Conference on Acoustic, Speech, and Signal Processing (ICASSP 2003)*. 2003.
- [Lameiro et al., 2011] C. Lameiro, A. Nazábal, F. Gholam, J. Vía, and I. Santamaría. “Capacity region of the two-way multi-antenna relay channel with analog tx-rx beamforming”. In *3rd International ICST Conference on Mobile Lightweight Wireless Systems (MOBILIGHT 2011)*. Bilbao, Spain, 2011.
- [Li et al., 2007a] S. Li, D. Huang, K. Letaief, and Z. Zhou. “Multi-stage beamforming for coded OFDM with multiple transmit and multiple receive antennas”. *IEEE Transactions on Wireless Communications*, volume 6, no. 3, pages 959–969, 2007.
- [Li et al., 2007b] S. Li, D. Huang, K. Letaief, and Z. Zhou. “Pre-DFT processing for MIMO-OFDM systems with space-time-frequency coding”. volume 6, no. 11, pages 4176–4182, 2007.
- [Ma and Giannakis, 2002] X. Ma and G. B. Giannakis. “Complex field coded MIMO systems: performance, rate, and trade-offs”. *Wireless Communications and Mobile Computing*, volume 2, no. 7, pages 693–717, 2002.
- [Marshall and Olkin, 1979] A. W. Marshall and I. Olkin. *Inequalities: Theory of Majorization and its Applications*. Academic Press, New York, NY, 1979.
- [Mayer and Willke, 1973] L. Mayer and T. Willke. “On biased estimation in linear models”. *Technometrics*, volume 15, pages 497–808, 1973.
- [Mayer et al., 2009] U. Mayer, M. Wickert, and R. Eickhoff. “D4.2 - Design of transceiver front-end”. Deliverable D4.2, MIMAX Project, Dresden, Germany, 2009.
- [Mayer et al., 2010] U. Mayer, M. Wickert, and R. Eickhoff. “D4.4 - Redesign of the MIMAX transceiver”. Deliverable D4.4, MIMAX Project, Dresden, Germany, 2010.
- [MIMAX Web, 2008] MIMAX Web. “MIMAX: Advanced MIMO systems for maximum reliability and performance”. <http://www.ict-mimax.eu>, 2008.
- [Mobile WiMAX, 2006] Mobile WiMAX. “Mobile WiMAX - Part I/II: A technical overview and performance evaluation”. 2006.
- [Mohimani et al., 2009] G. H. Mohimani, M. Babaie-Zadeh, and C. Jutten. “A fast approach for overcomplete sparse decomposition based on smoothed l0 norm”. *IEEE Transaction on Signal Processing*, volume 57, no. 1, pages 289–301, 2009.
- [Okada and Komaki, 2001] M. Okada and S. Komaki. “Pre-DFT combining space diversity assisted COFDM”. *IEEE Transactions on Vehicular Technology*, volume 50, no. 2, pages 487–496, 2001.

- [Palomar and Fonollosa, 2005] D. Palomar and J. Fonollosa. “Practical algorithms for a family of waterfilling solutions”. *IEEE Transaction on Signal Processing*, volume 53-2, pages 686–695, 2005.
- [Palomar et al., 2003] D. P. Palomar, J. M. Goeffi, and M. A. Lagunas. “Joint Tx-Rx beamforming design for multicarrier MIMO channels: A unified framework for convex optimization”. *IEEE Transactions on Signal Processing*, volume 51, no. 9, pages 2381–2401, 2003.
- [Palomar and Jiang, 2006] D. P. Palomar and Y. Jiang. “MIMO transceiver design via majorization theory”. *Found. Trends Commun. Inf. Theory*, volume 3, no. 4, pages 331–551, 2006.
- [Phan et al., 2009] K. Phan, S. Vorobyov, N. Sidiropoulos, and C. Tellambura. “Spectrum sharing in wireless networks via QoS-aware secondary multicast beamforming”. *IEEE Transactions on Signal Processing*, volume 57, no. 6, pages 2323–2335, 2009.
- [Proakis, 1988] J. Proakis. *Digital Communications*. Prentice Hall, NJ, USA, 1988.
- [Rahman et al., 2004] M. Rahman, K. Witrisal, S. Das, F. Fitzek, O. Olsen, and R. Prasad. “Optimum pre-DFT combining with cyclic delay diversity for OFDM based WLAN systems”. In *IEEE 59th Vehicular Technology Conference (VTC 2004-Spring)*, volume 4, pages 1844–1848. 2004.
- [Renyi, 1976] A. Renyi. “Some fundamental questions of information theory”. in *Selected papers of Alfred Renyi*, volume 2, pages 526–552, 1976.
- [S. Jeon and Itoh, May 2002] Y. Q. S. Jeon, Y. Wang and T. Itoh. “A novel smart antenna system implementation for broad-band wireless communications”. *IEEE Transactions on Antennas and Propagation*, volume vol. 50, page 600–606, May 2002.
- [Sampath and Paulraj, 2002] H. Sampath and A. Paulraj. “Linear precoding for space-time coded systems with known fading correlations”. *IEEE Communications Letters*, volume 6, no. 6, pages 239–241, 2002.
- [Sandhu and Ho, 2003] S. Sandhu and M. Ho. “Analog combining of multiple receive antennas with OFDM”. In *IEEE International Conference on Communications (ICC '03)*, volume 5, pages 3428–3432. 2003.
- [Santamaría et al., 2010] I. Santamaría, R. Eickhoff, Z. Stamenkovic, O. Gago, M. Andreou, J. Ibáñez, J. Vía, and M. W. K. Tittelbach-Helmrich. “D6.2 - Benchmarking of the network front-end”. Technical report, MIMAX Project, 2010.
- [Santamaría et al., 2011] I. Santamaría, R. Eickhoff, Z. Stamenkovic, O. Gago, D. Christofi, J. Ibáñez, M. Wickert, K. Tittelbach, A. Nazábal, and Óscar González. “D6.3 - System integration and demonstration”. Technical report, MIMAX Project, 2011.
- [Santamaría et al., 2009a] I. Santamaría, J. Vía, V. Elvira, J. Ibáñez, J. Pérez, R. Eickhoff, and U. Mayer. *Handbook of Smart Antennas for RFID Systems*, chapter Low cost and compact RF-MIMO transceivers. Wiley, 2009.
- [Santamaría et al., 2009b] I. Santamaría, J. Via, J. Pérez, J. Ibáñez, and V. Elvira. “D5.1 - Development of MIMO algorithms”. Technical report, MIMAX Project, 2009.

- [Santamaría et al., 2008] I. Santamaría, V. Elvira, J. Vía, D. Ramírez, J. Pérez, J. Ibáñez, R. Eickhoff, and F. Ellinger. “Optimal MIMO transmission schemes with adaptive antenna combining in the RF path”. In *16th European Signal Processing Conference (EUSIPCO 2008)*. Lausanne, Switzerland, 2008.
- [Santamaría et al., 2002] I. Santamaría, D. Erdogmus, and J. C. Principe. “Entropy minimization for supervised digital communications channel equalization”. *IEEE Transactions on Signal Processing*, volume 50, no. 5, pages 1184–1192, 2002.
- [Sidiropoulos et al., 2006] N. Sidiropoulos, T. Davidson, and Z.-Q. Luo. “Transmit beamforming for physical-layer multicasting”. *IEEE Transactions on Signal Processing*, volume 54, no. 6, pages 2239–2251, 2006.
- [Stamenkovic et al., 2010] Z. Stamenkovic, K. Tittelbach-Helmrich, M. Krstic, J. Ibáñez, V. Elvira, and I. Santamaría. “Mac and baseband hardware platforms for RF-MIMO WLAN”. In *Proceedings of the 5th European Conference on Circuits and Systems for Communications*. Belgrade, Serbia, 2010.
- [Stoica and Selen, 2004] P. Stoica and Y. Selen. “Cyclic minimizers, majorization techniques, and the expectation-maximization algorithm: a refresher”. *IEEE Signal Processing Magazine*, volume 21, pages 112–114, 2004.
- [Tarokh et al., 1998] V. Tarokh, N. Seshadri, and A. R. Calderbank. “Space-time codes for high data rate wireless communications: Performance criterion and code construction”. *IEEE Transactions on Information Theory*, volume 44, no. 2, pages 744–765, 1998.
- [Telatar, 1999] I. E. Telatar. “Capacity of multi-antenna Gaussian channels”. *European Transactions on Telecommunications*, volume 10, no. 6, pages 585–595, 1999.
- [Troya et al., 2002] A. Troya, K. Maharatna, M. Krstic, E. Grass., and R. Kraemer. “OFDM synchronizer implementation for an IEEE 802.11(a) compliant modem. In: IASTED international conference on wireless and optical communication”. In *IASTED International Conference on Wireless and Optical Communication*. Banff, Canada, 2002.
- [Tse, 2005] D. Tse. *Fundamentals of Wireless Communication*. Cambridge University Press, 2005.
- [Vía et al., 2010a] J. Vía, I. Santamaría, V. Elvira, and R. Eickhoff. “A general criterion for analog Tx-Rx beamforming under OFDM transmissions”. *IEEE Transactions on Signal Processing*, volume 58, no. 4, pages 2155–2167, 2010.
- [Vía et al., 2010b] J. Vía, I. Santamaría, V. Elvira, and R. Eickhoff. “A general pre-FFT criterion for MIMO-OFDM beamforming”. In *IEEE International Conference on Communications (ICC 2010)*. Cape Town, South Africa, 2010.
- [Vía et al., 2009] J. Vía, I. Santamaría, V. Elvira, J. Ibáñez, and R. Eickhoff. “OFDM system with pre-FFT processing for MIMO systems”. In *FP7 Workshop on Advanced MIMO and Cooperative Communications*. EU Commission, Brussels, Belgium, 2009.
- [Vía et al., 2009a] J. Vía, V. Elvira, J. Ibáñez, and I. Santamaría. “Optimal precoding for a novel RF-MIMO scheme in transmit correlated rayleigh channels”. In *IEEE Workshop on Signal Processing Advances in Wireless Communications (SPAWC 2009)*. Perugia, Italy, 2009.

- [Vía et al., 2009b] J. Vía, V. Elvira, I. Santamaría, and R. Eickhoff. “Analog antenna combining for maximum capacity under OFDM transmissions”. In *IEEE International Conference on Communications (ICC 2009)*. Dresden, Germany, 2009.
- [Vía et al., 2009c] J. Vía, V. Elvira, I. Santamaría, and R. Eickhoff. “Minimum BER beamforming in the RF domain for OFDM transmissions and linear receivers”. In *IEEE International Conference on Acoustics, Speech and Signal Processing (ICASSP 2009)*. Taipei, Taiwan, 2009.
- [Wang et al., 2007] F. Wang, A. Ghosh, C. Sankaran, and S. Benes. “WiMAX system performance with multiple transmit and multiple receive antennas”. In *IEEE 65th Vehicular Technology Conference (VTC-Spring)*, pages 2807–2811. 2007.
- [Wang et al., 2008] F. Wang, A. Ghosh, C. Sankaran, P. Fleming, F. Hsieh, and S. Benes. “Mobile WiMAX systems: performance and evolution”. *IEEE Communications Magazine*, volume 46, no. 10, pages 41–49, 2008.
- [Winters, 1987] J. Winters. “On the capacity of radio communication systems with diversity in a rayleigh fading environment”. *IEEE J. Sel. Areas Commun.*, volume 871-8, 1987.
- [Xin et al., 2003] Y. Xin, Z. Wang, and G. Giannakis. “Space-time diversity systems based on linear constellation precoding”. *IEEE Transactions on Wireless Communications*, volume 2, no. 2, pages 294–309, 2003.
- [Zheng and Tse, 2003] L. Zheng and D. Tse. “Diversity and multiplexing: A fundamental tradeoff in multiple-antenna channels”. *IEEE Transactions on Information Theory*, volume 49, no. 5, pages 1073–1096, 2003.